17

THE GEOLOGY AND GEOCHEMISTRY OF THE ETENDEKA FORMATION QUARTZ LATITES, NAMIBIA.

by

SIMON CHARLES MILNER

Department of Geochemistry
University of Cape Town
May 1988

Thesis submitted in fulfilment of the requirements for the degree of Doctor of Philosophy in the Department of Geochemistry at the University of Cape Town.

ABSTRACT

The Etendeka Formation volcanics of north-western Namibia form part of the Karoo Igneous Province of southern Africa and consist of a series of basalts interbedded with quartz latites and minor volumes of latite. This thesis examines various aspects of the geology and geochemistry of the quartz latites, in particular the volcanological and petrogenetic origin of these rocks. This study has involved the geological mapping of *ca*. 5000 km^2 of the southern Etendeka region and the documentation of the field and petrographic characteristics of the quartz latites. 183 whole rock quartz latite samples have been analysed for 32 elements by x-ray fluorescence spectrometry and 17 of these samples were selected for detailed mineral analyses by electron microprobe.

The quartz latites make up a significant proportion of the succession (> 25 %) and constitute as much as 60 % of the outcrop in the southern Etendeka region. They occur as voluminous (80 - 800 km^3), widespread (up to 4500 km^2) sheet-like units, typically between 40 and 300 m thick. Individual units consist of basal, main and upper zones. The main zone usually constitutes over 70 % of the unit and typically consists of featureless devitrified quartz latite. In contrast the basal and upper zones of the flow are characterised by flow banding, pitchstone lenses and breccias which may contain rare pyroclastic textures. The quartz latites are sparsely porphyritic (< 10 %) with glassy or devitrified groundmass textures. The phenocrysts consist of plagioclase, pyroxene, titanomagnetite and rare ilmenite. Pyroxene and plagioclase geothermometry indicate high (1000 - 1100 °C) temperatures of crystallisation, which coupled with an absence of primary hydrous phases, indicate that the quartz latites were relatively hot, H_2O-undersaturated magmas.

The quartz latites display features common to both rhyolite lavas and ignimbrites and are clearly the products of an unusual eruption style. The local preservation of pyroclastic textures and the broad areal extent of these units have led to the conclusion that the quartz latites were erupted as dense, high-temperature ash flows which underwent en masse lava-like flowage prior to their final emplacement (i.e. they are rheoignimbrites). A combination of high eruption temperatures and relatively low viscosity help to explain the often completely welded, homogeneous textures encountered at most outcrops. The apparent mobility of the quartz latite ash flows, coupled with their high temperatures and strongly welded nature require high rates of magma production

and/or descent from very high eruption columns.

Apart from some systematic differences between pitchstone and devitrified quartz latite, largely explained by alteration processes, individual quartz latite units exhibit remarkably uniform compositions with no significant vertical or lateral variation. It has been possible to use geochemistry as a primary criterion for the correlation of major quartz latite units over much of the southern Etendeka, and this has enabled the reconstruction of a stratigraphic model for the Etendeka Formation in this region.

A comparison of the composition of quartz latites from the southern Etendeka with those from the more northerly, Sarusas region reveal that the latter show notable enrichments in Ba, Sr, Nb, Zr, P, Ti, Y and LREE. In the Karoo and Paraná Igneous Provinces a laterally extensive geochemical discontinuity separates relatively incompatible trace and minor element "enriched" basalts in the north from compositionally more "normal" basalts in the south. This feature is also apparent in the Etendeka quartz latites.

Petrogenetic modelling indicates that the quartz latites are minimum partial melts of mid- to lower-crustal material of basic to intermediate composition. Melting probably occurred at depths of 30 - 35 km (8 - 10 kb), induced by the underplating or ponding of basaltic magma within the lower crust. The major and trace element and isotopic (Sr and O) composition of the quartz latites indicates that they underwent little mixing or interaction with basaltic magma, and further precludes their derivation from a basaltic precursor either by simple closed system fractional crystallisation or by differentiation and crustal contamination.

Mineral composition data and geochemical modelling indicate that variation trends defined by different groups of quartz latites in the southern Etendeka are not the result of magmatic differentiation. However, small compositional variations within individual groups of quartz latite are probably the result of limited degrees of fractional crystallisation. The compositional differences between different groups of quartz latite are probably due to slight variations in the composition of the source, its mineralogy and the degree of partial melting.

Simple trace element modelling and geodynamic considerations indicate that the "enriched" Sarusas quartz latites are not the products of partial melting of "enriched" underplated basalt, as might be implied from their trace element and

isotopic characteristics. If one accepts that the "enriched" basalts were derived from enriched sub-continental mantle, then it is possible that the enrichment process(es) may also have affected the source regions of the quartz latites at the base of the lower crust.

TABLE OF CONTENTS

LIST OF FIGURES

LIST OF TABLES

ACKNOWLEDGEMENTS

I would like to express my gratitude to my supervisors, Profs. Tony Erlank and Andy Duncan for their guidance, support and encouragement during the research and preparation of this thesis. I have also benefitted from discussions with Goonie Marsh and the late Peter Betton. I am grateful to Prof. James Willis and Drs. Stuart Smith and Dave Reid for their advice, particularly with regard to XRF analysis and the preparation of samples. Andy Duncan and Dave Hill are thanked for patiently introducing me to the Departmental computer system, and in particular to a whole host of data handling and computer graphics programs which have been invaluable in the interpretation and presentation of data. Russell Sweeney is thanked for analysing several new quartz latite samples for Sr-isotopes at the NPRL, Pretoria.

This project was largely funded by the SWA/Namibia Committee of Research Priorities (CRP) through the Geological Survey of SWA/Namibia. I would also like to thank Tony Erlank for the studentship from the CSIR (FRD) which I received during 1987/88.

Field work played a major role in this study and could not have been achieved without the logistical support of the Geological Survey of SWA/Namibia and the greatly appreciated efforts of its Director Dr. Roy Miller, and his staff. In particular I wish to thank my field assistants, Fikameni Jeremias and Michael Gondombolo, for their help and companionship in the field. Officers of Nature Conservation in the Skeleton Coast Park, particularly Rudi Loutit (then at Ugabmond), are thanked for their advice and hospitality, and for their tolerance of geologists whose apparent aim in life is to scare off all the game and make tracks in the desert!

My visits to Windhoek have always been something to look forward to and I would particularly like to thank Roger Swart, Brian Hoal, Bruce and Collwyn Bulley and Dudley and Linda Corbett for their kind hospitality during numerous stop-overs in Windhoek.

Brian Hoal, Jon McStay, Chris Harris and Ron Watkins are thanked for their comments on earlier drafts of this work, and the timely assistance of Nadi Ebrahim, Jon McStay and Chris Harris during the final collation of the thesis was greatly appreciated. I would also like to thank Charlie Basson (photographer) for his advice and for the final production of the black and white plates in Chapter 3.

Finally I would like to thank all those people who have offered their moral support, especially during the arduous period of "writing up". In particular, thanks go to my parents and sisters whose support and encouragement is most appreciated. Special thanks must go to Debbie Smith who has been a constant source of encouragement over the past 18 months and who has cheerfully put up with the irrationalities of someone gripped by "thesis" mania.

CHAPTER 1

INTRODUCTION

1.1 THE KAROO IGNEOUS PROVINCE

Disruption of the Gondwana supercontinent was preceded by an intensive phase of igneous activity which occurred during the Jurassic and early Cretaceous. Manifestations of this igneous activity are widespread, with remnants in southern Africa (Karoo), South America (Paraná), Antarctica (Kirwan, Ferrar Group) and in Tasmania. A later phase of volcanic activity in late Cretaceous - early Tertiary times gave rise to the Deccan traps (India). A pre-drift reconstruction of Gondwanaland and the distribution of these outcrop remnants is illustrated in Fig. 1.1 (Gondwana model after De Wit *et al.*, 1988).

In southern Africa flood lavas and intrusive dykes and sills were emplaced after the extensive and prolonged sedimentation of the Karoo Supergroup, and form what is broadly referred to as the Karoo Igneous Province. The majority of Karoo igneous rocks, particularly those of central and eastern southern Africa, date from the earlier part of the Jurassic period (*ca.* 195 - 177 Ma, Fitch and Miller, 1984; and Allsopp *et al.*, 1984a) prior to the opening of the Indian Ocean (*ca.* 145 - 150 Ma, Segoufin, 1978). During the upper Jurassic - early Cretaceous period a later phase of igneous activity occurred in north-western Namibia, coincident with the Paraná volcanism. The timing of this activity is not tightly constrained but is thought to have preceded the opening of the South Atlantic, *ca.* 123 - 127 Ma (Duncan *et al.*, 1984).

Remnants of the Karoo Igneous Province are distributed throughout southern Africa (Fig. 1.2) and have a present outcrop area of approximately 140,000 km^2 (Eales *et al.*, 1984). Detailed descriptions of the different regions of the Karoo Province are given by Eales *et al.* (1984) and a summary of the overall geological characteristics of the main outcrop areas is given below.

1.1.1 Lebombo Monocline and Nuanetsi.

The Lebombo monocline is a north - south flexure which runs for about 700 km from Natal to the Limpopo River and then strikes north-east into the Nuanetsi syncline of south-eastern Zimbabwe (Fig. 1.2). Estimates for the total

Fig. 1.1 Mesozoic Continental Flood Basalt Provinces of Gondwanaland.

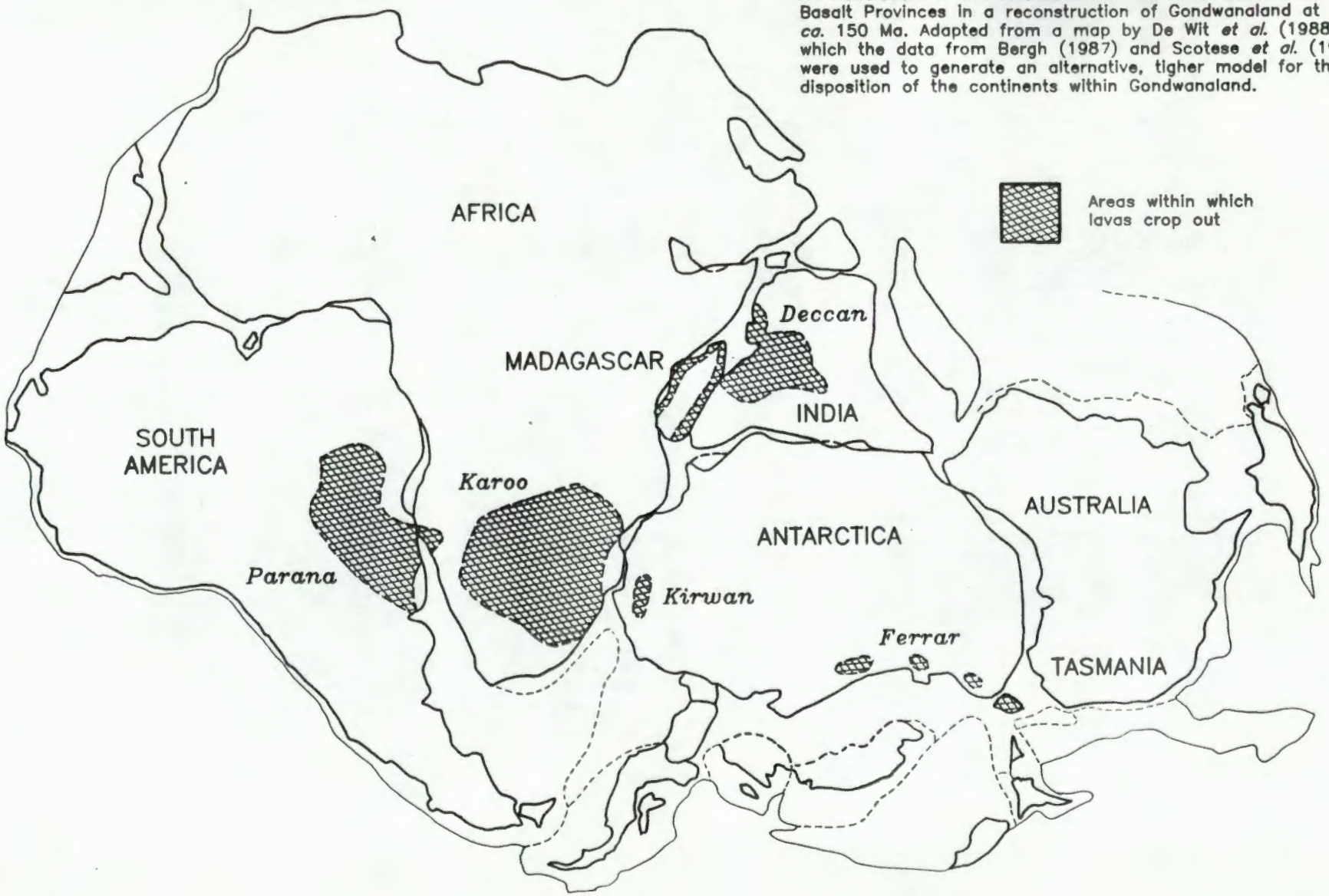

FIG. 1.2 Distribution of Karoo Volcanics in southern Africa.

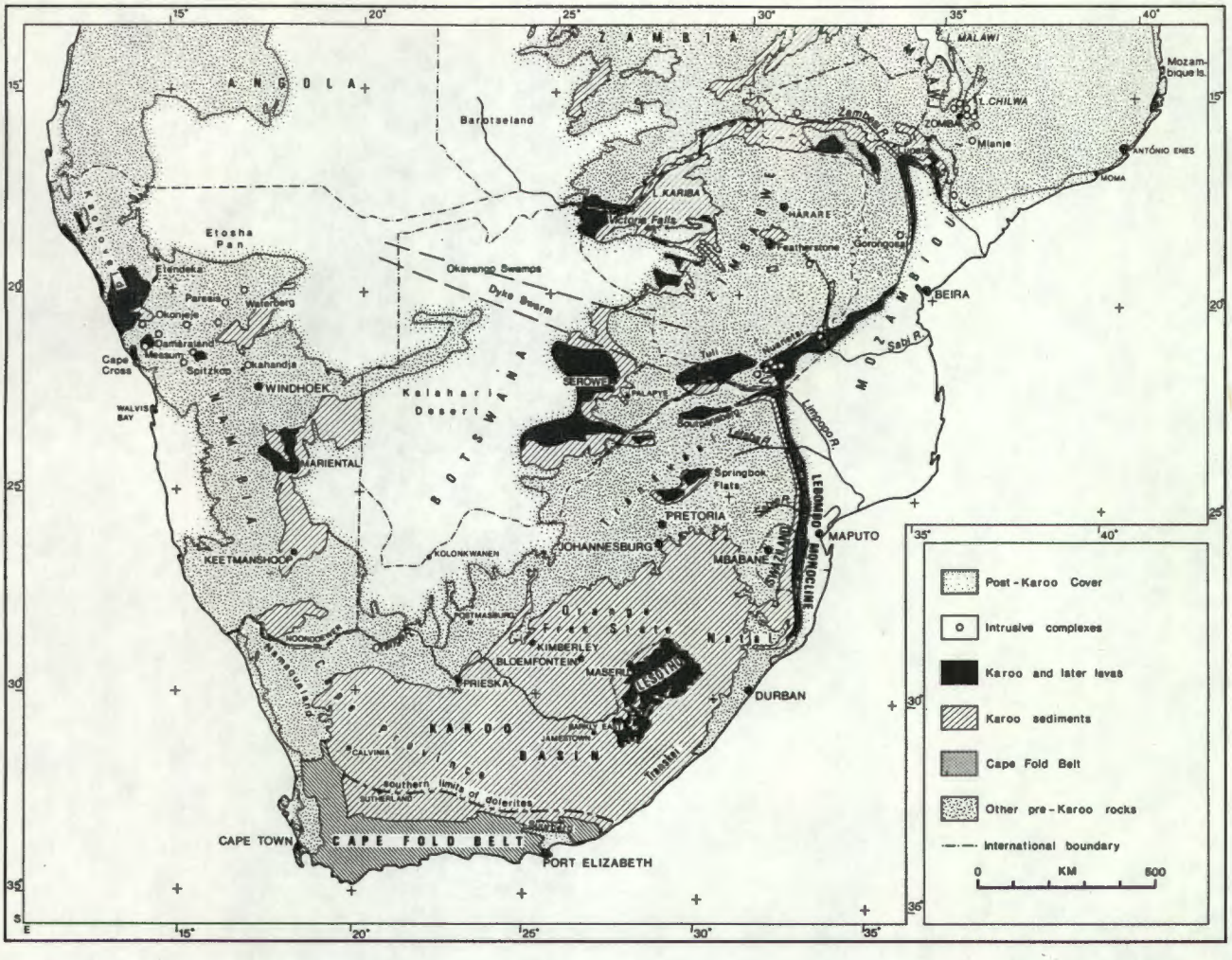

Simplified geological map of southern Africa showing the distribution of Karoo lavas and sediments. Map copied from Eales *et al.* (1984).

thickness of volcanics in this structure vary from 6600 m in Nuanetsi (Cox, 1965) to over 12000 m in Swaziland (Cleverly, 1977). The stratigraphy of the Lebombo lavas is defined by Cleverly and Bristow (1979). The lower half of the section in the northern Lebombo - Nuanetsi area consists of nephelinites and related rock types of the Mashikiri Formation overlain by tholeiitic picrite basalts of the Letaba Formation, in turn overlain by basalts and tholeiitic andesites of the Sabie River Basalt Formation. The upper half of the section consists of the Jozini Rhyolite Formation in the northern Lebombo and the Nuanetsi rhyolite, with some interbedded basalt, in the Nuanetsi area (Duncan *et al.*, 1984). In the southern Lebombo the Sabie River Basalt Formation forms the base of the succession and is overlain by the Jozini Rhyolite Formation which is in turn overlain by the locally developed Mbuluzi Rhyolite Formation. Above the main Rhyolite sequence lies the Movene Basalt Formation which is largely confined to Mozambique.

1.1.2 **Central Area** (Lesotho and north-eastern Cape Province)

The volcanic succession of this area consists of essentially flat lying units and has a maximum observed thickness of 1400 m. The lower part of the sequence consists of several compositionally diverse basalt formations which are associated with small volumes of andesitic and dacitic lavas and intrusives. These are succeeded by large volumes of compositionally uniform basalts comprising the Lesotho Formation. The Lesotho Formation "magma type" (Marsh and Eales, 1984) is overwhelmingly dominant throughout the central area and is known to occur over an enormous area of southern Africa, being represented by lavas in southern Namibia (Mariental) and in southern Botswana (Serowe), and by the majority of dolerites in the south-western Karoo basin.

1.1.3 **North-western Namibia** (Etendeka Formation)

In north-western Namibia remnants of lava crop out over large areas of the Skeleton Coast Park (Namib Desert) and the western areas of Damaraland and Kaokoland. The largest of these remnants is referred to as "the Etendeka", a geographical area which encompasses the main lava field and is the type area of the Etendeka Formation. The Etendeka Formation volcanics, which are contemporaneous with the Paraná volcanics (Brazil) represent a relatively small proportion (*ca.* 78,000 km^2, Erlank *et al.*, 1984) of the Paraná

flood basalt province which covers an estimated 1,200,000 km^2 (Bellieni *et al.*, 1984). The Etendeka Formation is described in more detail in a later chapter, but basically consists of a suite of basalts and "evolved basalts" interbedded with quartz latites and small volumes of latite.

1.1.4 Intrusive rocks

Dolerite dykes and sills, which probably acted as feeders for basalt eruption, occur throughout the Karoo Igneous Province and generally have the same compositional characteristics as the main basalt magma-types of a particular area. The Horingbaai (Namibia) and Rooi Rand (southern Lebombo) dolerites are compositionally and isotopically similar to MORB, and it is thought that they were derived from asthenospheric MORB-type source regions during the initial stages of sea-floor spreading (Duncan *et al.*, 1984).

In Damaraland a linear belt of late- to post-Karoo sub-volcanic ring complexes and plutons (Martin *et al.*, 1960) are closely associated with the Etendeka volcanics and consist of highly differentiated tholeiitic and alkaline rock types and carbonatite. In the Lebombo several large granophyre intrusions occur close to the top of the Sabie River Basalt Formation and in Nuanetsi numerous granophyres intrude the volcanic succession.

1.2 ACID VOLCANISM

The Karoo volcanics are clearly bi-modal (acid - basic) in character. The acid volcanics are only found in areas adjacent to the continental margins, and are believed to be a thermal consequence of crustal thinning and rifting preceding the disruption of Gondwanaland (Duncan *et al.*, 1984). Since this study deals almost exclusively with the quartz latites of the Etendeka Formation it is appropriate to outline some of the characteristics of the Lebombo rhyolites for comparison with them.

The rhyolites (*sensu lato*) of the Jozini and Mbuluzi Formations are by far the largest volume of acid volcanics in the Karoo Igneous Province, with an estimated thickness of 5,000 m and a total volume of 35,000 km^3 (Cleverly *et al.*, 1984). Individual flows are typically sheet-like, from 50 - 350 m thick and traceable along strike for up to 50 km. Many of the flow units contain

features which suggest that they are ignimbritic in origin (Bristow and Cleverly, 1979). The Jozini and Mbuluzi Formation rhyolites are geochemically similar but can be distinguished from one another by the presence of quartz phenocrysts and lower Zr concentrations in the latter. Minor intercalated rhyolite units also occur in the Sabie River Basalt Formation. The most important of these are the Mkutshane Beds which, with their distinctly lower trace element abundances and enriched radiogenic Sr ($^{87}Sr/^{86}Sr$ initial ratios 0.715 - 0.741), are thought to be either crustal melts or have been highly contaminated by crustal material (Cleverly *et al.*, 1984). For the majority of Lebombo rhyolites, however, a combination of high concentrations of incompatible elements coupled with low $^{87}Sr/^{86}Sr$ initial ratios (0.704 - 0.708) led Cleverly *et al.* (1984) to propose that they were derived by the partial melting of basalt.

It is important to note that the interbedding of acid and basic volcanics in the Etendeka Formation is in sharp contrast to the individual basalt and rhyolite formations of the Lebombo-Nuanetsi succession.

1.3 PREVIOUS STUDIES

The earliest account of the lavas in the Etendeka is given by Reuning (1929) who described basic melaphyres, glassy intermediate rocks and orthoclase porphyries, and listed chemical analyses showing that the intermediate rocks contained 46 - 56 wt % SiO_2 and that the "orthoclase" porphyries contained 65 - 68 wt % SiO_2. Subsequent studies by Siedner and Miller (1968), Gidskehaug *et al.* (1975) and Siedner and Mitchell (1976) have concentrated on dating the lavas in order to determine the time of initial rifting of the South Atlantic Ocean, but have documented little of the geology and compositional characteristics of the Etendeka sequences. The lavas are also mentioned by Korn and Martin (1954), Martin *et al.* (1960), Frets (1969), Hodgson (1970) and Hodgson and Botha (1975), however these descriptions are fairly superficial and in some cases inaccurate. The first comprehensive account of the Etendeka volcanics is by Erlank *et al.* (1984), who concentrated their efforts on the geochemistry and petrogenesis of the basic suite. Erlank *et al.* (1984) present major, trace element and Ar-, Sr-, Nd- and Pb-isotopic data for a variety of mafic and felsic volcanics belonging to the Etendeka Formation, and also present a stratigraphic type section of the lavas at Tafelberg and a

provisional geological map of the Etendeka based mainly on photogeological interpretation.

1.4 AGE OF THE ETENDEKA FORMATION

The timing of the Etendeka volcanic episode is important in determining the relationship between rifting and volcanism. A considerable number of ages have been published for the lavas and dolerites in Namibia and these are reviewed in some detail by Erlank *et al.* (1984). Various dating techniques have yielded ages between 110 - 150 Ma with some anomalously high K - Ar ages, which are thought to have resulted from excess argon. Re-interpreting the K - Ar data of Gidskehaug *et al.* (1975) Siedner and Mitchell (1976) obtained a well constrained $^{40}Ar/^{36}Ar$ - $^{40}K/^{36}Ar$ isochron age of 121 ± 2 Ma. Although this age has gained some acceptance in the literature there is some evidence to suggest that the lavas may be considerably older. Using a $^{40}Ar/^{39}Ar$ step heating technique to analyse plagioclase and pyroxene separates Erlank *et al.* (1984) obtained ages of between 125 - 130 Ma for two Horingbaai dolerites, and Allsopp *et al.* (1984a) obtained an Rb - Sr isochron age of 132 ± 2.2 Ma for gabbroic rocks of the Messum Igneous Complex. Both the Horingbaai dolerites and the Messum complex intrude Etendeka Formation lavas indicating that the latter are almost certainly older than 130 Ma. Indirect lines of evidence also suggest an older age. The similarity of the Karoo sedimentary sequence beneath the Etendeka Formation with that of the central Karoo basin in South Africa suggests that they are closely associated in time. There is no evidence in the sedimentary record in north-western Namibia to indicate that a prolonged period of time (some 70 Ma using currently available dates) existed between the eruption of the Central area and Lebombo volcanics in South Africa and the eruption of the Etendeka Formation in Namibia (J. Ward pers. comm., 1987). An Rb - Sr errorchron age of 154 ± 21 Ma for the quartz latites (Allsopp *et al.*, 1984b) is considered (by these authors) to be anomalously high, in that it exceeds those of other studies. Zeolite - host rock tie lines for the quartz latites have slopes indicating ages of approximately 150 Ma and it is suggested (Allsopp *et al.*, 1984b; Erlank *et al.*, 1984) that the introduction of Sr-rich zeolite and calcite into the quartz latites may be responsible for the high errorchron age. However, these authors claim that many of their samples were free from secondary mineralisation and geochemical studies (Chapter 6)

suggest that much of the Sr and Ca in these secondary minerals may ultimately have been derived from the quartz latites themselves (i.e. with the same $^{87}Sr/^{86}Sr$ initial ratio as the host) such that an age of 150 Ma may be significant. The identification of several different groups of quartz latite, which can be modelled as having slightly different crustal source regions (Chapters 6 and 7), suggest that the large errors on the Rb - Sr isochron is probably due to slight isotopic heterogeneity in the source. Clearly, further Rb - Sr studies, involving whole rock and mineral separates (phenocrysts and secondary phases) from individual quartz latite units are required to see if the lavas can be dated more precisely. In order to avoid confusion and permit direct comparison with data in Erlank *et al.* (1984) an age of 121 Ma has been retained when making age corrections to isotopic data. The use of this age and not an older age does not alter the discussions in later chapters.

1.5 AIMS OF THIS STUDY

The work presented in this thesis forms part of a continued programme of research on the Etendeka Formation and concentrates specifically on the quartz latites of the succession.

Detailed investigations have been carried out in the southern part of the Etendeka and the principle aims of this study are summarised as follows:

(1) To map out the distribution of the quartz latites and determine the stratigraphic relationships within the Formation.

(2) To document the nature of the quartz latite flow units in order to determine their volcanological characteristics.

(3) To determine the whole rock and mineral compositional characteristics of the quartz latites.

(4) To propose and test models for the petrogenesis of the quartz latites and to assess their role in the geodynamics of continental rifting.

Additional reconnaissance sampling of quartz latite units from the Sarusas district, further north, has also been carried out and has allowed a comparison of the petrographic and compositional characteristics of quartz latites from different localities.

CHAPTER 2

THE GEOLOGY OF THE SOUTHERN ETENDEKA QUARTZ LATITES

2.1 INTRODUCTION

Quartz latites of the Etendeka Formation are prominent, widespread units which cover several thousand km^2. Correlation of quartz latite units across the southern Etendeka has revealed fine stratigraphic detail within the Etendeka lava pile not previously recognised. The quartz latites crop out mostly as massive, featureless units, although rare exposures of flow contacts reveal important information on the mechanisms of eruption and emplacement.

In this chapter the results of field studies on the distribution and character of the quartz latites of the southern Etendeka are presented. These studies have defined the broad geological characteristics of individual units and their stratigraphic position within the Etendeka Formation. A more detailed account of the structure of quartz latite units is also presented together with discussion of some prominent alteration zones. Remnants of the Etendeka Formation lavas crop out over a wide area of north-western Namibia and a brief description of the underlying Karoo sediments and basement rocks indicates the conditions prevailing at the onset of volcanism, and places the volcanics in a regional geological context. The spatial distribution of the lava remnants and the overall stratigraphy of the Etendeka Formation is also discussed.

It has not been possible to make detailed field studies of the quartz latites which crop out in the Sarusas region north of the main Etendeka lava field, and for this reason the geology of the these units is not discussed in this chapter. However, a suite of samples has been collected and in subsequent chapters the petrographic and compositional characteristics of these quartz latites are discussed and compared with quartz latites from the main study area.

2.2 GEOLOGICAL SETTING

2.2.1 Introduction

The Etendeka Formation volcanics form the uppermost unit of the Karoo succession in Namibia. They conformably overlie laterally impersistent deposits of the Karoo sedimentary sequence and frequently overstep the latter to lie

directly on pre-Karoo basement of both Pan-African (Damara) and mid-early Proterozoic age. The distribution of the Etendeka Formation outcrops and the rocks over which they lie is presented in a simplified geological map of north-western Namibia, Fig. 2.1.

2.2.2 Mid-Early Proterozoic Basement

Along the north-eastern edge of the Etendeka the volcanics lie on the pre-Damara basement rocks of the Kamanjab inlier. This inlier is of early Mokolian age (1.7 - 1.9 Ga) and consists of para- and ortho-gneisses and meta-sediments of the Huab Complex (Frets, 1969) and the overlying Khoabendus Group (SACS, 1980) which are intruded by the Fransfontein Granite suite dated at 1.8 ± 0.1 Ga (Burger *et al.*, 1976).

Further north, the Karoo and Damara sequences overlie a succession of metamorphosed volcanics and sediments of the Epupa crustal segment which are widely migmatised and altered to porphyroblastic gneiss. The Kunene Complex dated at *ca.* 2.1 Ga (De Caruallio, 1970 and Da Silva, 1973) gives a minimum age to the Epupa Complex which it intrudes.

2.2.3 Damara Sequence

The Damara succession underlying the Karoo sequence in north-western Namibia constitutes the northern or coastal arm of the Damara Orogen and is chiefly composed of schistose metasedimentary rocks.

Between the Etendeka and Gobobosebberge lava fields (Fig. 2.1) the Damara sequence is composed of a turbiditic succession of pelitic, psammitic and calcareous rocks of the Khomas Subgroup (Swakop Group). Regional metamorphism between Brandberg West and Doros is of low grade and does not exceed the biotite isograd (Ahrendt *et al.*, 1983). The succession is affected by at least two phases of deformation, the first resulting in north-south trending isoclinal folds, conspicuous on aerial photographs and Landsat imagery.

North of the Etendeka the Damara is divided into the western, central and eastern zones of the Kaoko belt (Miller, 1983). Medium to high grade eugeosynclinal schists of the Khomas and Ugab Subgroups in the western and central zones are thrust over the eastern zone along the Sesfontein Thrust (Fig. 2.1). The eastern zone consists of low grade mio-geosynclinal deposits of

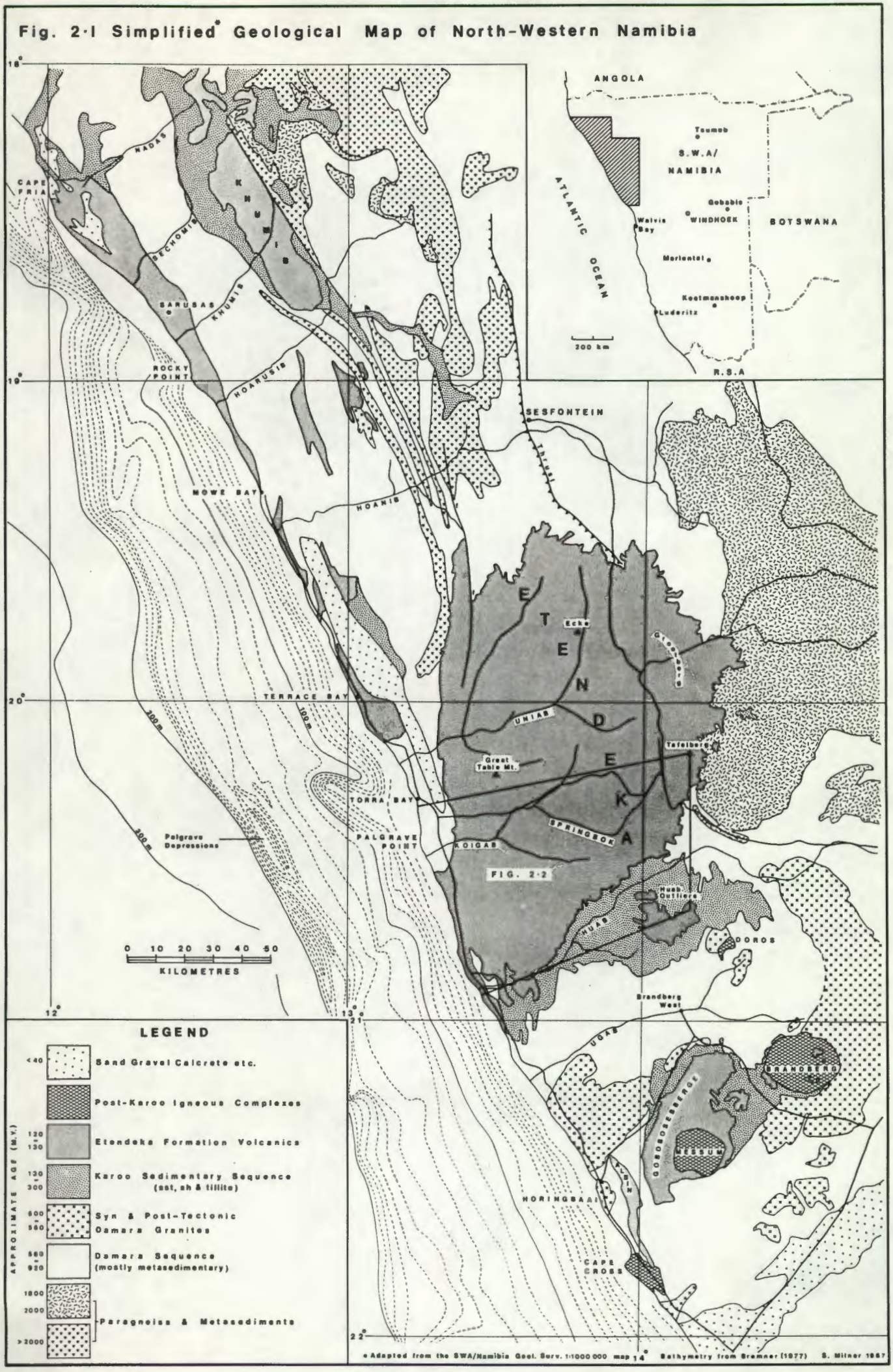
Fig. 2·1 Simplified* Geological Map of North-Western Namibia
ANGOLA
Tsumeb
S.W.A/
NAMIBIA
Gobabis
WINDHOEK
Walvis Bay
BOTSWANA
Mariental
Keetmanshoop
Lüderitz
ATLANTIC OCEAN
200 km
R.S.A
CAPE FRIA
NADAS
SECHOMIB
KHOMAS
SARUSAS
KHUMIS
ROCKY POINT
HOARUSIB
SESFONTEIN
HOANIB
MOWE BAY
TERRACE BAY
ETENDEKA
Echo
UMIAB
Great Table Mt.
TORRA BAY
PALGRAVE POINT
Palgrave Depressions
KOIGAB
SPRINGBOK
FIG. 2·2
Huab Outliers
HUAB
DOROS
Brandberg West
UGAB
BRANDBERG
GOBOBOSEBERGE
WESSUM
HORINGBAAI
CAPE CROSS
200 m
100 m
0 10 20 30 40 50
KILOMETRES
LEGEND
APPROXIMATE AGE (M.Y.)
<40 Sand Gravel Calcrete etc.
Post-Karoo Igneous Complexes
120 - 130 Etendeka Formation Volcanics
120 - 300 Karoo Sedimentary Sequence (sst, sh & tillite)
500 - 560 Syn & Post-Tectonic Damara Granites
560 - 920 Damara Sequence (mostly metasedimentary)
1800 2000 >2000 Paragneiss & Metasediments
* Adapted from the SWA/Namibia Geol. Surv. 1:1000 000 map
Bathymetry from Bremner (1977)
S. Milner 1987

the Tsumeb and Abenab Subgroups overlain by the exo-geosynclinal deposits of the Mulden Group (Ahrendt *et al.*, 1983). Schistose rocks of the Mulden Group also occur as a basement horst north of the Huab River mouth.

The Damara schists are intruded by syn- and post-tectonic granites and granodiorites which are dominantly calc-alkaline in character. These are well developed in the area south of Brandberg West (Fig. 2.1) where they underlie the Karoo succession of the Gobobosebberge. Scattered granitic intrusions also occur throughout the Kaoko belt.

2.2.4 Karoo Sedimentary Sequence

Sedimentary formations of the Karoo sequence in north-western Namibia (Fig. 2.1) are summarised in Table 2.1 (after SACS, 1980). Karoo sediments, which are Carboniferous-Jurassic in age, occur in the vicinity of, and along, present-day river valleys. Sedimentation was strongly influenced by the pre-Karoo topography, particularly east-west trending Dwyka-age glacial valleys which are currently being re-excavated by the Nadas, Sechomib, Hoarusib, Hoanib and Huab river courses (Martin, 1973; Fig. 2.1). Palaeocurrent directions in the Formations below the Etjo sandstones indicate that arenaceous material was deposited from many directions, and are consistent with deposition within the confines of valleys (Hodgson, 1970).

The sedimentary sequence outlined above is well developed in the Huab River region, particularly beneath outlying remnants of the main lava field in an area called the Huab Outliers (Fig. 2.1). However, the Dwyka Tillite is preserved only locally and the Prince Albert Formation usually forms the base of the Karoo succession in this area. Glacial and periglacial deposits of the Dwyka are better developed north of the Etendeka where they occur round the Khumib lava remnant (Fig. 2.1) and show local thickening in the Dwyka-age valleys.

The cumulative thickness of the Prince Albert and Gai-as Formations increases from approximately 130 m in the Doros region to around 340 m at the coast. The sedimentary succession is often incomplete and there are considerable variations in stratigraphic sequence and thickness. This is particularly apparent in the faulted region north of the Huab River mouth. Borehole cores and stratigraphic sections (Erlank *et al.*, 1984) have shown a more extensive stratigraphic sequence is often preserved or thickened in down faulted blocks. In adjacent horst structures however, certain stratigraphic

Table 2.1 Summary of the Karoo sedimentary sequence in northwestern Namibia.

Formation	Lithology	*Thickness
Etjo	Dune bedded, fine to medium grained, yellow–orange Aeolian sandstone.	125 m
Gai–as	Red–purple mudstone, shale, siltstone and subordinate sandstone.	50 m
Probeer	Upper– Massive grey limestone Lower– Varicoloured limestones with chert horizons	60 m
Prince Albert	Upper– Sandstone (Draaihoek Member) Middle– Interbedded white and black shales Lower– Carbonaceous shales	10 m 70 m
Dwyka	Tillite with quartz, schist and quartzite pebbles	Localised

Lithological detail from Hodgson (1970). *Thicknesses recorded just north of Doros.

units may be missing and marked variations in thicknesses of some of the Formations over short distances suggest that faulting occurred periodically both during and after sedimentation (Erlank *et al.*, 1984).

In the Doros-Huab River area the sedimentary Formations pinch out to the north and south, the aeolian Etjo sandstones over-stepping the lower Formations around the eastern margin of the Etendeka to lie directly on basement. The Etjo sandstones are well developed in the Huab Outliers area (Fig. 2.1) where they often form cliffs and display large scale, high-angle cross-bedding. Locally they are separated from the upper fluvial sandstones of the Gai-as Formation by a basal conglomerate up to 4 m thick (Frets, 1969). The conglomerate is composed of quartz and schist pebbles and Hodgson (1970) ascribes its presence to a strong inwash from the north, probably from the upland Huab massif which today forms part of the Kamanjab inlier. Interbedding of the Etjo sandstones with the volcanics is well developed in the Huab Outliers with lenses and bands of sandstone occurring as much as 130 m above the base of the lavas. Sandstones interbedded with basalt often take the form of "fossilised" dunes which have been flooded by the early basalt flows; a spectacular development of this occurs just south of Awahab (Fig. 2.2) where one such "dune" is 80 - 90 m high. Interbedding of the Etjo sandstone with the lavas also occurs 15 km north of Terrace Bay (Erlank *et al.*, 1984). North of the Huab River the sandstones thin and are themselves over-stepped by volcanics, although thin lenses of sandstone do occur locally beneath the lavas between the farm Vrede and the area just north of Tafelberg, where basalts rest on basement.

2.2.5 Etendeka Formation

The Etendeka Formation consists of basic to intermediate lavas of a tholeiitic series interbedded with more acid quartz latite units and some minor latite. Basaltic dykes and sills are associated with the Formation and dense dyke swarms are observed cutting Damara granites south-west of the Ugab River mouth (Erlank *et al.*, 1984). A large dolerite sill intruded between the basement and overlying Karoo sediments is developed along the Huab River between the river mouth and the Huab outliers, where it reaches an estimated thickness of 200 m. Remnants of the Etendeka Formation lavas are scattered over 78,000 km^2 of north-western Namibia (Erlank *et al.*, 1984) and must once have formed part of extensive flood lava fields. The main outcrop remnants occur between Cape Cross and Cape Fria (Fig. 2.1) with the main lava field

covering some 12,000 km^2 and reaching an observed maximum thickness of 880 m at Tafelberg in the east. The original maximum stratigraphic thickness of volcanics is unknown, although it is thought to have exceeded 2 km (Reuning and Martin, 1957). In most areas the volcanics are sub-horizontal at outcrop and the name "Etendeka", which is derived from the Ovahimba word meaning a place of flat topped hills, describes the classic trap morphology of the lavas (Plate 2.1) and the impressive flat topped mountains which occur along the eastern margin of the main lava field. Along the coast between Albin and Cape Fria (Fig. 2.1) the lavas generally dip between 5° and 30° ENE in a belt of coast-parallel faulting that extends up to 30 km inland.

The Etendeka Formation (proposed by Hodgson, 1970) has its type locality (SACS, 1980) in the Tafelberg region on the eastern edge of the main lava field (Fig. 2.1). While the stratigraphy in this area is representative of a fairly large proportion of the northern Etendeka, that of the Etendeka Formation as a whole varies considerably from one outcrop remnant to another. To facilitate discussion of the volcanics, geographical names have been assigned to the principal lava remnants (Fig. 2.1), the chief characteristics of which are outlined below.

2.2.5.1 The Etendeka and the Huab Outliers

Detailed mapping of the southern part of the Etendeka and the Huab outliers (an area simply referred to as the southern Etendeka; Figs. 2.1 & 2.2) has revealed differences in quartz latite stratigraphy which have led to the identification of two lava sequences, the Springbok and Tafelberg successions (see section 2.3 and 2.5). With the aid of geochemical studies (Milner and Duncan, 1987) the Tafelberg lavas can be correlated with a thick succession of quartz latites in the faulted coastal region (Interbedded Coastal quartz latites). Note that the basaltic lavas of the Etendeka are predominantly aphyric and are referred to as the Tafelberg-type basalts by Erlank *et al.* (1984).

2.2.5.2 The Gobobosebberge Remnant

The lavas of the Gobobosebberge reach a maximum thickness of 350 m and are intruded by the Messum sub-volcanic complex (Korn and Martin, 1954). Little is known of the stratigraphy of this area, although reconnaissance sampling has indicated the existence of an interbedded basalt and quartz latite sequence with the quartz latites being petrographically and geochemically similar to those of

PLATE 2.1

Flat-lying trap-like volcanics of the Etendeka Formation. View looking north-west from the Huab Outliers across the Huab River (middle distance) to the main Etendeka lava field beyond.

the Springbok succession further north.

2.2.5.3 Albin Remnant

The Albin section consists of a tilted sequence of predominantly plagioclase-phyric basalts (the Albin-type basalts of Erlank *et al.*, 1984) approximately 200 m thick. These lavas conformably overlie Etjo sandstones and are interbedded with aphyric Tafelberg-type basalts in the upper part of the section. A porphyritic quartz latite forms the uppermost unit of the sequence and also shows similarities in petrography and geochemistry to the Springbok quartz latites.

2.2.5.4 Khumib Remnant

The Khumib remnant consists of flat-lying basalts approximately 750 m thick which conformably overlie Karoo sediments and which are down-faulted against early Proterozoic basement in the east (Fig. 2.1). These basalts are generally aphyric to sparsely phyric and are characterised by chemical compositions that are "enriched" in TiO_2, P_2O_5 and large ion lithophile elements relative to "normal" Tafelberg-type basalts. Some interbedding between "normal" and "enriched" basalts occurs in the upper portion of the succession. No quartz latite is observed in this section. The "enriched" lavas are referred to as the Khumib-type basalts and are currently being studied as part of a collaborative investigation in this Department.

2.2.5.5 Sarusas Remnant

Reconnaissance sampling carried out between the Hoarusib River and Cape Fria indicates that most of the ridges parallel to the coast south of the Sechomib River consist of quartz latite units which dip between 5° and 10° NE. A traverse across the sequence at Sarusas mine (Fig. 2.1) has revealed the presence of at least six quartz latite units, although it is not clear whether some of these have been repeated by faulting. North of the Sechomib River both quartz latite and basalt (predominantly "Khumib-type") are encountered. Faulting in this coastal region makes the stratigraphic relationships between the quartz latites and the basalts unclear, and it is not known whether the quartz latites are interbedded with basalt or whether they form a separate succession of units. The thickness of the volcanic succession in this area is unknown. The quartz latites from this region are geochemically and petrographically distinct from the quartz latites of the southern Etendeka and

are referred to as the Sarusas quartz latites in this work.

2.2.5.6 Summary

The terminology used in this work can be summarised as follows. The main Karoo lava field in north-western Namibia is referred to as the **Etendeka**, the southern portion of which, the **southern Etendeka** (the area covered by Fig. 2.2, see Fig. 2.1) is composed of the **Springbok** and **Tafelberg successions**. Lavas of the Tafelberg succession cover a substantial portion of the northern part of the main Etendeka lava field and some of the units can be correlated with the **Interbedded Coastal quartz latites** in the coastal region. Note that the **Tafelberg-type** basalt of Erlank *et al.* (1984) includes basaltic lavas from both the Tafelberg and Springbok successions. Quartz latites of the **Gobobosebberge** and **Albin** remnants show some compositional and petrographic similarity to the Springbok quartz latites. North of the Etendeka the **Khumib** outcrop is the type area for the "enriched" **Khumib-type** basalts and the **Sarusas** remnant is the type area for the **Sarusas quartz latites**.

As more information on the Etendeka Formation becomes available it may be possible to formalise a more detailed stratigraphic terminology for these lavas, although at present there is insufficient data to do so. On the basis of current observation the author suggests that it may be desirable to promote the Etendeka Formation to Group status and use terms such as Springbok, Tafelberg and Khumib as Formation names, with prominent quartz latite units as Members.

2.3 MAPPING

The results of geological mapping in the southern Etendeka are presented in Figs. 2.2 and 2.3a.

Fig. 2.2 covers approximately 5,100 km^2 (about one third) of the Etendeka lava field between the Skeleton Coast Park and western Damaraland, and its primary function is to show the distribution of quartz latite in this area. Details of this map have been incorporated into a 1:250,000 scale map of the Cape Cross region (Geological Survey of SWA/Namibia, 1988) and these maps are the most comprehensive of the Etendeka currently available. In Fig. 2.2 the limits of the basement have been indicated in accordance with Geological Survey

LEGEND

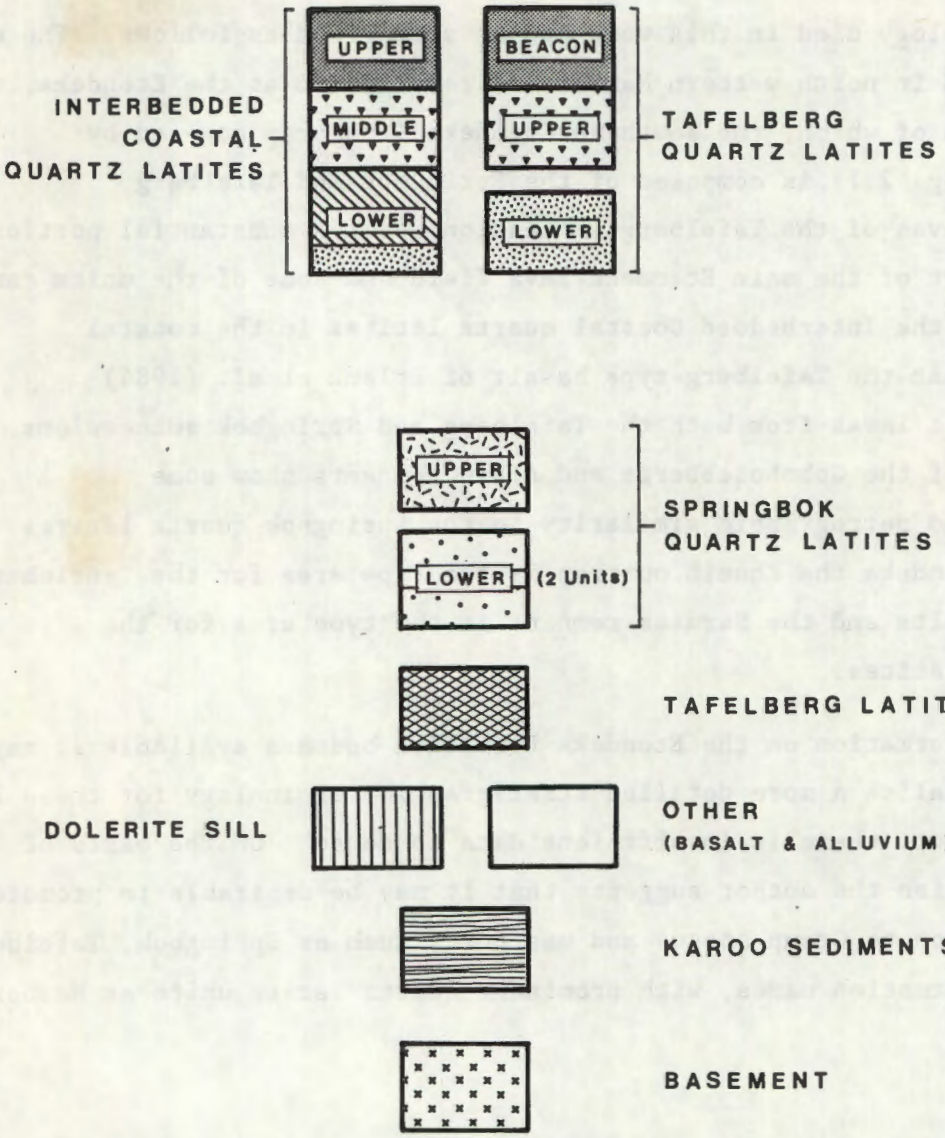
INTERBEDDED COASTAL QUARTZ LATITES
UPPER
MIDDLE
LOWER
BEACON
UPPER
LOWER
TAFELBERG QUARTZ LATITES
UPPER
LOWER
(2 Units)
SPRINGBOK QUARTZ LATITES
TAFELBERG LATITE
DOLERITE SILL
OTHER
(BASALT & ALLUVIUM)
KAROO SEDIMENTS
BASEMENT
FAULT
30
DIPS
SALT PAN

Fig. 2·2 Geological map of the southern Etendeka Volcanics.

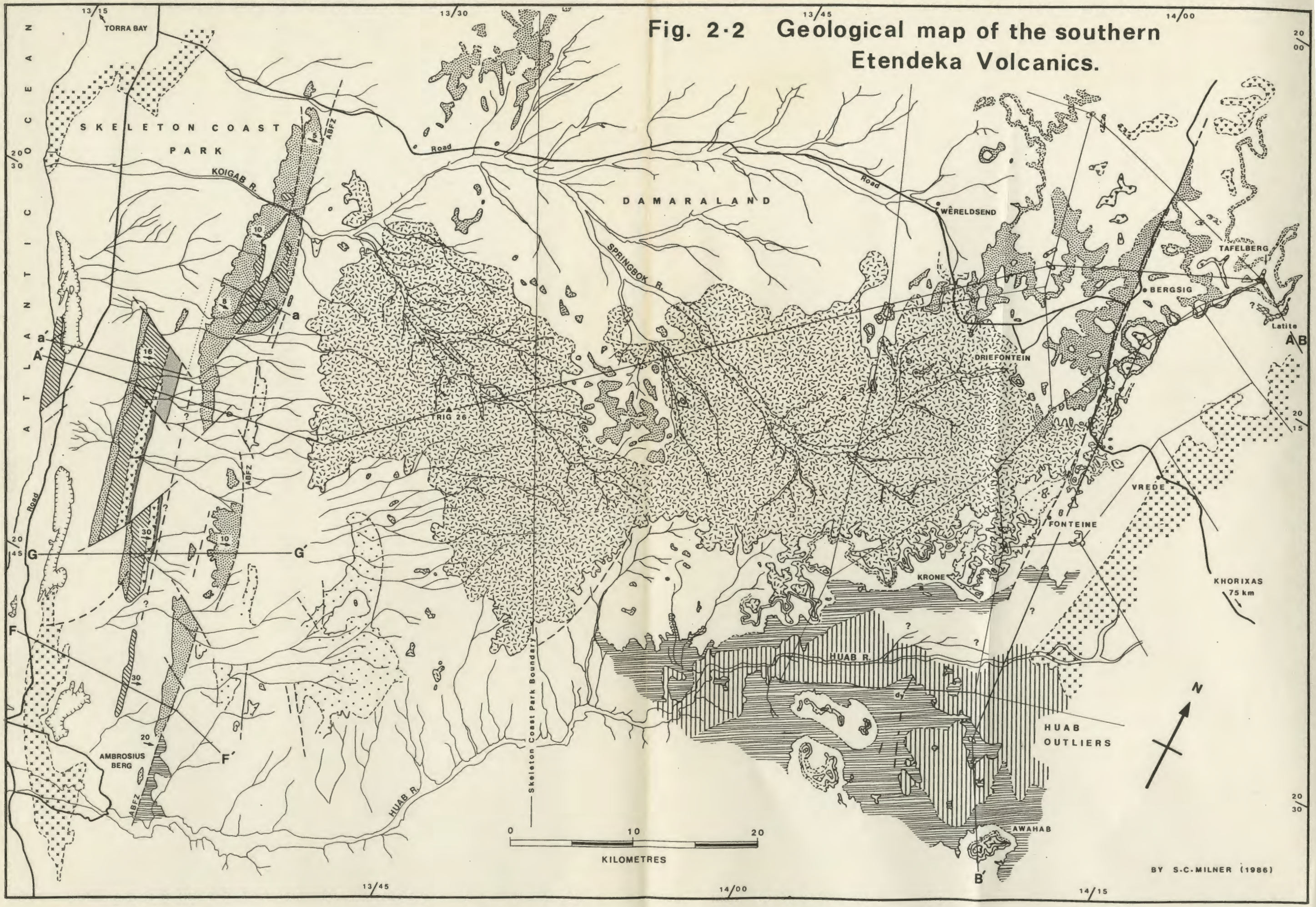

Fig. 2·3a

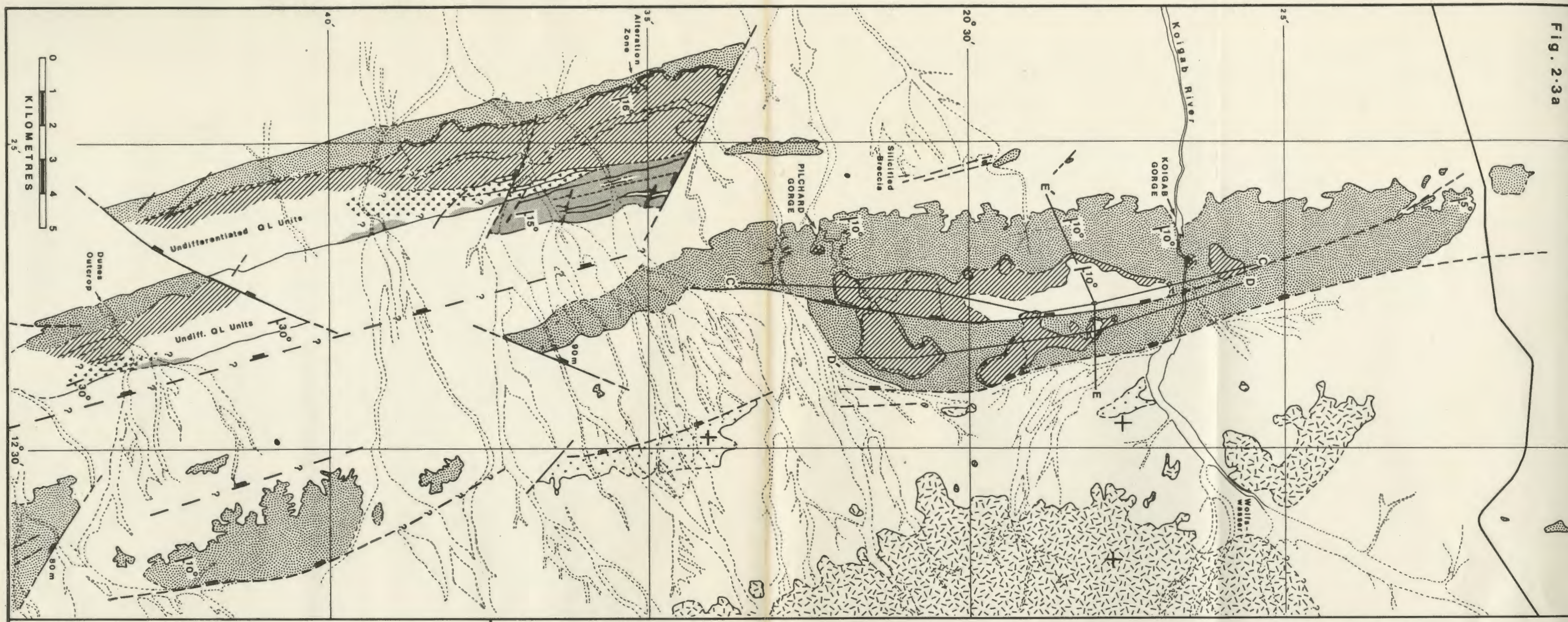

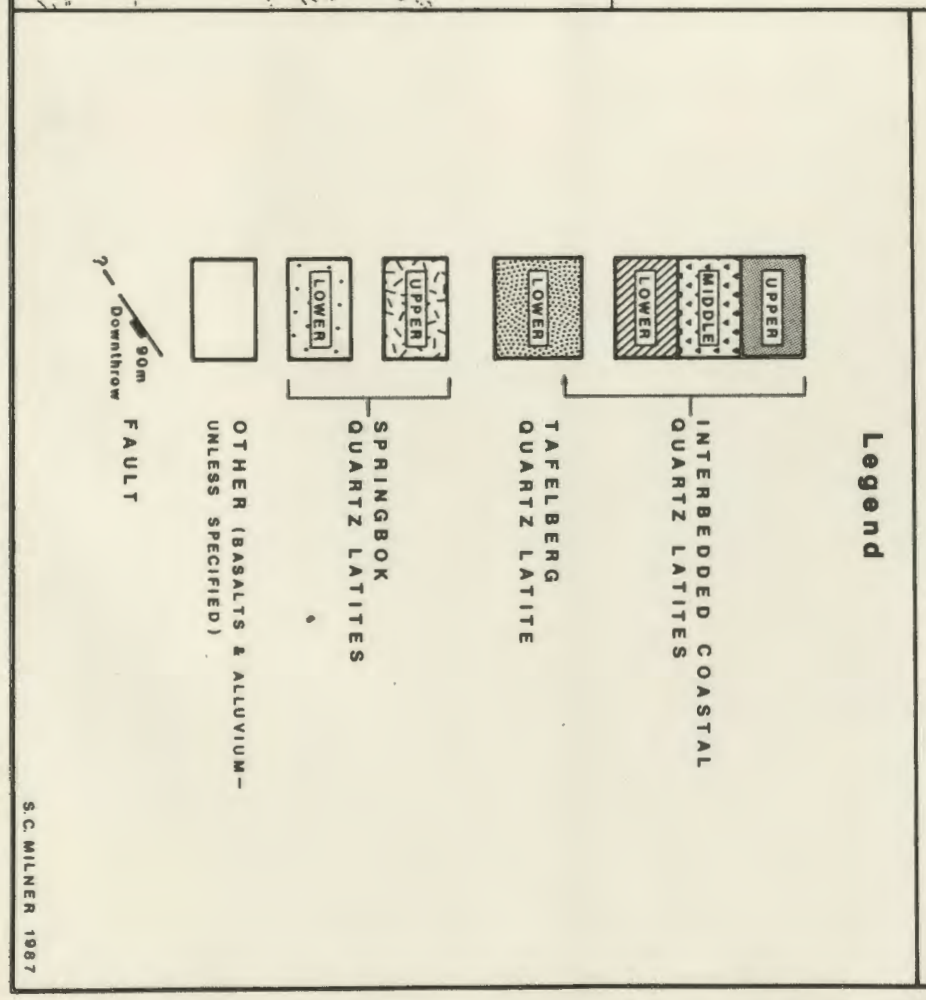

Fig. 2·3b

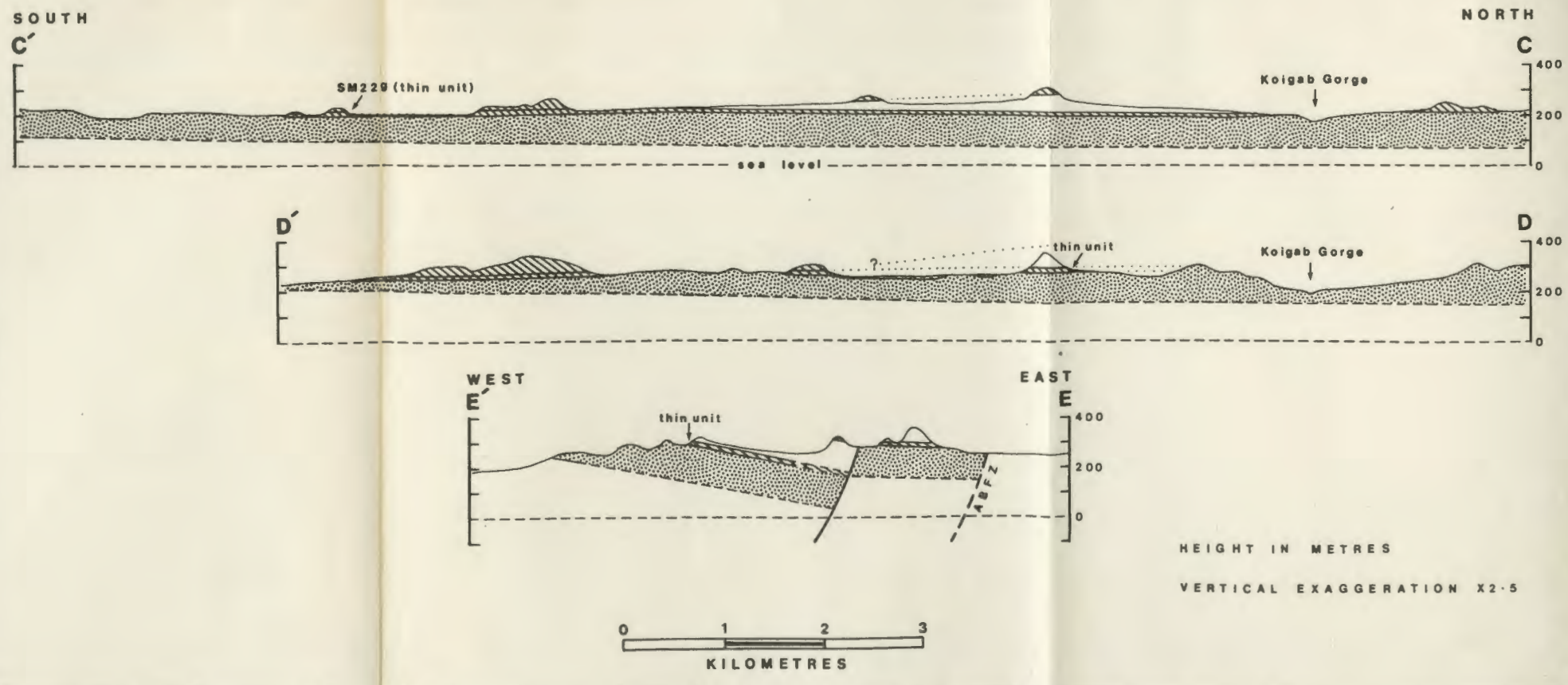

findings (*op cit*) and Frets (1969). Details of the strongly faulted area north of the Huab River mouth are given in Figure 2 of Erlank *et al.* (1984), and are not repeated here. The legend in Fig. 2.2 depicts the stratigraphy of the quartz latites across this area, of particular note is the stratigraphic equivalence of some of the Interbedded Coastal quartz latites with those of the Tafelberg sequence.

Fig. 2.3a is a larger scale presentation of the quartz latite outcrop near the coast and shows individual quartz latite units in more detail. Also indicated are localities of particular interest described in the text. Areas of "undifferentiated" quartz latite outcrop are the result of gentle relief and superficial cover (sand and scree) which make the contacts between the quartz latite units difficult to define.

The maps were constructed from field information gathered on 1:75,000 scale aerial photographs (1:50,000 in the Huab Outlier region) and transferred to 1:50,000 and 1:250,000 topographic maps (Director General of Surveys, Pretoria).

2.4 STRUCTURE

2.4.1 Introduction

The area covered by Fig. 2.2 is divided into two structural regions by the Ambrosius Berg Fault Zone (ABFZ). This zone of faulting can be traced for more than 60 km north of Ambrosius Berg and constitutes a major structural break (see also Figs. 2.4 and 2.5). East of the ABFZ the succession is characterised by predominantly flat-lying units (Plate 2.1) with a slight westerly dip of the order of 0.5° or less. West of the ABFZ, a coastal zone approximately 20 km wide is dominated by faults parallel to the coast which have tilted the volcanics between 5° and 30° east (Fig. 2.3).

Syn-volcanic erosion of the lavas and the pre-existing topography play an important role in the structure of the lava pile, affecting the outcrop pattern and the spatial distribution of the volcanics.

Cross-sections through the Etendeka Formation are presented in Fig. 2.4 and the section lines A-A′ (also a-a′) and B-B′ are indicated on Fig. 2.2. In Fig. 2.3b more detailed cross-sections (C-C′, D-D′ and E-E′) are used to illustrate the effects of palaeotopography encountered in the area south of the

Fig. 2·4a East-West Section Across The Southern Etendeka.

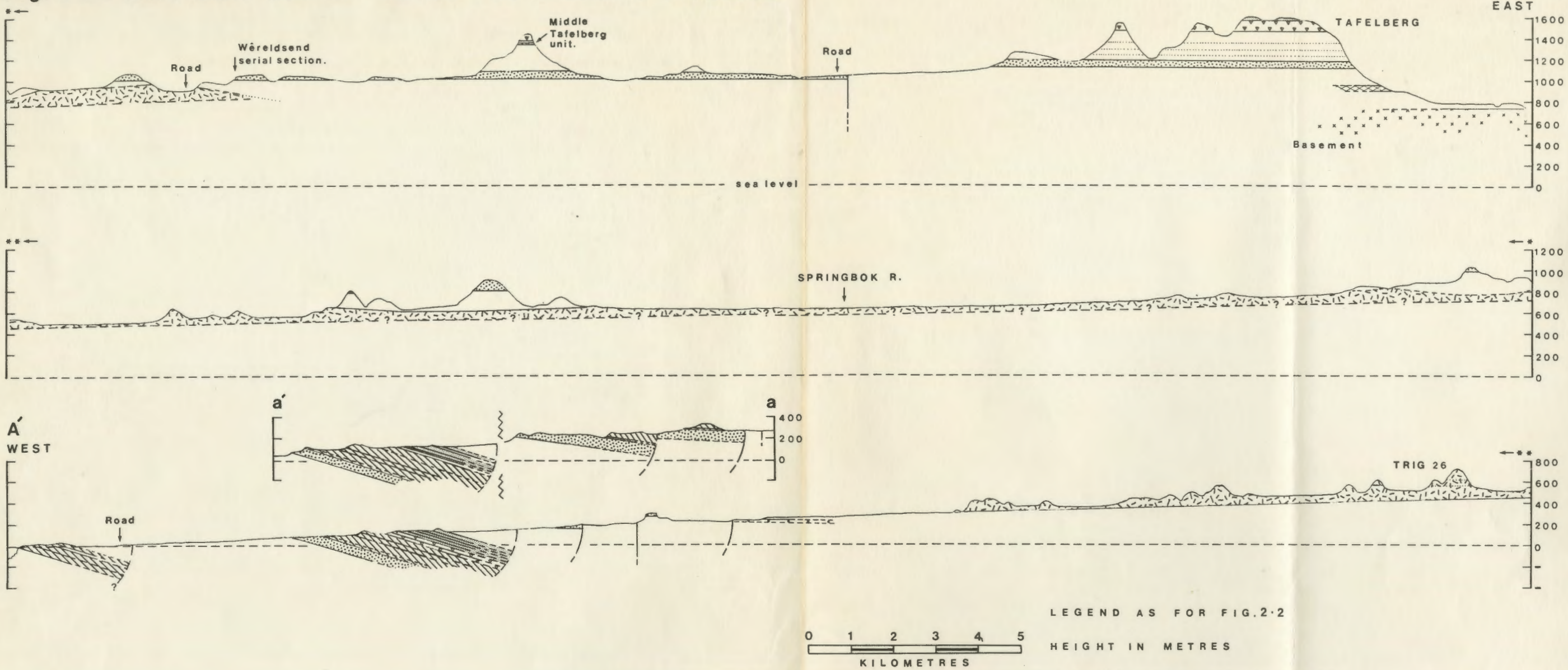

Fig. 2·4b North-South Section Across The Southern Etendeka.

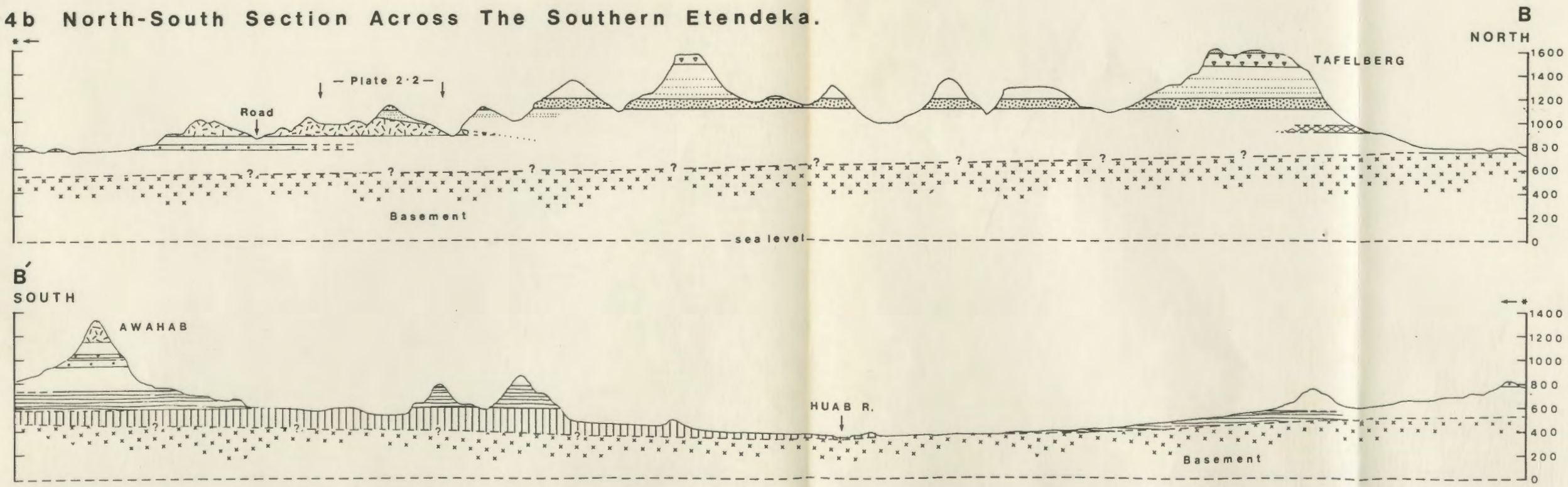

Fig. 2.5 Sections* Across the Basement Horst Structure North of the Huab River Mouth.

* Reproduced from the SWA/Namibia Geological Survey 1:250 000 Cape Cross Sheet (1988). Geological Interpretation by R. McG. Miller.

Legend as for Fig. 2.2. Height in Metres.

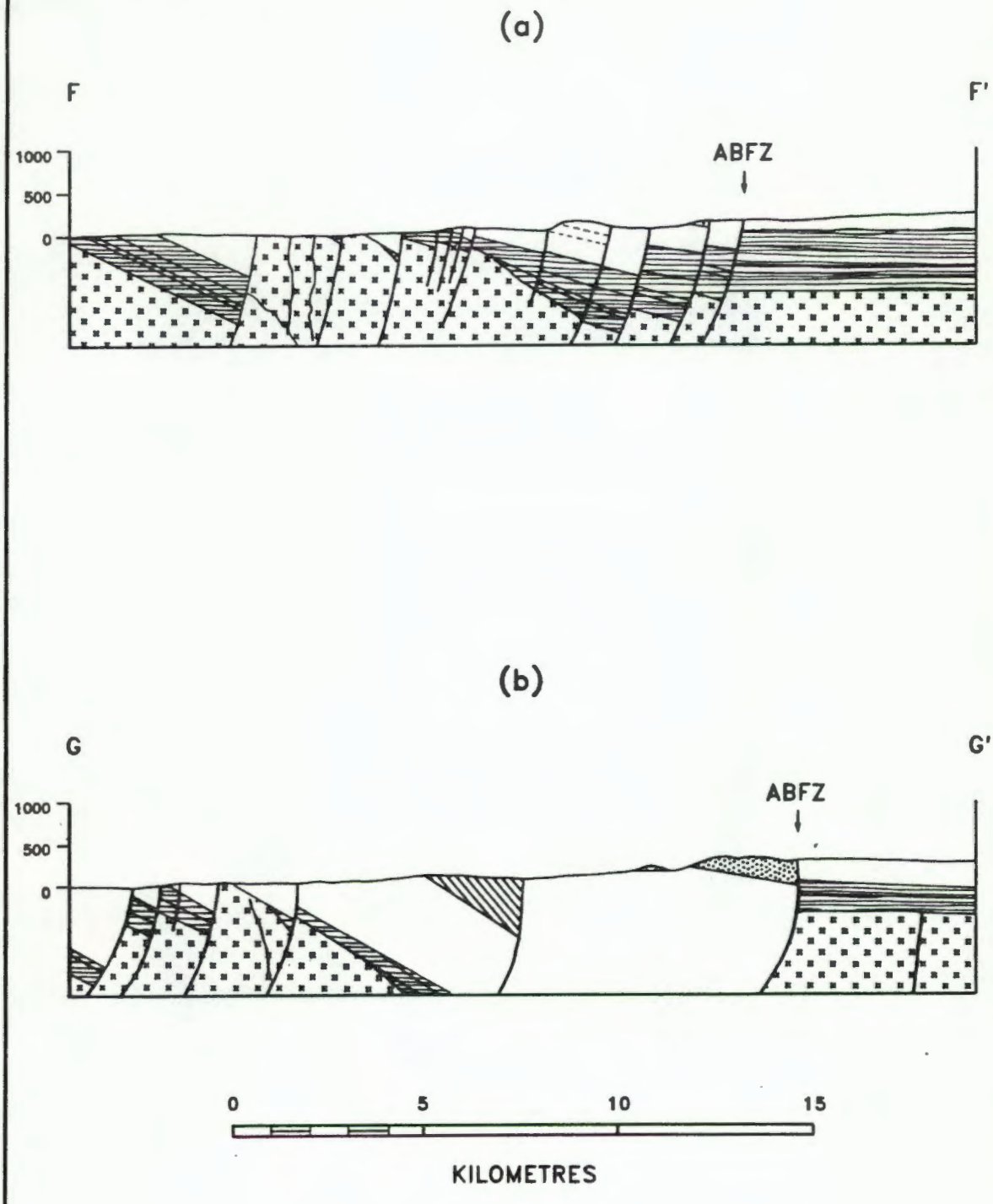

Koigab Gorge (Fig. 2.3a). An interpretation of the geological structure of the faulted coastal region by Miller (1988) is reproduced in Fig. 2.5 (section lines F-F' and G-G', Fig. 2.2) to indicate the nature of the basement horst structure north of the Huab River mouth.

2.4.2 Faulting

Detailed discussion of the nature, effects and timing of faulting in the southern Etendeka, particularly west of the ABFZ, is not possible on the strength of field observation alone. Although the outcrop distribution and geomorphology of the coastal area is dominated by faulting (Fig. 2.3) the fault planes are often obscured by alluvial or scree material in areas of low relief, and are thus rarely observed. Faults are occasionally indicated by trails of calcite or silicified breccia on the desert surface. In the Koigab Gorge a north-south trending "vein" of calcite, with a variable thickness (maximum 30 - 40 cm), appears coincident with a north-south trending fault traced to the gorge at this point (Fig. 2.3). Occurrences of silicified breccia are rare, although patches with quartz and calcite in a zone about 10 m wide and 50 - 60 m long occur in an area having several small faults (see Fig. 2.3a for location). In some instances faults may be inferred from abrupt changes in the amount or direction of dip of the volcanics. Note that an accurate measurement of the angle of dip in the volcanic section is generally not possible due to the absence of base-parallel reference planes and poorly exposed contact relationships.

Few faults occur east of the ABFZ. The north-south trending Bergsig Fault runs parallel to the road north and south of Bergsig lowering the volcanic sequence approximately 100 m to the west (see Figs. 2.2 and 2.4a). Landsat images of the Etendeka show N-S trending linear features to the west of the Bergsig Fault which extend from the north and die out as they reach the Upper Springbok quartz latite sheet. Some of these lineations are indicated as faults on the Geological Survey 1:1,000,000 scale map, but to the authors knowledge these have not been substantiated by field studies.

West of the ABFZ two different styles of faulting are evident and can be briefly outlined as follows:

(1) North-south trending faults are believed to have developed as a response to tectonic extension during continental break-up. Differential rotation of the volcanic units in successive fault blocks to the west of the ABFZ is indicated by an overall increase in easterly dip in that direction, suggesting that the faults bounding these blocks are listric rather than planar in character (Wernicke and Burchfiel, 1982). The difficulty in making accurate dip measurements and the lack of information on fault geometry (fault angle, curvature etc..) make an estimate of the amount of crustal extension across the area difficult. However, the low dip angles on the strata, generally less than 20° E, indicate that extension was less than 15 % (Wernicke and Burchfiel, 1982).

(2) Conjugate sets of SSW and SE trending, normal faults cut across the strike of the volcanics (Figs. 2.2 and 2.3). The most conspicuous of these cut the Interbedded Coastal quartz latite block, the southerly fault having a down-throw of approximately 90 m to the NW. Bremner (1977) suggests that the unusual shoal which extends for up to 40 km north-west of Palgrave Point (Fig. 2.1) originated through basement faulting. It is interesting to note that the trace of the fault which cuts the northern end of the Interbedded Coastal quartz latite block (Fig. 2.2) coincides with the south-western side of this shoal and with the southern outcrop limit of basement near the Koigab River mouth. Likewise, the trace of the fault bounding the southern end of the Interbedded Coastal quartz latite block coincides with the northern end of the basement horst structure north of the Huab River mouth (Fig. 2.2), and it seems likely that these faults have rejuvenated old basement structures.

Most of the faulting which affects the southern Etendeka is probably post-volcanic, although some syn-volcanic fault movements may also have occurred in the period between the eruption of the Upper Springbok quartz latite and the Lower Tafelberg quartz latite. This is suggested by the absence of the Springbok succession quartz latites in any section west of the ABFZ.

The development of listric faults appears to post-date, and be partially controlled by, the normal faults. This is clearly demonstrated at the northern end of the Interbedded Coastal quartz latite sequence where the affect of an obscured listric fault (Fig. 2.3a), which tilts the quartz latites 15 - 16° E, is not observed north of the normal fault which truncates the outcrop.

2.4.3 Palaeo-Topography

2.4.3.1 Pre-Karoo Topography

As indicated in the subsection on the Karoo sedimentary sequence (2.2.4) sedimentation was strongly influenced by Dwyka-age glacial valleys and by a block-faulted graben system in the coastal region.

Fig. 2.4b shows the palaeo-Huab valley indicated by a gentle dip of the basement-cover rock contact towards the present Huab River, and by a thickening of the Karoo sediments and lavas. The combined thickness of the Karoo sediments and the Springbok succession lavas beneath the Upper Springbok quartz latite at Awahab is approximately 560 m (excluding dolerite) which can be compared with about 300 m at a point 20 km north of the Huab River where the sediments have wedged out and the volcanics thinned.

In the strongly faulted coastal region the interpretation of the stratigraphy and structure with respect to palaeo-topography is more difficult. The deposition of both sediments and lavas appears to have been affected by a basement horst structure (Fig. 2.5) north of the Huab River mouth. This structure, which diminishes northward (compare Figs. 2.5a and b), almost certainly acted as a topographic barrier during volcanism and may be responsible for the abrupt thinning of the Interbedded Coastal quartz latite sequence with which it is juxtaposed (Fig. 2.2).

2.4.3.2 Intra-Volcanic Relief

The Tafelberg succession transgressively overlies the Upper Springbok quartz latite from the north (Fig. 2.4 and Plate 2.2) indicating that considerable intra-volcanic relief existed during the eruption of the Etendeka lava pile, with the Upper Springbok quartz latite forming a significant topographic barrier to the spread of the lower part of the Tafelberg succession. The absence of flow top features (Section 2.6), at the contact with the overlying basalts or of any indication of distal thinning, suggests that the abrupt termination of the Upper Springbok unit is not a primary eruptive feature. The available evidence suggests that this quartz latite unit was truncated by erosion prior to the eruption of the Tafelberg Succession. The contact between the Upper Springbok quartz latite and the overlying Tafelberg units is often irregular with local variations of between 40 - 50 m elevation. Between the Springbok River and Trig 26 (Fig. 2.2) a lobe of the Tafelberg lavas appears to fill a NW trending palaeo-valley in the Upper Springbok quartz

PLATE 2.2

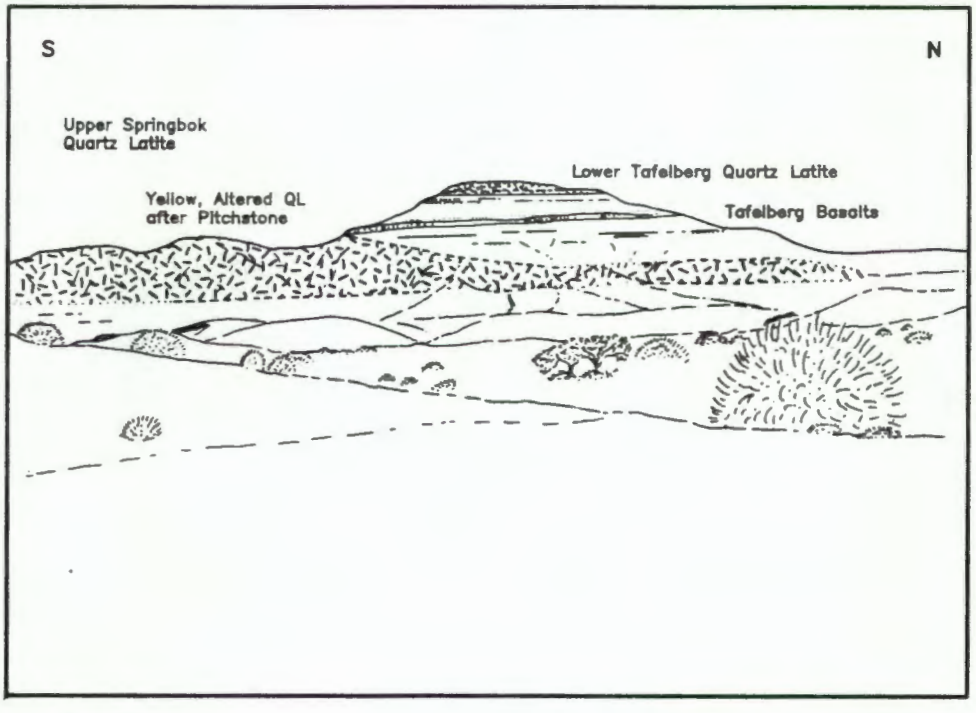

Flat-lying units of the Tafelberg Sucession transgress the Upper Springbok quartz latite from the north demonstrating the unconformity between the two successions. The height from the base of the hill to the top is approximately 350 m. See Fig. 2.4b for the exact locality.

latite, with the quartz latite at Trig 26 forming the high ground to the west of this valley (Fig. 2.4a). In the area west of Fonteine (Fig. 2.2) the Upper Springbok quartz latite shows its thickest development (295 m) and is unconformably overlain by basalts of the Tafelberg succession, which have a stratigraphic level some 40 m above the Lower Tafelberg quartz latite. At its upper contact the Upper Springbok unit consists of a massive, sparsely vesicular, variably altered quartz latite which has an irregular uneven surface with depressions up to 15 m deep and 30 m wide filled with basalt. Angular clasts of non-vesicular quartz latite, 0.1 - 10 cm in diameter, are observed filling cracks in the quartz latite near the contact zone, and appear to be colluvial in origin. Also of interest in this area are two small outcrops of Lower Tafelberg quartz latite, between the farms Krone and Fonteine (Fig. 2.2), which lie in topographic hollows within the Upper Springbok quartz latite.

The evidence for intra-formational erosion is supported by the occurrence of Dwyka deposits north-east of Tafelberg (Fig. 2.1) which indicate the presence of an east-west trending palaeo-valley at this latitude (Martin, 1973; Figure 4). This intra-volcanic relief almost certainly indicates a considerable hiatus in volcanic activity between the eruption of the Springbok and Tafelberg successions. North of the Upper Springbok unit the effects of palaeo-relief at the base of the Tafelberg Succession appear to have been rapidly eliminated, with successive lava flows being erupted onto an essentially flat lying topography, yielding the classic trap morphology of the Tafelberg region.

Less dramatic palaeo-relief has been recognised in the area west of the ABFZ. Fig. 2.3b illustrates cross-sections of the geology in the area south of the Koigab Gorge (Fig. 2.3a). The Lower Tafelberg quartz latite has an uneven erosional top (no flow top features observed) overlain in places by the Gemini quartz latite, a thin (10 - 15 m) poorly welded unit (see section 2.5 for detail), which often appears to fill hollows. Just south of the Koigab Gorge this unit is overlain by up to 60 m of basalt, comprising three flows. The basalt thins rapidly to the south and is transgressively overlain by a sparsely porphyritic quartz latite which directly overlies the Gemini quartz latite unit at the SM-229 locality (Fig. 2.3b). It is likely that palaeo-relief of a similar magnitude may affect the quartz latite units of the Interbedded Coastal sequence contributing to the difficulties encountered during the mapping of this area.

Small depressions, filled by quartz latite of the overlying unit, are frequently encountered in the Lower Tafelberg quartz latite west of the ABFZ. Notable examples occur in the Koigab Gorge, Pilchard Gorge and at the northern end of the Interbedded Coastal sequence (Fig. 2.3a). The occurrence of these depressions appears to be associated with zones of alteration and volatile fluxing which are described in more detail in section 2.8. Plate 2.3 illustrates the Koigab Gorge occurrence; the upper 6 - 7 m of the section consists of a sparsely porphyritic pitchstone which has an irregular undulose contact with a rather altered deposit consisting of a pumice-like breccia and some pitchstone. The relationship between this deposit and the Lower Tafelberg quartz latite is unclear, although it is probably the equivalent of the Gemini unit encountered south of the gorge.

2.4.4 Effect of Intrusion on Structure

The only notable example of displacement of the volcanics by intrusion occurs in the Huab Outliers where the elevation of the base of the Upper Springbok quartz latite is 270 m greater than that observed just north of the Huab River (Fig. 2.4b). Although some of this difference may be due to slight northward dip of the Springbok Succession towards the Huab River, much of it can apparently be attributed to the injection of a thick (up to 130 m) dolerite sill beneath the lavas on the southern side of the Huab River valley. The sill has its maximum thickness (A.R. Duncan, pers. comm., 1988) centered about a point approximately 5 km north-west of Awahab (Fig. 2.2). The upper and lower contacts of the sill are highly irregular. In the Huab River valley the sill intrudes mainly along the Karoo sediment-basement interface, but towards the centre of the structure the dolerite intrudes up into the Etjo sandstones and further east is intruded entirely into basement.

2.5 STRATIGRAPHY OF QUARTZ LATITES

2.5.1 Introduction

Erlank *et al.* (1984) demonstrated that the earlier literary accounts of the Etendeka lavas (Reuning, 1929; Korn and Martin, 1954; Martin *et al.*, 1960; and Siedner and Miller, 1968) are imprecise and conflicting with regard to the stratigraphy of the Etendeka region. Erlank *et al.* (1984) showed that

PLATE 2.3

An illustration showing two quartz latite units which fill a topographic hollow in the Lower Tafelberg quartz latite unit in the Koigab Gorge. The contact between the two units is an irregular feature which occurs between 3 and 5 m above the river bed. The upper unit is hypersthene/plagioclase phyric (SM-180) and consists predominantly of pitchstone, and is easily distinguished from the sparsely plagioclase phyric Lower Tafelberg quartz latite. The lower unit consists of sparsely plagioclase phyric pitchstone (bottom left) and strongly altered clastic material with some pumice blocks (bottom right). The relationship between this unit and the Lower Tafelberg quartz latite is uncertain.

the lava succession at Tafelberg consisted of basalt interbedded with quartz latite (two units) and a single latite unit, and also indicated the presence of a thick sequence of easterly dipping quartz latites near the coast, south of Torra Bay. A more detailed account of the Etendeka Formation stratigraphy is presented here with particular emphasis on the nature of individual quartz latite units. The term "unit" is used here to describe individual quartz latite occurrences in any particular section, as their overall massive nature at outcrop often precludes the use of more precise terminology such as flow unit, cooling unit or compound cooling unit terms defined by Fisher and Schmincke (1984). An "ideal" section through a quartz latite unit consists of basal, main and upper zones. The basal and upper zones are characterised by features such as flow banding, pitchstone lenses and breccias and the main zone of the unit normally consists of massive devitrified quartz latite with little textural variability. A more detailed treatment of the quartz latite unit structure is presented in Section 2.6.

2.5.2 Springbok Succession

2.5.2.1 Introduction

The Springbok succession lavas are the earliest lavas erupted in the southern Etendeka and crop out over an area covering approximately 3200 km^2, between the Springbok River and the Huab Outliers (Fig. 2.2). Thickest development of the succession is observed in the Huab Outlier region where it reaches a maximum of 560 m at Awahab (Plate 2.4). Here the succession comprises basalts interbedded with three porphyritic quartz latite units which constitute approximately 50 % of the section. The volcanics overlie sandstones of the Etjo Formation and interbedding, of the sandstones with basalts in the lower portion of the succession is shown in Plate 2.5. A more detailed representation of the stratigraphy at Awahab is presented in Fig. 2.6.

2.5.2.2 Lower Springbok Quartz Latites

The two lower quartz latite units in the Springbok succession are collectively termed the Lower Springbok quartz latites as they have a close stratigraphic association (Fig. 2.6) and appear very similar in outcrop and hand-specimen. At Awahab these units form two prominent cliffs half way up the section (Plate 2.4), with the base of the lower unit approximately 160 m above the base of the Formation. Both units have well developed basal and flow top

PLATE 2.4

The Springbok Succession at Awahab (right). The mountains are capped by the Upper Springbok quartz latite and the two lowest bench formers on the mountain to the left are the Lower Springbok quartz latites. The hills in the middle distance are composed of Karoo sediments which overlie Damara rocks of the foreground.

PLATE 2.5

The lower portion of the Springbok Succession (130 m) is characterised by friable, altered basalts interbedded with bands and lenses of sandstone. This then gives way to more massive volcanics. The first major cliff former is the lowest of the Lower Springbok quartz latites, notice its planar contact with the underlying basalt. View from Awahab looking south, Brandberg is visible in the far (60 km) distance.

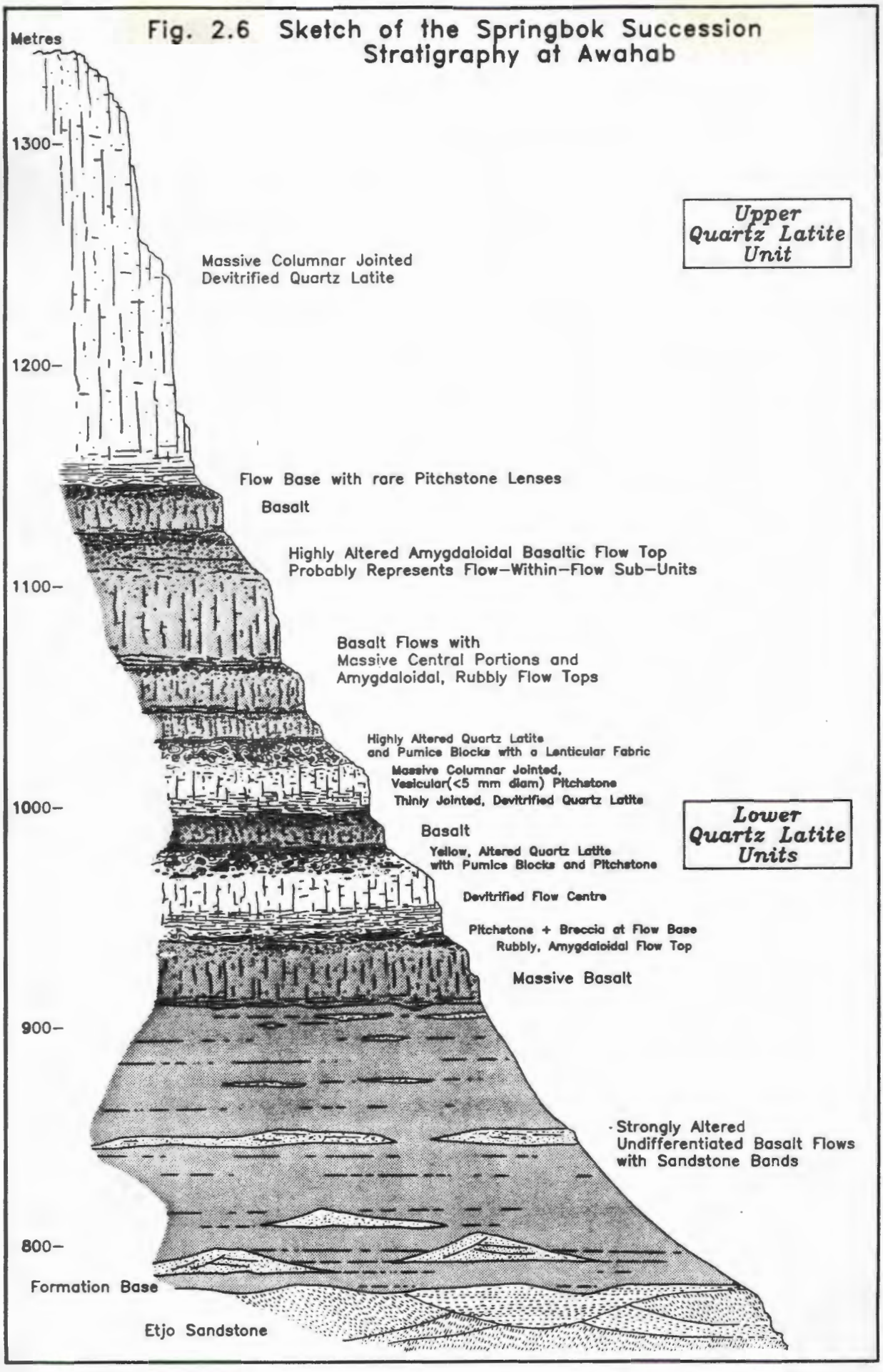
Fig. 2.6 Sketch of the Springbok Succession
Stratigraphy at Awahab
Metres
1300–
1200–
1100–
1000–
900–
800–
Upper
Quartz Latite
Unit
Massive Columnar Jointed
Devitrified Quartz Latite
Flow Base with rare Pitchstone Lenses
Basalt
Highly Altered Amygdaloidal Basaltic Flow Top
Probably Represents Flow–Within–Flow Sub–Units
Basalt Flows with
Massive Central Portions and
Amygdaloidal, Rubbly Flow Tops
Highly Altered Quartz Latite
and Pumice Blocks with a Lenticular Fabric
Massive Columnar Jointed,
Vesicular(<5 mm diam) Pitchstone
Thinly Jointed, Devitrified Quartz Latite
Basalt
Yellow, Altered Quartz Latite
with Pumice Blocks and Pitchstone
Devitrified Flow Centre
Pitchstone + Breccia at Flow Base
Rubbly, Amygdaloidal Flow Top
Massive Basalt
Lower
Quartz Latite
Units
Strongly Altered
Undifferentiated Basalt Flows
with Sandstone Bands
Formation Base
Etjo Sandstone

facies and planar flow contacts (Plate 2.5). The Lower Springbok quartz latites can be traced for up to 35 km between Awahab and the farms Fonteine and Krone. The lower of the two units maintains a fairly uniform thickness of 40 - 45 m over this distance, while the upper unit shows signs of a gradual thinning from 35 m at Awahab to 25 - 30 m just south of Fonteine. The basalt unit separating the two units also thins slightly towards the north.

A significant change in the characteristics of the Lower Springbok quartz latites is observed in a small stream bed 5 km north of Fonteine, immediately east of the Bergsig Fault. At this locality the upper of the two units appears to have thinned markedly and lies directly on the lower unit, without any intervening basalt. The thinning is accompanied by a considerable change in the character of the flow, such that the contact between the two units is unrecognisable. The combined unit has an estimated thickness of about 50 m, although the base is not seen. The lower 8 m of the exposure consists of a friable, thinly jointed quartz latite which gives way to 20 - 25 m of flow banded and brecciated material, with clasts up to 30 - 40 cm in diameter. Plates 2.6 - 2.8 illustrate the nature of this upper zone and show the relationship between the flow banded contorted quartz latite and the breccia blocks. Generally blocks become more amygdaloidal and pumice-like towards the top of the flow (Plate 2.8), with non-amygdaloidal (denser) quartz latite forming the majority of clasts lower down (Plate 2.7). The increasingly pumiceous nature of breccia blocks towards the top of a flow is a feature commonly observed in other quartz latite units (see Section 2.6). It appears that the upper portion of the deposit represents a combination of the flow top material of the lower quartz latite unit overlain by a distal portion of the upper unit. The "distal" facies displays characteristics common to both basal and flow top facies without the familiar massive central portion of the unit. Whilst the change in character of the upper unit is abrupt, the rate of thinning appears gradual, as indicated by a horizontal base and an upper surface dipping at approximately 0.2°.

In the south-western part of the study area (Fig. 2.2) the Lower Springbok quartz latite crops out discontinuously over a wide area of the low lying alluvial plain east of the ABFZ, and occurs as far north as the Koigab River (Fig. 2.2). It appears that the outcrops represent a single, thin (10 - 20 m) unit lying 150 - 180 m above the base of the Etendeka Formation. Contact relationships of this unit with the underlying basalts appear to be

PLATE 2.6

Horizontal pavement of flow banded and brecciated material in the composite Lower Springbok quartz latite unit just north of Fonteine. The dark bands to the left of centre are of pitchstone. To the right of the centre a zone of breccia separates the pitchstone bands from flow folded quartz latite (far right).

PLATE 2.7

Breccia composed of large clasts of quartz latite in a much finer grained purplish-grey matrix. In most cases the clasts are only sparsely amygdaliodal. Viewed near the base of the flow banded and brecciated zone in the Lower Springbok quartz latite near Fonteine, and stratigraphically below the outcrop in Plate 2.6.

PLATE 2.8

(a)

(b)

Pumice block breccias encountered near the top of the composite Lower Springbok unit near Fonteine. Note that the amygdales in some of the blocks are flattened and that the orientation of this fabric varies from block to block.

transgressive, providing evidence, supported by variations in stratigraphic height (20 - 30 m), for the existence of palaeo-relief prior to eruption. No evidence to suggest the presence of two Lower Springbok units in this area has been observed.

The area encompassed by the outcrop limits of the Lower Springbok quartz latites (Fig. 2.2) is approximately 2700 km^2. Assuming an average thickness of 30 m, this represents 80 km^3 as an absolute minimum for the volume of a single eruptive unit. It is conceivable that the Lower Springbok quartz latites may cover a much larger area (> 6500 km^2), although confirmation of this must wait for the results of studies on the Albin and Gobobosebberge quartz latites (Fig. 2.1).

2.5.2.3 Upper Springbok Quartz Latite

The Upper Springbok quartz latite forms the uppermost unit of the Springbok succession and is separated from the Lower Springbok quartz latites by 60 - 100 m of basalt at Awahab (Fig. 2.6). Outcrops of this unit generally form large boulder strewn hills, such as the flanks of the hill at Wolfswasser (Fig. 2.3) illustrated in Plate 2.9.

As discussed in a previous section the upper surface of this unit is eroded and the complete thickness of the quartz latite unit is unknown. It has a maximum observed thickness of 295 m about 6 km west of Fonteine, and thickness measurements of 270 m and 190 m at Trig 26 and Awahab respectively indicate that this unit is very thick over much of its outcrop area. Approximately 2750 km^2 are encompassed by the limits of the present outcrop (Fig. 2.2), forming part of what once was undoubtedly a much more extensive sheet. Assuming a thickness of 250 - 290 m over the outcrop area yields a volume of 700 - 800 km^3 for this unit, an estimate which is probably considerably less than the original erupted volume.

Pyroclastic flow sheets are sometimes composed of several flow units that may be difficult to distinguish. Differences in the structure of the Upper Springbok quartz latite unit compared to an idealised section through a quartz latite unit, coupled with its great thickness, suggest that it may comprise several flow units. However, the structure of the unit varies substantially between different outcrops as indicated below.

PLATE 2.9

Columnar-jointed cliffs of the Upper Springbok quartz latite at Wolfswasser (Fig. 2.3a). This unit overlies basalt and the contact is clearly visible. The cliff is approx. 100 m high, and the boulder strewn flanks of the hill are typical of the outcrop encountered over much of the Upper Springbok sheet.

PLATE 2.10

The Tafelberg Succession at Tafelberg. The Upper Tafelberg quartz latite forms the steep columnar-jointed cliffs near the top of the mountain. This is overlain at the summit (top left) by the Tafelberg Beacon quartz latite. Lower down in the succession two prominent cliff-forming basalt units overlie the Lower Tafelberg quartz latite. The Tafelberg latite occurs at the top of the first bench beyond the foreground bushes. The traverse of Erlank *et al.* (1984) was made up the gulley on the right-hand side of the photograph.

(1) At Awahab the Upper Springbok quartz latite unit forms the uppermost cliffs of the section (Plate 2.4) where it is well exposed. The basal zone of the unit is generally poorly developed with a few narrow (< 0.5 m) pitchstone lenses and some contorted flow banding. Above this, the unit consists of massive, devitrified, columnar-jointed quartz latite with no significant textural variability in 190 m of section.

(2) About 6 km west of Fonteine a more complicated picture emerges. Fig. 2.7a illustrates a number of different textural zones encountered in a traverse through 200 m of the unit beneath the southernmost basalt-capped hill in that area (Fig. 2.2). The lower part of the section consists of pitchstone and devitrified quartz latite with zones of contorted flow banding and altered amygdaloidal material, which may represent contacts between flow units. About 1 km north of this traverse, however, the unit consists entirely of massive, thickly jointed, non-vesicular, devitrified quartz latite with little indication of textural variability within the unit.

(3) The best evidence for flow unit contacts occurs at Trig 26 (Fig. 2.2), illustrated in Fig. 2.7b. Here at least two contacts between flow units are marked by zones of contorted banding, hydraulic fracturing and breccias similar to those seen at the bases of other flow units. Owing to scree cover the lateral extent of these contacts is unknown.

Differences in the post-depositional temperature profiles of ash-flow deposits composed of several flow units may result in either simple or compound cooling units (Fisher and Schmincke, 1984). A simple cooling unit results when a single or successive flows cool as one unit with no sharp changes in the temperature gradient. Alternatively, a compound cooling unit occurs if there is an interruption in the temperature gradient, which may result from a finite delay in the eruption of successive flows. The outcrop at Trig 26 provides reasonably good evidence that the Upper Springbok unit is composed of at least three flow units. In most instances this unit appears to have behaved as a simple cooling unit with a fairly uniform cooling history. The textural variations outlined above are probably due to the variable development of flow base and flow top features (e.g. banding, breccia and pitchstone) in the individual units which constitute the Upper Springbok unit. Note that flow base and flow top features show variable development in many of the Etendeka quartz latite units. Both sections in Fig. 2.7 indicate the presence of considerable amounts of pitchstone in the lower part of the unit, while the upper portion is

Fig. 2.7 Field Sketches of the Upper Springbok Unit

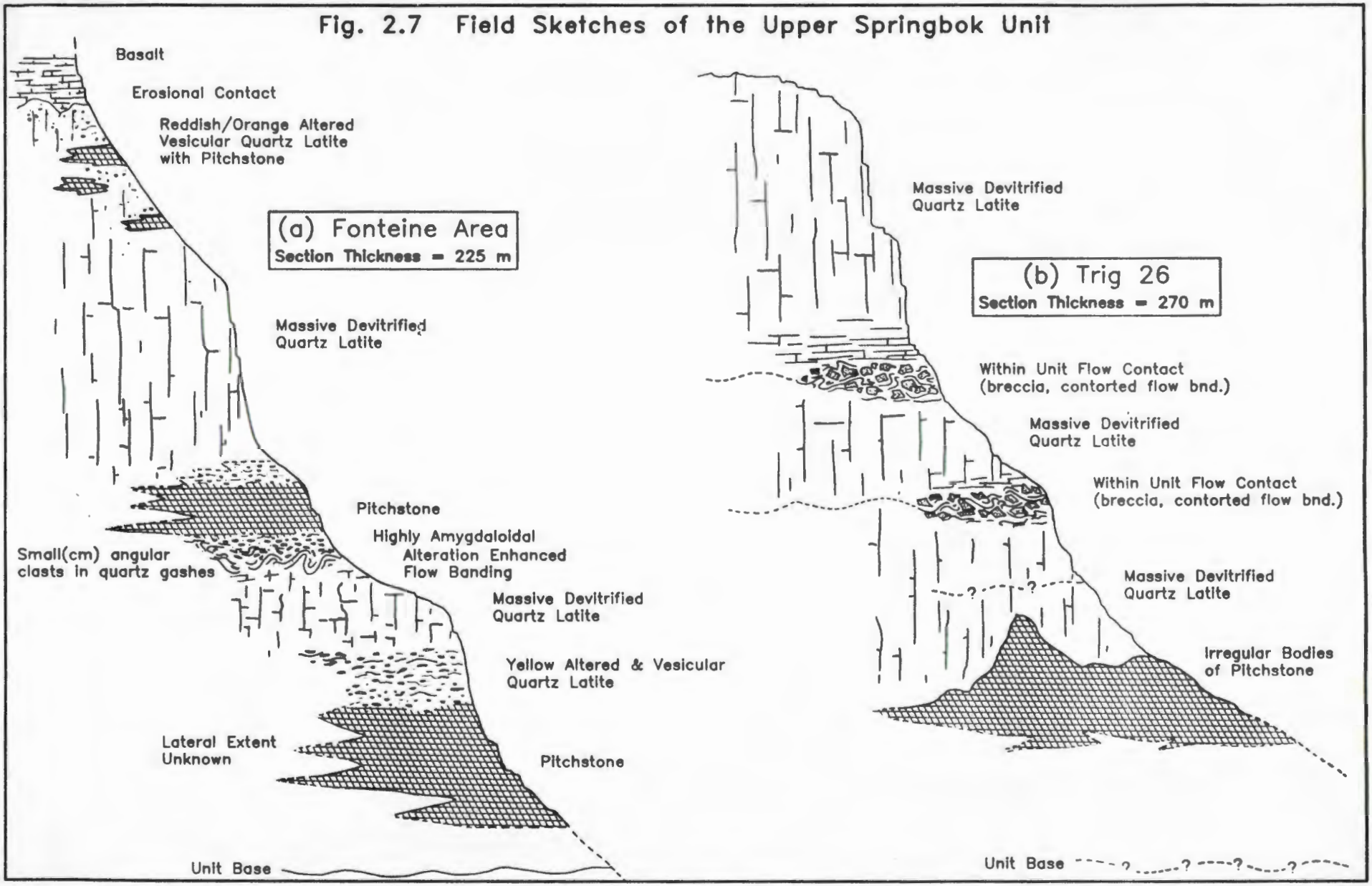

dominated by massive, devitrified quartz latite. This difference is often encountered throughout the Upper Springbok quartz latite sheet, where fairly thick bodies of massive pitchstone and highly amygdaloidal, altered quartz latite frequently occur within 50 - 60 m of the base.

At the Huab Outlier 13 km due west of Awahab (Fig. 2.2) the Upper Springbok quartz latite exhibits an unusual basal zone forming a compound unit with the underlying basalt. The basalt is approximately 6 m thick and rests on the amygdaloidal flow top of the underlying flow, and is undoubtedly extrusive in origin. The petrography and composition of samples collected in a vertical section through the contact zone show that there is a gradational change from basalt to quartz latite over a thickness of 1 - 2 m. No attenuation of the vertical joint pattern occurs across the contact zone and the most plausible explanation for this feature is the almost synchronous eruption of basalt and quartz latite, resulting in a simple cooling unit similar to those described above. However, this does not readily explain the gradation in composition. It is interesting to note that none of the features equated with rapid basal chilling, such as pitchstone, breccia and contorted flow banding, are observed along what is obviously a high temperature contact. A similar contact is observed 15 km to the NNW, north of the Huab River. These are, however, the only localities at which this unusual feature is observed and at Awahab the Upper Springbok unit overlies rubbly amygdaloidal basalt and exhibits a basal facies. This very interesting feature will receive further investigation subsequent to this thesis.

2.5.3 Tafelberg Succession

2.5.3.1 Introduction

The Tafelberg succession transgresses the Springbok succession from the north. It covers approximately 1,600 km^2 (excluding the Interbedded Coastal sequence) of the area studied (Fig. 2.2) and crops out over much of the northern Etendeka, covering an estimated 8,000 - 10,000 km^2 in total. The thickest development of the succession (880 m) occurs at Tafelberg, which is the main sequence of lavas described by Erlank *et al.* (1984). The succession consists of interbedded basalt, quartz latite and minor volumes of latite, with thickness proportions of 70 %, 24 % and 6 %, respectively. Plate 2.10 illustrates the Tafelberg type section, the stratigraphy of which is illustrated in Fig. 2.8.

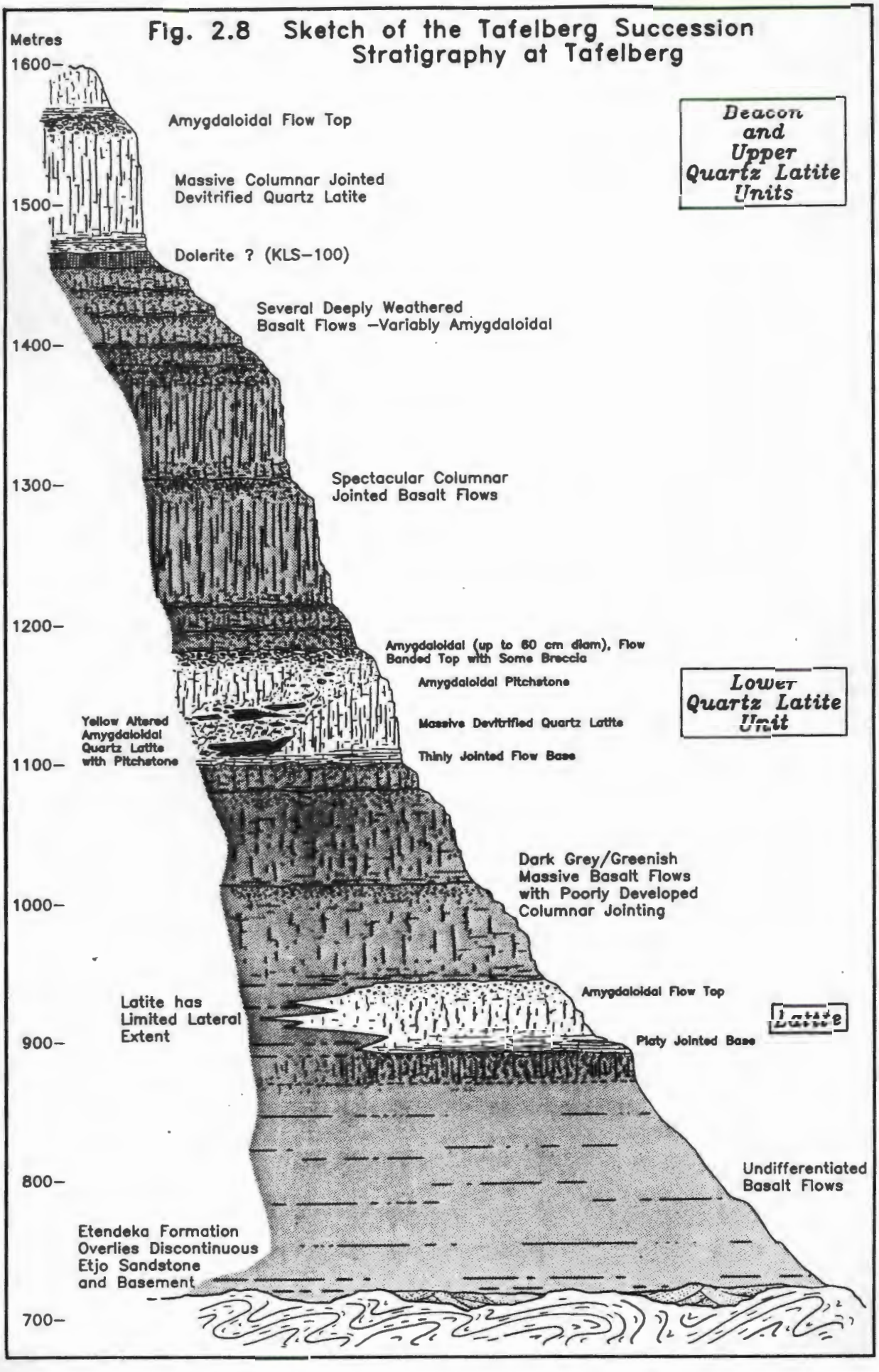
Fig. 2.8 Sketch of the Tafelberg Succession
Stratigraphy at Tafelberg
Metres
1600
1500
1400
1300
1200
1100
1000
900
800
700
Amygdaloidal Flow Top
Massive Columnar Jointed
Devitrified Quartz Latite
Dolerite ? (KLS–100)
Several Deeply Weathered
Basalt Flows –Variably Amygdaloidal
Spectacular Columnar
Jointed Basalt Flows
Amygdaloidal (up to 60 cm diam), Flow
Banded Top with Some Breccia
Amygdaloidal Pitchstone
Massive Devitrified Quartz Latite
Thinly Jointed Flow Base
Yellow Altered
Amygdaloidal
Quartz Latite
with Pitchstone
Dark Grey/Greenish
Massive Basalt Flows
with Poorly Developed
Columnar Jointing
Amygdaloidal Flow Top
Platy Jointed Base
Latite has
Limited Lateral
Extent
Undifferentiated
Basalt Flows
Etendeka Formation
Overlies Discontinuous
Etjo Sandstone
and Basement
Deacon
and
Upper
Quartz Latite
Units
Lower
Quartz Latite
Unit

The principal quartz latite units of the succession consist of a lower and two upper units (Upper Tafelberg and Tafelberg Beacon quartz latites), however, an additional quartz latite unit is observed about 17 km west of Tafelberg (see Fig. 2.4a). This unit consists of 15 - 20 m of vesicular, sparsely porphyritic quartz latite with a pitchstone base. It crops out 15 - 20 m below the Upper Tafelberg quartz latite and is referred to as the Middle Tafelberg unit. The latite is an isolated occurrence which has only been observed at Tafelberg. It occurs as a single unit with a maximum thickness of 50 m and can be traced over a limited distance of 2 - 3 km. It pinches out between basalt units to the north and is obscured by scree on the southern flank of Tafelberg.

2.5.3.2 Lower Tafelberg Quartz Latite

The Lower Tafelberg quartz latite is a sparsely porphyritic, predominantly felsitic rock at outcrop, although pitchstone bands and lenses may be observed near the flow contacts. In the north-eastern part of the study area it forms a significant step in the topography, commonly forming a low cliff line; further west it forms a moderately thick capping to the hills north of the Torra Bay-Bergsig road, west of the Skeleton Coast Park boundary; and forms prominent hills north and south of the Koigab Gorge, west of the ABFZ (Fig. 2.2). Outcrops of this unit are also encountered at Ecke and the Grootberg range in the northern Etendeka (Fig. 2.1). The area covered within the limits of the outcrop remnants is approximately 4,500 km^2, making this the most extensive unit mapped. The unit thickens from the north-east to the south-west and the following thicknesses are recorded:

Ecke (50 km NNW of Wêreldsend)	~ 50 m
Tafelberg and Wêreldsend	~ 70 - 80 m
Great Table Mountain (Fig. 2.1)	~ 130 m*
Koigab Gorge	~ 150 m*

* - note that in both of these instances the upper portion of the unit has been removed by erosion.

Where the flow-top facies does occur it is quite well developed (subsection 2.6.2) and has a tendency to be more amygdaloidal than the equivalent facies in the Springbok quartz latites. East of the ABFZ the base of the Lower Tafelberg unit is characterised by 1 - 2 m of fine grained, devitrified, laminar flow-banded quartz latite with little or no pitchstone or basal breccia. West of the ABFZ, however, it displays quite well developed basal characteristics

(subsection 2.6.4) with pitchstone bands, breccias and contorted flow banding. The differences in character of the basal facies may be a function of the terrain over which the unit was erupted, the terrain being more uneven west of the ABFZ compared to the generally flat planar palaeo-surfaces of the east. A thickening of the unit to the west indicates a closer proximity to the where depositional conditions may also have been more turbulent.

Unlike the Upper Springbok quartz latite there is no evidence to suggest that the Lower Tafelberg quartz latite is a composite unit consisting of more than one flow. At Tafelberg a zone with massive pitchstone, glassy, friable pitchstone and highly altered yellowish quartz latite is exposed in the gully at the south-eastern end of the mountain (Plate 2.10). This was initially thought to represent contacts between two or more flow units. However, exposure on the north side of the gully does not show these features and consists of 40 - 50 m of massive, columnar jointed, devitrified quartz latite and pitchstone overlain by 15 m of the flow top facies. The zone of textural variability appears to cut the flow diagonally and is highly vesicular throughout (Fig. 2.8 shows a schematic representation). Agate, quartz and zeolite fill cavities and joints in the rock, which coupled with fairly extensive alteration, indicate considerable fluid interaction with the rock in this zone. Further descriptions of alteration zones within quartz latite units are given in Section 2.8.

2.5.3.3 Upper Tafelberg Quartz Latite

The Upper Tafelberg quartz latite crops out over an area of 1,300 km^2 between Tafelberg and Grootberg (Fig. 2.1). It forms the uppermost unit of the spectacular flat-topped mountains and can be traced visually for more than 30 km northwards from Tafelberg. At Tafelberg the unit is approximately 80 m thick and forms almost vertical, columnar-jointed cliffs (Plate 2.10). At outcrop it is a massive, devitrified, aphanitic rock which often looks like a fine-grained arenaceous sediment on weathered surfaces. The flow base shows predominantly laminar flow banding, although some contorted banding is observed within the lower-most 3 - 4 m. No breccias or pitchstone bands have been observed. Towards the upper part of the flow the unit becomes increasingly vesicular and gives way to a highly amygdaloidal, flow-banded rock characteristic of the flow top facies (subsection 2.6.2).

2.5.3.4 Tafelberg Beacon Quartz Latite

The Tafelberg Beacon quartz latite unit is very similar in hand specimen to the Upper Tafelberg quartz latite. It has only been recognised at Tafelberg where it forms a small outcrop at the summit of the mountain (Plate 2.10). It directly overlies the Upper Tafelberg unit and has an observed maximum thickness of 40 m; the upper part of the flow having been removed by erosion. This unit originally had a much wider extent but has been eroded from neighbouring hills.

2.5.4 Interbedded Coastal Quartz Latites

The sparsely porphyritic quartz latites of the Interbedded Coastal succession occur in the faulted region west of the ABFZ (Figs. 2.2 & 2.3), where they commonly form prominent north-south trending ridges. As a consequence of low relief and superficial cover the stratigraphy of the succession is not as clearly defined as it is for the horizontally bedded sequences inland. Contact relationships are generally inferred from the presence of pitchstone and variously coloured quartz latite in the desert float or from obvious changes in the nature of the quartz latite between successive ridges.

The succession is the thickest single accumulation of quartz latites encountered in the Etendeka having an estimated thickness of 800 - 1,000 m (Fig. 2.4a). Petrographic and geochemical evidence indicates that this sequence is the westerly equivalent of the Tafelberg succession, the lowest unit in the succession being the Lower Tafelberg quartz latite unit (Fig. 2.3). Tilting and faulting in the coastal area make it impossible to estimate the areal extent of the units above the Lower Tafelberg unit. Some of the lower units can be traced for up to 25 km along strike suggesting that they covered a considerable area. Bathymetric studies by Bremner (1977) revealed the presence of a series of longitudinal troughs and ridges, the Palgrave Depressions (Fig. 2.1), occurring in a zone which extends 110 km south of Palgrave Point, about 50 km offshore on the landward side of the inner shelf break. Individual depressions are up to 40 km long, 5.5 km in width and about 35 m deep. Thin-sections of dredge samples (kindly loaned by M. Bremner) reveal the presence of sparsely porphyritic quartz latite which is similar to that encountered in the Interbedded Coastal sequence. It seems likely that this ocean floor feature represents a westerly extension of the Interbedded Coastal quartz latites, increasing substantially their known areal coverage.

On the basis of geochemistry (Milner and Duncan, 1987) the Interbedded Coastal succession can be subdivided into lower, middle and upper portions which are indicated on Fig. 2.3. A traverse across the northern end of the fault block reveals at least eleven different quartz latite units, which do not appear to have been repeated by faulting. At the southern end of the main fault block the Upper Interbedded units are not as well developed as those further north, accordingly the succession appears to be slightly thinner with only seven mappable units. The lower units appear to be laterally persistent and vary from 10 - 20 m to over 200 m in thickness. They are also found outcropping at the coast 15 km south of the Koigab River mouth and in the area south of the Koigab Gorge (Fig. 2.3). Higher in the sequence contacts between units are less distinct. The units appear thinner and laterally impersistent and are interbedded with several thin basalt lava flows. Whether the lateral impersistence is a feature of the original deposition or of subsequent erosion of the quartz latite units is unknown.

One of the most interesting units encountered among the Interbedded Coastal quartz latites is the Gemini quartz latite, a thin (15 - 20 m) flow unit which overlies the Lower Tafelberg unit south of the Koigab Gorge (Fig. 2.3). The entire unit is composed of friable pitchstone, varicoloured, contorted flow banded quartz latite and altered clastic material. The type locality for this unit, SM-229, indicated on Fig. 2.3b, is illustrated in Plate 2.11 which shows about 8 m of the deposit overlain by massive devitrified quartz latite of a subsequent flow. The outcrop characteristics of this deposit are outlined below:

(1) The deposit consists of interspersed irregular shaped bodies of pitchstone, flow banded quartz latite and altered clastic material, which are not confined to specific horizons (Plate 2.11).

(2) Contacts between vitreous friable pitchstone and the flow banded, varicoloured quartz latite are mostly sharp (Plate 2.12).

(3) The breccia is dominantly composed of a soft, yellowish-brown rock which is an alteration product after pitchstone. Some clasts still contain pitchstone (Plate 2.13), and clastic zones are often gradational with the pitchstone bodies.

(4) Clasts range in size from 1 to 15 cm in diameter and are commonly highly amygdaloidal. The amygdales are often drawn out and flattened producing a

PLATE 2.11

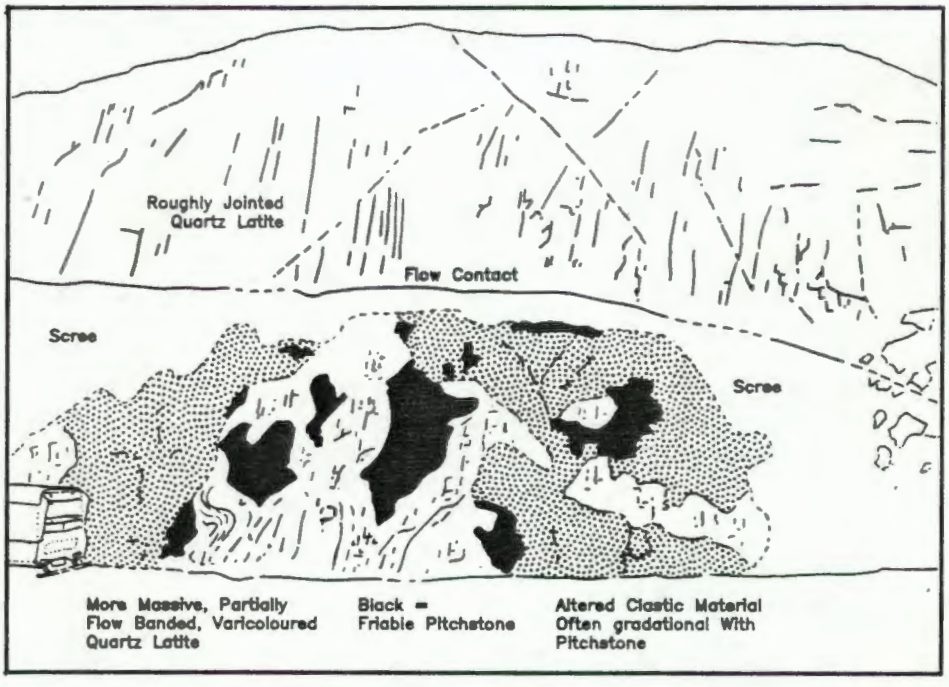

The general outcrop characteristics of the Gemini quartz latite unit at the SM-229 locality (see Fig. 2.3b). The Gemini quartz latite which consists of a chaotic assortment of friable pitchstone, altered clastic material and flow banded quartz latite, forms the lower part of the section and is overlain by more massive featureless quartz latite of the overlying unit.

PLATE 2.12

Gemini quartz latite unit (SM-229 locality). Close association of flow banded and contorted devitrified quartz latite with glassy friable pitchstone (left). Photograph taken just to the right of the vehicle in Plate 2.11.

PLATE 2.13

Altered, poorly consolidated breccia of the Gemini quartz latite unit at the SM-229 locality. Note that some of the clasts still contain pitchstone.

linear fabric. Orientation of the flattening appears to be random indicating that the clasts may have already been flattened prior to their deposition. Note that the pitchstones are not generally vesicular.

(5) Flattened amygdales, distorted clasts and a eutaxitic texture are commonly observed in the more massive portions of the unit (Plate 2.14).

Important petrographic information presented in Chapter 4 shows that in comparison with most of the quartz latite units studied this unit is poorly welded, and better illustrates the pyroclastic nature of the quartz latite units.

Outcrops of a similar type of material with identical stratigraphic associations to the SM-229 locality occur above the lowest unit in the main Interbedded Coastal sequence. This unit may thus be usable as a stratigraphic marker separating the Lower Tafelberg quartz latite from the overlying Interbedded Coastal quartz latite succession, providing corroborative evidence for the stratigraphic reconstructions of Milner and Duncan (1987).

2.6 DETAILED QUARTZ LATITE UNIT STRUCTURE

2.6.1 Introduction

Until the present study, brief details of which have already been presented in Milner (1986), little had been documented about the nature of the acid flows of the Etendeka Formation. The general appearance of the quartz latite units in the field suggests that they represent rather featureless, monotonous flows and there is little to indicate a precise mode of origin. The generally characterless nature of the exposure is largely a result of outcrops typically being formed from the more massive central portions of the flow, with the more altered contact zones being commonly obscured by scree and other superficial material.

A unit can be conveniently divided into basal, main and upper zones, the boundaries of which are broadly defined by changes in textural character. The most informative portions of the unit are the basal and upper zones. In these zones, features such as banding, pitchstone lenses and breccias, are preserved and may have been induced by rapid chilling either by contact with the ground surface or with the atmosphere. Careful study of field relationships of

PLATE 2.14

Fine detail in more massive devitrified Gemini quartz latite is enhanced by alteration. Note that the central clast is deformed and that similar material above and slightly to the right shows signs of flowage. A strong eutaxitic texture is developed in the bottom right-hand corner. Vesicles, which are filled with quartz, (above the lens cap) are flattened in the direction of flow. Outcrop locality is approx. 5 km south of the Koigab Gorge.

PLATE 2.15

Tight centimetre-scale contorted flow banding. Two or three small clasts of quartz latite are just visible above the marker pen and below the main fold nose. Photograph taken at the base of an Interbedded Coastal quartz latite unit, Grid. Ref. 13°29'59"E 20°47'50"S.

these features, coupled with petrographic study of polished slabs and thin-sections (Chapter 4), has provided considerable insight into the mode of eruption and emplacement of these units.

The overall similarity in structure of the different quartz latite units permits a general discussion of the flow features observed. Both the Lower Springbok and Lower Tafelberg quartz latites have well developed flow zones and much of the information used to describe a "typical" quartz latite unit comes from these units. By way of a summary, idealised sections through typical Springbok and Tafelberg quartz latite units are presented in Fig. 2.12. Two sections are presented to illustrate the slight differences encountered between the Springbok and Tafelberg units. It is important to note that not all features described for the upper and basal zones may be present at any one locality. Often the zones themselves are absent, or only poorly developed, or unexposed. Table 2.2 gives an indication of the frequency with which certain flow characteristics are observed.

2.6.2 Basal Zone

The basal part of a quartz latite unit exhibits the majority of flow features and consequently yields most information as to the mode of eruption of these units. The basal facies includes flow banding, pitchstone lenses, and breccia as well as more massive quartz latite, and ranges from less than a metre to 5 - 6 m in thickness. Quite large variations in the development of the basal zone occur between the Springbok and Tafelberg quartz latite units. In the east the latter have relatively thin basal zones which show uncontorted laminar flow banding with little brecciation or presence of pitchstone, and contrast with thicker basal zones of the Springbok units. However, the basal zone of the Lower Tafelberg quartz latite changes in character west of the ABFZ. Here it is better developed with pitchstone lenses, breccia and contorted banding. Field sketches from localities where flow base characteristics are particularly well developed are presented in Figs. 2.9 and 2.10. Characteristics of the main flow features are outlined below.

2.6.2.1 Banding

In devitrified quartz latite banding is often enhanced by alteration which colours differentially the bands in shades of red, orange and grey. Banding is also observed in pitchstone bodies, indicated by different degrees of

Table 2.2

(a) The percentage of sections* exhibiting recognisable flow features

ZONE	Featureless/ No Outcrop	Flow Features Recognised
UPPER	52 %	48 %
MAIN	86 %	14 %
BASAL	55 %	45 %

* This data is semi–quantitative and encompasses 19 randomly selected sections which encountered an equivalent of 29 quartz latite units.

(b) The occurrence of specific flow features as a percentage of the total number of zones which exhibit upper and basal facies development. Data for both the Springbok and Tafelberg quartz latite units are presented

FEATURE	SPRINGBOK %		TAFELBERG %
Contorted Banding	66		43
Breccia	66		29
Pitchstone	100	UPPER ZONE	71
Amygdaloidal	33		100
Altered	100		100
Contorted Banding	50		41
Laminar Banding	5		35
Breccia	25		21
Pitchstone	85	BASAL ZONE	28
Basalt Clasts	0		41
Amygdaloidal	20		28

~Data are semi–quantitative and have been compiled from field notes on numerous outcrops, and are not confined to the 19 sections indicated above.

Fig. 2.9 Field Sketch of a Flow Base Occurrence in a Lower Springbok Quartz Latite Unit, Awahab

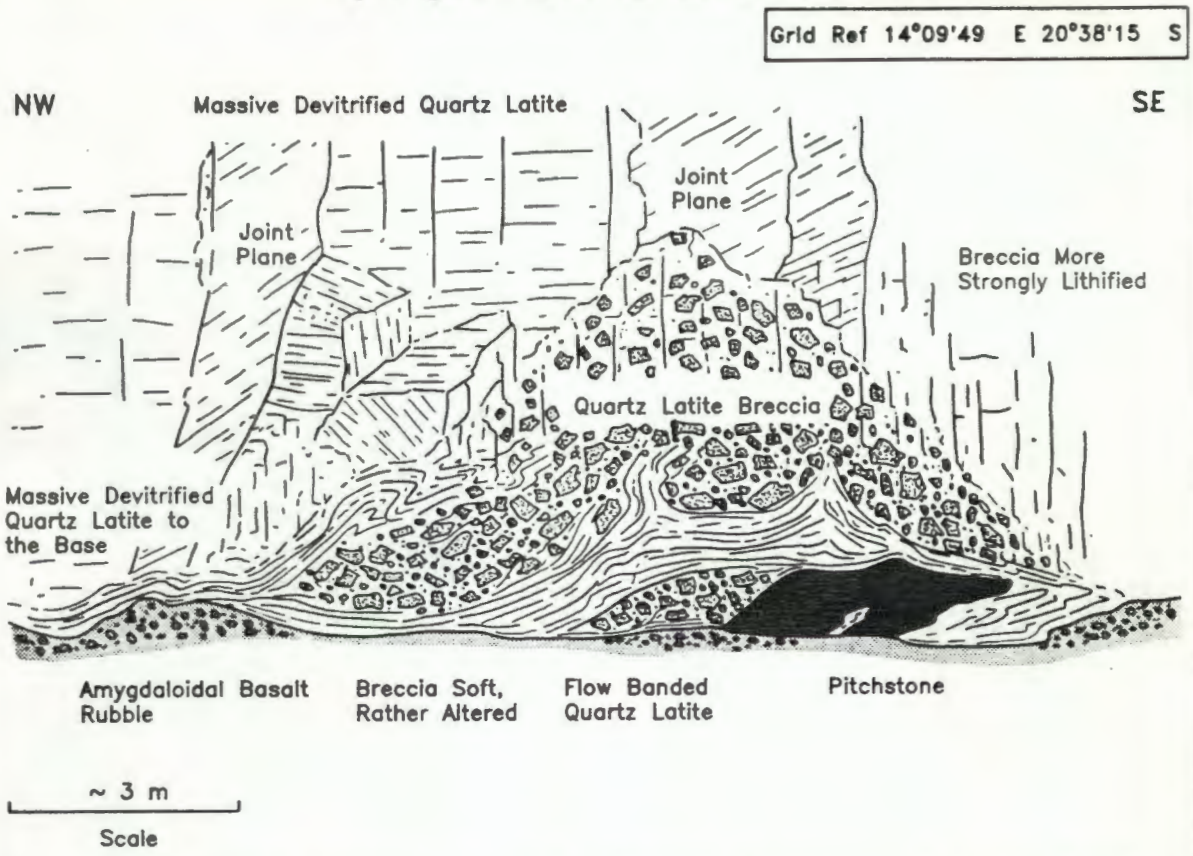

Fig. 2.10 Field Sketch of the 'Dunes' Outcrop. A Flow Base from the Interbedded Coastal Quartz Latite Block

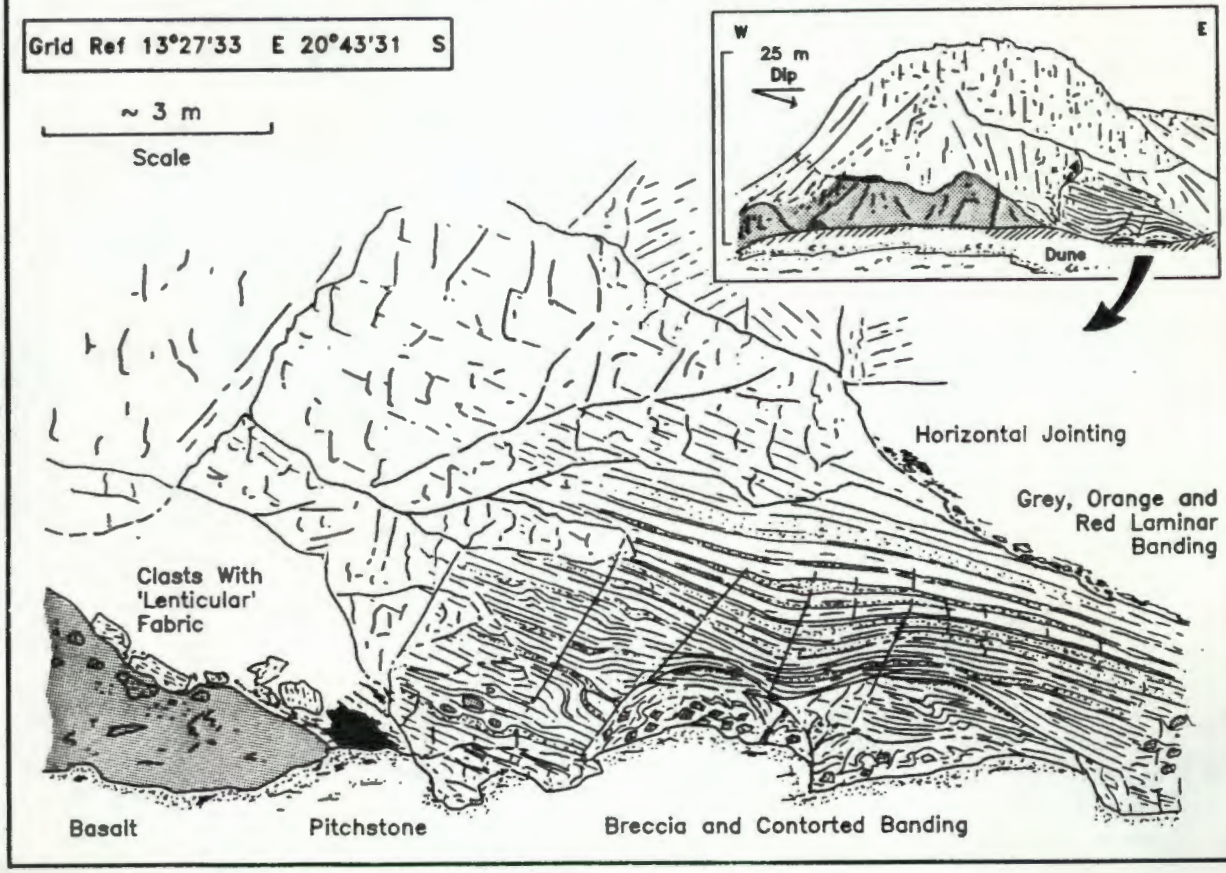

devitrification. Banding typically occurs on a millimetre to decimetre scale. Near the base of the unit, normally within the lowermost 2 - 3 m, the banding is frequently contorted and often intimately associated with basal breccia. Contortions occur vertically and laterally within the units and vary from tight centimetre-scale folds to more open structures of up to a metre or more. The contortions frequently give way upwards to more laminar banding which is often associated with a strong centimetre-scale jointing in the same plane. More rarely joint patterns are also contorted, the joints forming between different bands in a contorted flow structure. Samples collected from the laminar banded region at the "Dunes" outcrop (Fig. 2.10) contain fiammé-like structures (further details of which are presented in Chapter 4). Plates 2.15 - 2.17 show the nature of some of the banding observed.

2.6.2.2 Pitchstone

Pitchstone normally occurs as irregular pods and lenses within 2 to 3 m of the base of a quartz latite unit. These lenses and pods range from thin stringers, 10 - 15 cm wide and 1 - 2 m long, to larger bodies up to 3 m thick and 30 m long. The pitchstone is normally homogeneous, massive and only sparsely amygdaloidal, and may show either sharp or gradational contacts with the more devitrified portions of the flow. Some pitchstones contain structures similar to the "spherulites" described by Bonnichsen and Citron (1982). These spherulites consist of roughly spherical masses of devitrified quartz latite (up to 50 cm in diameter) which commonly have a central shrinkage cavity filled with quartz and/or zeolite. Plates 2.18 and 2.19 illustrate pitchstone occurrences from the south-western outcrop area of the Lower Springbok quartz latite and from the Lower Tafelberg unit in the Koigab Gorge. Some pitchstone occurring at the base of the Lower Tafelberg and Interbedded Coastal quartz latite units forms glassy, friable, perlitic zones which exhibit welded clastic textures in thin-section. Significantly larger pitchstone bodies up to 10 m thick, encountered in the Upper Springbok quartz latite unit (see previous section), are not confined to the basal zone but extend 50 - 60 m up into the unit. An interesting feature of these particular pitchstone bodies is that they frequently display a flattened amygdaloidal fabric, not dissimilar from that observed in brecciated material.

PLATE 2.16

Large-scale open flow banding. The form of the flow banding has been enhanced by alteration which colours alternate bands in shades of orange and purplish-grey. The hammer is just over 0.5 m long. Lower Springbok quartz latite cropping out in the south-western alluvial plain.

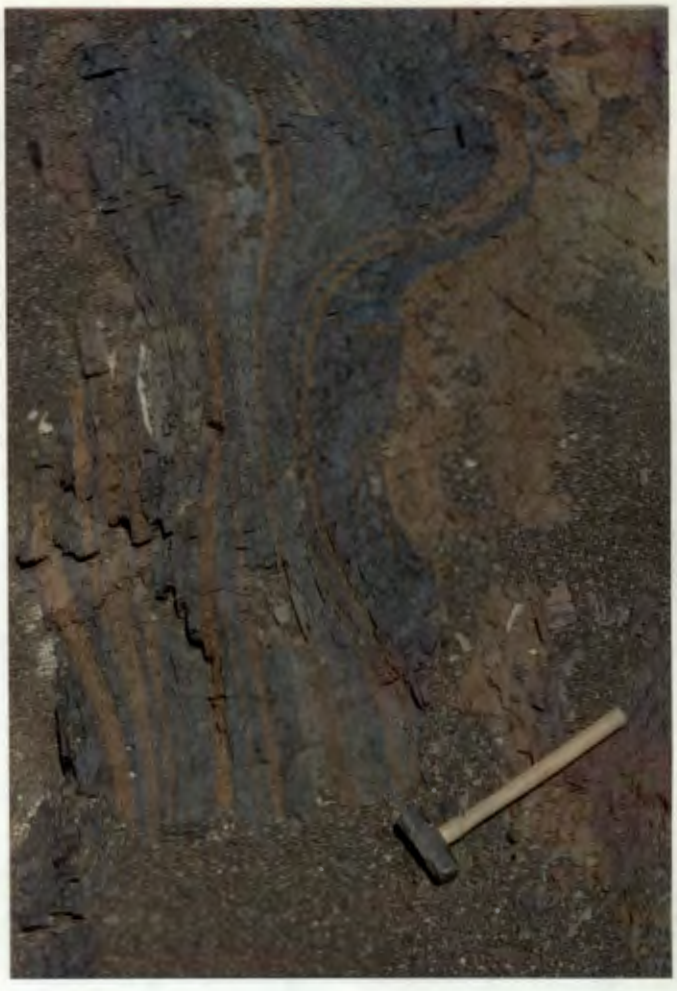

PLATE 2.17

Different degrees of devitrification enhance contorted flow banding in a block of Lower Springbok quartz latite pitchstone, Awahab.

PLATE 2.18

Pitchstone body at the base of the Lower Springbok quartz latite unit in the south-western part of the southern Etendeka. Note that it has a sharp contact with the overlying devitrified portions of the flow unit. The devitrified quartz latite which has well developed vertical joints also exhibits a strong horizontal jointing which is a common flow base feature.

PLATE 2.19

The base of the Lower Tafelberg quartz latite unit in the Koigab Gorge. A basal pitchstone lens (approx. 0.5 m thick) overlies rubbly, vesicular basalt. The white material which occurs along the contact is a recent deposit of gypcrete. Above the pitchstone the unit is predominantly devitrified, although several thin stringers of pitchstone do occur higher up.

2.6.2.3 Breccia

Basal breccias display a variety of textures reflecting differing amounts of matrix material present and the degree of welding to which they have been subjected. Unwelded or partially welded breccias yield some of the most convincing pyroclastic textures observed in the quartz latites. These are fully described and illustrated in Chapter 4.

Breccia occurs in discontinuous zones of limited extent, although some fairly thick accumulations (7 - 8 m maximum) are observed at the base of the Lower Springbok quartz latites at Awahab (Fig. 2.9). The breccias vary from clast-supported to matrix-supported and are composed of angular to subrounded clasts of quartz latite, whose maximum dimensions range from 1 to 50 cm. The matrix is composed of fragmented pumice, glass and phenocrysts (Subsection 4.2.1). Clasts are predominantly devitrified and are sparsely to moderately amygdaloidal, frequently displaying a flattened fabric. Breccias containing pitchstone clasts (e.g. Plate 4.23) are rare. The breccias are chaotic in nature with no grading of clast size. Random orientation of the flattened amygdaloidal fabric of the clasts indicates that the flattening occurred prior to their final emplacement and that the clasts were relatively cool and rigid at this time. Generally the matrix shards become increasingly welded upwards (towards the centre of the flow) and clasts well above the base are often surrounded by massive quartz latite (Plate 2.21). It is important to note however, that breccia horizons may be underlain by or pervaded by massive flow banded quartz latite even when the matrix shards appear relatively undeformed (Fig. 2.9). Plates 2.20 and 2.22 show some of the breccia horizons.

In the lowest of the Lower Springbok quartz latites at Awahab contorted flow banding in quartz latite is ruptured producing angular clasts (Plates 2.23 - 2.24). Occasionally this flow brecciation produces fairly large blocks, some up to a metre or more in length.

The Lower Tafelberg quartz latite west of the ABFZ contains widespread clasts of amygdaloidal basalt usually less than 20 cm in diameter. These clasts are present up to 2 - 3 m from the flow base, having been incorporated from the scoriaceous top of the underlying basalt lava (Plate 2.25 and 2.26).

2.6.3 Main Zone

This zone commonly forms in excess of 70 % of the unit as a whole. It is characteristically massive with little or no internal structure, except for an

PLATE 2.20

(a)

Well developed basal breccia showing unsorted clasts set in an altered matrix. (a) shows competent flow banded material below the breccia, highlighting the contemporary nature of the breccia with flowage in the quartz latite. Photographed at Awahab, the outcrop illustrated in Fig. 2.9. Compass for scale.

(b)

Similar to (a). The hammer is about 0.5 m long and demonstrates the size of some of the blocks at this locality.

PLATE 2.21

Clast-supported breccia horizon gives way to a matrix supported regime with clasts incorporated into massive quartz latite higher up. Note the amygdaloidal nature of the clasts and their chaotic orientation. Lower Springbok quartz latite in the south-western area, same flow base outcrop as that illustrated in Plate 2.18.

PLATE 2.22

Elongate blocks of ruptured flow banded quartz latite incorporated into a more strongly brecciated horizon, similar to those illustrated in Plate 2.20. The hammer is approx. 0.75 m long .

PLATE 2.23

Good example of ruptured flow banding with shearing through the nose of the fold structure. Lower Springbok quartz latite, Awahab - observed at the same outcrop as that illustrated in Plate 2.22.

PLATE 2.24

Strong overfolding of quartz latite. This photograph was taken to the left and slightly above Plate 2.23 (Plates actually match up).

PLATE 2.25

Basalt - quartz latite (Lower Tafelberg) contact illustrating the incorporation of amygdaloidal basaltic rubble into the base of a quartz latite flow unit. Apart from some weak laminar banding this is the only flow base feature identified at this locality. Photographed in the Koigab Gorge 15 - 20 m from the outcrop illustrated in Plate 2.19.

PLATE 2.26

Basaltic clasts caught up in the laminar flow banded zone at the base of the Lower Tafelberg quartz latite at the 'Dunes' locality (see Fig. 2.10). The amygdaloidal nature of the clasts is consistent with their derivation from the underlying basalt flow top.

occasional horizontal lamination, and forms the vertical, crudely columnar-jointed cliffs seen at Awahab and Tafelberg (Plate 2.4 and 2.10). The homogeneous nature of this zone is borne out by petrographic studies which normally reveal monotonous devitrification textures common to both phyric and aphyric units alike.

Some units do, however, contain significant amounts of pitchstone within the main zone. Thinner units, such as the Lower Springbok quartz latites and the thinner parts of the Lower Tafelberg quartz latite at Tafelberg and Grootberg (Fig. 2.1), often have massive, vertically jointed pitchstone in the upper part of the main zone (see Fig. 2.12). These pitchstones, which may be as much as 15 - 20 m thick, contain numerous spherical amygdales and normally give way to the more altered and amygdaloidal flow top facies.

2.6.4 Upper Zone

In general this zone is the most strongly altered and amygdaloidal portion of a flow unit. Fig. 2.11 illustrates a section through the upper zone of a Lower Springbok quartz latite at Awahab and typifies the chaotic nature of the flow-top facies. Sections through the upper zones of the Tafelberg quartz latites reveal very similar features although the rocks are considerably more amygdaloidal. The thickness of the upper zone varies. In most cases it is 7 - 10 m thick although in occurrences of the Tafelberg quartz latites it may be up to 15 - 20 m thick. Many of the features encountered in the upper zone, such as contorted banding (Plate 2.27), pitchstone lenses and breccia, are similar to those already described for the basal zone, although there are a few notable differences which are outlined below.

2.6.4.1 Flow Top Breccia

As with the basal facies, breccia horizons are closely interspersed with flow-banded material, and vertical "dykes" of quartz latite cut accumulations of breccia. One such dyke in a Lower Springbok quartz latite unit in the Huab Outliers emerges from the main zone of the unit and extends upwards for at least 7 - 8 m (a diagrammatic representation is given in Fig. 2.12). Contacts between flow-banded material and breccia may be either sharp or gradational; the latter occur just above the main zone where clasts have become incorporated into the flow-banded quartz latite and have been streaked out and deformed. In other places the contorted quartz latite shows signs of flow brecciation and some of

Fig. 2.11 Section Logged through the Upper Zone of a Lower Springbok Quartz Latite Unit.

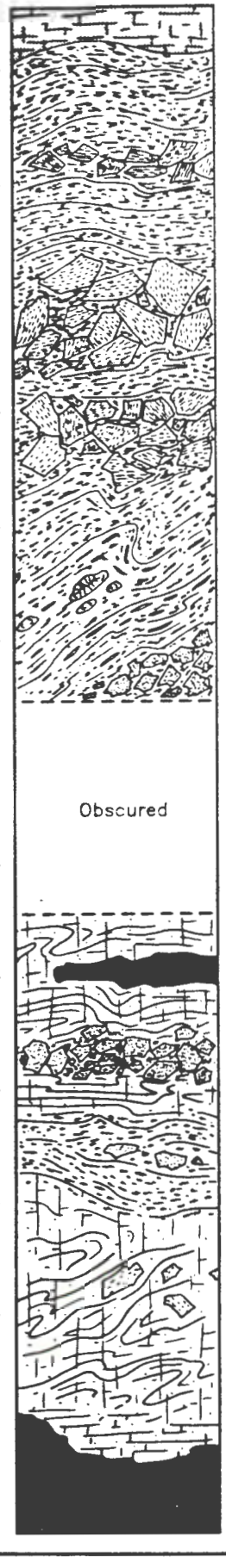

Basalt

Grid Ref 14°09'21 E 20°38'32 S

Flow Top is Highly Altered such that it is difficult to distinguish between Quartz Latite and Pumice Blocks

Pumice Block Breccia

Flow Banded – Highly Altered

Pumice Block Breccia

Yellow, Highly Altered and Amygdaloidal with some Flow Banding. Amygdales are Elongated in the Direction of Flow (Sizes range from 2–3 mm to 10–15 cm diam. ~ Quartz Filled)

Breccia

Devitrified, Sparsely Amygdaloidal Amygdaloidal Pitchstone

Varicoloured – Contorted

Breccia

Flow Banded – more Compitent

Amygdaloidal Contorted Quartz Latite with Clasts

Occasional Vesicular Clast

Orange/Red Contorted Banding

Orangy–Red Quartz Latite

Massive, Amygdaloidal Pitchstone (Amygdales Spherical < 10 mm diam.)

PLATE 2.27

Contorted flow banding in the upper zone of the Lower Tafelberg quartz latite at Wêreldsend.

PLATE 2.28

Extensive breccia horizon in the upper zone of the Lower Tafelberg quartz latite at Wêreldsend. (see Plate 3.5 for an illustration of the section at Wêreldsend).

PLATE 2.29

A more detailed illustration of the flow top breccia shown in Plate 2.28. The clasts are sparsely vesicular and are set in a fine-grained, purple-grey matrix which is strongly cemented by silica.

PLATE 2.30

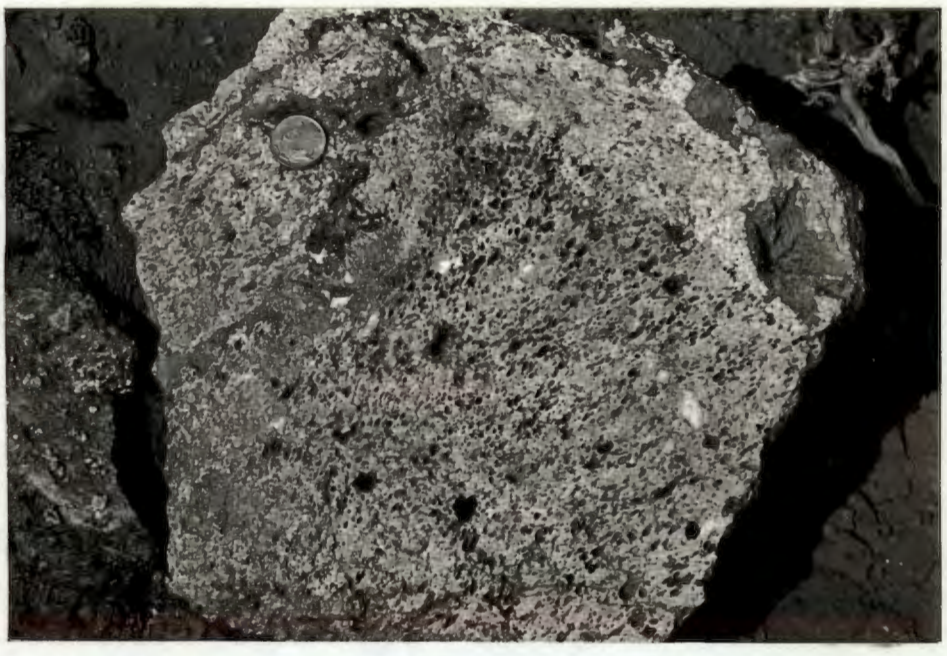

Pumice block from the contact zone illustrated in Plate 2.3. Blocks of a similar nature are observed in the flow top zones of the Lower Springbok quartz latite units (Fig. 2.11) in the Huab Outliers region, although they tend to be more deformed.

the resultant clasts are themselves flow-banded. The matrix within the breccias is very similar to that encountered in the basal breccias (Chapter 4), consisting of fragmented glass and crystals. Plates 2.28 and 2.29 show breccia near the top of the Lower Tafelberg unit at Wêreldsend (photographs taken just above the SM-198 sample site, see Plate 3.5 in the following chapter).

An important aspect of the flow top breccia is that the clasts become increasingly amygdaloidal towards the top of the flow unit. The clasts which range in size from a few centimetres to 50 - 60 cm across, are concentrated towards the top of the flow. The blocks are strongly altered to a soft, yellow material similar to the alteration products of glass seen elsewhere. Originally these blocks probably consisted of highly vesicular glass (pumice). Plate 2.30 shows the nature of one of these clasts and Plate 2.8 shows their overall mode of occurrence. It is likely that the pumiceous blocks were quite buoyant during eruption and emplacement, resulting in their concentration towards the top of the flow. Gentle flattening of the amygdales and the close-packed nature of the breccia suggest that they may have been compressed slightly, probably by the lithostatic load of the overlying units. Plate 2.31 illustrates the basalt-quartz latite contact in the lowest of the two Lower Springbok units in the Huab Outliers region.

2.6.4.2 Amygdales and Vesicles

The size and concentration of amygdales and vesicles increases from the upper part of the main zone through the upper zone; this is particularly noticeable in the Tafelberg and certain Interbedded Coastal quartz latite units. Amygdales and vesicles range in size from < 1.0 cm to 30 - 40 cm in diameter with those between 5 - 10 cm diameter being the most common. They display a variety of shapes, including spherical, ovoid and complex flattened structures, which are often aligned in the direction of flow, and may be partially or completely filled with secondary minerals (Plate 2.32). In the Tafelberg quartz latites, particularly the upper unit, there is a tendency for the vesicles to remain free of secondary minerals in the transition between the main and upper zones. Amygdale fillings are normally silica (quartz and agate), zeolite and calcite with rare instances of prehnite. In the Sarusas area gem-quality amethyst has been mined from such geoids. Agate, commonly deposited around the outer margins of the geoids, frequently contains angular fragments of quartz latite which appear to have spalled off the cavity walls.

PLATE 2.31

Flow top of a Lower Springbok quartz latite (Huab Outliers), overlain by dark, fine grained basalt. The quartz latite flow top material is strongly altered and friable with some pumice blocks, although these are difficult to recognise.

PLATE 2.32

Quartz and agate filled amygdales, collected from the upper zone of the Lower Tafelberg quartz latite at wêreldsend where they are particularly abundant. South African 20° piece for scale (2.5 cm diameter).

2.6.5 Summary

Fig. 2.12 presents composite sections through the Springbok and Tafelberg quartz latite flow units giving an overall representation of the structure of an Etendeka quartz latite unit. Also indicated are the differences observed between units of the two successions; note in particular the strongly amygdaloidal nature of the upper zone of the Tafelberg units, and the more strongly developed basal facies of the Springbok units. In terms of the unit structure, the Interbedded Coastal quartz latites most closely resemble the "Tafelberg-type" unit. Note that the basal facies indicated for the latter is more representative of that observed west of the ABFZ and the reader is referred to Plate 3.5 in the next chapter for an illustration of the basal facies of the Tafelberg units of the east.

2.7 XENOLITHS

Rare fragments of quartzite and granite occur as xenoliths in the quartz latite and are most frequently encountered in the Springbok quartz latites.

Fragments of quartzite, up to 20 cm long, are the most common xenolith. Apart from one isolated occurrence in the Lower Tafelberg unit at Ecke (Fig. 2.1), these xenoliths have only been found in the Springbok quartz latites, notably the upper unit. Both angular and rounded, resorbed clasts (Plate 2.33) are observed. In thin-section the quartzite is seen to consist of clear, anhedral grains of quartz up to 4.0 mm across. The colourless quartz is surrounded by a turbid, milky white quartz which appears to represent a recrystallisation of the larger grains and occurs along grain boundaries and intra-grain fractures. Fairly strong optical continuity exists between the large quartz grains and the surrounding recrystallised material, with triple junctions between regions of different optical orientation. Plate 2.34 illustrates the textures observed in these xenoliths. Whole rock XRF analysis show that the quartzite is composed of 98.7 % SiO_2 with Fe_2O_3, Al_2O_3, CaO and trace alkalis making up the remaining 1.3 %. Most trace element concentrations were below detection limits with the exception of Sr(31 ppm), Ba(23 ppm) and Cu(12 ppm).

Granite xenoliths occur less frequently and are again most common in the Springbok quartz latites. A medium-grained granite xenolith observed in a Lower

Fig. 2.12 Schematic Sections Through Idealised Etendeka Quartz Latite Flow Units.

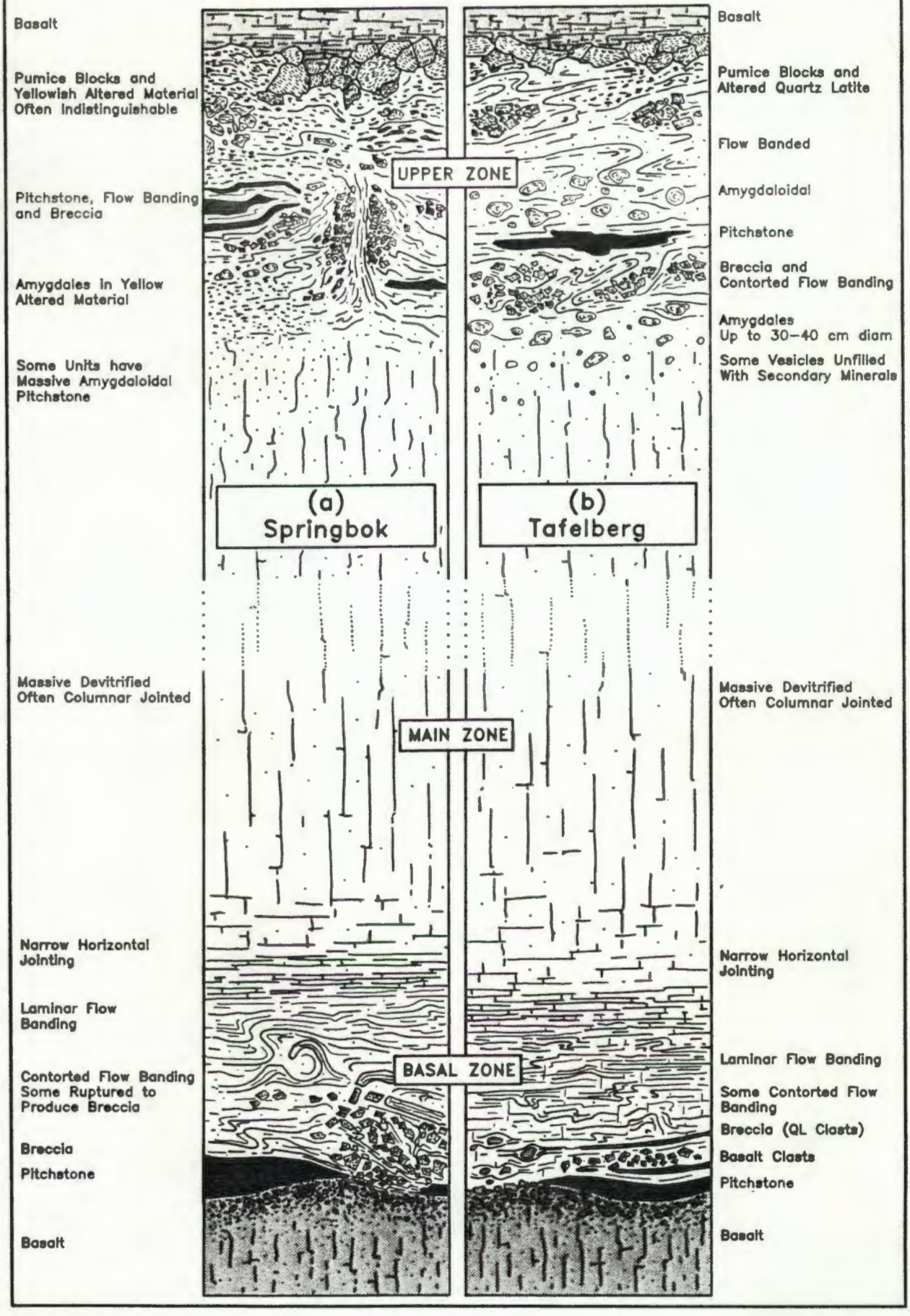

PLATE 2.33

Quartzite xenoliths in the Upper Springbok quartz latite at Awahab. These xenoliths are commonly rounded and embayed, although angular slab-like quartzite xenoliths have also been observed.

PLATE 2.34

X 20

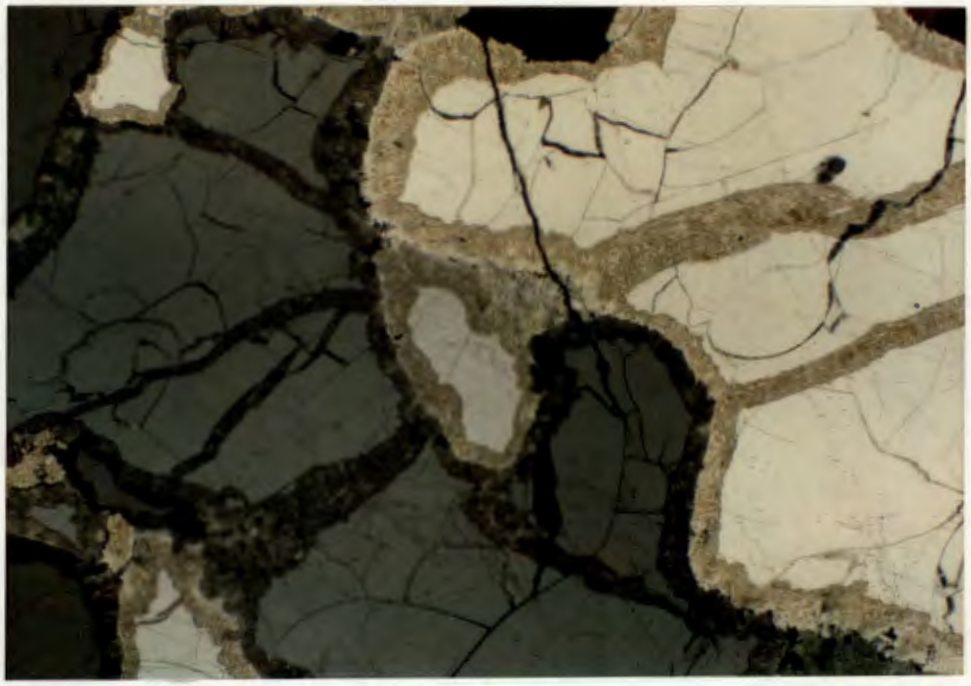

Photomicrograph of the quartzite xenolith material in thin section (crossed polarised light). The quartzite appears to have recrystallised along fractures and grain boundaries. Note that the recrystallised quartz is in optical continuity with the large clear grains of quartz.

Springbok quartz latite at Awahab was rather friable and altered and showed a slight increase in the amount of quartz near the rim. Anhedral, strongly resorbed quartz and feldspar crystals are separated by a buff-brown coloured mesostasis, which frequently exhibits radial devitrification textures and microlites, indicating that partial melting had occurred along grain boundaries. A single zircon crystal was observed within this mesostasis. In an isolated occurrence two large granite xenoliths (2 - 3 m long and 0.75 - 1.0 m thick) have been observed in basalt between the two Lower Springbok quartz latite units at Awahab. One xenolith contained large (2 - 3 cm) alkali-feldspar phenocrysts resembling some of the syn- and post-tectonic Damara granites in the Brandberg area (pers. comm., R.McG. Miller).

Isolated xenocrysts of quartz and of alkali-feldspar also occur within the quartz latites, predominantly the Springbok units. These xenocrysts are probably the result of disaggregation of larger xenoliths.

2.8 ALTERATION ZONES

Alteration is normally encountered in the basal and upper facies of the quartz latite flow unit, where it is often associated with precipitation of secondary minerals such as quartz and zeolite in vesicles. Zones of alteration affecting the entire unit are more rare. One such zone in The Lower Tafelberg unit at Tafelberg is described in subsection 2.5.3.

Another alteration zone of interest, indicated on Fig. 2.3a, occurs in the Interbedded Coastal succession, 2 - 3 km south of the northern limit of outcrop. The alteration in this case is confined to the lowest unit (the Lower Tafelberg) and extends for a distance of about 1 km north and south of the locality indicated. Plate 2.35 shows the outcrop where the most intense alteration was observed. The alteration has coloured the quartz latite shades of red, orange and purplish-grey enhancing primary flow features such as banding and pyroclastic, eutaxitic-like textures, illustrated in Plate 2.36. An interesting aspect of the outcrop is the occurrence of a post depositional brecciation and a network of veins containing quartz, zeolite and calcite (Plate 2.37). The rock appears to have been "expanded" and hydraulically fractured with breccia and secondary minerals filling angular cavities and fractures (Plate 2.36). The breccia clasts are highly angular and clasts with different alteration colours

PLATE 2.35

A zone of alteration in the Interbedded Coastal quartz latite block (see Fig. 2.3a for its locality). The dome-shaped outcrop consists of altered, variously coloured quartz latite which exhibits varying degrees of fracturing. The alteration appears to be confined to lower unit and does not affect the overlying unit which crops out above the alteration zone.

PLATE 2.36

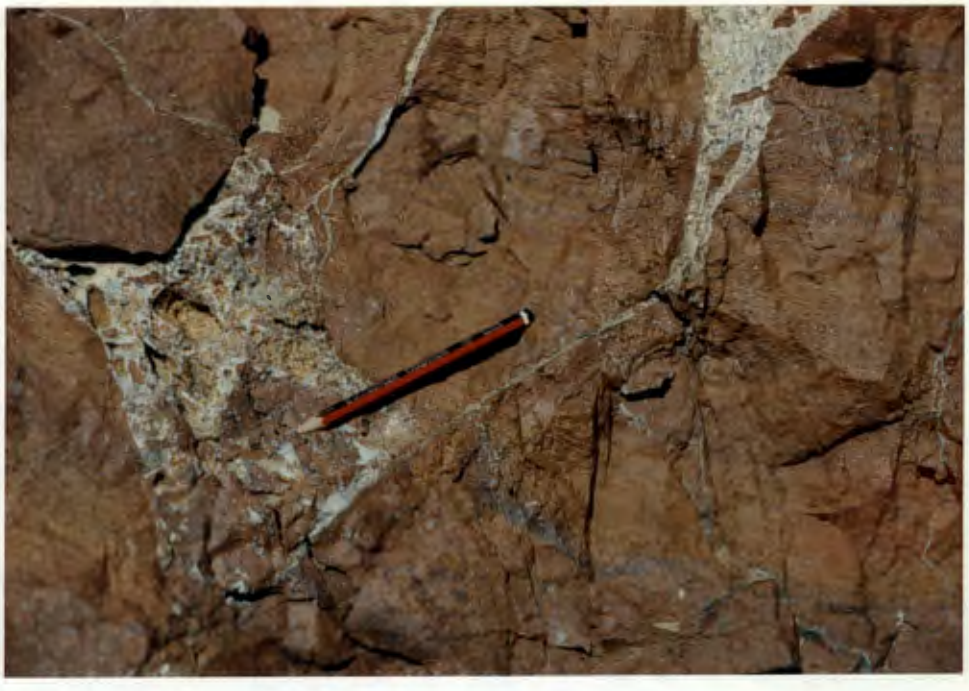

Alteration enhanced flow banding and fiammé-like features occur in the altered zone illustrated in Plate 2.35. Angular fracture cavities also occur and are filled by small clasts of quartz latite cemented by quartz, zeolite and calcite.

PLATE 2.37

Brecciated and fractured quartz latite from the alteration zone illustrated in Plate 2.35. The fractures are filled with quartz and zeolite. Quartz latite clasts with different alteration colours (centre to centre top) appear to occupy small breccia "pipes" suggesting that the alteration was accompanied by minor explosive activity.

are often juxtaposed. In general the outcrop is quite strongly lithified and bears little resemblance to the breccia horizons described for the basal and upper flow zones. It appears that this zone formed a hollow prior to the eruption of the overlying unit. Evidence for this is two fold; firstly outcrops of phyric pitchstone, identical with those from the overlying unit, are found "out of section" near the base of the hill in Plate 2.35. Secondly, there is a change in the attitude of cm-scale jointing in the overlying unit, this jointing which is normally sub-horizontal plunges steeply towards the altered zone lending support to the notion of a palaeo-topographic depression. The paucity of good outcrop and the blanketing of this zone by the overlying unit make it difficult to identify the cause of the alteration and brecciation. Such features may well be explained by explosive phreatic or hydrothermal activity, as discussed later in this thesis.

Some of the features described above have also been identified at other localities within the Lower Tafelberg quartz latite unit. At the head of Pilchard Gorge (Fig. 2.3a) a palaeo-topographic depression, filled by the Gemini quartz latite unit (subsection 2.5.4), is associated with strong alteration and some hydraulic fracturing of the Lower Tafelberg unit. Likewise in the Koigab Gorge two areas show similar features, one near the head of the gorge about 1 km west of the trace of the ABFZ (Fig. 2.3a) and the other in the region of the topographic hollow illustrated in Plate 2.3. In both cases "pipes" of fractured quartz latite occur, one up to 2 - 3 m in length. Furthermore, a dark fine-grained sample (SM-006) collected from the head of the gorge contained anomalously high concentrations of K_2O (~ 7.4 %) which is presumably due to some alteration process.

2.9 SUMMARY

In this Chapter the basic geological features of the Etendeka Formation in the southern Etendeka region have been described, and a more detailed account has been given of the outcrop characteristics of the quartz latites. This information will be integrated with petrographic and geochemical data in later sections to enable a reconstruction of the overall Etendeka Formation stratigraphy in this region, and to elucidate the petrogenesis and the volcanogenic origin of the quartz latites. A brief summary of the main points arising from this chapter are given below.

(1) The Etendeka Formation volcanics crop out over *ca.* 78,000 km^2 of northwestern Namibia and consist of a series of interbedded basalts, quartz latites and minor volumes of latite. In most areas the volcanics are sub-horizontal, although west of the ABFZ the lavas generally dip between 5° and 30° ENE in a belt of predominantly coast-parallel faulting that extends up to 30 km inland.

(2) The faulting is syn- to post-volcanic in age and is dominantly listric in character. The listric faulting appears to be predated by, and in some instances controlled by, conjugate sets of SSW and SE trending normal faults which cut the strike of the volcanics, and are thought to represent a reactivation of old basement structures.

(3) In the southern Etendeka the Etendeka Formation is composed of two distinct lava sequences which can be differentiated on the basis of their quartz latite stratigraphy. The Springbok Succession is the oldest sequence and crops out along the southern margin of the lava field east of the faulted coastal region. Towards the north the upper part of this sequence is truncated by intra-formational erosion and is transgressively overlain by lavas of the Tafelberg Succession. The stratigraphic position of the Interbedded Coastal quartz latite sequence is not readily apparent from field studies alone, but it will be shown in subsequent sections that it can be correlated with the Tafelberg Succession.

(4) The quartz latites occur as widespread sheet-like units typically between 40 and 300 m thick. Most of the quartz latite units observed appear to be single cooling units. However, differences in the structure of the Upper Springbok quartz latite, coupled with its great thickness (~300 m), suggest that it may be a compound cooling unit composed of several flows. The quartz latites are undoubtedly the products of exceedingly large eruptions. The Springbok quartz latites each cover an area of approximately 2,700 km^2 and the Lower Tafelberg quartz latite crops out over an area of *ca.* 4,500 km^2. The preserved volumes of individual quartz latite units range between 80 - 800 km^3 and must be considerably less than the original erupted volumes.

(5) A gradual thinning of the Lower Springbok quartz latite units towards the north indicates that their eruptive centre(s) was to the S or SSE. Similarly, thickening of the Lower Tafelberg quartz latite towards the SW

suggests that its eruptive centre probably lay to the west of the present coast line.

(6) The Gemini quartz latite unit, which consists of a chaotic assortment of altered clastic material, friable pitchstone and flow folded devitrified quartz latite, is of particular interest as it illustrates the pyroclastic nature of the quartz latite units.

(7) A quartz latite unit can be divided into basal, main and upper zones (Fig. 2.12). The main zone usually constitutes over 70 % of the unit and typically consists of featureless, devitrified quartz latite which yields little information as to the mode of eruption. The basal and upper zones of the flow are commonly 5 - 6 m and 7 - 10 m thick respectively and are characterised by flow banding, pitchstone lenses and breccia which contain rare pyroclastic textures.

(8) Extensive alteration zones in the Lower Tafelberg quartz latite unit are characterised by orange, red and purple colouration, post depositional brecciation and net-work veins of quartz, zeolite and calcite. These zones are probably the result of explosive phreatic or hydrothermal activity which took place as the unit cooled.

CHAPTER 3

PETROGRAPHY OF THE ETENDEKA FORMATION QUARTZ LATITES

3.1 INTRODUCTION

A description of the petrography of the Etendeka Formation quartz latites can be conveniently divided into two categories, namely, (1) the mineralogy and the textural fabrics displayed by the majority of the quartz latite samples, and (2) the rare, but significant, pyroclastic textures observed in some of the more rapidly chilled horizons of the quartz latite flow units. To highlight the importance of these different types of information they are presented separately, in this and the following chapter, and inferences drawn from them are discussed together in terms of quartz latite volcanology in a later chapter.

The first four sections of this chapter give a descriptive account of the textures, mineralogy and alteration encountered in most of the quartz latite samples collected. These are then followed by a section which shows the relationship between petrography and the volcanic stratigraphy, and indicates the type of petrographic variations observed within individual flow units. The southern Etendeka quartz latites and the Sarusas quartz latites and latites show significant differences in petrographic character. In order to emphasise these differences the southern Etendeka and Sarusas rocks are discussed in separate sections of this Chapter and a summary given in Table 3.3. The main petrographic features of the Tafelberg latite described by Erlank *et al.* (1984) are also included in Table 3.3.

Due to similarities in mineralogy and texture between the different groups of quartz latite in the southern Etendeka (Chapter 2) their petrography is presented in an integrated form to avoid lengthy repetition. Detailed petrographic descriptions of selected quartz latites and latites are documented in Appendix 1 and modal analyses are presented in Table 3.1. The samples for which data are given in Table 3.1 are considered to be representative of the quartz latite units discussed in Chapter 2. In Table 3.1 the quartz latite unit represented by a particular sample is indicated by an abbreviation. An explanation of these abbreviations is given in Table 3.2. It is important to note that these abbreviations are also used in subsequent tables and figure legends in this thesis.

Table 3.1 Modal Analyses of Main Quartz Latite Units and of two Sarusas Latites (Vol %).

ND ~ Not Determined * ~ Mt + Ilm

Sample and Unit N°	Plagioclase Phenocryst	Hypersthene Phenocryst	Pigeonite Phenocryst	Augite Phenocryst	Pyroxene Pseudomorph Phenocryst	Magnetite Phenocryst	Plagioclase Micro-phenocryst	Clinopyroxene Micro-phenocryst	Opaque Micro-phenocryst	Groundmass	Apatite (Ap) Vesicle (V)	Total Counts
SM-212 LS	6.0	–	1.6	–	–	1.0	–	–	–	91.4	0.02 Ap	4487
SM-212A LS	5.1	–	1.9	–	–	0.6	–	–	–	92.1	0.3 V	2705
SM-168 US	6.3	1.0	0.3	–	–	0.4	10.2	6.6	1.9	73.3	–	4959
SM-172 US	8.5	–	2.3	–	–	0.8	5.9	5.5	2.6	74.4	–	2619
SM-220 US	3.9	0.8	0.2	–	–	0.3	9.3	5.0	1.7	78.8	–	2993
SM-220A US	5.5	–	–	–	1.3	0.7	ND	ND	ND	92.5	–	3042
SM-179 LT	2.7	–	–	–	–	0.4	–	–	–	95.8	1.1 V	4096
SM-196 LT	1.9	–	–	–	–	1.1	5.3	4.9	3.1	83.7	–	2853
SM-060 MT	2.1	0.5	–	–	–	0.4	4.0	2.8	0.8	88.1	1.3 V	2546
SM-059 UT	–	–	–	–	–	–	13.5	4.5	4.2	77.8	–	1000
SM-007 TB	–	–	–	–	–	–	14.5	5.1	3.6	76.8	–	1000
SM-150 LIC	5.0	–	–	–	1.1	0.7	ND	ND	ND	93.2	–	2765
SM-160 LIC	1.4	0.9	–	–	–	0.4	10.3	12.1	3.5	71.4	–	2342
SM-103 MIC	–	–	–	–	–	–	12.6	4.6	3.5	79.3	–	1000
KLS-275 MIC	–	–	–	–	–	–	15.5	6.2	3.7	74.6	–	1500
SM-040 UIC	1.5	–	–	0.7	–	0.1	ND	ND	ND	97.7	–	4030
SM-163 UIC	4.5	–	–	0.8	–	0.4	ND	ND	ND	94.1	0.2 V	5183
SM-110 SQL	15.5	–	–	1.4	0.3	2.4*	ND	ND	ND	76.7	3.7 V	3520
SM-115 SQL	6.8	–	–	2.1	–	0.6	3.3	2.9	0.6	83.5	0.2 Ap	2279
KLS-315 SQL	–	–	–	–	–	–	8.0	8.4	3.1	80.5	–	2000
KLS-311 SL	16.9	–	–	1.1	1.3	1.2*	–	–	–	79.1	0.4 Ap	2541
KLS-327 SL	4.8	–	0.9	0.9	–	0.8*	ND	ND	ND	92.1	0.5 Ap	3035

TABLE 3.2

Abbreviations used in Tables and in Figure legends to denote the different types of quartz latite. 1 - 10 are groups of quartz latite from the southern Etendeka.

(1)	**LS** - Lower Springbok Quartz Latite
(2)	**US** - Upper Springbok Quartz Latite
(3)	**Alb** - Albin and Gobobosebberge Quartz Latite
(4)	**LT** - Lower Tafelberg Quartz Latite
(5)	**MT** - Middle Tafelberg Quartz Latite
(6)	**UT** - Upper Tafelberg Quartz Latite
(7)	**TB** - Tafelberg Beacon Quartz Latite
(8)	**LIC** - Lower Interbedded Coastal Quartz Latite
(9)	**MIC** - Middle Interbedded Coastal Quartz Latite
(10)	**UIC** - Upper Interbedded Coastal Quartz Latite
(11)	**SQL** - Sarusas Quartz Latite
(12)	**SL** - Sarusas Latite

3.2 SOUTHERN ETENDEKA QUARTZ LATITES

3.2.1 Introduction

The quartz latites which outcrop in the southern Etendeka region (Fig. 2.2) are generally porphyritic to microporphyritic lavas with glassy to devitrified groundmass textures. The photomicrographs in Plates 3.1 and 3.2 illustrate the range of textures observed in these rocks and provide a focus around which the petrography of the quartz latites can be discussed.

The quartz latites have total phenocryst contents of generally less than 10 modal % (Table 3.1), which is typical of many rhyolites from bimodal (acid - basic) associations (Ewart, 1979). Individual subhedral to euhedral, phenocrysts of plagioclase, pyroxene and titanomagnetite are commonly associated in glomeroporphyritic aggregates of these phases (Plate 3.1a-c). The microphenocrysts normally show a random distribution, although they may exhibit a subparallel alignment in flow banded rocks. The quartz latites exhibit a variety of groundmass textures from holohyaline, occasionally with abundant microlites and flow banding, to devitrified samples with spherulitic cryptocrystalline and interstitial granophyric areas. A continuous range of textures can be demonstrated between these two extremes indicating a rather complex devitrification history.

Occasionally a continuous range in crystal sizes makes the distinction between the phenocryst and microphenocryst populations difficult using a simple grain size discriminant. However, crystal morphology and distribution throughout the rock, coupled with the overall grain size, help to distinguish different crystal generations.

The mineral phases in pitchstone material sampled from various quartz latite units are essentially unaltered and this has proved invaluable in characterising primary quartz latite textures and mineralogy. Phenocrysts encountered in the quartz latites include plagioclase, hypersthene, pigeonite, augite and titanomagnetite. It is important to note that no primary hydrous phases have been observed. The southern Etendeka quartz latites can be classified into six different groups on the basis of their phenocryst assemblage:

(1) Non-porphyritic.

(2) Plagioclase + titanomagnetite; quartz latites with this assemblage are commonly sparsely porphyritic.

PLATE 3.1

3.1a Lower Springbok quartz latite, pitchstone (SM-017). PPL
Slightly rounded phenocrysts of plagioclase, pigeonite and titanomagnetite form compact glomeroporphyritic aggregates. The groundmass consists of a grey glass with very fine microlites, and shows slight alteration along fractures and around sparse vesicles.

3.1b Upper Springbok quartz latite, pitchstone (SM-061). PPL
An aggregate of subhedral phenocrysts of plagioclase and hypersthene with smaller grains of titanomagnetite. A rim of pigeonite is clearly developed on the outer surfaces of the hypersthene, but is absent where the hypersthene and plagioclase are intergrown. The partially devitrified glassy groundmass encloses microphenocrysts of plagioclase, pigeonite and titanomagnetite.

3.1c Upper Springbok quartz latite, pitchstone (SM-172). PPL
Subhedral phenocrysts of plagioclase, pigeonite and titanomagnetite are commonly associated together in aggregates. Microphenocrysts of the same phases are enclosed in a partially devitrified, microlitic glass. Flow banding in the groundmass is due to a varying abundance of microphenocrysts, microlites and a dusty opaque material.

3.1d Upper Springbok quartz latite, devitrified (SM-174). PPL
Devitrified equivalent of Plate 3.1c. Phenocrysts show signs of alteration, the plagioclase is turbid and the pigeonite altered along fractures. The groundmass consists of cryptocrystalline material (medium to dark grey) with irregular patches of quartz and alkali-feldspar (small whitish areas).

3.1e Lower Interbedded Coastal quartz latite, pitchstone (SM-066). PPL
Phenocrysts of plagioclase, hypersthene and titanomagnetite enclosed in a partially devitrified, glassy groundmass with microlites of plagioclase, clinopyroxene and titanomagnetite. Unlike the Upper Springbok sample the hypersthene in this sample is not rimmed by pigeonite.

3.1f Lower Interbedded Coastal quartz latite, devitrified (SM-150). PPL
An aggregate of altered plagioclase and hypersthene phenocrysts, the latter completely pseudomorphed by a green clay mineral. The groundmass which contains microphenocrysts of plagioclase, clinopyroxene and titanomagnetite consists of cryptocrystalline spherulitic areas (dark and medium grey) with interstitial areas of quartz and alkali-feldspar (pale grey and white).

3.1g Middle Interbedded Coastal quartz latite, devitrified (SM-103). PPL
Quenched microphenocrysts and microlites of plagioclase and grains of titanomagnetite enclosed in a buff coloured cryptocrystalline groundmass. Clinopyroxene is also present, but is not easily identified in this plate.

3.1h Upper Interbedded Coastal quartz latite, devitrified (SM-161). XPL
Aggregates of plagioclase, augite and titanomagnetite phenocrysts enclosed in a groundmass of dark cryptocrystalline material and interstitial granophyre. Notice that while the plagioclase has a turbid altered appearance the augite is relatively unaltered.

PPL = Plane Polarised Light

XPL = Cross Polarised Light

PLATE 3.1

(a) 1.0 mm

(b) 0.5 mm

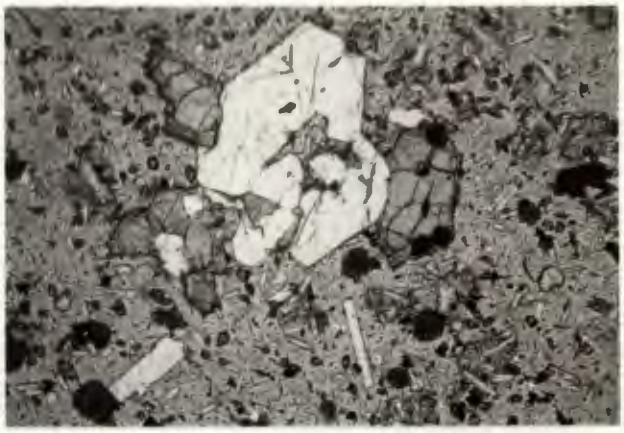

(c) 1.0 mm

(d) 1.0 mm

(e) 0.5 mm

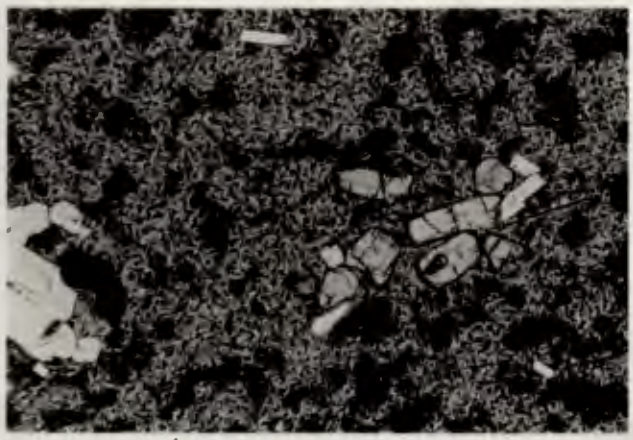

(f) 1.0 mm

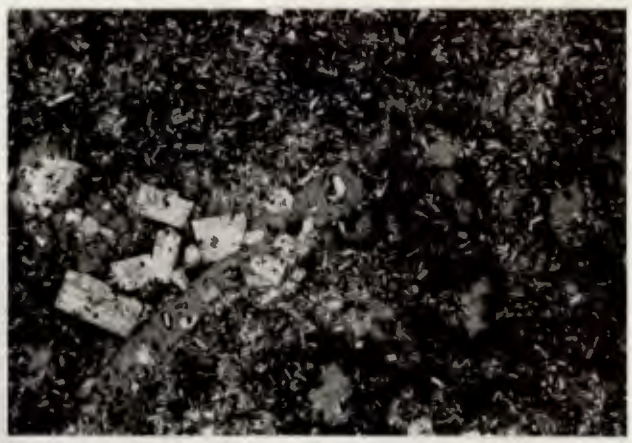

(g) 0.5 mm

(h) 1.0 mm

PLATE 3.2

3.2a (i) Lower Interbedded Coastal quartz latite (SM-154). XPL
Sieve textured plagioclase phenocryst showing multiple twinning. The entire structure is in optical continuity and the dark areas within the crystal are isotropic groundmass glass.

(ii) Lower Springbok quartz latite (SM-212). PPL
Plagioclase phenocryst showing a rounded inclusion rich central portion, with a poorly developed sieve texture, surrounded by an overgrowth of inclusion-free material. No optical zonation is observed across this crystal.

3.2b Lower Springbok quartz latite, pitchstone (SM-208). PPL
A predominantly monomineralic aggregate of plagioclase phenocrysts (with the exception of four small pigeonite grains). Large, blocky, subhedral to euhedral crystals appear to have nucleated around a central core consisting of much smaller anhedral crystals of plagioclase and minor magnetite. The core has a metamorphic-style texture in XPL and may be xenolithic in origin.

3.2c Tafelberg Beacon quartz latite, devitrified (SM-007). XPL
Microphenocrysts of plagioclase, augite and titanomagnetite set in a cryptocrystalline to granophyric groundmass. The phenocrysts have acted as centres for devitrification and are commonly surrounded by cryptocrystalline material (medium to dark grey). The devitrification texture is over-printed by the crystallisation of quartz and alkali-feldspar (pale grey - whitish areas) which is most strongly developed interstitially.

3.2d Tafelberg Beacon quartz latite, devitrified (SM-007). XPL
Interstitial granophyre. The clear areas (centre right) are mainly quartz crystals which have sparse rod-like inclusions. In contrast the alkali-feldspar (centre) has a very turbid appearance with densely crowded inclusions of the devitrified material.

3.2e Sarusas quartz latite, pitchstone (SM-115). PPL
Sparse, subhedral to euhedral phenocrysts of plagioclase and augite enclosed in a grey, sparsely microporphyritic glass with densely crowded microlites. Microphenocrysts are of plagioclase, augite and titanomagnetite. The white crystals adhering to, and included in, the large augite phenocryst (right) are apatite.

3.2f Sarusas quartz latite, devitrified (KLS-315). PPL
Long acicular crystals of altered clinopyroxene, and microphenocrysts of plagioclase and magnetite are enclosed in a devitrified groundmass with a strongly developed granophyric to micrographic texture. Laths and quenched needles are crudely aligned (bottom left to top right).

3.2g Sarusas quartz latite, devitrified (KLS-313). PPL
Sparse microphenocrysts of plagioclase, clinopyroxene and magnetite are enclosed in a spherulitic to granophyric textured groundmass. The spherulites (centre right and centre top) have a radiating fabric.

3.2h Sarusas latite, holocrystalline (KLS-327). PPL
Glomeroporphyritic aggregates of subhedral plagioclase, pigeonite (cracked morphology), augite and opaques (Ti-Mt and Ilm) are set in a groundmass of stubby laths of feldspar (some anorthoclase), equant grains of clinopyroxene and opaque and interstitial quartz and alkali-feldspar. The white bladed crystals in the aggregate are apatite.

PLATE 3.2

(a) (i) 0.5 mm (ii) 0.5 mm

(b) 1.0 mm

(c) 0.5 mm

(d) 0.25 mm

(e) 1.0 mm

(f) 1.0 mm

(g) 1.0 mm

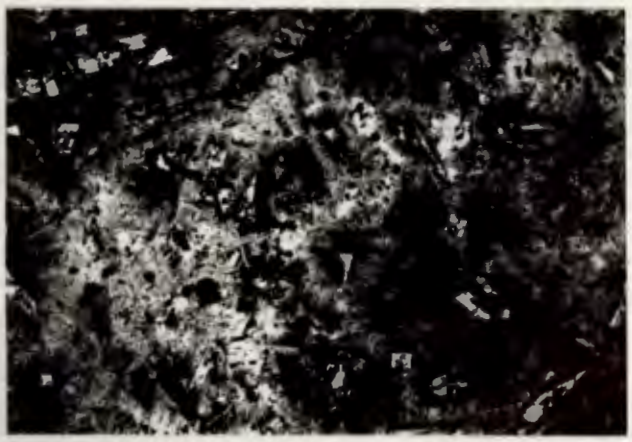

(h) 1.0 mm

(3) Plagioclase + pigeonite + titanomagnetite.

(4) Plagioclase + hypersthene + titanomagnetite ± pigeonite; where the hypersthene is rimmed by pigeonite.

(5) Plagioclase + hypersthene + titanomagnetite ± pigeonite.

(6) Plagioclase + augite + titanomagnetite ± pigeonite.

The occurrence of these petrographic types in the various quartz latite units is discussed in more detail in Section 3.5 and is summarised in Table 3.4.

Table 3.1 presents detailed modal analyses of the petrographic type examples described in Appendix 1. Phenocryst abundances in the porphyritic varieties range from 2.3 to 11.6 modal % with an average of approximately 5.5 %. The microphenocrysts range between 7.6 and 25 modal %, when present, and have an average of approximately 19 %. Typical plagioclase:pyroxene:titanomagnetite ratios estimated for the phenocryst and microphenocryst populations are 9:3:1 and 4:2:1 respectively.

3.2.2 Phenocryst Mineralogy

3.2.2.1 Plagioclase

Plagioclase is the most abundant phenocryst phase constituting between 1.5 and 8.5 % of the mode (Table 3.1). It commonly forms blocky, subhedral to euhedral crystals (Plate 3.1a-f,h). Bladed, elongate morphologies are observed in the Upper Interbedded group of quartz latites. Occasionally broken or fractured crystals are encountered and in some instances plagioclase phenocrysts are somewhat rounded (Plate 3.1a). Most crystals range in size between 0.25 and 2.5 mm, although larger, frequently sieve-textured, crystals up to 4.5 mm have been observed (Plate 3.2a(i)). Plagioclase phenocrysts commonly display simple Carlsbad twinning and to a lesser degree poly-synthetic albite twinning. Fairly weak compositional zonation with both continuous and discontinuous variations is not uncommon. Both normal and reverse zonation is encountered. More rarely plagioclase phenocrysts exhibit a zonal arrangement of melt inclusions which are parallel or sub-parallel to the crystal faces.

Sieve-textured plagioclase phenocrysts occur as both discrete and interlocking crystals and often show multiple twinning (Plate 3.2a(i)). A feature commonly observed is that of an anhedral sieve-textured central portion

with a complete or partial syntactic overgrowth. The subsequent plagioclase growth commonly shows subhedral to euhedral crystal faces, although in some cases it may also have an embayed, anhedral form. This overgrowth texture is best displayed when the central area is inclusion rich and the subsequent rim inclusion free (Plate 3.2a(ii)). Compositional zonation may or may not be present in sieve-textured crystals and where it does occur it is similar to that described earlier. Most of the sieve-textured crystals determined by microprobe analysis have a similar range in composition to the complete crystals. Some large (~15 mm) anhedral grains occasionally encountered are probably xenocrystic in origin and do not normally exhibit overgrowth textures.

Microphenocrysts of plagioclase (Plate 3.1) have modal proportions of 0 - 15.5 % (Table 3.1). They commonly occur as subhedral to euhedral lath shaped crystals (0.025 - 0.5 mm), although skeletal and quench textured morphologies are also observed (Plate 3.1g).

3.2.2.2 Hypersthene

Hypersthene occurs as sparse phenocrysts and microphenocrysts and constitutes no more than 0.5 - 1.0 % of the mode (Table 3.1). Hypersthene usually forms blocky to bladed, subhedral crystals, although a full range of anhedral to euhedral morphologies are encountered (Plate 3.1b,e). These crystals display a continuous range of sizes between 0.1 and 3.5 mm, the elongate, bladed crystals yielding the larger dimensions. No twinning or compositional zonation has been observed. In the Upper Springbok quartz latite, hypersthene is distinctively rimmed by pigeonite and there is a tendency for the crystals to be more blocky and slightly rounded. The pigeonite coronas are often complete, but are notably absent where the crystal is closely intergrown with plagioclase and magnetite. This is illustrated in Plate 3.1b where the pigeonite rims are clearly visible except where the hypersthene abuts against plagioclase.

3.2.2.3 Pigeonite

Phenocrysts of pigeonite (Plate 3.1a,c,d) commonly constitute approximately 2 % of the mode, although their modal proportion in hypersthene-bearing rocks is much lower (Table 3.1). Crystals of pigeonite occur in a continuous range of sizes from 0.1 to 1.5 mm, exhibit a blocky, anhedral to subhedral morphology and are often quite strongly rounded. Small phenocrysts which occur in the hypersthene-phyric quartz latites have a tendency to be more euhedral and have

less rounded outlines. Pigeonite phenocrysts occasionally exhibit simple twinning but are not compositionally zoned.

Microphenocrysts of pigeonite occur as subhedral to anhedral grains and laths 0.05 to 0.3 mm in size. Because of their size they are not easily distinguished from more calcium-rich clinopyroxenes other than by microprobe analysis, and in Table 3.1 'clinopyroxene' microphenocrysts, inclusive of pigeonite, constitute between 3 and 12 % of the mode.

3.2.2.4 Augite

Augite phenocrysts occur as very sparse blocky to bladed crystals which constitute less than 1.0 % of the mode and range in size between 0.2 and 3.0 mm. These crystals are subhedral to anhedral in form and are often quite strongly resorbed with rounded margins and lobate embayments (Plate 3.1h). No compositional zonation or twinning has been observed. In rare instances augite phenocrysts have cores of pigeonite.

Microphenocrysts of augite occur as subhedral to anhedral grains and laths between 0.05 and 0.3 mm in size and are not easily distinguished from pigeonite; although, some of the larger crystals in the non-porphyritic Upper Tafelberg and Tafelberg Beacon units have a characteristic greenish tinge.

3.2.2.5 Titanomagnetite

Titanomagnetite occurs as sparse phenocrysts in most quartz latites and has modal proportions of between 0.3 and 1.1 %. It forms predominantly subhedral to anhedral, often rounded crystals, 0.1 to 0.5 mm in diameter.

Equant microphenocrysts of titanomagnetite have modal proportions of between 0.8 and 4.2 %. They exhibit a complete range of anhedral to euhedral shapes and a grain size of the order of 0.05 - 0.1 mm.

Titanomagnetite grains exhibit a variety of oxidation textures which are described in section 3.4.

3.2.3 Phenocryst Inter-relationships

Phenocrysts of the phases described above are commonly associated in glomeroporphyritic aggregates and the principal textures observed in these aggregates are summarised below:

(1) Phenocrysts which occur towards the centre of a tightly intergrown cluster are commonly anhedral, apparently having competed for growth space with neighbouring crystals. Those crystals on the outer edge of the aggregate exhibit a more euhedral form, as do the phenocrysts in more open clusters (Plate 3.1a-c).

(2) Both poly- and mono-mineralic aggregates are observed, the latter usually of plagioclase (Plate 3.2b). Sieve-textured plagioclase crystals are rarely associated with polymineralic aggregates and tend to form discrete crystals or small aggregates on their own.

(3) Unusual aggregates of plagioclase and magnetite are occasionally observed in the Springbok quartz latites and are similar to the predominantly plagioclase aggregate in Plate 3.2b. They consist of a dense, rounded, central area of small, equigranular crystals of plagioclase and magnetite surrounded by larger, more euhedral, plagioclase phenocrysts, some of which may be sieve textured. The origin of these clusters is unclear, although one possible explanation is that the central area represents xenolithic material which has acted as a nucleation point for magmatic crystallisation. Betton (1978) reported similar occurrences from the Lebombo rhyolites, which he interpreted as being cognate cumulates ripped up from the magma chamber or conduit during eruption. In the Etendeka quartz latites the close association of large plagioclase phenocrysts with this material indicates its existence in the magma chamber for some time prior to eruption.

No preferred order or sequence of crystallisation can be deduced for the phenocryst assemblages observed. The close association of many phenocrysts in glomeroporphyritic aggregates suggests that crystallisation was broadly synchronous. In some instances plagioclase partially encloses crystals of pyroxene and magnetite which may be due to the more rapid growth of plagioclase. Occasionally, magnetite and euhedral crystals of apatite occur towards the centre of large phenocrysts indicating that they may have been some of the earliest phases to start crystallising.

3.2.4 Groundmass Petrography

Some of the groundmass textures displayed by the Etendeka quartz latites are illustrated in Plates 3.1 and 3.2. A range of textures between glassy and devitrified or felsitic occur, and a description of the transition from one type

to the other is given in Section 3.4. In this section the main textural features of the glassy and devitrified samples are presented.

3.2.4.1 Glassy Groundmass

Two types of glassy groundmass are recognised in the quartz latites:

(1) The most common variety of glassy groundmass consists of a grey to clear glass with abundant microlites and crystallites (Plate 3.1a-c,e). Weak polarisation colours exhibited by the microlites enable the identification of feldspar and clinopyroxene, as well as small grains of magnetite. Occasionally feldspar and clinopyroxene form acicular crystals up to 0.5 mm long (0.02 mm wide), but more usually form grains and laths less than 0.01 mm in size. The microcrystalline material exhibits a range of habit with globular, rod-like and hair-like crystals often showing branching, radiating and dendritic quench textures.

Banding is frequently observed and is caused by: (1) differences in the abundance of microlites and microphenocrysts, (2) occasional subparallel alignment of microlites and microphenocrysts, and (3) differences in glass colour, brought about by variable concentrations of a submicroscopic, dusty opaque material (Plate 3.1c).

(2) The second type of glass encountered is brown and contains no microcrystalline material. In handspecimen pitchstones with this type of groundmass exhibit a bright vitreous lustre. Whole rock loss-on-ignition values, greater than 3 % (Chapter 6), indicate that this type of glass is quite strongly hydrated. Contorted bands, flame structures and abrupt changes in the glass colour are evidence of a welded clastic origin; features which are described in more detail in Chapter 4.

3.2.4.2 Devitrified Groundmass

The term "devitrified" is used in a broad sense to describe non-glassy quartz latites although it is not always certain that the groundmass textures observed are the result of devitrification from a wholly glassy state. Some of the textures encountered are illustrated in Plates 3.1, 3.2 and 3.3. They range from completely cryptocrystalline (Plate 3.1g) to a network of cryptocrystalline material with interstitial intergrowths of quartz and alkali feldspar (Plates 3.2c,d and 3.3c,d). The cryptocrystalline material is generally buff to dark brown in colour and exhibits a faint, patchy, often radial anisotropy.

PLATE 3.3

3.3a Lower Tafelberg quartz latite, pitchstone (SM-065). PPL
Microphenocrysts of plagioclase, clinopyroxene and titanomagnetite enclosed in a spherulitic glass. The spherulites, which are clearly visible, have a radiating habit which is sometimes centered about a microphenocryst. The white interstitial areas are glass.

3.3b Lower Tafelberg quartz latite, pitchstone (SM-065). PPL
Spherulite at higher magnification. As devitrification proceeds the interstitial glass is invaded by fine black needles which are then replaced by a more even textured material (bottom right) which has a faint radial anisotropy. A microphenocryst of clinopyroxene in clearly visible in the glass (top left).

3.3c Lower Tafelberg quartz latite, devitrified (SM-190). PPL
Completely devitrified groundmass texture with anastomosing spherulites and interstitial granophyric quartz and alkali-feldspar. Compare with the texture in Plate 3.3a.

3.3d Lower Tafelberg quartz latite, devitrified (SM-151). XPL
Strongly developed micrographic texture (quartz and alkali-feldspar) which over-prints an earlier devitrified fabric (dark grey turbid areas). Microphenocrysts of plagioclase are barely recognisable.

3.3e Lower Tafelberg quartz latite, devitrified (SM-194). PPL
Titanomagnetite (dark grey) showing progressive oxidation to titanomaghemite (pale grey). The reaction proceeds along curved fractures which are thought to result from changes in volume induced by the inversion of the spinel structure to that of a cationic deficient spinel.

3.3f Lower Tafelberg quartz latite, devitrified (SM-198). PPL
Titanomagnetite phenocrysts showing C_2 - C_3 stage, high temperature, oxidation. Trellis ilmenite lamellae are exsolved along the {111} planes and the host magnetite (medium grey) shows retrogressive alteration to hematite (white), which has resulted in an increased reflectivity of the phenocrysts.

3.3g Sarusas quartz latite, devitrified (KLS-316). PPL
Titanomagnetite showing the C_4 stage of high temperature oxidation. Fine and coarse grained trellis ilmenite lamellae show pseudomorphic oxidation to ferri-rutile (medium grey) and ferri-ilmenite (pale grey). The host magnetite (dark grey) is largely altered to hematite (white) and shows exsolved needles (black) of pleonaste-magnesioferrite$_{ss}$.

3.3h Sarusas quartz latite, devitrified (KLS-316). XPL
Expanded view of the titanomagnetite phenocryst in Plate 3.3g illustrating the extent of the ilmenite exsolution. The ilmenite lamellae display a distinct anisotropism as does the hematite replacing magnetite.

PLATE 3.3

(a) 0.5 mm

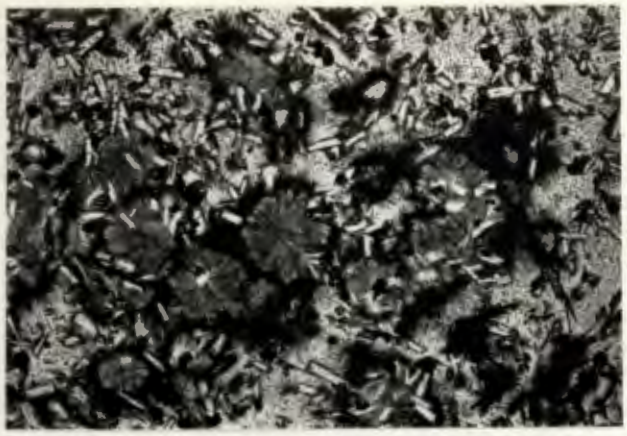

(b) 100 μm

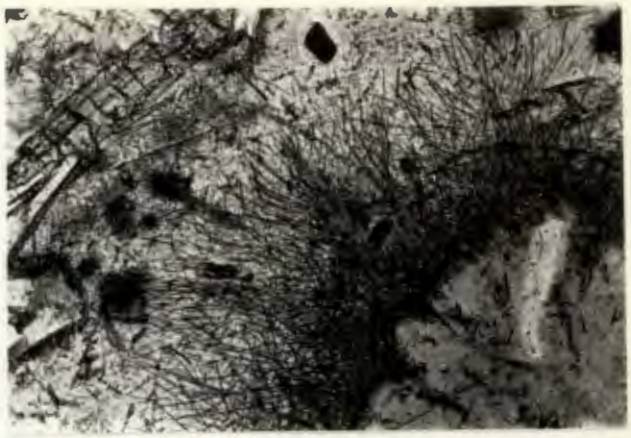

(c) 0.5 mm

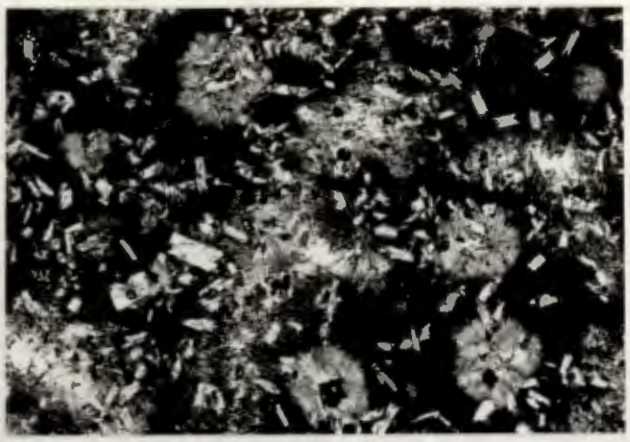

(d) 0.5 mm

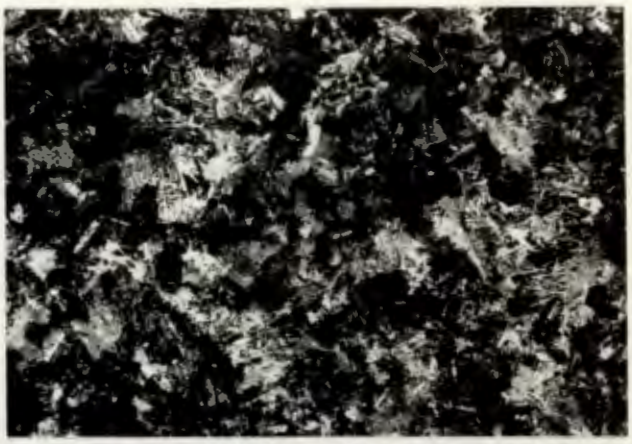

(e) 50 μm

(f) 100 μm

(g) 20 μm

(h) 50 μm

Spherulites, which are illustrated in Plates 3.1f and 3.3a-c, are quite common and often display delicate radiating fabrics which "penetrate" the interstitial areas occupied by quartz and alkali feldspar. Anhedral grains of quartz and alkali feldspar have granophyric and micrographic textures which are illustrated in Plates 3.2c,d and 3.3d respectively. Alkali feldspar is typically turbid in appearance with material included from the spherulitic regions and often forms continuously zoned syntactic coronas round plagioclase microphenocrysts. Unlike alkali feldspar, quartz occurs as fairly clear crystals with relatively few inclusions (Plate 3.2c,d).

The size of the granophyric and cryptocrystalline domains varies considerably and appears to be a function of flow thickness and stratigraphic height within a single unit. The changes in texture observed in a single flow unit are illustrated for the Wêreldsend serial section in Plate 3.5, in which one can clearly see an increase in grain size towards the centre of the flow.

The relationship between the cryptocrystalline and granophyric material is not always clear. However, in the majority of cases the growth of anhedral quartz and alkali feldspar, which often include delicate devitrified material, apparently post-dates an initial devitrification event and requires the subsolidus development of quartz and alkali feldspar.

3.2.5 Accessory Minerals and Inclusions

3.2.5.1 Apatite

Apatite forms euhedral, elongate, hexagonal prisms and is the most common accessory mineral encountered. It is frequently associated with glomeroporphyritic aggregates, where it is often present as inclusions in other minerals. Isolated crystals also occur in the groundmass. Apatite appears to have crystallised early and in many cases apparently provided nucleation centers around which the main phenocryst phases crystallised.

3.2.5.2 Ilmenite

Primary ilmenite is an extremely rare accessory phase in the southern Etendeka quartz latites and has only been identified in one of the Lower Springbok samples. In this instance it forms part of two composite grains with titanomagnetite and despite the presence of secondary trellis ilmenite in the adjacent titanomagnetite it was almost certainly primary.

3.2.5.3 Sulphide

Sulphide, predominantly chalcopyrite, has been observed in several fresh pitchstone specimens. It occurs as small isolated blebs and small blocky crystals (<0.01 mm) often associated with titanomagnetite. Small sulphide inclusions have also been seen in titanomagnetite crystals.

3.2.5.4 Inclusions in minerals

The most common inclusions observed in the main phenocryst phases are of glass, although occasional inclusions of apatite and magnetite also occur. Inclusions of glass take on a variety of forms from small micron-sized blebs to larger inclusions which exhibit a variety of shapes and may contain crystallites. The larger inclusions often occur towards the centre of plagioclase crystals and have a tendency to be dark and murky. Clear, oval inclusions (~0.01 mm) of unaltered glass have been encountered in several pigeonite phenocrysts. Microprobe analyses of these inclusions show them to be rhyolitic in composition.

3.3 SARUSAS QUARTZ LATITES AND LATITES

Differences in petrographic character between the Sarusas quartz latites and latites and the southern Etendeka quartz latites are generally quite subtle, and are summarised in Table 3.3. Most of the textural observations, for example, crystal habit, glomeroporphyritic aggregates and devitrification textures, are very similar to those described for the southern Etendeka quartz latites in the previous section. For more detailed descriptions of type examples the reader is referred to Appendix 1 and to Table 3.1 for modal analyses. Plates 3.2e-h illustrate the textures and mineralogy observed in some units.

One of the main differences between the Sarusas rocks and the southern Etendeka quartz latites is that augite is the main pyroxene phenocryst in all the porphyritic units sampled in the Sarusas district, whereas in the southern Etendeka the augite bearing phenocryst assemblage is restricted to a few thin flows in the Upper Interbedded Coastal succession. The following assemblages have been observed:

Table 3.3 Comparison of the Quartz Latites and Latites of the Sarusas and southern Etendeka Areas.

	Phenocryst Assemblage	Phenocryst Contents	Plagioclase	Pyroxene	Accessory Phases	Groundmass Texture
SARUSAS QUARTZ LATITES	(1) Non–Porphyritic (2) Pl + Aug + Ti–Mt ± Pig ± Ilm	Up to 20 %	Frequently zoned and twinned. Few sieve textured crystals. Andesine composition. Some large up to 10 mm long.	Principally augite. Some pigeonite pseudomorphs.	Apatite is common and ilmenite is rare	Predominantly de–vitrified. Although glassy and holo–crystalline varieties also occur.
SARUSAS LATITES	(1) Pl + Aug + Pig + Ti–Mt + Ilm	7 – 20 %	Similar to above	Principally augite and pigeonite.	Apatite and ilmenite are common. Up to 0.5 modal % apatite	Holocrystalline.
SOUTHERN ETENDEKA QUARTZ LATITES	(1) Non–Porphyritic (2) Pl + Ti–Mt (3) Pl + Pig + Ti–Mt (4) Pl + Hyp + Ti–Mt ± Pig (5) Pl + Aug + Ti–Mt ± pig	Generally < 8 %	Frequently sieve textured. Labradorite compos–itions. Generally < 3.0 mm diametre.	Mainly hypersthene and pigeonite with subordinate augite	Apatite and ilmenite are rare.	Glassy to devitrified
TAFELBERG LATITE	(1) Clinopyroxene + Albite (the latter presumed xenocrystic)	–	Generally absent, only found as presumed xenocrysts of pure albite.	Elongate comb text–ured prisms ≤ 5 mm long are charcter–istic. Subcalcic augite to pigeonite.	–	Holocrystalline with acicular Cpx, eu–hedral K–feldspar laths, magnetite and interstitial quartz

Sarusas quartz latites

(1) Non-porphyritic

(2) Plagioclase + augite + titanomagnetite ± pigeonite.

Sarusas latites

(1) Plagioclase + augite + pigeonite + titanomagnetite ± ilmenite.

The phenocryst content in most samples is less than 10 modal %, but occasionally phenocryst abundances of up to 20 modal % are observed (Table 3.1). Phenocryst contents tend to decrease in the more evolved samples (~ 70 wt % SiO_2) and in these samples the phenocrysts, particularly augite, have a more anhedral, embayed habit.

Apatite is a more common accessory phase in the Sarusas quartz latites and latites than in the southern Etendeka quartz latites, with modal proportions of up to 0.5 % in some latite samples. Apatite occurs as euhedral to subhedral, elongate hexagonal prisms which are commonly associated with glomeroporphyritic aggregates and as inclusions in the main phenocryst phases (Plate 3.2h).

The latites and some of the quartz latites have holocrystalline groundmass textures which are not encountered in the southern Etendeka quartz latites. This texture consists of an equigranular fabric (0.05 - 0.2 mm) of stubby plagioclase laths, grains of pyroxene and opaque material set in a granophyric intergrowth of anhedral quartz and alkali feldspar (Plate 3.2h). Plagioclase is often zoned and may be syntactically overgrown by alkali feldspar.

3.4 QUARTZ LATITE ALTERATION

3.4.1 Introduction

Some of the geochemical variation encountered in the Etendeka quartz latite data set can be linked with post-eruptive alteration processes. This section describes some of the petrographic features attributed to alteration and provides some petrographic constraints on how alteration may have affected the whole rock chemical compositions. Devitrification, which affects the majority of samples collected, is considered to be the main alteration process occurring in the quartz latites. The alteration of pitchstone by hydration also occurs, and may be accompanied by secondary mineralisation. Devitrification is normally

accompanied by phenocryst alteration. Little work has been carried out on the conditions or products of plagioclase and pyroxene alteration. However, a study of the oxidation textures in titanomagnetite has revealed information related to the post-eruptive cooling and oxidation of a quartz latite unit and this is reported in Section 3.5.

3.4.2 Alteration of Silicate Minerals

Plagioclase and pyroxene display a variety of alteration products which, without extensive X-ray diffraction studies are not easily identified. The susceptibility of these phases to alteration varies, but can be generalised as follows where augite represents the most resistant mineral:

Hypersthene + Plagioclase < Pigeonite < Augite

Fresh cores of pigeonite and unaltered augite may occur when plagioclase is quite strongly altered, and in some instances unaltered pigeonite coronas occur round completely pseudomorphed hypersthene.

3.4.2.1 Plagioclase

The alteration of plagioclase is characterised by a turbid appearance and a patchy extinction pattern. Albitisation and replacement of plagioclase by zeolite minerals is well known (Deer *et al.*, 1963) and minerals such as sericite, carbonate and a green clay mineral are also observed. Plate 3.1d,f,h shows the appearance of altered plagioclase typical to many of the quartz latites observed. Primary twin and zonation structures disappear on alteration and in some strongly devitrified samples microphenocrysts of plagioclase are so severely altered that they are barely recognisable.

3.4.2.2 Pyroxene

Hypersthene is commonly replaced by a bright green-yellow pleochroic mineral (Plate 3.1f) which has a radiating habit and is similar to the iron-rich smectite, nontronite (Deer *et al.*, 1966). Pigeonite is replaced by an amorphous greenish-brown material (Plate 3.1d) and in some of the Sarusas quartz latites appears to be replaced by serpentine. Carbonate also replaces pyroxene. Alteration of augite is seldom observed.

3.4.3 Oxidation of Titanomagnetite and Ilmenite

Two distinct types of temperature-related oxidation texture are observed in titanomagnetite crystals, these correspond to the two main reaction mechanisms discussed in detail by Haggerty (1976). The first, oxidation at low pressure between 400 - 600 °C yields cationic-deficient spinels of the titanomaghemite (Usp-Mt-γFe_2O_3) series; which may subsequently invert to an ilmenite-hematite$_{ss}$ (αFe_2O_3) at temperatures between 250 and 550 °C (Haggerty; Lindsley; 1976). The second involves an oxidation exsolution reaction which occurs at temperatures above 600 °C (at low to moderate pressures) and is followed by pseudomorphic reactions as oxidation becomes more advanced. Haggerty (1976) recognises seven stages of alteration between homogeneous titanomagnetite and a final pseudobrookite$_{ss}$-hematite$_{ss}$ assemblage, these can be summarised as follows:

Exsolution reactions;

C_1 Homogeneous titanomagnetite.

C_2 Magnetite enriched ulvospinel$_{ss}$ with a small number of exsolved ilmenite lamellae along the {111} spinel parting.

C_3 Ulvospinel poor magnetite$_{ss}$ with densely crowded exsolved ilmenite lamellae, forming a trellis texture along {111} planes. Saturation of magnetite with Al and Mg, due to ilmenite exsolution and the preferred partitioning of Al and Mg into the spinel structure results in the exsolution of pleonaste$_{ss}$ and magnesioferrite$_{ss}$.

Pseudomorphic reactions;

C_4 Is characterised by a mottling of the ilmenite-titanomagnetite intergrowth. This is caused by: (a) fine serrations that develop at the exsolution interfaces. (b) formation of exsolved transparent spinels in magnetite. (c) the development of ferri-rutile in ilmenite.

C_5 In this stage rutile and titanohematite develop extensively in the meta-ilmenite lamellae and begin to develop within the titanomagnetite.

C_6 Characterised by the incipient development of pseudobrookite from rutile and titanohematite along relict {111} planes.

C_7 The final stage characterised by the assemblage pseudobrookite$_{ss}$ and hematite$_{ss}$.

Note that the progression of oxidation through these stages is dependent on oxygen fugacity and not a progressive elevation in temperature.

Plate 3.3e illustrates the progressive oxidation of titanomagnetite (dark even grey) to titanomaghemite (whitish). The alteration reaction tends to occur along curved cracks and fractures and the pale grey areas represent intermediate stages in the transition. Note that both minerals are cubic and hence isotropic.

Several stages of high temperature oxidation are encountered in titanomagnetite phenocrysts, the highest corresponding to Haggerty's C_4 stage. In many cases the residual magnetite between the ilmenite lamellae also shows low temperature alteration to hematite. This alteration may occur without an intermediate maghemite stage and is more typical of Ti-deficient magnetite$_{ss}$ compositions. Plate 3.3f illustrates the C_2 - C_3 stage of alteration with well developed trellis ilmenite and the retrogressive alteration of the host magnetite to titanohematite. Plate 3.3g,h are examples of the C_4 stage (Haggerty, 1976). Lamellae of ilmenite are mottled due to the presence of ferri-rutile and the host magnetite, which shows alteration to hematite, has exsolved black needles of pleonaste$_{ss}$ and magnesioferrite$_{ss}$.

Discrete primary ilmenite crystals undergo a similar oxidation reaction to the meta-ilmenite lamellae in titanomagnetite (Haggerty, 1976). Ilmenite which occurs in some of the Sarusas quartz latites shows alteration to the C_4 stage of titanomagnetite alteration which corresponds to the R_4 stage of Haggerty (1976).

3.4.4 Alteration of Glass

Groundmass textures observed in the majority of quartz latite samples (Subsection 3.2.4) are consistent with the existence of an early glass phase. Two types of alteration process have been recognised. The first, involves the development of cryptocrystalline material and granophyric intergrowths of quartz and alkali feldspar; producing the devitrification textures most commonly encountered. The second, involves hydration of the glass followed by its replacement with secondary silica, zeolites and clay minerals.

3.4.4.1 Devitrification of Glass

The progressive replacement of glass by cryptocrystalline material during the devitrification process is illustrated in Plate 3.3a-d. Incipient devitrification occurs in some of the freshest pitchstone samples and is characterised by alteration along cracks and as small(0.05 - 0.25 mm), buff coloured spots. Devitrification and spherulite growth often occur radially from a central point, such as a microphenocryst or vesicle, starting with the formation of an opaque fibrous material which penetrates the surrounding glass (Plate 3.3a,b). As the spherulite grows the fibrous material is replaced by a buff coloured material with a faint radial anisotropism. Although the components of the spherulite are too small for optical measurement, the central portion is probably an intergrowth of cristobalite and feldspar (Smith, 1974), and the dark hair-like material the unwanted components rejected by the advancing crystals. In many devitrified samples the spherulite texture is overprinted by a granophyric intergrowth of quartz and alkali feldspar (Plate 3.3d). Spherulite development does not always occur with devitrification and some samples are composed of a homogeneous cryptocrystalline material with little structure.

3.4.4.2 Hydration of Glass and Secondary Mineralisation

This type of alteration is found in friable, vitreous pitchstones and is only well developed in poorly welded lapilli-tuff material (Chapter 4). Alteration proceeds via an initial stage of hydration resulting in the formation of perlite, characterised by curved concentric (perlitic) cracks. The hydrated glass, which is isotropic and dark brown in colour, alters to a slightly anisotropic, orangy-yellow product. This alteration develops at the margins of glassy fragments and along perlitic fractures forming coronas around fresher cores of glass. More intense alteration results in the replacement of these glassy cores by a strongly anisotropic material which often exhibits a fibrous or vermicular habit. Minerals replacing the glass generally have a low birefringence and probably consist of an assemblage of opaline silica, zeolite and clay minerals, similar to those precipitated in pore spaces. Instances of optical continuity between minerals filling pore spaces and the altered 'glassy' fragments support this. A precise identification of the replacement minerals would, however, require an x-ray diffraction and microprobe study beyond the scope of this thesis. Examples of this type of alteration are illustrated in Plate 3.4a,b, and are similar to the diagenetic changes which affect rhyolitic

PLATE 3.4

(a)

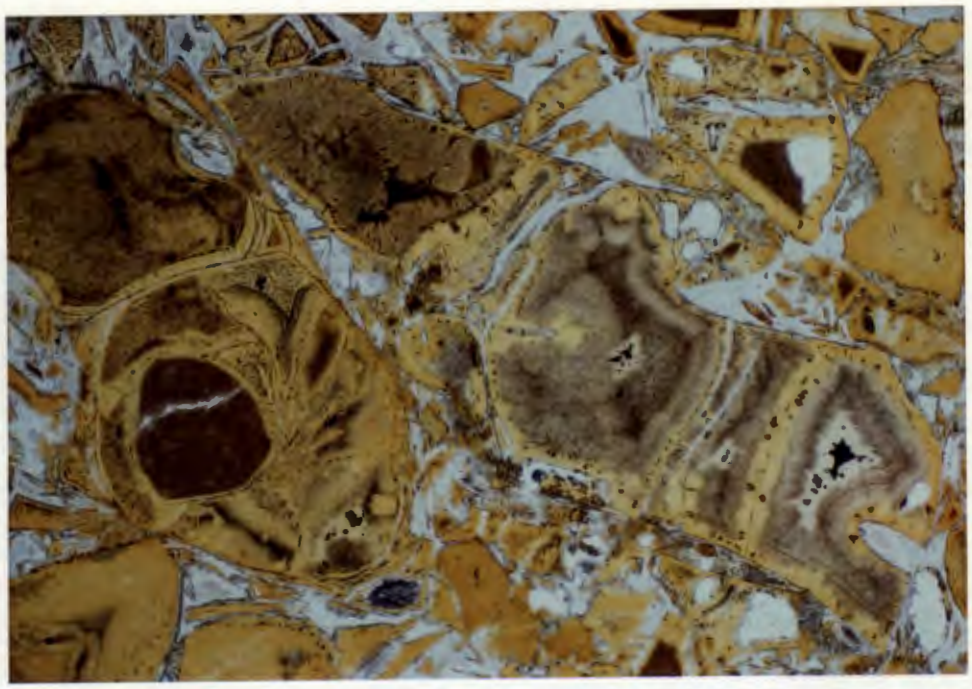

0.5 mm

(b)

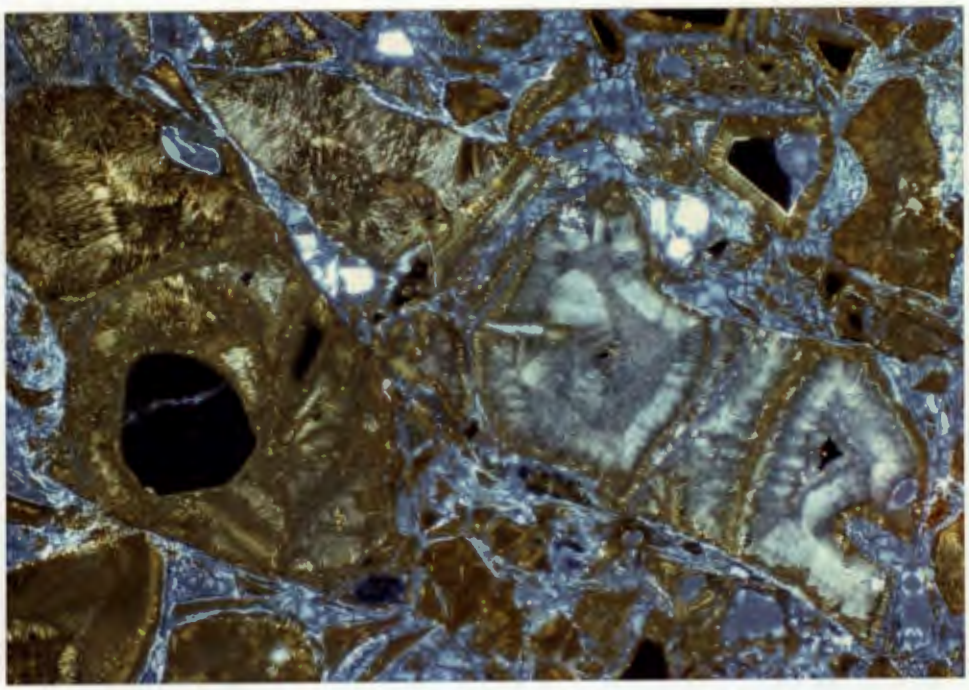

0.5 mm

Gemini quartz latite, lapilli-tuff (SM-229C).

This plate illustrates the progressive alteration of fragments and shards of glass. Alteration starts with the hydration and perlitic fracturing of the glass, some of which remains in the cores in some of the fragments (dark brown, isotropic). As alteration proceeds a slightly anisotropic, orangy-yellow material develops round the margins of the shards and along fractures. Following this the central glassy material is replaced by more strongly anisotropic material with a radiating habit. These latter stages are well developed in the large fragment right of centre. The shards are cemented by amorphous silica and the white crystals in (b) are pyrogenic crystals of plagioclase which show surprisingly little alteration.

tuffs, Fisher and Schmincke (1984).

3.5 RELATIONSHIPS BETWEEN PETROGRAPHY AND GEOLOGY

3.5.1 Introduction

In this section some of the petrographic features described in an integrated form in the preceding sections are placed in context with geological observations of Chapter 2. Due to the reconnaissance nature of the Sarusas quartz latite sampling this section only deals with the southern Etendeka quartz latites.

3.5.2 Petrography and Stratigraphy

The use of petrography as a primary stratigraphic indicator in the Etendeka is restricted by fairly uniform groundmass textures and by alteration, which often makes the identification of phenocryst assemblages difficult. The stratigraphy of the southern Etendeka has been defined by the correlation of geochemically similar groups of quartz latite units (Milner and Duncan, 1987). Table 3.4 summarises the phenocryst assemblages (subsection 3.2.1) encountered in these groups, and sets them out in accordance with the stratigraphic model proposed for the southern Etendeka by Milner and Duncan (1987). Table 3.4 shows that a good petrographic correlation exists between the quartz latites of the Tafelberg and Interbedded Coastal successions and supports the geochemical stratigraphic model. Because of the different number of quartz latite units encountered in the Tafelberg and Interbedded Coastal sections, the comparison of quartz latite groups and their petrography in Table 3.4 is not intended as an absolute correlation of individual units. However, it is believed that the Lower Tafelberg quartz latite and the lower-most flow unit in the Interbedded Coastal block are the same unit. Three main reasons for this belief are, (1) indistinguishable whole rock compositions, (2) identical phenocryst assemblage (plagioclase + titanomagnetite), and (3) the use of the Gemini quartz latite unit as a stratigraphic marker (Chapter 2). Above the Lower Tafelberg unit further direct correlation of quartz latite units is difficult because of the large amount of interbedded basalt in the Tafelberg sequence (Fig. 2.8). Samples from the Lower and Upper Springbok groups with the same plagioclase + pigeonite + titanomagnetite phenocryst assemblage are easily distinguished from

Table 3.4 Correlation of petrography with Stratigraphy

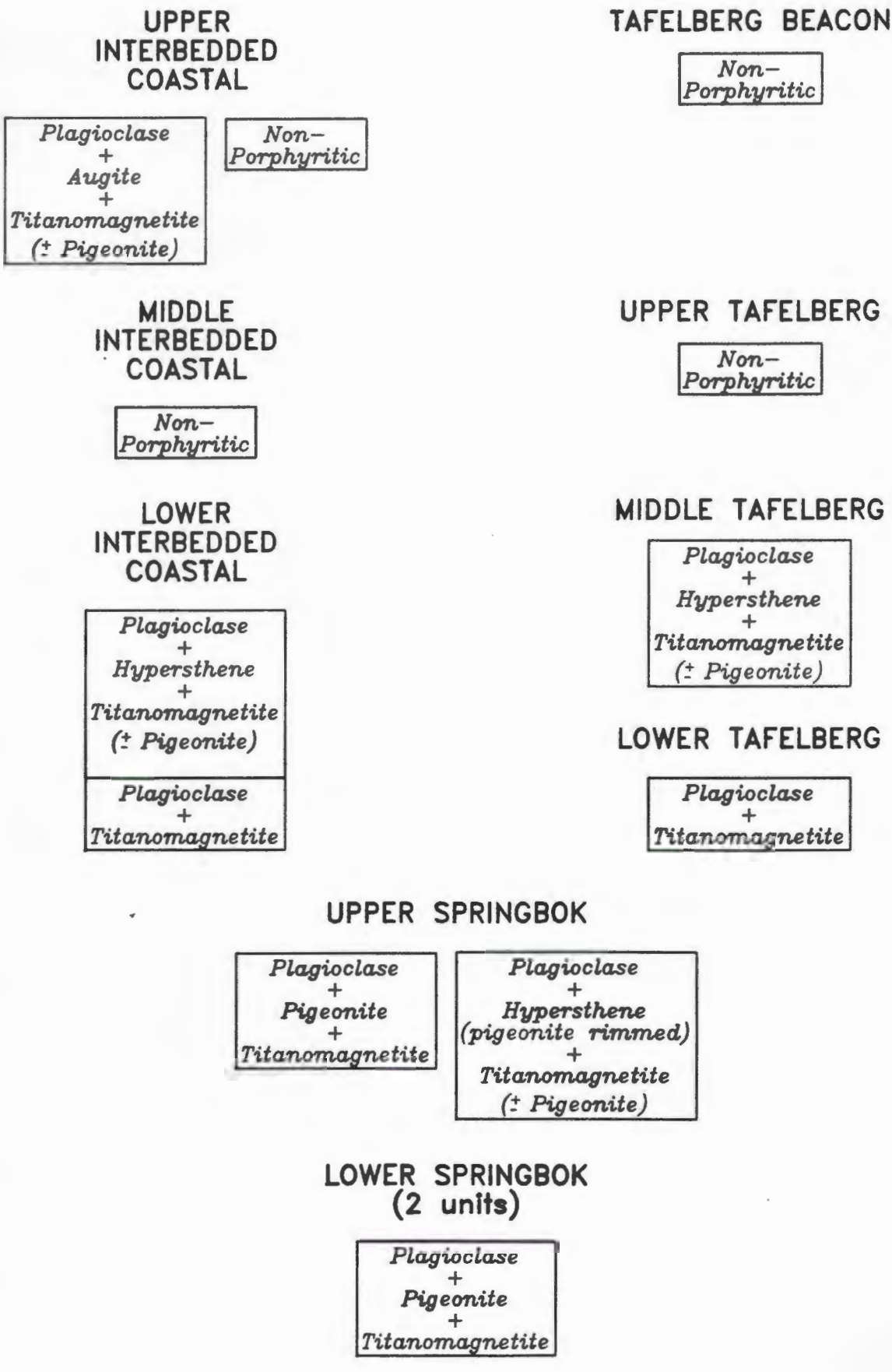

each other in thin section due to the microporphyritic nature of the latter, compare Plate 3.1a and 3.1c (see Appendix 1 for descriptions of type examples).

3.5.3 Petrographic Variation Within Quartz Latite Units

3.5.3.1 Mineralogical Variation

In general no changes in mineralogy and phenocryst abundance have been detected either vertically or laterally in the individual units studied. One notable exception to this are the two phenocryst assemblages displayed by the Upper Springbok unit (see Table 3.4). The distribution of these assemblages and the relationships between them are not tightly constrained due to the alteration of pyroxene in the majority of samples, and the lack of suitable serial sections. Samples in which pigeonite is the only pyroxene occur in the south-western part of the Upper Springbok sheet (near Trig 26) and at Awahab (Fig. 2.2). These areas represent some of the thickest parts of the unit and in both cases samples with this assemblage occupy the central portions of the unit, with the hypersthene-bearing rocks at the base and at the top (note that for the upper samples observations were made on devitrified samples). In the south-western area the Upper Springbok quartz latite appears to be a composite cooling unit made up of several flows (Fig. 2.7). Whether individual flows display a single assemblage of phenocrysts or exhibit a gradational change from one assemblage to the other is unclear. Several samples with roughly equal proportions of hypersthene and pigeonite phenocrysts have been encountered, possibly representing an intermediate stage in the change from one type of pyroxene phenocryst to the other. Both assemblages have been found in quenched pitchstone samples and there is little doubt that these changes in mineralogy are of a primary magmatic origin.

3.5.3.2 Textural Variation

The main petrographic variations observed in individual quartz latite units are textural changes which can be linked to the post-eruptive cooling and oxidation history.

Plate 3.5 illustrates variations in the groundmass texture and plagioclase microphenocryst grain size distribution in a section through the Lower Tafelberg quartz latite unit at Wêreldsend. The groundmass texture changes from a fine grained, homogeneous, cryptocrystalline material at the base (Plate 3.5e) to a spherulitic fabric with interstitial granophyre in the flow centre. This

PLATE 3.5

Shows a sketch of a serial section through the Lower Tafelberg quartz latite at Wêreldsend and illustrates progressive changes in the groundmass texture and the plagioclase microphenocryst grain size with stratigraphic height. All photographs were taken in plane polarised light.

3.5a (SM-200) Highly altered and fractured glassy material with quenched microlites. No plagioclase microphenocrysts are present. The flattened amygdale (centre top) is filled with orangy-brown silica.

3.5b-d (SM-198, SM-197 and SM-194 respectively) These samples contain microphenocrysts of plagioclase, clinopyroxene and titanomagnetite. The plagioclase laths are noticeably larger in the central part of the flow. The medium to dark grey areas consist of cryptocrystalline devitrified material and the pale grey to white areas are intergrowths of quartz and alkali-feldspar.

3.3e (SM-192) Shows a predominantly cryptocrystalline groundmass with very fine grained plagioclase laths.

All the samples contain sparse phenocrysts of altered plagioclase and titanomagnetite. Notice that the size of the plagioclase phenocrysts varies little through the flow (3.3b-e) indicating that they were present in the quartz latite magma prior to its eruption.

For details concerning the textural changes in the sketch section see Chapter 2, Fig. 2.12.

PLATE 3·5

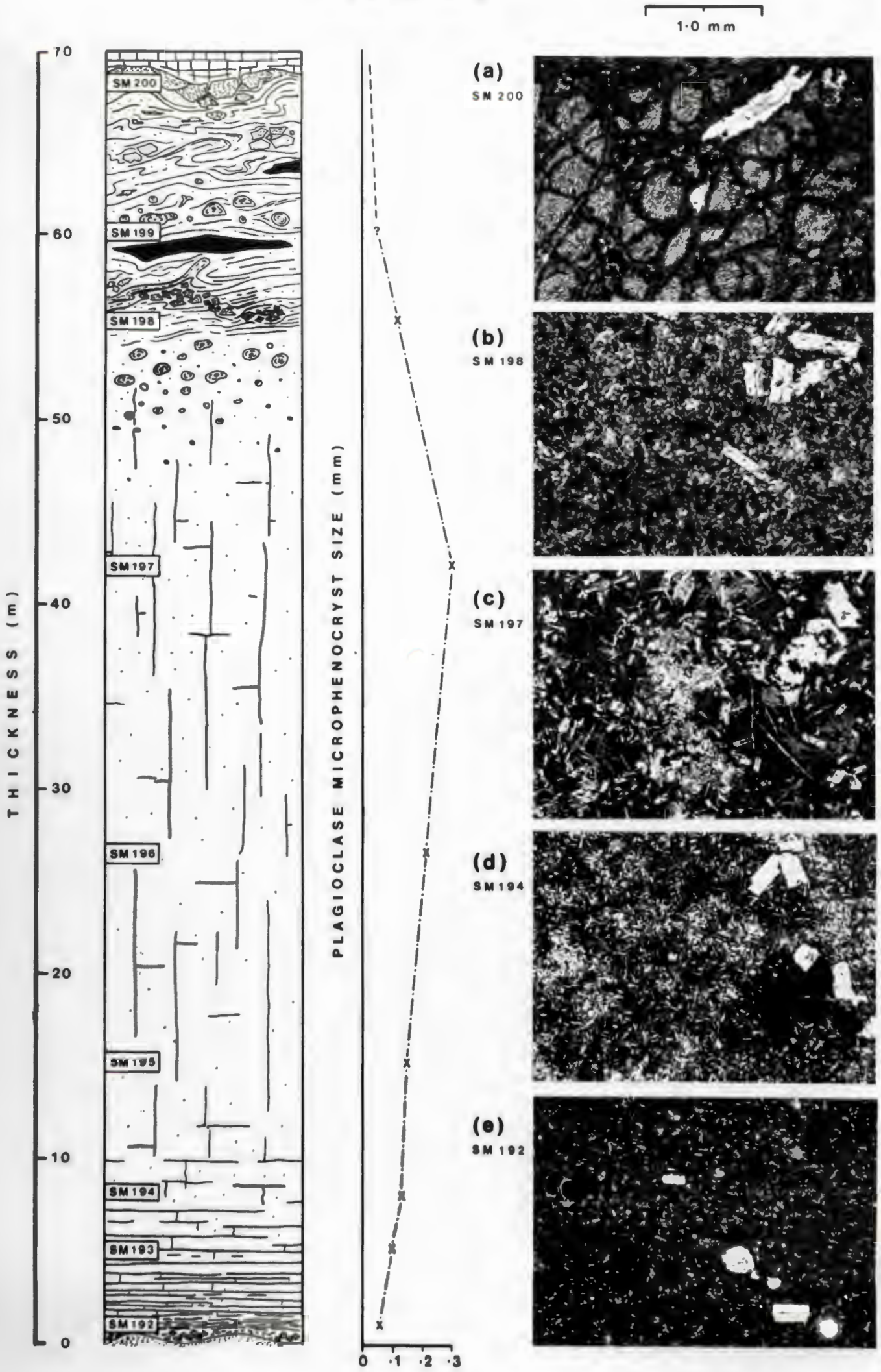
1·0 mm
THICKNESS (m)
70
60
50
40
30
20
10
0
SM 200
SM 199
SM 198
SM 197
SM 196
SM 195
SM 194
SM 193
SM 192
PLAGIOCLASE MICROPHENOCRYST SIZE (mm)
0
·1
·2
·3
(a)
SM 200
(b)
SM 198
(c)
SM 197
(d)
SM 194
(e)
SM 192

texture shows its strongest development in the sample SM-196, where approximately 45 % of the groundmass has a granophyric texture. The groundmass of the upper-most samples becomes predominantly cryptocrystalline again with the highest sample, SM-200, exhibiting an altered glassy texture (Plate 3.5a). The maximum plagioclase microphenocryst grain size also increases towards the centre of the flow, ranging from 0.025 mm near the base (Plate 3.5e) to 0.25 mm in the upper central portions of the flow (Plate 3.5c).

Plate 3.6 illustrates variations in the oxidation textures of titanomagnetite in the Lower Tafelberg serial section at Wêreldsend. Although the intensity of the oxidation may vary slightly within individual samples, the textures illustrated are representative of the majority of phenocrysts observed in a particular sample. At the rapidly chilled upper and lower surfaces of the flow titanomagnetite shows relatively low temperature (< 600 °C) alteration to maghemite (Plate 3.6a,h). Towards the centre of the flow, where cooling was obviously much slower, titanomagnetite shows high-temperature (> 600 °C) oxidation exsolution of trellis ilmenite. The intensity of this oxidation varies considerably as a function of stratigraphic height within the flow, and can be estimated using the C_1 - C_7 notation of Haggerty (1976). Oxidation reaches a maximum intensity of C_3 - C_4 about 15 m above the base of the flow (Plate 3.6e,f). Towards the centre of the flow the intensity of the oxidation becomes much less and approximates to the C_1 - C_2 stage (Plate 3.6c,d), and thereafter it increases slightly (C_2 - C_3) towards the upper central part of the flow (Plate 3.6b). The coexistence of C_3 and C_4 stage grains in the same thin section (Plate 3.6e,f) serves to illustrate the heterogeneous nature of the oxidation process, which is probably sensitive to fluid movement along fractures and joint planes (Haggerty, pers. comm., 1987).

The C_4 stage oxidation texture illustrated in Plate 3.6e shows a departure from the oxidation scheme set out by Haggerty (1976). At this stage ilmenite normally oxidises to give hematite plus ferri-rutile (e.g. Plate 3.3g). A detailed optical and electron microprobe study of the lamellae in Plate 3.6e shows that they have a uniform titanohematite composition (Ilm_{30}) with no trace of rutile, and are therefore somewhat unusual (Haggerty pers. comm., 1987). It is possible that the rutile is submicroscopic in nature thus precluding its direct observation, however totals on analyses of the lamellae are good, indicating good stoichiometry with no rutile inclusions. Furthermore, since the development of hematite and rutile from ilmenite is a pseudomorphic

PLATE 3.6

An illustration of the oxidation textures displayed by titanomagnetite phenocrysts in a profile through the Lower Tafelberg quartz latite at Wêreldsend, see Plate 3.5 for sample localities. (The primary composition of these titanomagnetites is approximately Usp_{20}, see Chapter 5).

3.6a (SM-200) Grains are completely altered to titanomaghemite and are considerably more reflective than unaltered magnetite. No inversion of the titanomaghemite to titanohematite is observed among these particular phenocrysts, although other crystals in this sample are extensively altered.

3.6b (SM-198) Part of a euhedral phenocryst showing high temperature, C_2 - C_3 stage, oxidation exsolution of trellis ilmenite. Much of the host magnetite (medium grey) is altered to hematite (white).

3.6c (SM-197) (i) shows very fine grained, C_2 stage ilmenite lamellae. The host magnetite is altered to hematite. (ii) Incipient exsolution of ilmenite. Much of the host magnetite is still intact with some alteration to hematite at the grain boundary.

3.6d (SM-196) (i) incipient oxidation exsolution of ilmenite and the alteration of magnetite to hematite only occurs at the grain margin, the central portion remains unaltered. (ii) incipient exsolution of ilmenite and more extensive alteration of magnetite to hematite occurs adjacent to a fracture in the crystal. Away from this fracture the titanomagnetite is essentially unaltered (not shown).

3.6e (SM-195) C_4 stage oxidation is characterised by the exsolution of black pleonaste-magnesioferrite$_{ss}$ needles from the host magnetite (dark grey). The trellis lamellae are of a uniform titanohematite composition (Ilm_{30}) with no evidence of pseudomorphic rutile. Host magnetite is unaltered.

3.6f (SM-195) C_3 stage oxidation exsolution characterised by thick lamellae of ilmenite. Magnetite shows partial alteration to hematite adjacent to the ilmenite lamellae.

3.6g (SM-194) C_2 - C_3 stage oxidation exsolution of trellis ilmenite. Much of the host magnetite (dark grey, top right) has been altered to hematite (white). The oxidation shown by this sample is of a similar intensity to that shown by SM-198.

3.6h (SM-192) Progressive low temperature (< 600 °C) alteration of titanomagnetite (dark grey) to titanomaghemite (pale grey to white). Alteration is most strongly developed at the grain boundaries and along fractures.

PLATE 3.6

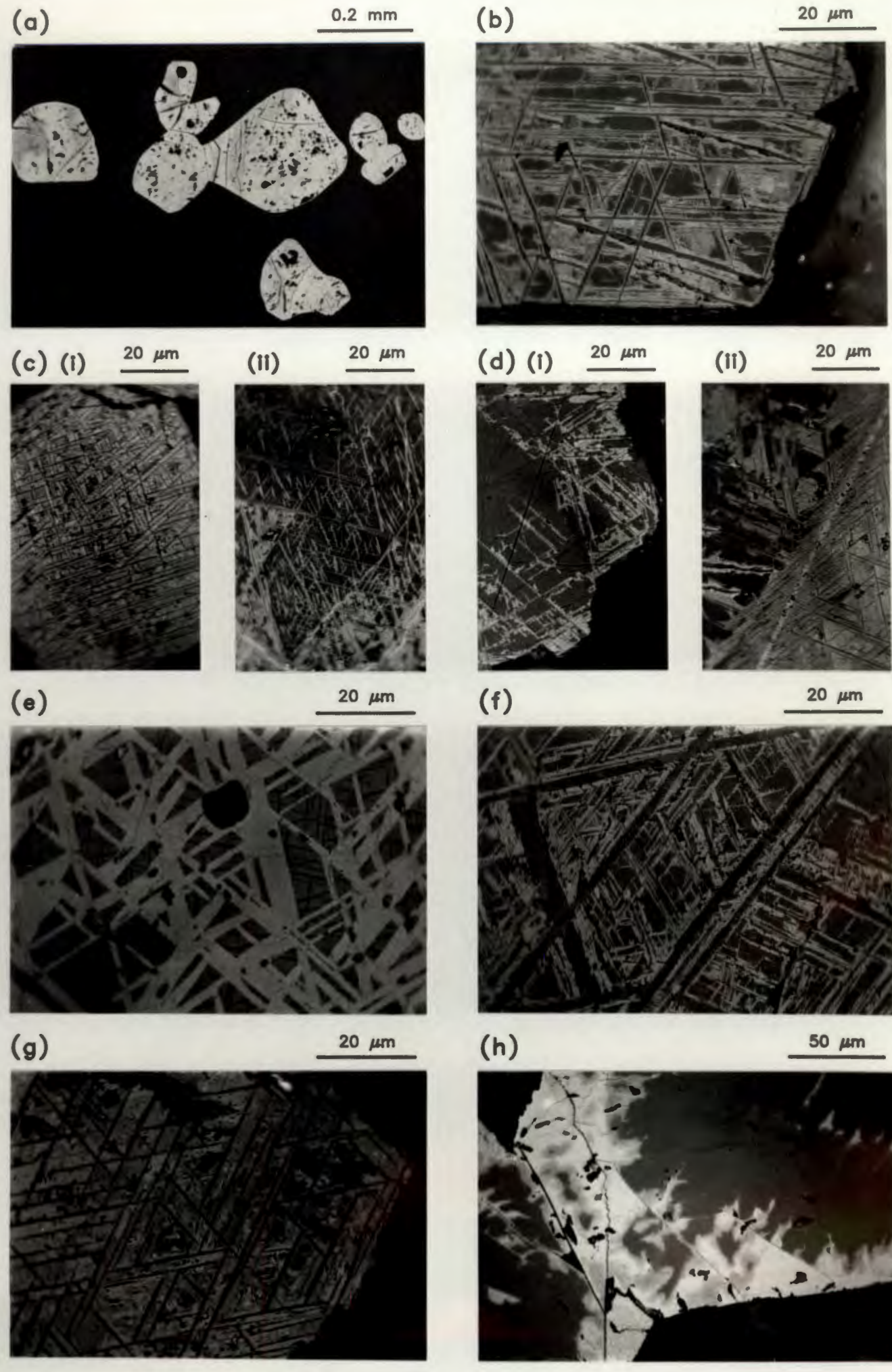
(a)
0.2 mm
(b)
20 μm
(c) (i)
20 μm
(ii)
20 μm
(d) (i)
20 μm
(ii)
20 μm
(e)
20 μm
(f)
20 μm
(g)
20 μm
(h)
50 μm

reaction, and assuming that the magnetite grain in Plate 3.6e is part of the phenocryst population, not a xenocryst, the primary titanomagnetite composition (Usp_{20}) of the Lower Tafelberg quartz latite (Chapter 5) is too Ti-poor to have exsolved the density of "meta-ilmenite" lamellae observed. If one compares the thickness and reflectivity of the lamellae in the C_4 stage grain (Plate 3.6e) with those of the C_3 stage grain (Plate 3.6f) it would appear that as oxidation progresses the lamellae become thicker and more iron-rich. Since the ilmenite-hematite solvus is interrupted at temperatures below 800 °C (Haggerty, 1976) this reaction must have occurred at temperatures greater than 800 °C.

The features illustrated in Plates 3.5 and 3.6 are consistent with the rapid cooling of the upper- and lower-most parts of the flow unit and the persistance of elevated temperatures (> 600 °C), possibly higher than 800 °C, in the centre of the flow for some time after eruption. The variation in the intensity of the high temperature titanomagnetite oxidation shows that the oxidising conditions were not uniformly developed within the flow. In oxidation profiles through basalt flows (Haggerty, 1976) the mechanism of high temperature oxidation is related to the trapping and accumulation of volatiles, the dissociation of H_2O and the preferential loss of hydrogen relative to oxygen due to the higher diffusivity constant of the former. The precise mechanisms involved in the oxidation of a quartz latite flow would require a more detailed statistical study of several sections through a single flow unit, and a careful assessment of how joint patterns and the intensity of jointing affects the oxidation profile.

3.6 SUMMARY

[1] The quartz latites of the Etendeka Formation are generally sparsely porphyritic to microporphyritic with glassy to devitrified groundmass textures.

[2] Phenocryst assemblages, which may include plagioclase, pyroxene, titanomagnetite and occasionally ilmenite, are characterised by the type of pyroxene present. Pyroxene phases observed include hypersthene, pigeonite and augite. No primary hydrous phases have been observed.

[3] Primary mineral phases are least altered in the rapidly quenched pitchstone

samples. The majority of samples collected are devitrified and often show the development of a granophyric intergrowth of quartz and alkali feldspar and the alteration of plagioclase, pyroxene and titanomagnetite.

[4] The petrography of the southern Etendeka quartz latites can not be used as a primary stratigraphic indicator. However, it can be correlated successfully with a stratigraphic interpretation based on a geochemical characterisation of quartz latite units.

[5] Petrographic variations within individual units are largely restricted to changes in texture which result from the progressive cooling and oxidation of the flow after eruption.

CHAPTER 4

PYROCLASTIC FEATURES WITHIN THE ETENDEKA QUARTZ LATITES

4.1 INTRODUCTION

As described in the previous chapter the majority of quartz latite samples collected in the Etendeka display homogeneous, glassy or devitrified groundmass textures which give little or no information regarding the eruptive character of these units. However, some samples collected from the basal and upper flow facies, particularly from the Gemini quartz latite unit south of the Koigab Gorge (Fig. 2.3), have textures which are clearly pyroclastic in origin. Although quite rare, these pyroclastic textures provide strong evidence to support an ignimbritic origin for the quartz latites and are thus important in defining the volcanological characteristics of these units. This chapter gives a descriptive account of the pyroclastic features observed and relies on photomicrographs and their accompanying captions for detail. A brief glossary of terms used in this chapter to describe the pyroclastic features is given in Table 4.1. Terms such as "unwelded" and "welded" are used *sensu stricto* and are not to be confused with post-cooling diagenetic processes which may have resulted in substantial lithification of unwelded deposits by cementation.

4.2 PYROCLASTIC FEATURES

4.2.1 Glassy Fragments and Pumiceous Material

In the Etendeka quartz latites unsorted lapilli-tuff material forms the matrix of many block breccias and more extensive portions of the Gemini quartz latite unit (Subsection 2.5.4). It is composed of shards and fragments of altered glass and pumice, with pyrogenic crystals of plagioclase, pyroxene and magnetite.

4.2.1.1 Unwelded Lapilli-Tuff

Unwelded lapilli-tuff is commonly coarse ash supported, although in patches the coarse fragments may be supported by fine ash. The fragments are cemented by quartz, opaline silica, zeolite and green amorphous clay minerals. In some specimens two different types of fragment can be identified on the basis of colour and morphology. Dark brown, non-perlitic fragments commonly have

Table 4.1

Glossary of terms used in the description of pyroclastic rocks

Fragment Origin

Juvenile

Pyroclasts derived directly from erupting magma, consisting of dense or inflated particles of chilled melt and crystals (pyrogenic).

Cognate

Fragmented co–magmatic volcanic rocks from previous eruptions of the same volcano. NB Also used here to describe 'Lithic Fragments' of quartz latite produced by rapid chilling and brecciation at the time of emplacement.

Accidental

Fragments derived from the sub–volcanic basement

Pyrogenic Crystals

Whole or broken phenocrysts which were present in the magma prior to eruption. May be enclosed by or separate from quenched magma

Fragment Size

	Clast Size	Deposit Name
Blocks	> 64 mm	Pyroclastic (block) Breccia
Lapilli	2 – 64 mm	Lapillistone
Ash	0.05 – 2 mm (coarse)	Tuff
	< 0.05 mm (fine)	(Lapilli + Ash = Lapilli–tuff)

Morphological Terms

Pumice

Highly vesicular volcanic glass

Fiamme

'Black glassy' lens–like inclusions with flame shaped cross sections. Interpreted as being collapsed pumice ~ micro– to macroscopic.

Glass Fragments

Angular to subrounded fragments of glass ~ often exhibit cuspate margins.

Shards

Highly angular, often cuspate glass fragments derived from the walls of and the junctions between tiny broken bubbles.

Textural Terms

Eutaxitic

Subparallel alignment of different fractions resulting in streaks, bands and lenses in a seemingly well ordered distribution.

Piperno

Similar to eutaxitic ~ characterised by conspicuous lenses of glass (fiamme).

After:

Fisher R.V. & Schmincke H.–U. (1984) Pyroclastic Rocks. (Chapter 5).

Ross, C.S. & Smith, R.L. (1961). Ash–Flow Tuffs: Their origin, geologic relations, and identification. *U.S. Geol. Surv. Prof. Paper,* **366**, 1 – 77.

well-rounded vesicles and angular outlines. Many have cuspate margins consistent with bubble rupture and the majority of finer grained bubble wall and bubble junction shards consist of this material. Perlitic, orangy-yellow quartz latite constitutes the other fragment variety. These fragments tend to be less angular and less vesicular than the dark brown variety and have vesicles which are often flattened and deformed. Both types of fragment have the same phenocryst assemblage. It is not known whether the differences between these fragment types reflect different origins (juvenile or cognate) or whether they are related to differences in the physical state of the fragments during the course of eruption. Flattened vesicles within the orangy-yellow, perlitic fragments are suggestive of a cognate origin, although the sub-round outlines may be due to the moulding of hot juvenile fragments at the time of eruption.

Plates 4.1 and 4.2 show the matrix material from the basal breccia illustrated in Plate 2.22 (Lower Springbok quartz latite, Awahab). In general the yellowish, perlitic fragments are more abundant than the darker clasts, the latter are noticeably more angular and often have cuspate margins. Plates 4.3 and 4.4 illustrate a similar matrix material from a flow-top breccia in a Lower Springbok quartz latite. Yellowish, perlitic glass constitutes the majority of fragments and pumice in this sample, but the larger clasts are predominantly lithic in character. Plagioclase, pigeonite and magnetite are clearly identifiable as isolated fragments and as phenocrysts within both pumice and lithic fragments.

Plates 4.5 - 4.8 show lapilli-tuff material (SM-229C) from the Gemini quartz latite unit. Glassy fragments and pumice are strongly perlitic and tend to be quite angular, differing in that respect from similar fragments in Plates 4.1 and 4.2. The glass fragments show progressive alteration from a dark brown isotropic (hydrated) glass at the cores of some of the fragments to yellow anisotropic material at the rims and along perlitic fractures. Note that this brown glass is texturally quite distinct from the dark brown fragments seen in other specimens. Cement and vesicle fillings which consist of opaline silica, fibrous zeolite and amorphous green clay minerals often show optical continuity with the yellow anisotropic material, indicating the replacement mineralogy of the fragments (Section 3.4). Despite the quite strong alteration of glass the pyrogenic plagioclase crystals remain largely unaltered. Fisher and Schmincke (1984) noted that the deposition of secondary minerals commonly followed extensive dissolution of glass. The presence of highly angular fragments and

PLATE 4.1

Unwelded lapilli-tuff, Lower Springbok quartz latite, Awahab. Matrix material of basal breccia illustrated in Plates 2.22 consisting of unsorted shards and fragments of quartz latite cemented by quartz.

PLATE 4.2

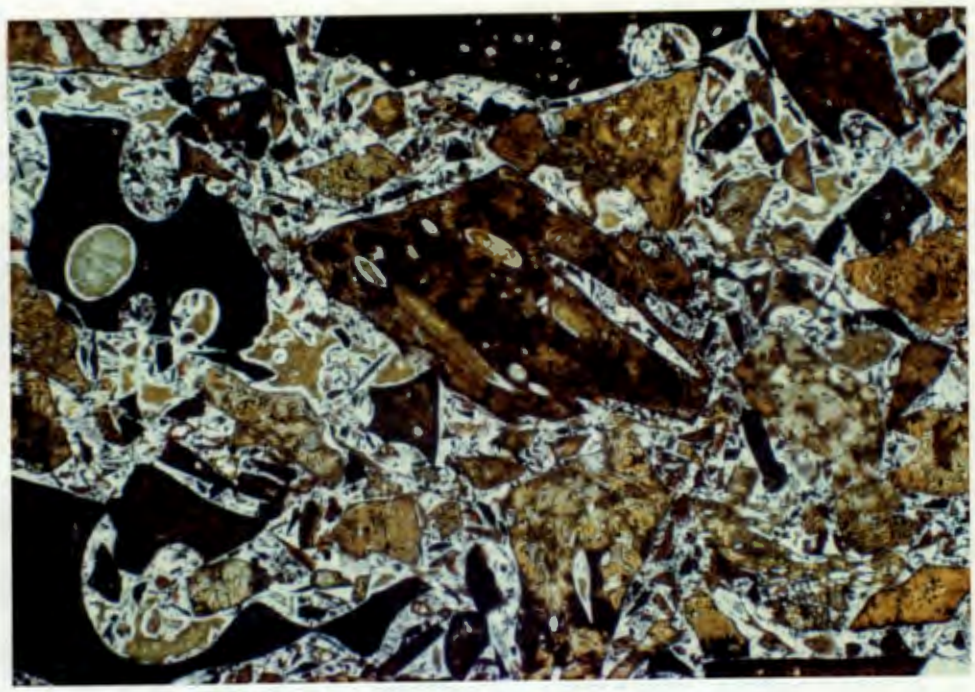

Unwelded lapilli-tuff, Lower Springbok quartz latite, Awahab. Part of Plate 4.1 showing more clearly the two types of fragment encountered. (1) Greenish-yellow to orange-brown variety commonly exhibit rounded outlines and flattened vesicles. (2) Very dark brown, almost opaque angular fragments with more spherical vesicles. Fragments are set in a poly-crystalline quartz cement with some pale green clay mineral.

PLATE 4.3

Unwelded lapilli-tuff, Lower Springbok quartz latite, (SM-221A). Matrix material from a flow top breccia. Most of the fragments are of completely altered yellow, perlitic glass. Many lapilli are pumiceous.

PLATE 4.4

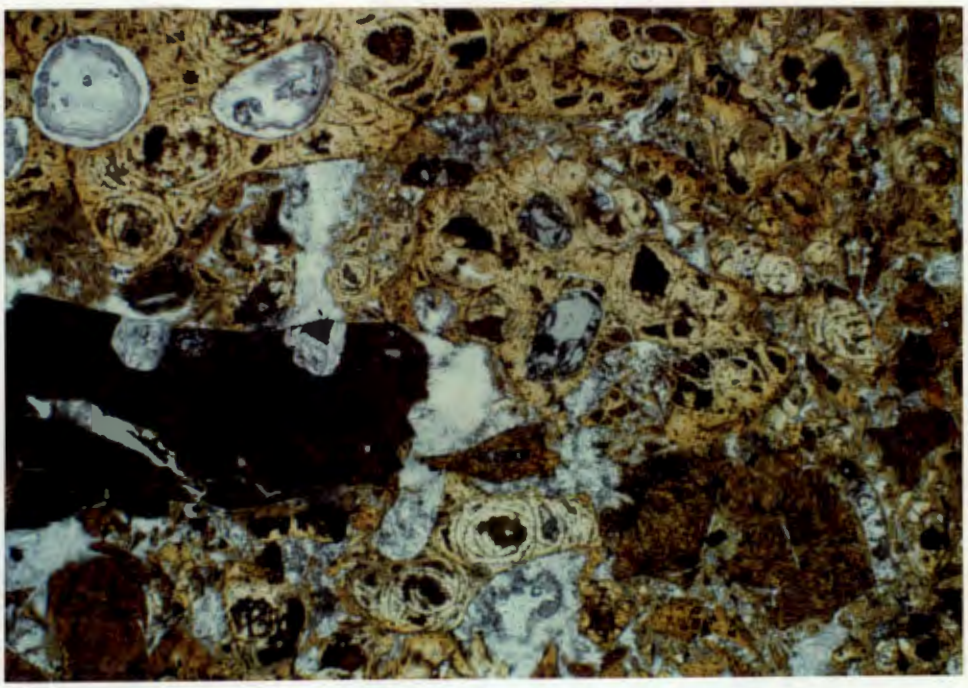

Unwelded lapilli-tuff, Lower Springbok quartz latite, (SM-221A). Part of Plate 4.3 illustrating the angular character of many fragments. Perlitic fractures are clearly visible as are phenocrysts of plagioclase (in dark fragment) and pigeonite (centre right). The fragments are cemented by quartz, zeolite and a greenish clay mineral.

PLATE 4.5

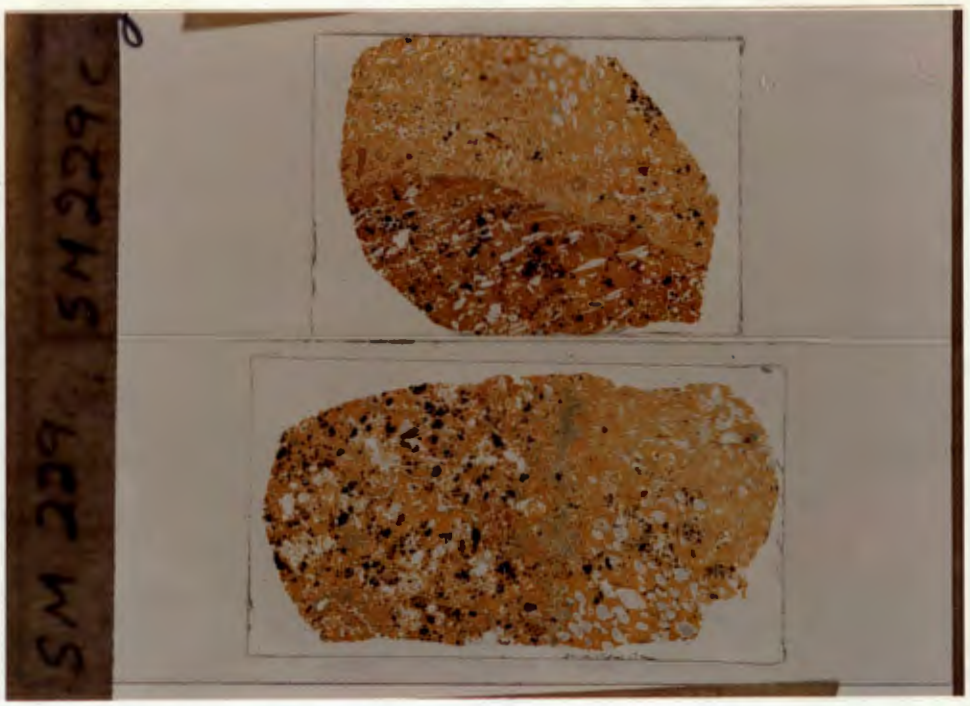

Unwelded lapilli-tuff, Gemini quartz latite, (SM-229C). Material collected from the brownish altered outcrop illustrated in Plate 2.11. Consists of altered, yellow fragments of glass and pumice lapilli.

PLATE 4.6

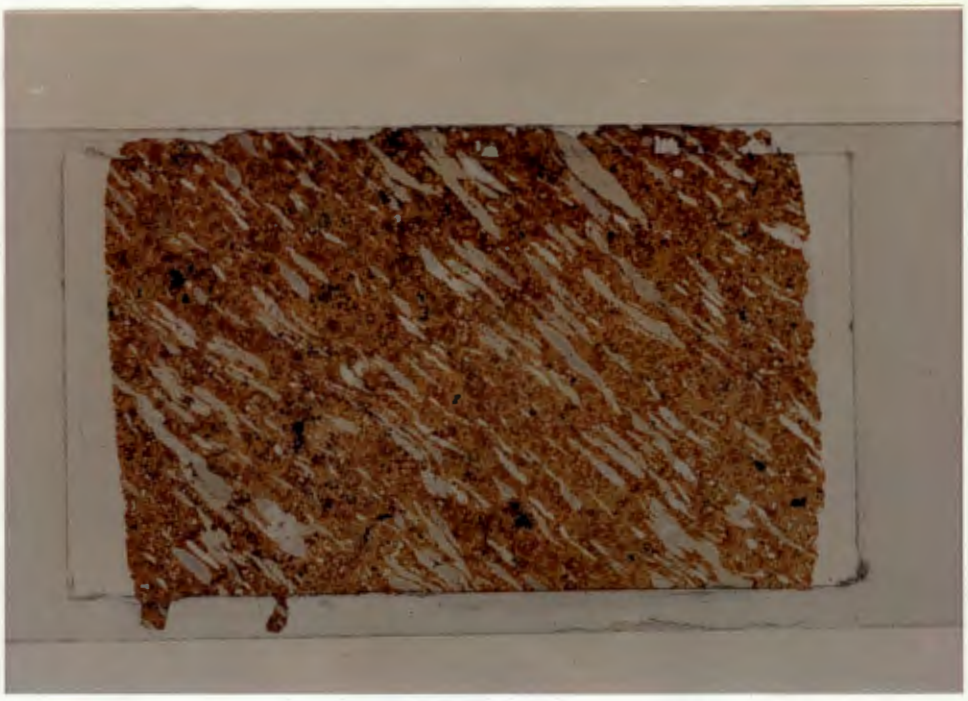

Pumice lapillus, Gemini quartz latite, (SM-229C). Slightly larger pumice clast forming part of the brown altered outcrop in Plate 2.11. The lapillus, which has been gently flattened, consists of altered perlitic glass. The vesicles are filled with silica.

PLATE 4.7

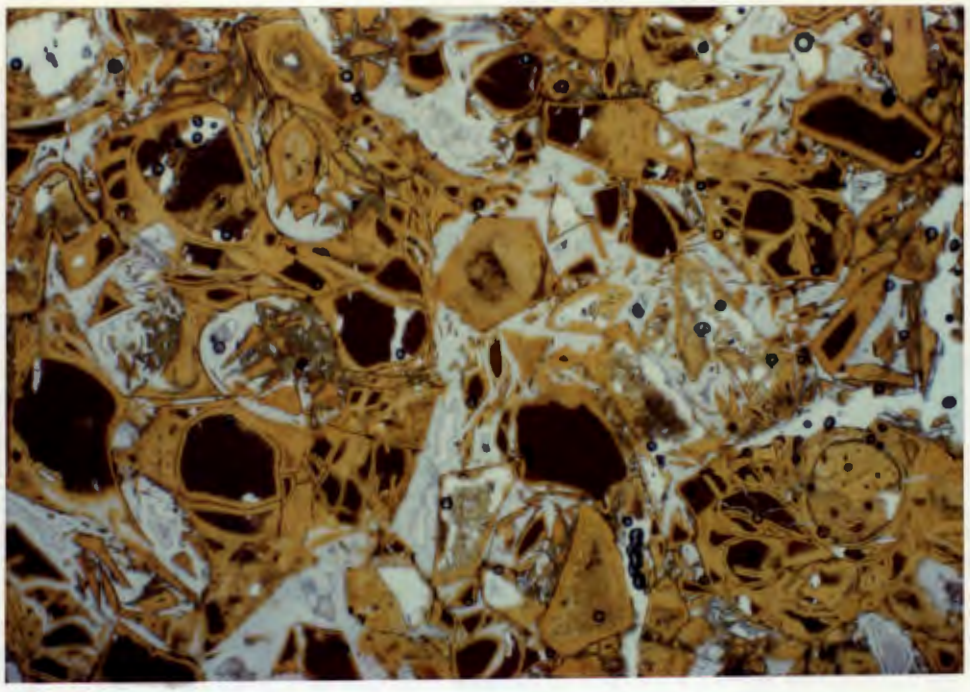

Unwelded lapilli-tuff, Gemini quartz latite (SM-229C). Part of Plate 4.5. Unsorted fragments of glass (right) and pumice (left) of juvenile character cemented by silica. Dark brown areas are relatively unaltered glass.

PLATE 4.8

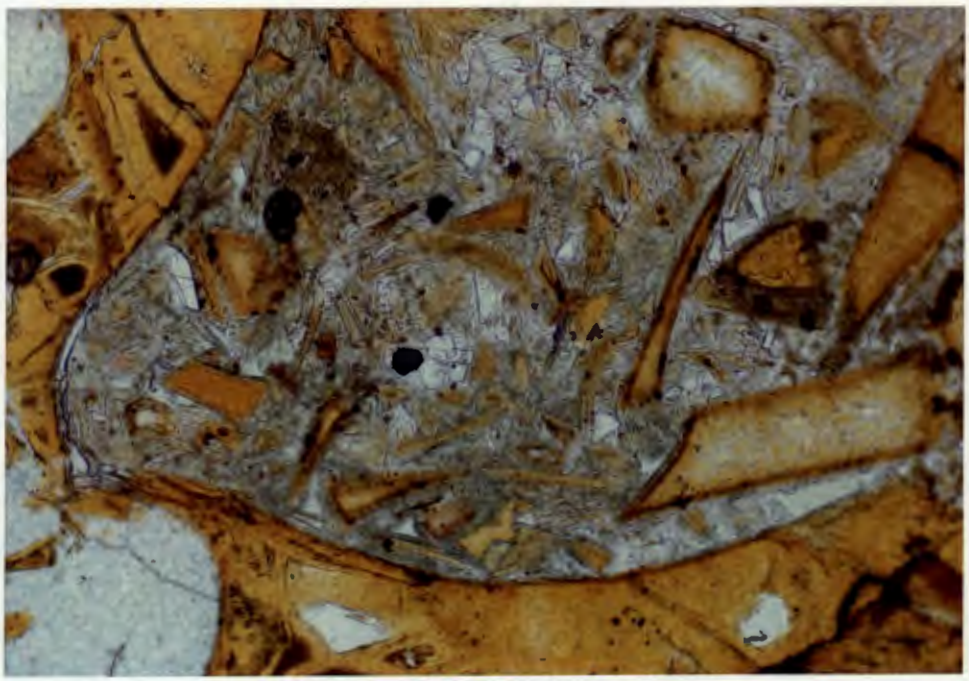

Unwelded lapilli-tuff, Gemini quartz latite (SM-229C). Part of Plate 4.5. Fine grained fragments and shards showing alteration to a green clay mineral. Fragmented pyrogenic crystals of plagioclase(white) and Ti-magnetite(black) are also present.

thin cuspate shards in SM-229C indicate that the dissolution of glass was not a major factor controlling the shape of these fragments and it is assumed that their morphology is of a primary volcanic nature.

4.2.1.2 Welded Lapilli-Tuff

Welding and compaction results in the progressive flattening of glass fragments and pumice lapilli producing eutaxitic or piperno-like textures. A dramatic reduction in porosity as a consequence of the tight compaction of glass fragments and the collapse of pumice lapilli occurs, with the result that pores spaces and vesicles become little more than relic features in homogeneous glass. Glass shards and fragments occasionally show deformation around pyrogenic crystals. Intense welding may be accompanied by rheomorphic flow banding and the development of microlites.

The Gemini quartz latite (Subsection 2.5.4) at the SM-229 locality demonstrates a number of features related to progressive welding and compaction, Plates 4.5 - 4.16. Plates 4.5 - 4.8 illustrate virtually unwelded lapilli-tuff material collected from the altered "clastic" portions of the flow (Plate 2.11). Welding and compaction of this material results in piperno-like pitchstones (Plates 4.9 - 4.14), which constitute the vitreous, extremely friable pitchstones illustrated in Plates 2.11 and 2.12. Notice that the amount of glass alteration in these specimens is a function of porosity, which in turn reflects the degree of welding. The most intensely welded material, Plates 4.15 and 4.16, comes from the devitrified, flow banded regions of the flow (Plate 2.11) providing strong evidence for rheomorphic processes.

4.2.2 **Breccias**

Breccias occur in both the basal and upper flow zones of a quartz latite unit, Section 2.5. They are composed of angular to subrounded lapilli- to block-sized clasts of reddish-brown quartz latite. The clasts are fine grained with homogeneous devitrification textures, similar to those seen in rapidly chilled material from the base of the Lower Tafelberg unit at Wêreldsend (Plate 3.5). The phenocryst assemblages in the clasts are the same as those within the host unit and many contain numerous microlites which may define flow banding. The clasts have a variable concentration of vesicles and in clasts from flow-base breccias the vesicles are often strongly flattened. Clasts with flattened vesicles or flow banding have a random orientation within the breccia,

PLATE 4.9

1.0 cm

Partially welded lapilli-tuff, Gemini quartz latite (SM-229G). Extremely friable pitchstone material (Plate 2.11). Fragments of glass and pumice show a crude compaction fabric

PLATE 4.10

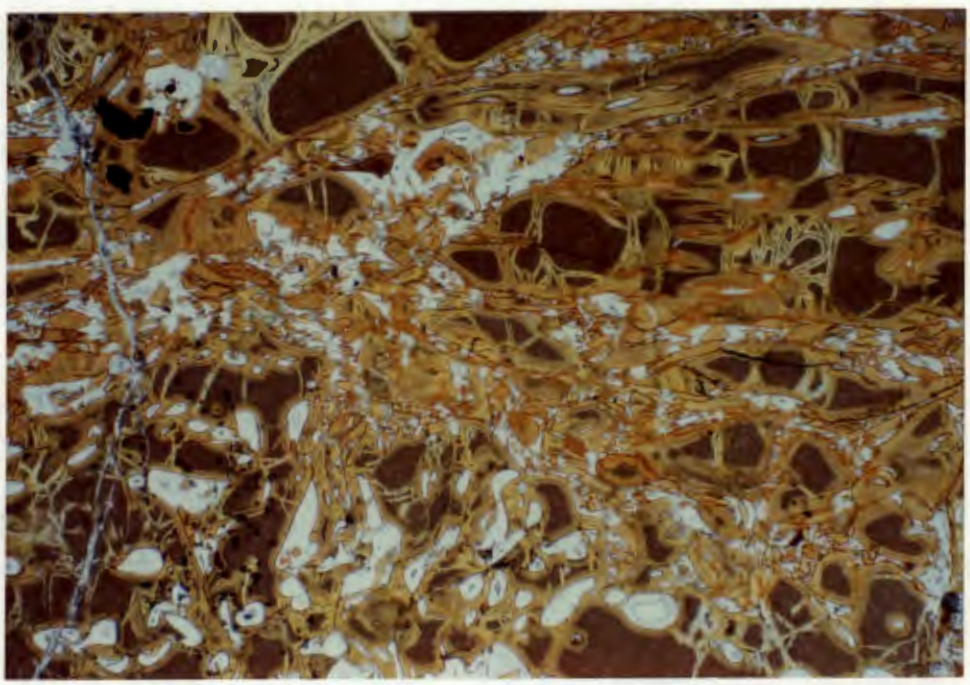

1.0 mm

Partially welded lapilli-tuff, Gemini quartz latite (SM-229G). Part of Plate 4.9. Fragments in the upper part of the photograph show the compaction fabric more clearly and some of the vesicles are flattened in the same plane. Lower down a pumice lapillus shows little compaction. Note that disaggregation of this clast would yield fragments with a morphology similar to those in Plate 4.7.

PLATE 4.11

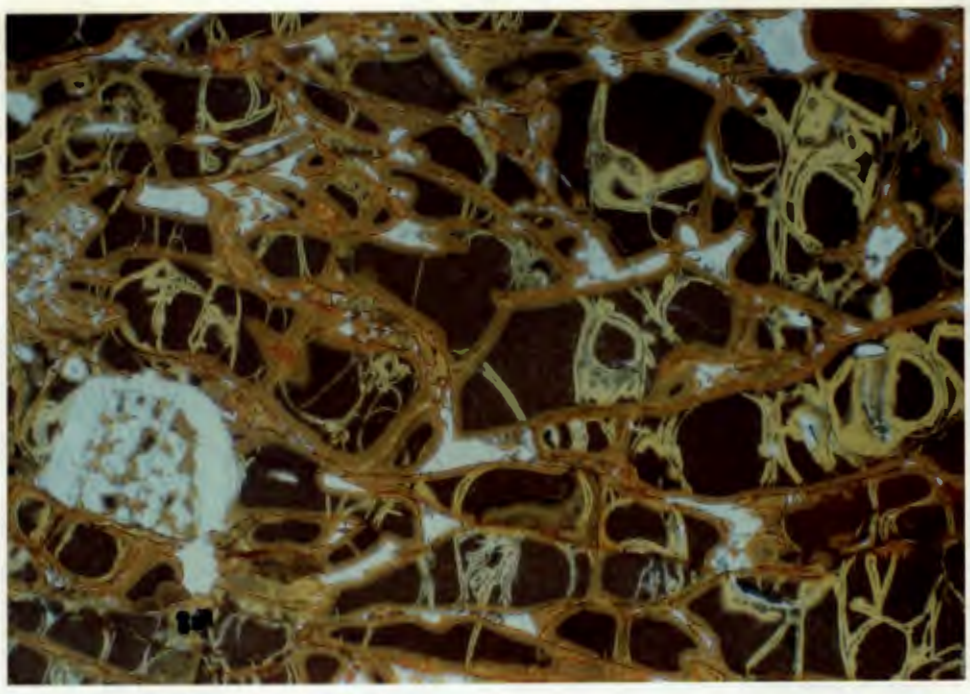

Partially welded lapilli-tuff, Gemini quartz latite (SM-229G). Part of Plate 4.9. Incipient welding and compaction of juvenile fragments which were once quite angular. Sieve textured plagioclase lower left. Comparison with Plate 4.7 highlights a reduction in both the porosity and the alteration of this sample

PLATE 4.12

More strongly welded lapilli-tuff, Gemini quartz latite (SM-229A). Friable pitchstone material (Plate 2.11) with piperno texture. Glassy fragments are more strongly flattened, compare with Plate 4.9. Note the poorly sorted nature, with submillimetre- to centimetre- sized fragments.

PLATE 4.13

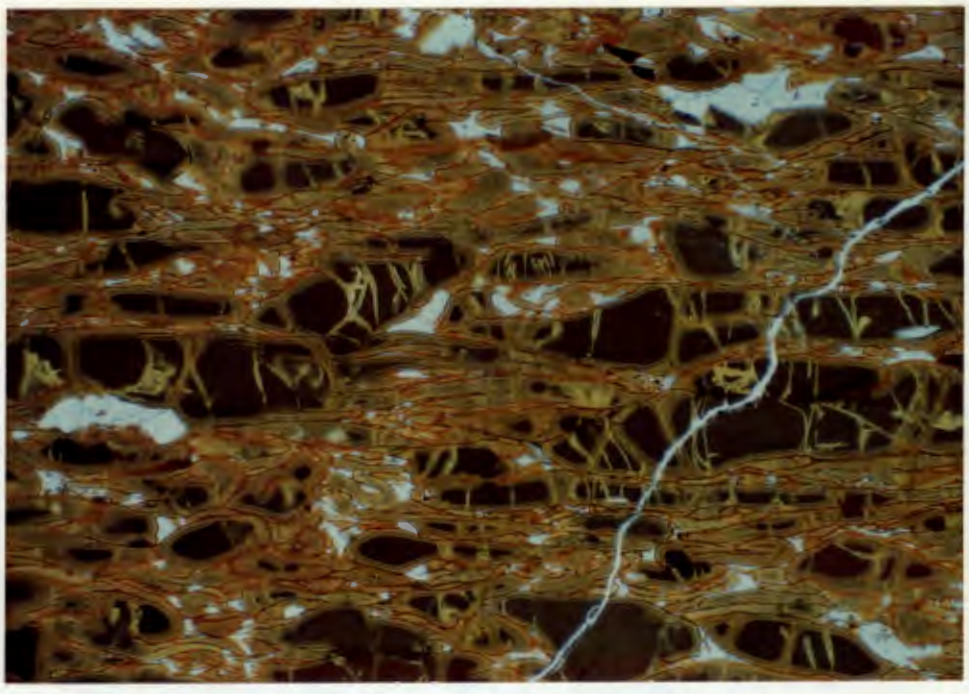

1.0 mm

More strongly welded lapilli-tuff, Gemini quartz latite (SM-229A). Part of Plate 4.13. Compaction and stretching of the glass fragments is more pronounced with an even greater reduction in porosity. Compare with Plates 4.10 and 4.11.

PLATE 4.14

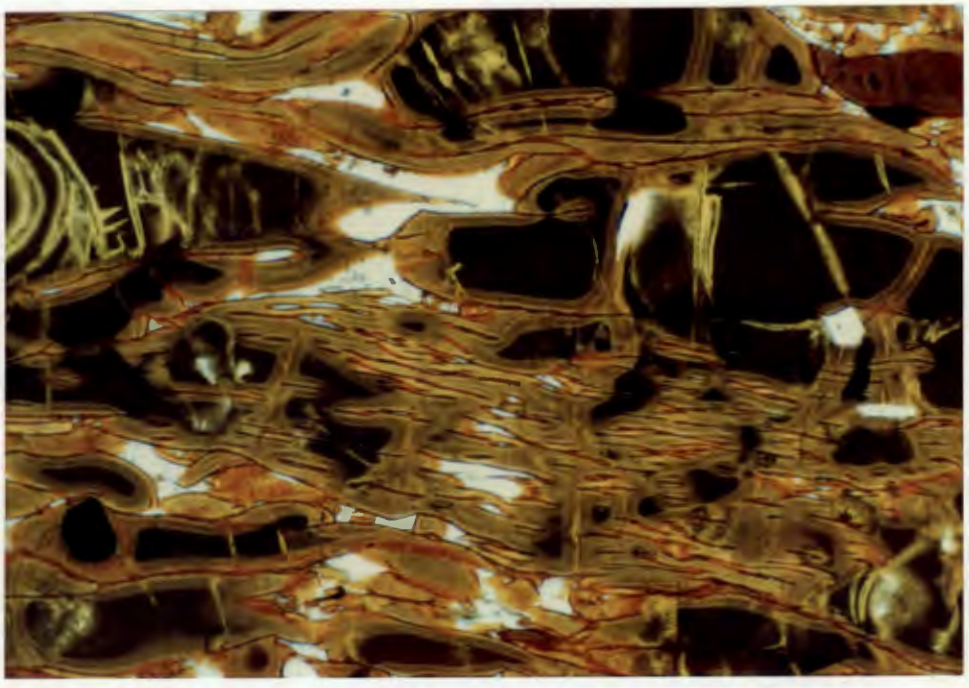

0.5 mm

More strongly welded lapilli-tuff, Gemini quartz latite (SM-229A). Part of Plate 4.13. Collapsed pumice fragment in which the vesicles have become completely flattened.

PLATE 4.15

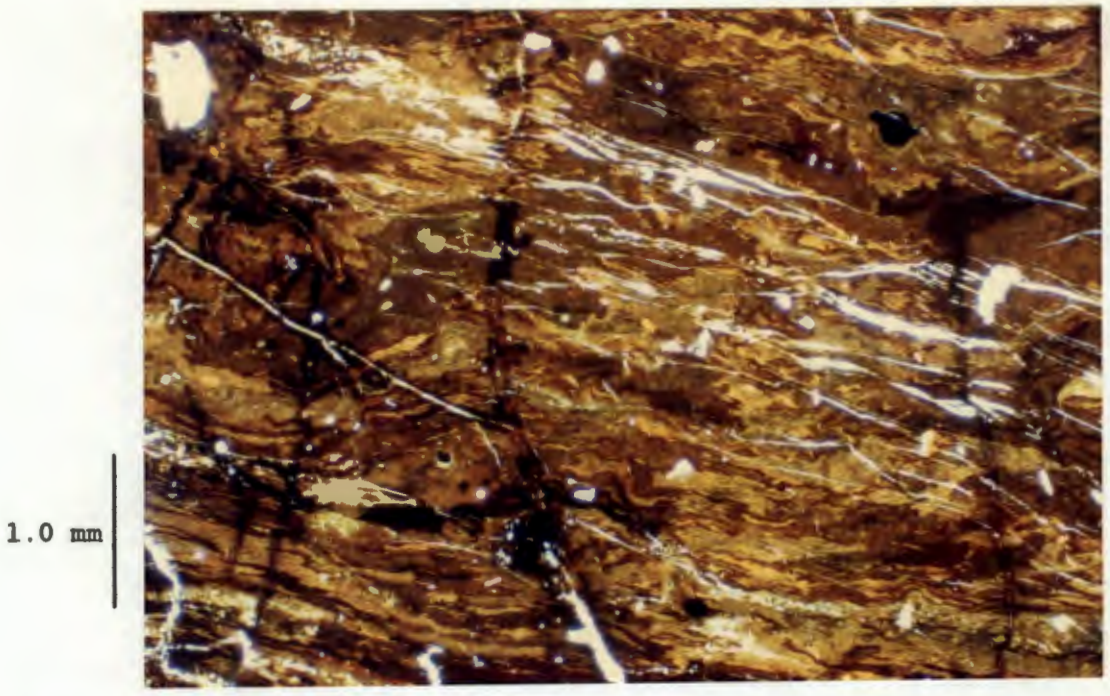

Flow-banded quartz latite, Gemini quartz latite (SM-229E). Orange-brown flow-banded material (Plate 2.11). Fragments are completely altered and devitrified, and show signs of extreme stretching and rheomorphism. White gashes are quartz-filled fractures which probably resulted from a reduction of volume on devitrification.

PLATE 4.16

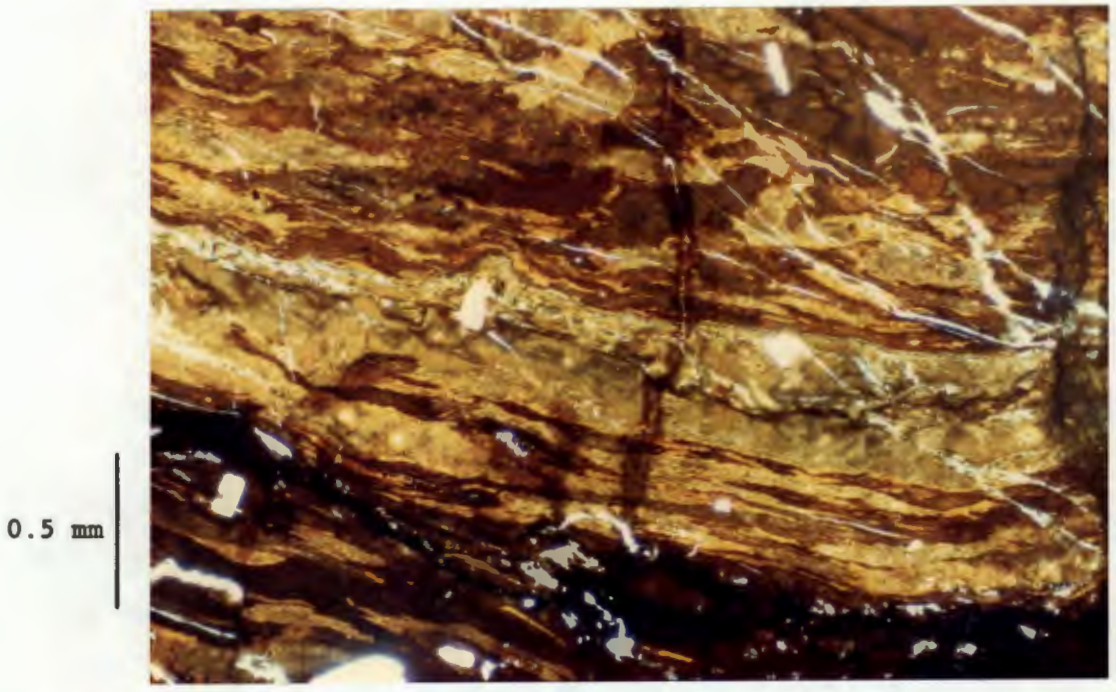

Flow-banded quartz latite, Gemini quartz latite (SM-229E). Part of Plate 4.15. Shows more clearly the streaks and flow textures which are interpreted as rheomorphosed fragments, and illustrates the final stage of the progressive welding and compaction of fragments illustrated in Plates 4.5 - 4.14.

indicating that these features were generated prior to the development of the breccia. For these reasons these clasts are considered to be cognate in character, distinct from the juvenile material discussed earlier. The breccias range from clast- to matrix-supported. The matrix consists of ash- and lapilli-sized fragments similar to that described in the previous section. An increase in the amount of matrix material and the degree of welding towards the main body of the flow, indicated in Chapter 2 (Subsection 2.6.2) is also noted petrographically. Plates 4.17 - 4.21 show some of the textures encountered in a flow base breccia in the Lower Tafelberg quartz latite (Pilchard Gorge, Fig. 2.3). Incipient welding is indicated by the moulding together of lithic fragments at their contact points (Plate 4.17). Notice that this specimen is clast-supported with little juvenile matrix material. Thin-sections of a more strongly welded breccia are illustrated in Plates 4.20 and 4.21. In this specimen the proportion of juvenile glass and pumice fragments is much greater, and the welding of lithic clasts and matrix material much more intense.

4.2.3 Pitchstones

Some pitchstones, notably those consisting of brown glass (Subsection 3.2.4), exhibit textures that are consistent with the welding of lapilli- and ash-sized fragments. Most of the fragments are apparently juvenile in origin (Plate 4.22) however, a pitchstone breccia in which some of the clasts are clearly cognate is illustrated in Plate 4.23. Cognate character is indicated by flow banding in some of the clasts which does not parallel the crude compaction fabric present, and by the fairly angular, non-vesicular morphology of such clasts.

The collapse of pumice fragments and the reduction of porosity during welding is often accompanied by compaction, although this is not always so. Plate 4.24 illustrates collapsed pore spaces between glassy fragments which show no discernible flattening. This texture is very similar to textures observed in globule ignimbrites at Mt. Suswa, Kenya (Hay *et al.*, 1979; Figure 5). Loss of interstitial volatiles probably occurred by diffusion along grain boundaries and Schmincke (1974) suggests that some "gas entrapped in pumice vesicles is redissolved in the glass when the pumice collapses during welding" which may further account for the reduction in porosity. Almost spherical vesicles sometimes coexist with flattened structures which represent relics of the primary porosity, Plates 4.25 and 4.26. Similar occurrences in peralkaline

PLATE 4.17

1.0 cm

Basal Breccia, Lower Tafelberg quartz latite, Pilchard Gorge. Cognate clasts of devitrified quartz latite cemented by quartz. Incipient welding occurs where the clasts touch. Notice the random orientation of clasts with flattened vesicles.

PLATE 4.18

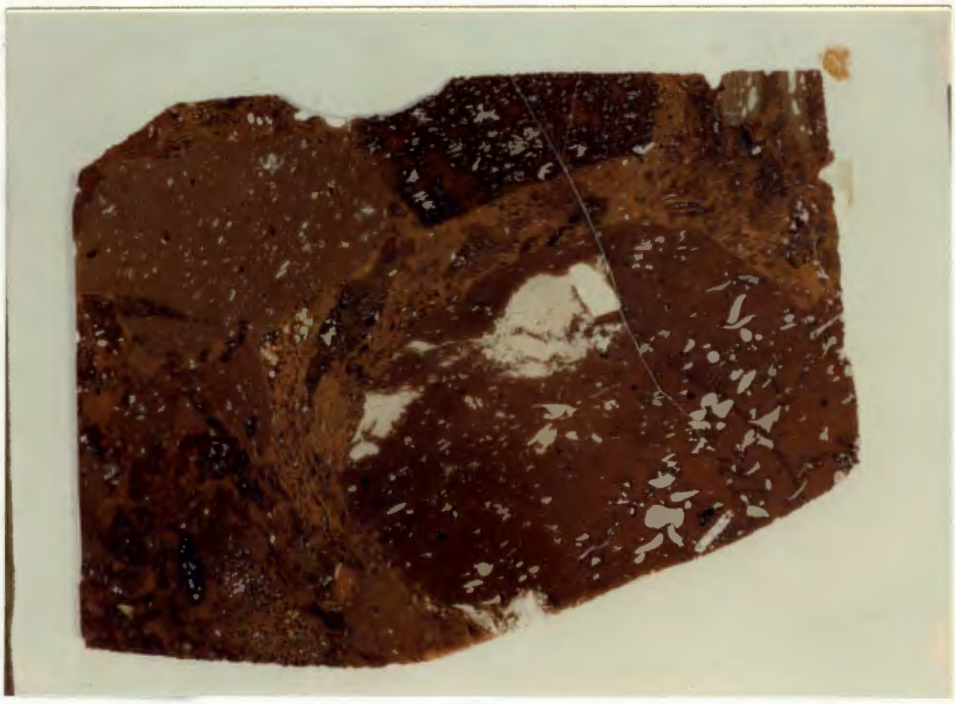

1.0 cm

Basal breccia, Lower Tafelberg quartz latite, Pilchard Gorge. Cognate clasts of quartz latite in a welded matrix of glass fragments and smaller lithic fragments.

PLATE 4.19

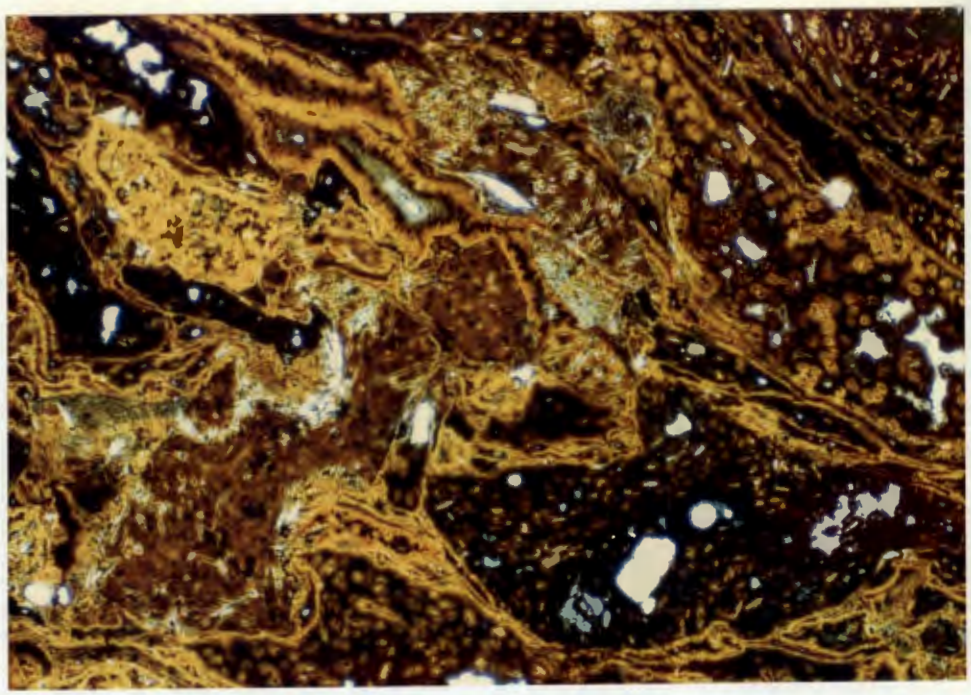

Matrix of basal breccia, Lower Tafelberg quartz latite, Pilchard Gorge. Part of Plate 4.18. Fragments of glass tightly packed together. Quenched microlites and spherulites are clearly visible.

PLATE 4.20

Strongly welded basal breccia, Lower Tafelberg quartz latite, Pilchard Gorge. Cognate clasts of quartz latite and juvenile pumiceous material in a welded matrix of finer grained fragmental material.

PLATE 4.21

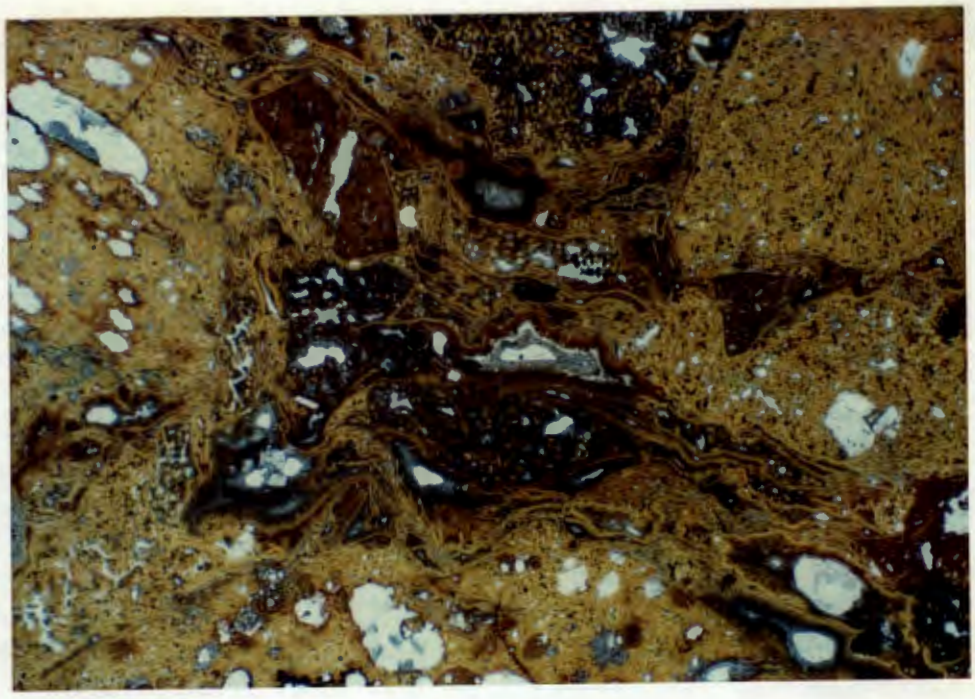

1.0 mm

Strongly welded basal breccia, Lower Tafelberg quartz latite, Pilchard Gorge. Part of Plate 4.20. Yellow, occasionally vesicular, clasts of quartz latite (extreme right, left and bottom) in a strongly welded matrix (centre). Notice that with this more intense welding the edges of the clasts become indistinct.

PLATE 4.22

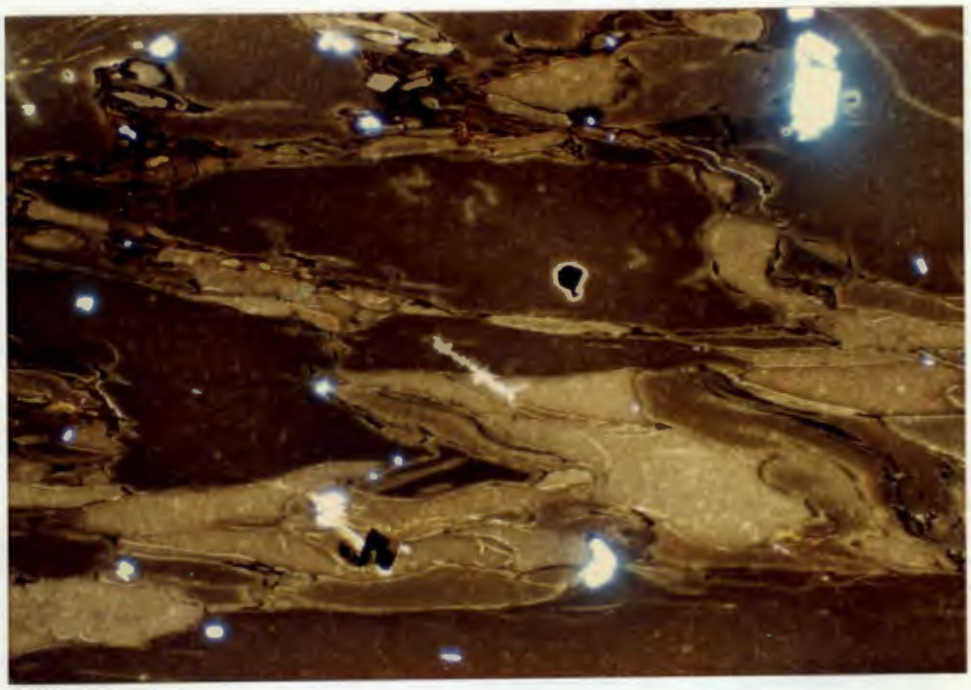

1.0 mm

Friable pitchstone, Gemini quartz latite(?) (SM-155). Strongly welded clasts of dark brown hydrated obsidian which show some flattening. Phenocryst of plagioclase(white) and Ti-magnetite(black) can also be seen. Clasts are thought to be juvenile in origin and some are undoubtedly pumiceous, see Plates 4.25 and 4.26.

PLATE 4.23

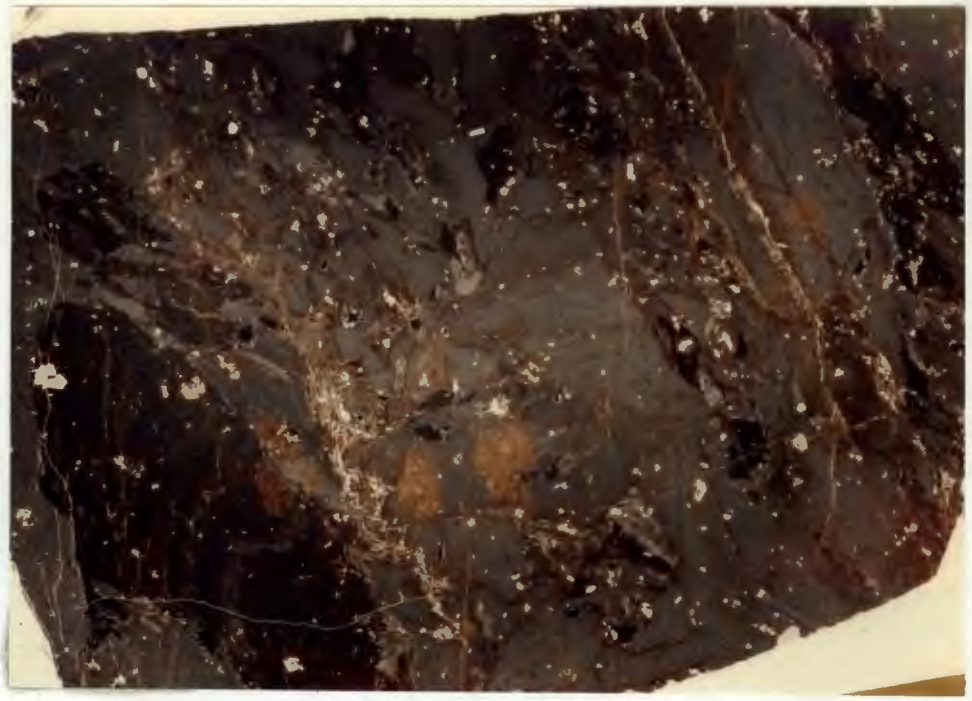

Welded pitchstone breccia, Lower Interbedded Coastal quartz latite (SM-152B). The cognate character of many of the clasts is indicated by flow- banding which does not parallel the crude compaction fabric, which runs diagonally, top left to bottom right. Notice also that the clasts are non-vesicular.

PLATE 4.24

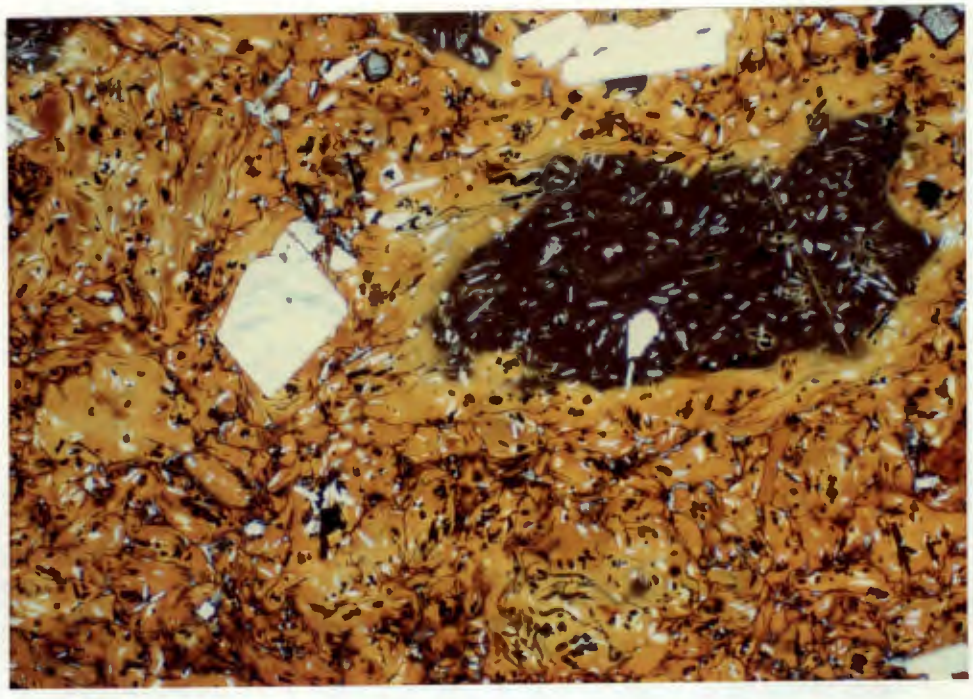

Globule pitchstone, Upper Springbok quartz latite (SM-220). Welded fragments of glass with no appreciable flattening or alignment gives the rock an unusual globule texture. Much of the glass is altered, the dark brown area representing fresher glass at the centre of a larger fragment. Phenocrysts of plagioclase (white), hyperstene (top right) and Ti-magnetite (black) are also present.

PLATE 4.25

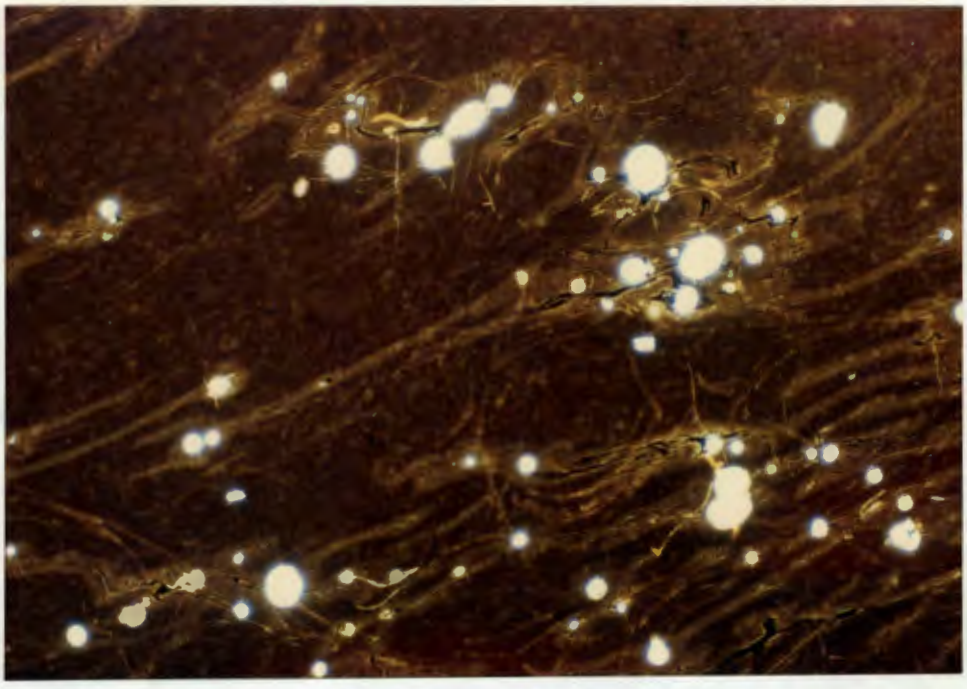

0.5 mm

Friable pitchstone, Gemini quartz latite (?) (SM-155). Thin pale brown lines running diagonally are relict vesicles which have collapsed completely. The round white structures are secondary vesicles which must have formed during late-stage exsolution of volatiles from the glass.

PLATE 4.26

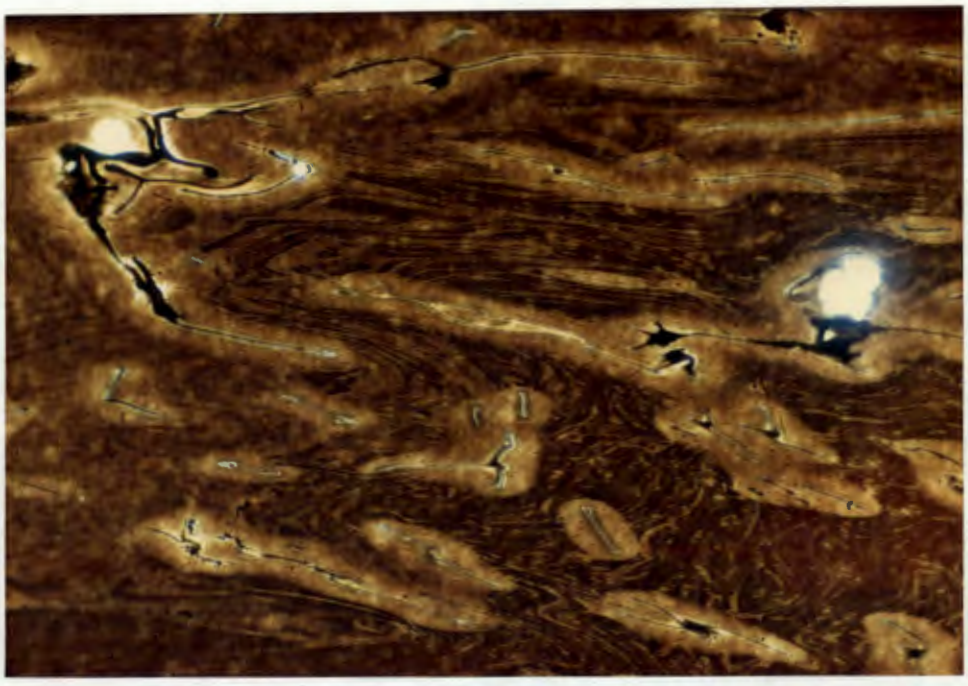

0.25 mm

Friable pitchstone, Gemini quartz latite (?) (SM-155). Collapsed vesicles at higher magnification. Notice that in most cases both walls of the vesicles can still be recognised.

ash-flow tuffs are described by Schmincke (1974) who regards them as secondary. Vesiculation of this nature is thought to have occurred after eruption and emplacement, and represents the exsolution of volatiles from the glass before final cooling.

Pitchstones containing clastic features are widely encountered, with examples from the Springbok, Tafelberg and Interbedded Coastal successions.

4.2.4 Laminar Banding and Fiammé

Laminar banded quartz latite represents strongly compacted and welded material which often contains collapsed pumice lapilli or fiammé. Differential alteration often picks out the fiammé in shades of purplish-grey against the orange matrix of the rock. The fiammé are often mottled due to the development of spherulites and granophyric intergrowths of quartz and alkali-feldspar. The fiammé have high length:thickness ratios, in some specimens averaging 20, indicating a high degree of compaction and welding (Fisher and Schmincke, 1984). Despite this, spherical secondary vesicles are commonly observed. Structures developed around rigid phenocryst are consistent with a degree of rheomorphic flow in some of the laminar banded quartz latites and are not merely a consequence of welding and compaction.

Plates 4.27 - 4.28 show the characteristics of banding and fiammé in specimens collected from the base of the Lower Tafelberg unit at the "Dunes" outcrop and Pilchard Gorge (Figs. 2.3 and 2.10).

4.3 SUMMARY

(1) Pyroclastic material of both juvenile and cognate character is recognised. The juvenile material consists of glassy fragments and shards, pumice and pyrogenic crystals. The cognate material consists of lithic fragments of devitrified quartz latite and pitchstone.

(2) Welding accompanied by compaction (in most cases) results in a marked reduction in porosity and a flattening of components producing eutaxitic and piperno textures with fiammé.

(3) Intense welding and compaction may be accompanied by flow features which

PLATE 4.27

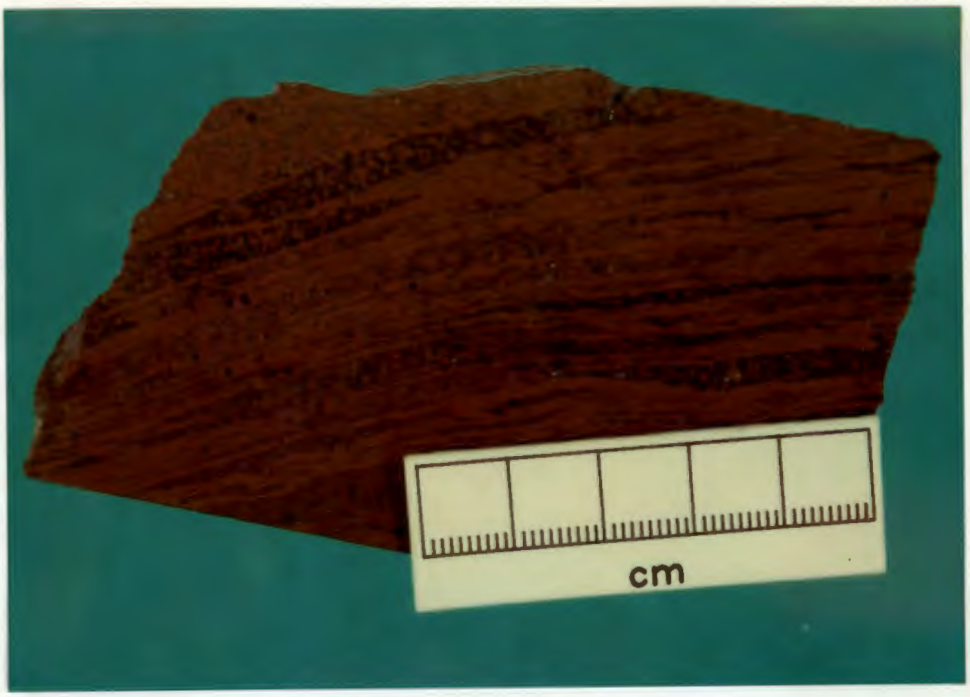

Fiammé textured quartz latite, Lower Tafelberg quartz latite, Pilchard Gorge. Polished slab of fiamme textured quartz latite from the laminar banded zone (Fig. 2.12). Flattened pumice fragments are clearly visible.

PLATE 4.28

Fiammé textured quartz latite, Lower Tafelberg quartz latite, Pilchard Gorge. Thin section of material illustrated in Plate 4.27. The pale grey horizontal bands with rust-coloured spots (spherulites) are the flattened pumice clasts. Notice the flame-like terminations to some of the clasts. The black spots are phenocrysts of Ti-magnetite.

indicate post-depositional rheomorphic flow.

(4) Despite the strong welding and compaction experienced by some pitchstones and fiammé-bearing specimens spherical vesicles are commonly observed. These are interpreted as secondary, resulting from the exsolution of volatiles from glass as the unit cools.

(5) Eutaxitic textures and fiammé are observed in rocks showing high temperature devitrification (spherulites with interstitial quartz and alkali-feldspar, Section 3.5). Indicating that although devitrification tends to obscure these textures to a certain degree it does not necessarily destroy them entirely.

(6) The intensity of low temperature glass alteration (Subsection 3.4.4) is dependent upon the degree of welding and the resultant porosity.

CHAPTER 5

MINERAL CHEMISTRY OF THE ETENDEKA FORMATION QUARTZ LATITES

5.1 INTRODUCTION

This chapter presents electron microprobe data for the principle mineral phases described in Chapter 3 and illustrates the compositional trends of plagioclase, pyroxene and Fe-Ti oxides within and between various groups of quartz latites. The compositions of individual minerals were determined by microprobe and a brief summary of the analytical procedures and conditions is presented in Appendix 2. A full listing of the microprobe data is given in Tables 25 - 30 on microfiche. Most of the microprobe work was carried out on pitchstone samples in which the mineral phases appear relatively unaltered (Chapter 3) and the majority of the analyses represent phenocryst compositions. A smaller number of determinations on microphenocryst and groundmass phases were also carried out. Table 5.1 lists those samples for which microprobe data is available, some of which are described in detail in Appendix 1 (with modal proportions in Table 3.1). Application of the Lindsley (1983) and Glazner (1984) geothermometers, using pyroxene and plagioclase respectively, indicate crystallisation temperatures between 975 and 1200 °C which are significantly higher than those usually envisaged for acidic melts.

5.2 FELDSPAR

5.2.1 Plagioclase

Data for plagioclase phenocrysts and microphenocrysts are presented separately so that their trends can be defined more clearly. Fig. 5.1 illustrates the range of phenocryst compositions displayed by the southern Etendeka quartz latites and the Sarusas quartz latites and latites. Analyses from the southern Etendeka range from An_{25} - An_{66} with the majority being labradoritic in composition. The Springbok quartz latites (Fig. 5.1a) exhibit a fairly tight compositional range (An_{53} - An_{61}) with no distinction between upper and lower units, whereas plagioclases from the Tafelberg and Interbedded Coastal quartz latites (Fig. 5.1b) show decreasing anorthite content with increasing stratigraphic height.

Table 5.1

List of samples and phases analysed by electron microprobe.

Quartz Latite Unit(s)	Sample Number	Phenocrysts	Micro-phenocrysts	Ground-mass
Lower Springbok	SM-017	Pl Pig Ti-Mt	–	–
	SM-208	Pl Pig Ti-Mt	–	–
	SM-212	Ti-Mt	–	–
	SM-215	Ti-Mt	–	–
Upper Springbok	SM-168	Pl Hyp Pig Ti-Mt	Pl Pig Ti-Mt	–
	SM-172	Pl Pig Ti-Mt	Pl Pig Ti-Mt	Glass
Lower Tafelberg	SM-179	Pl Ti-Mt	Pig Aug Ti-Mt	Glass
Lower Interbedded Coastal	SM-154	Hyp	Pig Aug	–
	SM-160	Pl Hyp Ti-Mt	Pl Pig Aug Ti-Mt	Glass
	SM-180	Pl Hyp Pig Ti-Mt	–	–
Upper Interbedded Coastal	SM-161	Pl Aug	–	–
	KLS-281	Pl Aug	–	–
Tafelberg Beacon	SM-007	Pl Aug	–	K-Spar
Sarusas (a-type)	SM-112	Pl Aug	Pl Aug	–
Sarusas (b-type)	SM-110	Pl Aug	–	K-Spar
	SM-115	Pl Aug Ti-Mt	Pl Ti-Mt	–
Sarusas Latite	KLS-327	Pl Pig Aug Ti-Mt Ilm	Pl	K-Spar

Pl = Plagioclase
Pig = Pigeonite
Aug = Augite
Ilm = Ilmenite
K-Spar = Potassium feldspar
Hyp = Hypersthene
Ti-Mt = Titano-magnetite

Fig. 5.1 Quartz Latite Plagioclase Phenocryst Compositions

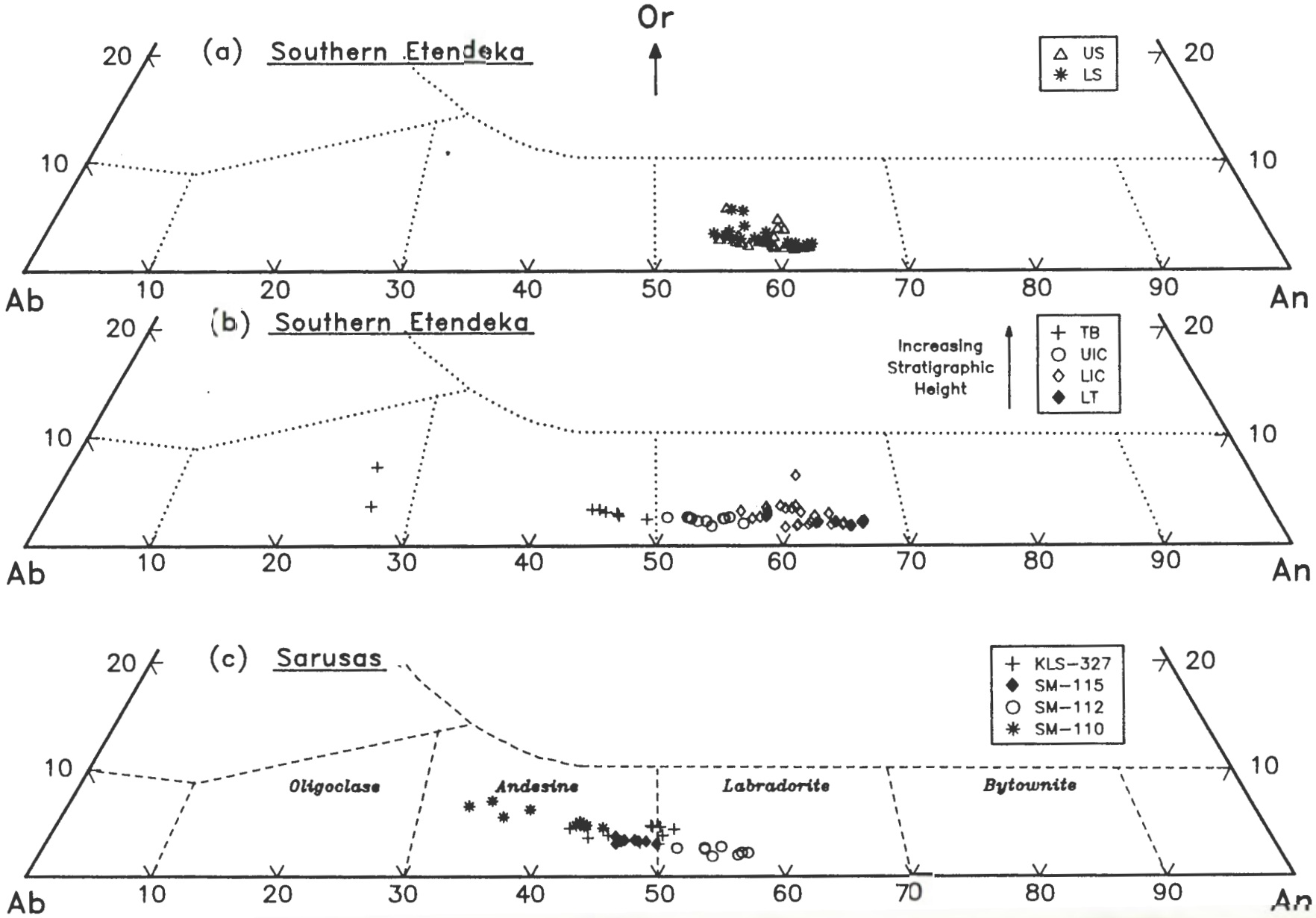

The Sarusas quartz latite and latite plagioclase compositions range from An_{32} - An_{56} (Fig. 5.1c). The trend observed is not simply related to either the stratigraphy or the whole rock chemistry. Sample SM-112 which exhibits the most "basic" plagioclase compositions has the most evolved whole rock composition which is quite distinct from the other samples. Note that the subhedral morphology of the plagioclase crystals in this sample indicates that they are not of a xenocrystic origin. Whole rock compositions of samples KLS-327, SM-115 and SM-110 are increasingly evolved (Tables 22 and 24 on microfiche), with the plagioclase compositions apparently defining a fractionation trend (note: SM-110 is the most porphyritic sample).

The compositions of plagioclase microphenocrysts are illustrated in Fig. 5.2. Microphenocrysts from the Upper Springbok and Lower Interbedded Coastal quartz latites show slightly more evolved compositions than coexisting phenocrysts. Plagioclase microphenocrysts determined in the Sarusas samples, SM-115 and KLS-327, also show more evolved compositions; note that they fall within the range displayed by the phenocrysts from SM-110 (Fig. 5.1a) but with a slightly lower orthoclase content.

The Fe content of the plagioclase varies between 0.4 and 1.4 wt% FeO (total Fe as FeO) and is broadly correlated with the plagioclase composition, Fig. 5.3. The tendency for iron to increase with An-content and with the temperature of crystallisation is well known (Smith, 1983). Smith (1983) indicates that the highest iron contents have been observed in volcanic bytownites at approximately 1.3 wt% FeO (1 wt% Fe), a concentration reached by several of the Etendeka quartz latite labradorites.

5.2.1.1 Plagioclase Zonation

Table 5.2 indicates the total variation in anorthite content of plagioclase phenocrysts from individual samples and shows the maximum degree of zonation observed within a single phenocryst from that sample. Although a detailed zonation study has not been attempted it appears that the zonation patterns are relatively simple, although some samples do contain plagioclases which exhibit both normal and reverse zonation. Many of the phenocrysts analysed show little compositional variation from core to margin and in some instances it is only the very outer rim of the crystal which shows any marked change.

Fig. 5.2 Quartz Latite Plagioclase Microphenocryst Compositions

Fields indicate phenocryst compositions

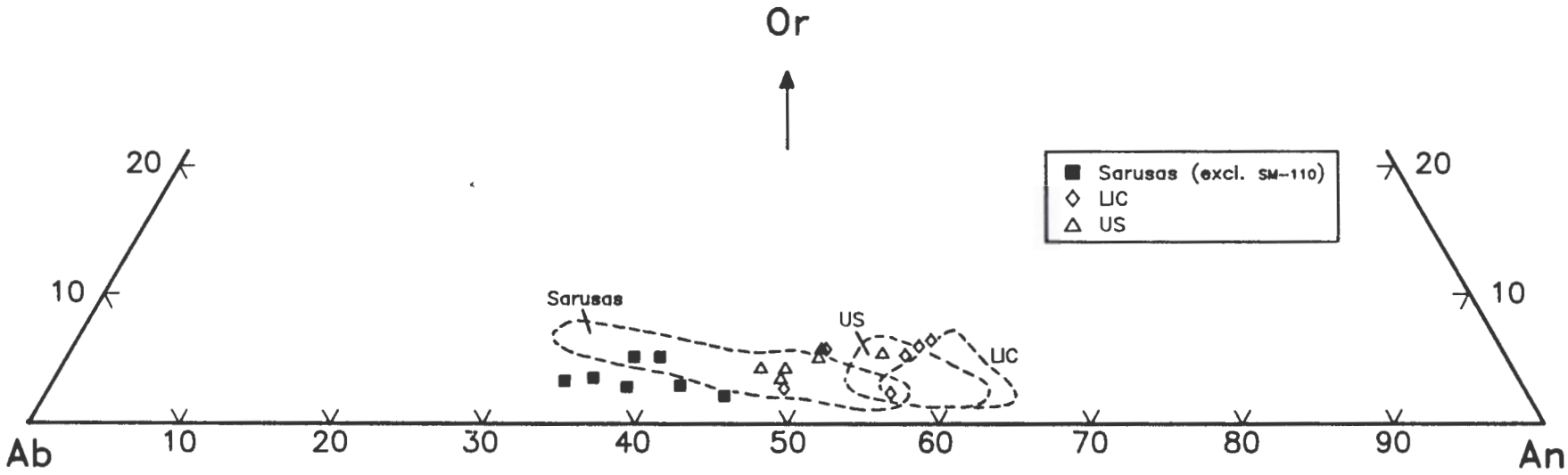

Fig. 5.3 FeO *vs.* Anorthite in Plagioclase.

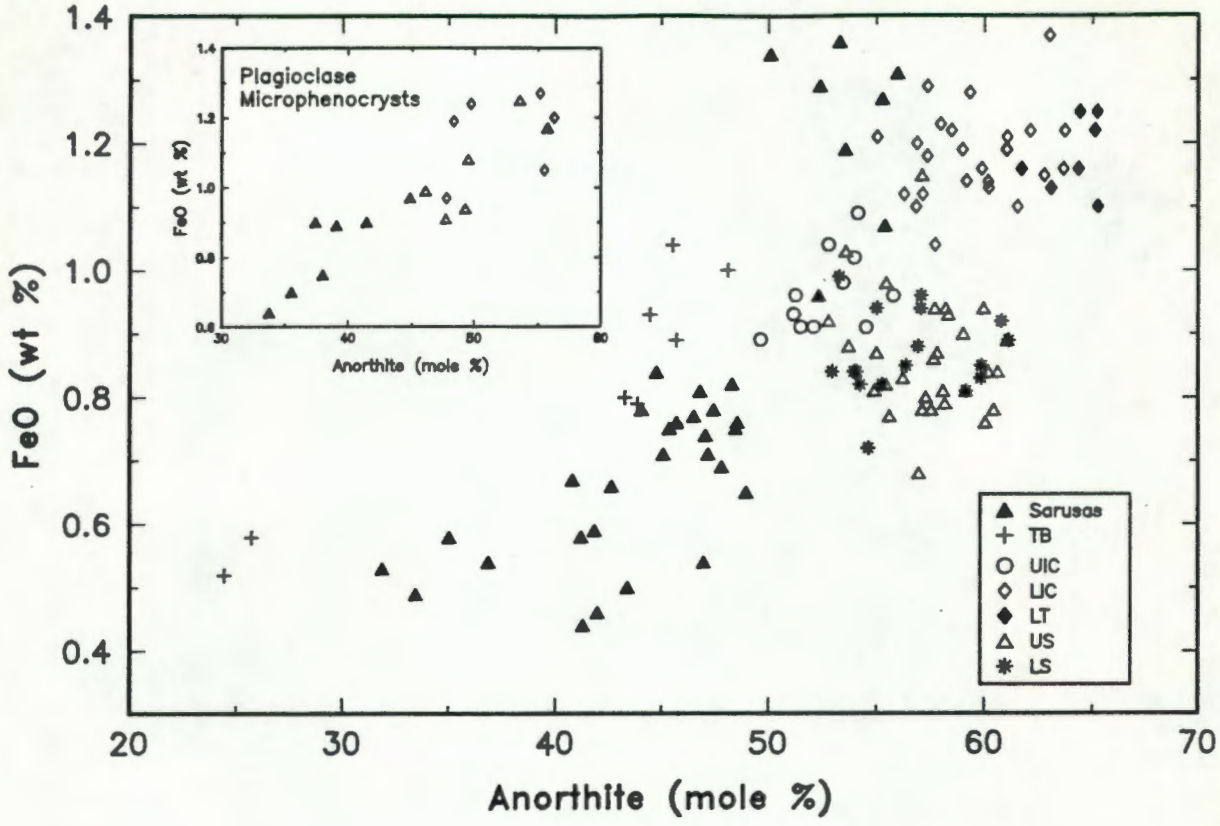

Table 5.2 The compositional range of plagioclase phenocrysts within individual samples and the maximum degree of zonation observed in that sample.

Sample Number	Compositional Range (mole % An)	Maximum Zonation –individual crystal (mole % An)	Zonation type– N = normal R = reverse
SM–017	7.0	5.2	N/R
SM–208	7.6	7.5	N
SM–168	8.5	2.0	N/R
SM–172	6.5	6.5	N
SM–179	3.5	–	–
SM–160	8.0	6.1	R
SM–180	8.5	3.8	N
SM–161	3.8	–	–
KLS–281	1.8	–	–
SM–007	22.0	nd	N
SM–110	10.0	10.0	N
SM–112	6.0	2.0	N
SM–115	3.5	1.0	N
KLS–327	8.0	3.0	N

5.2.2 Alkali-feldspar

The only alkali-feldspar analysed in the quartz latites and latites has been located in the groundmass mesostasis of devitrified or felsitic rocks. The summary below indicates the variable composition of alkali-feldspar.

Sample	An	Ab	Or
Tafelberg Beacon quartz	1.71	48.05	50.24
latite (SM-007):	0.80	41.37	57.83
Sarusas quartz latite	1.45	27.91	70.04
(SM-110):	1.09	30.10	68.81
	1.27	28.72	70.01
Sarusas latite (KLS-327):	3.55	44.78	51.67
	2.43	41.26	56.31
	1.83	36.21	61.96
	** 5.18	66.91	27.91

** Stubby lath-shaped crystal in the groundmass.

5.3 PYROXENE

Pyroxene phenocrysts in the southern Etendeka quartz latites (Fig. 5.4a) include Mg-rich hypersthene (En_{56-67}, $Wo_{3.4-3.8}$), intermediate pigeonite (En_{44-57}, Wo_{6-11}) and augite (En_{36-40}, Wo_{34-36}). The following observations are pertinent:

(1) Ca-poor pigeonites which coexist with hypersthene in the Upper Springbok unit (sample SM-168) have compositions which are distinct from those compositions obtained from the Upper Springbok unit (sample SM-172), where pigeonite is the only pyroxene present. Analyses of the latter are similar to the pigeonite compositions from the Lower Springbok and Upper Interbedded Coastal quartz latites

(2) The most Mg-rich hypersthene and pigeonite occurs in the Lower Interbedded Coastal quartz latites, which is consistent with the Ca-rich plagioclase compositions observed in these samples (Fig. 5.1b).

Fig. 5.4 Quartz Latite Pyroxene Phenocryst Compositions

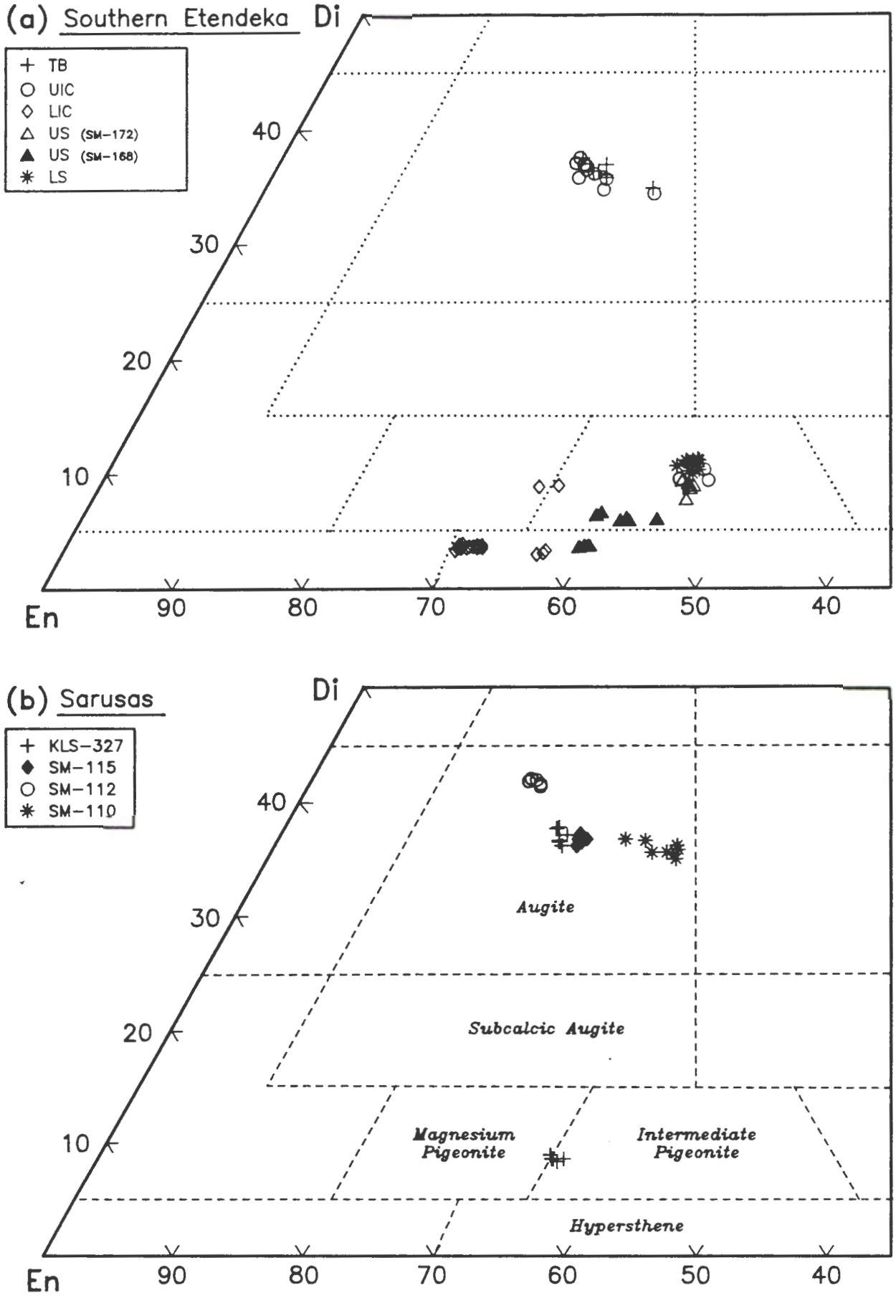

(3) Two distinct compositions for hypersthene, average En_{65} and En_{60} respectively, were obtained in one of the Lower Interbedded Coastal quartz latites (sample SM-154, Table 27 on microfiche). The more evolved compositions belong to three phenocrysts with a smaller than average grain size and probably represent relatively late stage crystallisation.

Pyroxene phenocryst compositions from the Sarusas quartz latites and latites (Fig. 5.4b) are dominated by augite with some minor pigeonite (En_{56} Wo_{8}). Augite compositions from samples KLS-327, SM-115 and SM-110 exhibit a range, En_{33-42} Wo_{35-38}, which defines a trend toward more Fe-enriched compositions in SM-110. This is in accord with a comparable trend towards more sodic plagioclase compositions observed in the these samples. The augite from sample SM-112 with an average composition En_{41} Wo_{42} is separated from this trend.

The composition of pyroxene microphenocrysts and microlites is presented in Fig. 5.5 which illustrates the following features:

(1) The composition of pigeonite in sample SM-168, which includes analyses of pigeonite mantling hypersthene, defines a trend towards more Ca- and Fe-rich pigeonite which is situated to the right of the main cluster of analyses for Springbok quartz latite pigeonite.

(2) Quenched pyroxene microlites in the Lower Tafelberg sample (SM-179) exhibit a wide range of compositions from Mg-rich pigeonite to augite. Compositions which fall in the field for subcalcic augite are consistent with observations made on rapidly cooled volcanic rocks (Deer *et al.*, 1966). Rapid crystallisation of metastable solid solutions is thought to give rise to such an extended compositional range, a feature indicated by the unmixing of some subcalcic augites on a cryptoperthitic scale (Deer *et al.*, 1966).

(3) Mg-rich pigeonite compositions from the Lower Interbedded Coastal quartz latite microphenocrysts, are similar to the compositions of phenocrysts in these rocks.

The presence of non-quadrilateral components in the pyroxene structure affects the activities of the Wo, En and Fs components (Lindsley, 1983) and is an important consideration regarding the use of pyroxenes as geothermometers (Section 5.4). Common non-quadrilateral constituents in pyroxenes include Ti,

Fig. 5.5 Quartz Latite Groundmass* Pyroxene Compositions

* Includes microphenocrysts, microlites and pigeonite rims on hypersthene (SM-168).

○ Sarusas (SM-112)
◇ LIC
◆ LT (SM-179)
△ US (SM-172)
▲ US (SM-168)

Fields indicate the range of phenocryst composition

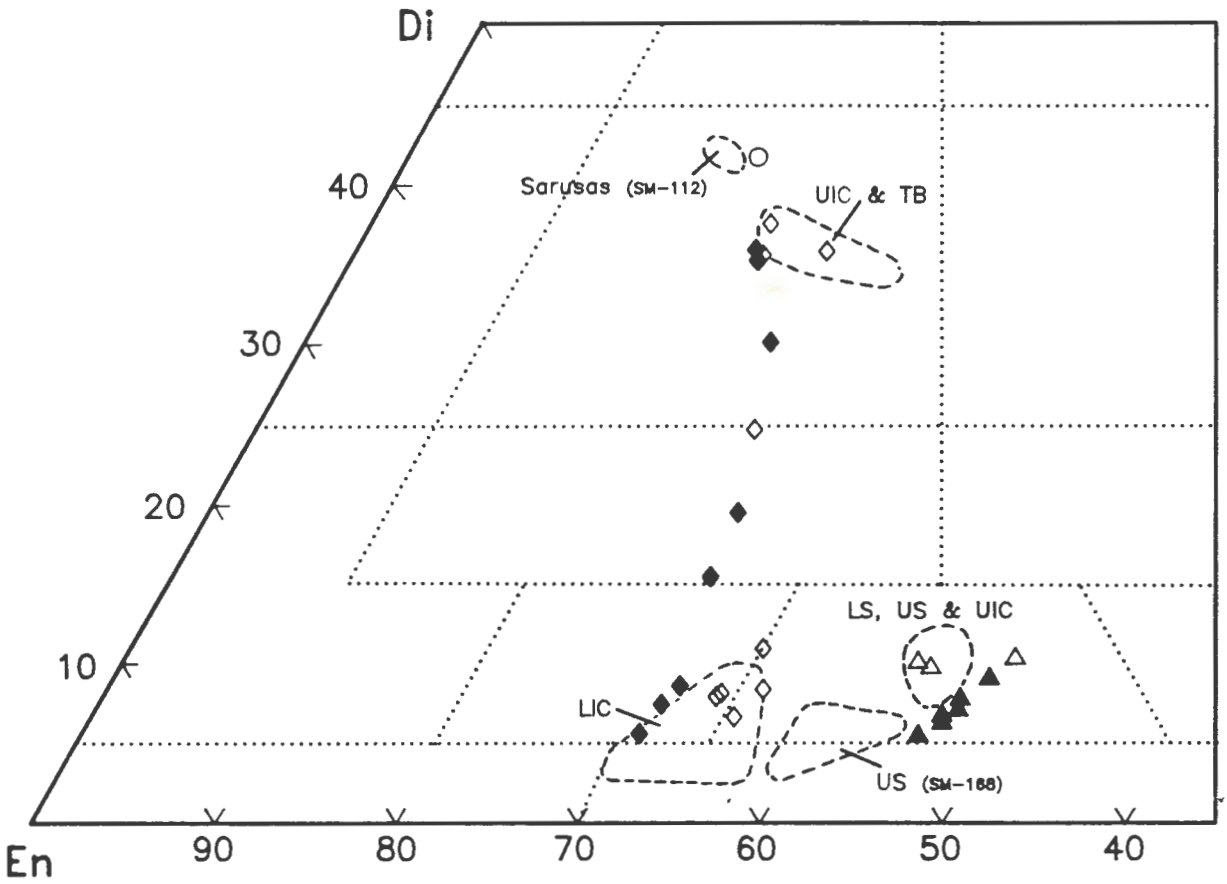

Al, Cr, Fe^{3+}, Mn and Na. Cr is below the microprobe detection limit (0.05 %) in all of the Etendeka Formation quartz latite pyroxenes and Na concentrations are low, <0.05, <0.1 and <0.3 wt% Na_2O for hypersthene, pigeonite and augite respectively. Fe^{3+} can only be inferred from the total iron obtained in a microprobe analysis using charge balance considerations (Lindsley, 1983). The main non-quadrilateral components in the quartz latite pyroxenes are Ti, Al and Mn (Fig. 5.6). Minor and trace element partitioning between coexisting pyroxenes and between pyroxenes and melt is poorly understood (Heubner, 1980) and only general observations are made here.

(1) Ti concentrations in the quartz latite pyroxenes (Fig. 5.6a) are similar to those quoted for pyroxenes by Deer *et al.* (1966). A correlation between the TiO_2 (wt%) content of the pyroxenes and that of the respective host rocks (see Chapter 6) indicates a whole rock compositional dependence of Ti in pyroxenes. This feature was also recognised by Bellieni *et al.* (1984), who obtained correlation coefficients of greater than 0.89 for pyroxene/host rock pairs during their investigation of the flood basalt to rhyolite suite of the Paraná, Brazil.

(2) Al varies from 0.6 - 2.5 wt% Al_2O_3 in the quartz latite pyroxenes and in hypersthene and augite there is a tendency for Al_2O_3 to increase with Mg/(Mg + Fe) as shown in Fig. 5.6c. This may reflect a temperature dependency for the partitioning of Al^{3+} into pyroxene or possibly a dependency on the Fe^{3+}/Fe^{2+} ratio of the bulk rock. The Al content of pigeonite is comparatively low, generally < 0.8 wt Al_2O_3, and there is often insufficient Al^{3+} in pigeonite to bring Si + Al to the ideal solution of 2 atoms per formula unit, introducing the possibility that Fe^{3+} and Ti may substitute in the tetrahedral site (Deer *et al.*, 1966).

(3) The distribution of Mn appears to be the inverse of that obtained for Al and generally reaches higher concentrations in the Fe-enriched pyroxenes, compare Fig. 5.6d with Fig. 5.6b. The correlation of MnO with FeO is illustrated in Fig. 5.6e.

Fig. 5.6 Minor elements in quartz latite pyroxene phenocrysts

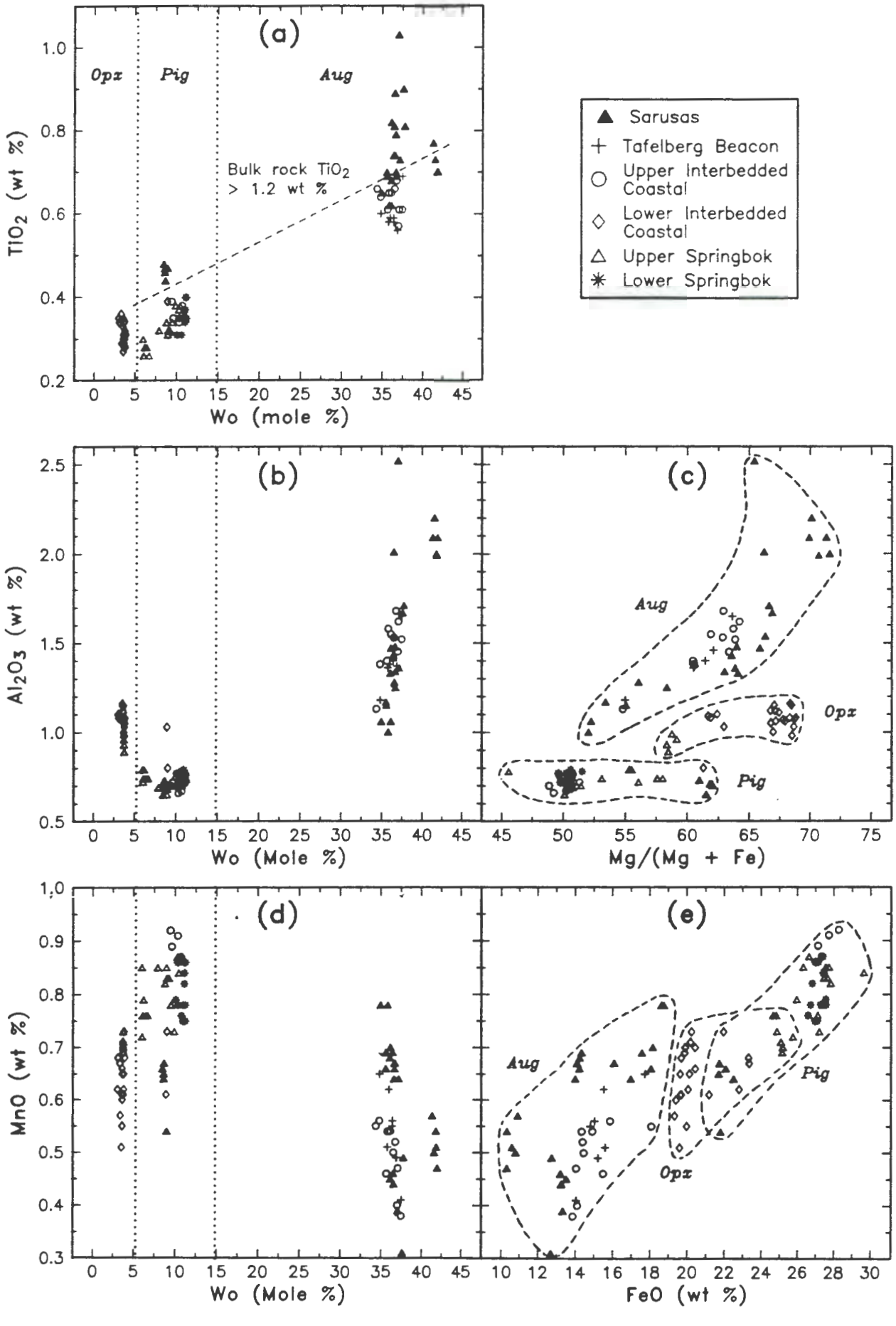

5.4 FE-TI OXIDES

5.4.1 Problems related to the oxidation of magnetite

Post-eruptive oxidation of Ti-magnetite, indicated by the exsolution of ilmenite or by progressive maghemitisation (Subsection 3.4.3), causes difficulties in determining the original composition of Ti-magnetite which crystallised from a quartz latite magma.

Exsolution of ilmenite obviously has a profound effect on the composition of the host magnetite, even during the early (C_2-C_3) stages (Chapter 3) of its development. For most quartz latite units it has been possible to avoid this problem by analysing magnetites from rapidly quenched glassy rocks. However, the lower temperature maghemitisation of magnetite is widespread and less easily avoided during sampling.

The calculation of atomic proportions, notably the Fe^{3+}:Fe^{2+} ratio, from microprobe data is based on the premise that a specific phase is stoichiometric. Analyses of many of the Etendeka quartz latite Ti-magnetites yielded low totals (96.5 - 100 %) when reduced on the basis of four oxygens (three cations). These low totals can be ascribed to the presence of maghemite, a cation-deficient spinel which is non-stoichiometric. The formation of maghemite, which generally leads to an increased reflectivity of the magnetite grain (see Subsection 3.4.3), does not destroy the cubic close-packed framework of the spinel structure (Lindsley, 1976) and the grain remains optically isotropic. Oxidation of magnetite to maghemite is therefore not the result of a simple addition of oxygen to the structure but more likely involves the removal of iron from the lattice by diffusion (Lindsley, 1976). Free oxygen at the surface of the magnetite grain is ionised by the oxidation of ferrous iron within the crystal by the reaction:

Ti-magnetite crystal Crystal margin

$$[\ 4Fe^{2+} \longrightarrow 4Fe^{3+} + 4e^-\ ] \quad [\ 4e^- + O_2 \longrightarrow 2O^{2-}\ ]$$

The charge balance of the lattice is restored by the diffusion of one in every three of the newly formed Fe^{3+} ions towards the grain boundary resulting in a cation deficiency. This oxidation mechanism is illustrated by Fig. 5.7a where Ti-magnetite analyses from a single quartz latite pitchstone (sample SM-180) show a good positive correlation between iron (all iron as FeO) and the analysis

Fig 5.7 The effects of maghemitisation on the composition of titanomagnetites from sample SM-180 (LIC).

(Total iron expressed as FeO*, r = correlation coefficient.)

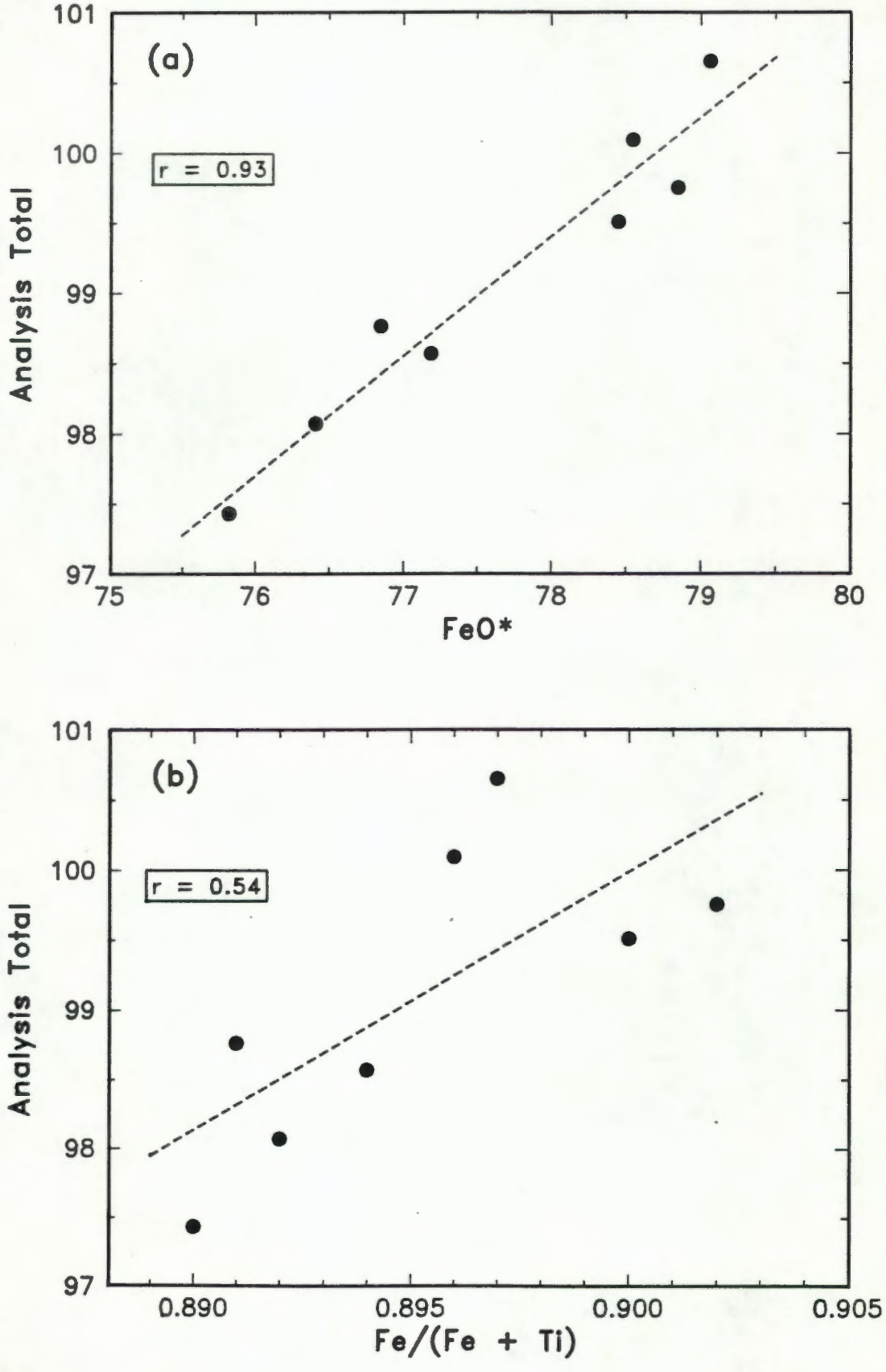

total (reduced on the basis of 4 oxygens). Diffusion of Fe from the structure is further supported by a decrease in the Fe:Ti ratio with decreasing total (Fig. 5.7b), note that the Fe:Ti ratio would remain constant if the low totals were due to in situ oxidation of Fe. The amount by which the analysis total differs from 100 % can be viewed as a qualitative measure of cation deficiency. Fe^{3+} ions which diffuse toward fractures or the margins of the grain may be removed in solution or be re-deposited as epitaxial growths of hematite or as new maghemite as an extension of the crystal structure (Lindsley, 1976). Ti-magnetite grains in the Sarusas sample (KLS-327) show an extensive development of hematite along fractures and grain boundaries, and particularly low totals of 95 to 96 % are obtained for analyses of the uniform textured, isotropic "magnetite" between fractures. Data of Akimoto and Katsura (1959) indicate that the Fe:Ti ratio is maintained during oxidation, suggesting that the Fe^{3+} is retained within an overall expanded structure (Lindsley, 1976). While this probably holds true for the entire grain, the localised analyses of the microprobe indicate a reduction in the Fe:Ti ratio with maghemitisation (Fig. 5.7b). The variation in Fe/(Fe + Ti) ratio (Fig. 5.7b) represents a difference of up to 2.5 mole % ulvospinel which is not due to magmatic fractionation. Maghemite compositions generally plot within the $FeTiO_3$ - Fe_2TiO_4 - Fe_3O_4 - Fe_2O_3 field on the TiO_2 - FeO - Fe_2O_3 ternary and in some cases may plot beyond the $FeTiO_3$ - Fe_2O_3 join (Lindsley, 1976). Ti-magnetite analyses plotted in Fig. 5.8a lie along the Fe_2TiO_4 - Fe_2O_3 join because the calculation of the Fe^{3+}:Fe^{2+} ratio on the basis of 4 oxygens does not account for any cation deficiency; many of the analyses should in fact lie within the shaded region of Fig. 5.8a.

5.4.2 Primary compositional variation

5.4.2.1 Titanomagnetite

The composition of Ti-magnetite phenocrysts in the quartz latites range from Usp_{23} in the Lower Tafelberg unit to Usp_{60} in some of the Springbok and Sarusas units (Fig. 5.8b), representing a variation of 8 - 21 wt% TiO_2. A comparison of microphenocryst and phenocryst compositions (Fig. 5.9) indicates that the magnetite becomes slightly more titanium rich (13 - 24 wt% TiO_2) as crystallisation proceeds and temperature decreases.

Factors which control the partitioning of elements among oxide minerals and between oxide and silicate minerals include temperature, oxygen fugacity

Fig. 5.8 Quartz Latite Fe:Ti Oxide Phenocryst Compositions

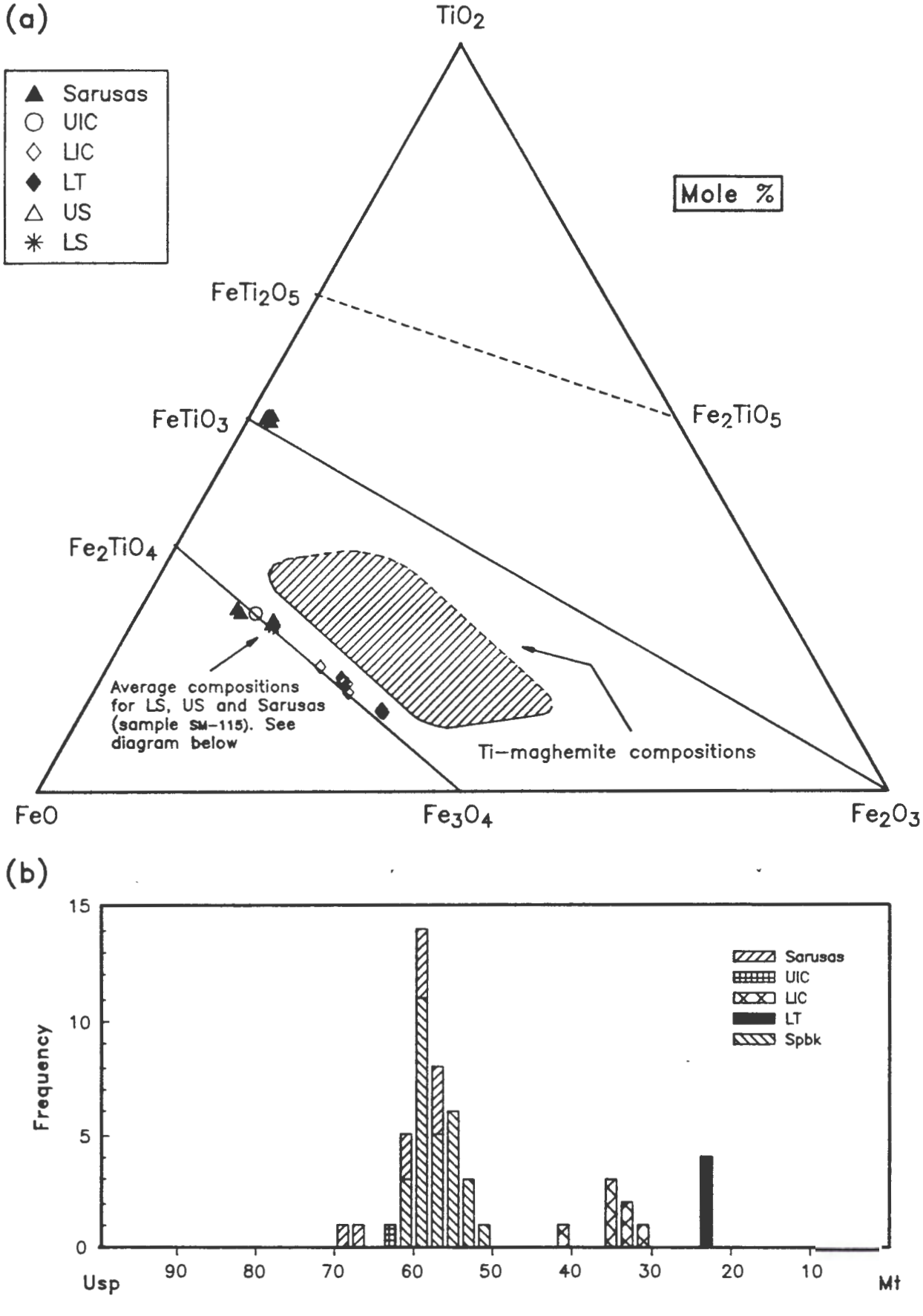

Fig. 5.9 Quartz latite titanomagnetite microphenocryst compositions.

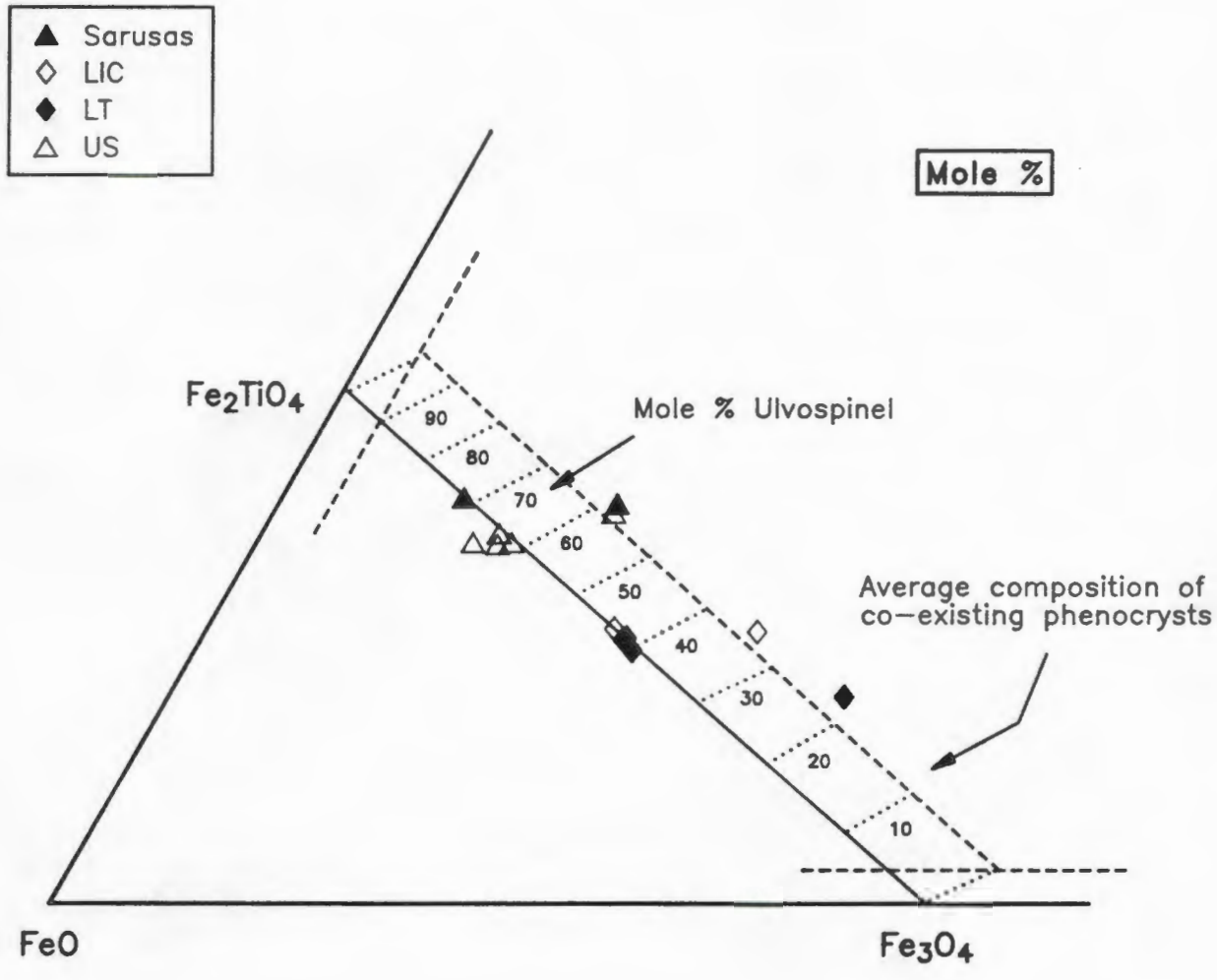

(fO_2) and bulk composition (notably the activity of silica). Most of the quartz latites, particularly from the southern Etendeka, exhibit a narrow range of bulk compositions, hence temperature and fO_2 are the main controls governing the variation in oxide compositions. Low fO_2 conditions favour the precipitation of Fe_2TiO_4-rich solid solutions and as fO_2 rises the ratio of Fe^{3+}:Fe^{2+} increases and stabilises more magnetite-rich solid solutions (Haggerty, 1976). At high values of fO_2 oxides crystallise in preference to Fe-rich silicates and as a consequence the pyroxenes which crystallise in apparently evolved systems may be surprisingly Mg-rich (Robinson, 1980). Some of these characteristics are observed in the quartz latites. Ti-magnetites from the Lower Coastal Interbedded units (samples SM-160 and SM-180) with a composition Usp_{30-34} coexist with hypersthene (En_{65}), whereas those from the Upper Springbok (Usp_{55}) coexist with hypersthene (En_{59}). The absence of ilmenite precludes an accurate assessment of fO_2 values in these samples although it may be safe to assume that the quartz latite magma of the Upper Springbok unit had an fO_2 which was low relative to that of the Lower Coastal Interbedded units, even after slight temperature differences are taken into account.

Minor constituents within the quartz latite Ti-magnetite include Al_2O_3, MgO and MnO (Fig. 5.10) which may exist as a variety of spinels in solid solution with the Usp-Mt_{ss}, viz:

Hercynite ($FeAl_2O_4$)	Spinel ($MgAl_2O_4$)
Magnesioferrite ($MgFe_2O_4$)	Magnesium Titanate (Mg_2TiO_4)
Jacobsite ($MnFe_2^{3+}O_4$)	

The concentrations of Al_2O_3 and MgO in the Ti-magnetites (Fig. 5.10) act as discriminants between the various groups of quartz latites. The concentration of Al_2O_3 has been found to increase with increasing temperature (Lipman, 1971) and this is particularly noticeable if one compares phenocryst and microphenocryst compositions for the same sample (Fig. 5.10). These data also suggest that the magnetite crystallising in the Lower Tafelberg quartz latite did so at a higher temperature than in the other groups of quartz latite.

5.4.2.2 Ilmenite

The ilmenite analyses plotted in Fig. 5.8a are from the Sarusas latite sample (KLS-327). Ilmenite is the dominant oxide phenocryst in this sample (average composition $Ilm_{91.9}Gk_{3.6}Hm_{4.5}$) and coexists with strongly

Fig. 5.10 Minor elements in quartz latite titanomagnetites

Fields enclosed by dashed lines indicate the microphenocryst compositions. Tie lines link microphenocrysts and phenocrysts from the same samles.

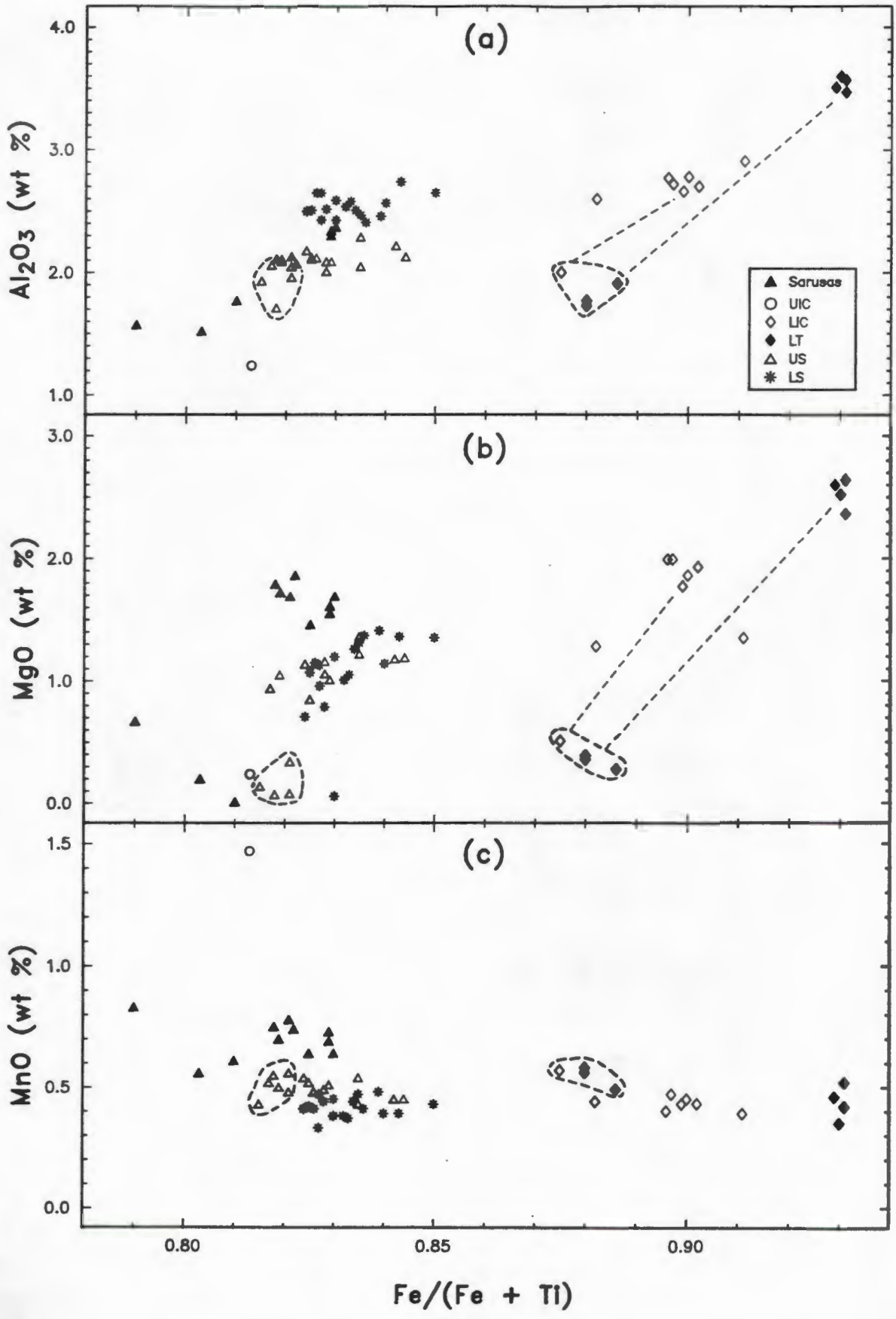

maghemitised Ti-magnetite (estimated composition Usp_{65}). Application of a thermobarometer (Spencer and Lindsley, 1981) to these compositions (end members recalculated in accordance with Stormer, 1983) yield values of T °C = 825 and $\log_{10} fO_2$ = -15. This temperature is considerably lower than the 1050 - 1100 °C estimated from pyroxene thermometry (Subsection 5.5.2) and it seems likely that these oxides, which plot somewhat below the FMQ buffer curve, have re-equilibrated at lower temperatures.

5.5 GEOTHERMOMETRY

5.5.1 Introduction

The geothermometer used most extensively in this study is the two pyroxene thermometer of Lindsley (1983), which utilises the partitioning of Ca between coexisting pyroxene phases. The minimum stability temperature of pigeonite, relative to augite and orthopyroxene (Lindsley, 1983), is also used to derive an estimate of the crystallisation temperature. Application of a geothermometer based on the activities of anorthite (and albite) in plagioclase and the melt from which it crystallised (Glazner, 1984) has been used in instances where pyroxene does not occur as a phenocryst phase. This thermometer is ideally suited to use on sparsely porphyritic, glassy rocks where the melt composition can be estimated from the whole rock composition. It is important to note, however, that this thermometer is highly sensitive to changes in CaO, Na_2O and K_2O in the whole rock(melt) composition and has therefore been used with caution. The absence of ilmenite in most samples precludes more extensive use of an Fe:Ti oxide thermometer e.g. Buddington and Lindsley (1964).

In such studies it is important to consider whether coexisting crystal phases or coexisting crystals and melt are in equilibrium with one another and the following are important considerations:

(1) Cumulus enrichment in porphyritic samples may result in a disequilibrium assemblage of crystals and melt. The subhedral to euhedral crystal shapes and compositional similarities between phenocrysts and microphenocrysts in the quartz latites, coupled with fairly uniform crystal distributions within individual quartz latite units, indicate that the process of cumulus enrichment is not significant in these rocks.

(2) Subsolidus reactions involving devitrification and hydration affect the

whole rock compositions of the quartz latites with respect to CaO, Na_2O and K_2O (Milner and Duncan, 1987). Therefore it is often invalid to assume that the whole rock composition approaches that of the original melt coexisting with crystals. The process of devitrification is often accompanied by the oxidation of titanomagnetite with the exsolution of trellis ilmenite, this makes the determination of primary titanomagnetite compositions by microprobe very difficult.

(3) Whether coexisting minerals crystallised at the same time or form part of a sequence of crystallisation is often difficult to determine petrographically and has an obvious bearing on the equilibrium-disequilibrium relationships of the minerals. Partition coefficients for Fe-Mg between equilibrium assemblages of pyroxenes, determined by Nakamura and Kushiro (1970), have been used to assess the degree of equilibrium attained by coexisting pyroxenes in the quartz latites (Subsection 5.5.2).

5.5.2 Pyroxene Thermometry

5.5.2.1 Equilibrium in Coexisting Pyroxenes

Nakamura and Kushiro (1970) determined $K_D(Mg\text{-}Fe^{2+})$ values between equilibrium pyroxene pairs in the Weiselberg andesite. The pyroxenes which were in contact gave the following average partition coefficients:

	[1] Hyp/Pig	[2] Hyp/Aug	[3] Pig/Aug
$K_D(Mg\text{-}Fe^{2+})$	1.08	0.81	0.75

The distribution coefficients were calculated using the following equations:

[1] $$\frac{X^{Hyp}}{1 - X^{Hyp}} \cdot \frac{1 - X^{Pig}}{X^{Pig}}$$

[2] $$\frac{X^{Hyp}}{1 - X^{Hyp}} \cdot \frac{1 - X^{Aug}}{X^{Aug}}$$

[3] $$\frac{X^{Pig}}{1 - X^{Pig}} \cdot \frac{1 - X^{Aug}}{X^{Aug}}$$

Where: X = Mg/(Mg + Fe)
Mg and Fe are atomic proportions based on six oxygens.

$K_D(Mg\text{-}Fe^{2+})$ values for coexisting pyroxenes in the Etendeka quartz latites are presented in Table 5.3. Pairs of pyroxene analyses with K_D values (figures in bold, Table 5.3) closest to the equilibration values of Nakamura and Kushiro (1970) have been used to calculate mineral crystallisation temperatures using the Lindsley (1983) thermometer. These analyses are listed in Table 5.4. The range of values calculated for these samples may be attributed to some sequential crystallisation of the pyroxene phases. The K_D value of 1.54 obtained for a coexisting hypersthene phenocryst and pigeonite microphenocryst (sample SM-168) serves to illustrate values for pyroxene pairs which are clearly at disequilibrium.

5.5.2.2 Lindsley (1983) Two Pyroxene Thermometer

Before the projection of pyroxene compositions onto the "thermometer quadrilateral" (Lindsley, 1983; Figure 9) the data were recalculated to account for the effects of non-quadrilateral components on the activities of Wo, En and Fs. Fe^{3+}, Cr and Ti were assigned to the M1 site and Al apportioned between the tetrahedral and M1 sites, while Ca and Na were restricted to the M2 sites only. Details of the recalculation scheme are given in Lindsley (1983). The compositions of coexisting pyroxenes together with the recalculated molecular proportions of Wo, En and Fs are presented in Table 5.4. A comparison of the recalculated molecular proportions with those calculated using the general formula $X = 100\ X/(Mg + {}^{*}Fe + Ca)$ where X = Ca(Wo), Mg(En) and Fe(Fs) ($^{*}Fe$ = total Fe) indicate that the correction is small for orthopyroxene, but significantly larger for both pigeonite (up to 2.2 mole% Wo) and augite (up to 1.9 mole% Wo). These corrections represent temperature differences of up to 70 °C indicating the importance of apparently small quantities of non-quadrilateral components on the activity of wollastonite. The Lindsley (1983) projection scheme does not, however, account for the Mn^{2+} present, possibly because it has little effect. Divalent cations in orthopyroxenes have two sites for substitution (M1 and M2) whereas the M2 sites in augite are almost completely filled with calcium ions. Ideal distribution of Mn between coexisting orthopyroxene and augite should yield D values of 0.5. A mean value of D = 0.55 (Heubner, 1980) indicates a close approach to ideality and the substitution of Mn on the Fe-Mg sites in pyroxene. Assuming that a relationship similar to that indicated by Heubner (1980) exists between pigeonite and augite, D values of 0.59 and 0.66 for KLS-281 and KLS-327 respectively indicate a

Table 5.3 K_D values for coexisting quartz latite pyroxenes

Sample Number	Hypersthene / Pigeonite	Pigeonite / Augite	Hypersthene / Augite
	Equilibrium K_D = 1.08	Equilibrium K_D = 0.75	Equilibrium K_D = 0.81
SM–168	1.05 1.01 – 1.28 (~1.54 Pig Microphenocryst) (~1.42 Pig mantling Hyp)	–	–
SM–154	**1.03** 0.94 – 1.32	**0.84** 0.84 – 1.15	**0.86** 0.86 – 1.39
SM–160	**1.16** 0.77 – 1.43	**0.82** 0.82 – 0.92	**1.07** 1.07 – 1.18
SM–180	**1.18** 1.18 – 1.39	–	–
KLS–281	–	**0.70** 0.63 – 0.82	–
KLS–327	–	**0.77** 0.77 – 0.86	–
		Order of crystallisation	
	< 1.08 Pig first > 1.08 Hyp first	< 0.75 Aug first > 0.75 Pig first	< 0.81 Aug first > 0.81 Hyp first

Footnote:
The equilibrium K_D values quoted for each pyroxene pair are from Nakamura and Kushiro (1970). The range of values for each sample has been calculated using the maximum and minimum X values (see page 147) obtained for each pyroxene phase. The values in bold are the distribution coefficients for pyroxene pairs which, from the limited number of determinations for each pair, are the closest to the equilibrium values of Nakamura and Kushiro (1970). The "order of crystallisation" is a theoretical indication of which pyroxene crystallised first.

TABLE 5.4

Quartz latite pyroxene compositions used for geothermometry (Fig. 5.11).

	(1) HYP	(1) PIG	(2) HYP	(2) PIG	(2) AUG	(3) HYP	(3) PIG	(3) PIG	(3) AUG	(4) HYP	(4) PIG	(5) PIG	(5) AUG	(6) PIG	(6) AUG
SiO_2	51.72	51.80	51.68	51.71	50.03	52.55	52.01	51.32	50.19	52.18	52.18	51.65	50.57	51.24	50.87
TiO_2	0.35	0.28	0.36	0.35	0.59	0.28	0.24	0.29	0.57	0.34	0.39	0.35	0.64	0.47	0.90
Al_2O_3	0.96	0.74	1.09	0.94	1.75	1.05	0.74	0.83	1.64	1.12	1.03	0.72	1.39	0.73	1.67
Cr_2O_3	nd	nd	nd	nd	nd	nd	nd	nd	nd	nd	nd	nd	nd	nd	nd
FeO	24.86	24.66	23.37	21.63	13.38	20.26	21.24	22.52	13.91	20.46	21.18	27.12	15.77	22.52	12.69
MnO	0.73	0.76	0.67	0.85	0.61	0.73	0.83	0.77	0.60	0.66	0.61	0.89	0.57	0.64	0.31
MgO	20.23	19.13	21.10	18.97	13.97	22.82	20.70	19.51	14.66	23.02	20.22	16.06	13.44	19.76	14.38
CaO	1.84	3.17	1.63	5.35	17.98	1.90	3.93	4.12	17.28	1.79	4.38	4.63	16.91	4.26	18.03
Na_2O	0.03	0.06	0.03	0.08	0.22	0.04	0.05	0.06	0.21	nd	0.06	0.08	0.24	0.07	0.25
K_2O	nd	nd	nd	nd	nd	nd	nd	nd	nd	nd	nd	nd	nd	nd	nd
Total	100.26	100.60	99.93	99.88	98.53	99.30	99.74	99.42	99.06	99.57	100.05	101.50	99.53	99.69	99.10
	ATOMIC PROPORTIONS BASED ON SIX OXYGENS														
Si	1.949	1.960	1.948	1.957	1.923	1.954	1.959	1.954	1.920	1.947	1.958	1.967	1.937	1.946	1.933
Ti	0.010	0.008	0.010	0.010	0.017	0.008	0.007	0.008	0.016	0.010	0.011	0.010	0.018	0.013	0.026
Al	0.043	0.033	0.048	0.042	0.079	0.046	0.033	0.037	0.074	0.049	0.046	0.032	0.063	0.033	0.075
Cr	-	-	-	-	-	-	-	-	-	-	-	-	-	-	-
Fe^{2+}	0.784	0.780	0.737	0.685	0.430	0.634	0.669	0.717	0.445	0.639	0.665	0.864	0.505	0.715	0.403
Mn	0.023	0.024	0.021	0.027	0.020	0.023	0.026	0.025	0.019	0.021	0.019	0.029	0.018	0.021	0.010
Mg	1.136	1.079	1.185	1.070	0.800	1.272	1.162	1.107	0.836	1.280	1.131	0.912	0.767	1.119	0.814
Ca	0.074	0.129	0.066	0.217	0.741	0.076	0.159	0.168	0.708	0.072	0.176	0.189	0.694	0.173	0.734
Na	0.002	0.004	0.002	0.006	0.016	0.003	0.004	0.004	0.016	-	0.004	0.006	0.018	0.005	0.016
K	-	-	-	-	-	-	-	-	-	-	-	-	-	-	-
Sum	4.021	4.018	4.019	4.015	4.028	4.017	4.020	4.022	4.035	4.019	4.011	4.010	4.022	4.027	4.014
Wo	3.72	6.47	3.31	11.00	37.57	3.84	7.97	8.44	35.61	3.60	8.93	9.62	35.29	8.64	37.61
En	56.96	54.27	59.63	54.27	40.60	64.18	58.40	55.57	42.02	64.32	57.35	46.41	39.02	55.72	41.72
Fs	39.31	39.26	37.06	34.73	21.82	31.98	33.63	35.99	22.37	32.08	33.71	43.98	25.69	35.64	20.66
Mg#	59.17	58.03	61.67	60.98	65.04	66.75	63.46	60.69	65.25	66.72	62.58	51.34	60.30	60.99	66.88
Pyroxenes recalculated for use on the Lindsley (1983) thermometer.															
Wo	3.74	7.45	3.30	12.85	35.70	3.60	8.85	9.20	34.10	3.39	10.60	11.80	34.25	8.80	36.85
En	57.70	54.34	60.57	54.02	43.85	65.47	58.58	55.87	45.05	65.42	56.93	45.76	41.10	56.02	43.13
Fs	38.55	38.21	36.14	33.12	20.45	30.94	32.68	34.93	20.85	31.19	32.47	42.44	24.65	35.18	20.02

(1) SM-168 - Upper Springbok Quartz latite.

(2) SM-154
(3) SM-160 - Lower Interbedded Coastal.
(4) SM-180

(5) KLS-281 - Upper Interbedded Coastal.

(6) KLS-327 - Sarusas Latite.

similar approach to ideality for Mn substitution in the Etendeka pyroxenes, further supported by the MnO *vs* FeO trend in Fig. 5.6e. If the above assumptions are correct, then minor amounts of Mn in the pyroxene structure should have little effect on the activity of Wo and hence the temperatures derived.

The compositions of coexisting pyroxenes have been projected onto the thermometer quadrilateral (1 atm.) in Fig. 5.11 and Table 5.5 gives the temperature for individual pyroxene phases and a mean temperature for each sample. Two main observations arise from the application of the thermometer. Firstly the narrowly spaced isotherms in the orthopyroxene part of the quadrilateral make the estimation of hypersthene temperatures difficult. Secondly there appears to be a systematic increase (Hyp < Pig < Aug) in the temperatures obtained for coexisting pyroxenes. This may be partly due to the difficulty in estimating hypersthene temperatures with the additional possibility that recasting the pyroxene analyses overestimates the effect of non-quadrilateral components. Bearing in mind the accuracy of the thermometer (±50 °C) the temperatures obtained for coexisting pyroxenes (Table 5.5) show fairly good agreement with each other.

5.5.2.3 The minimum stability of Pigeonite: an estimation of temperature.

The phase relationships for the pure Ca-Mg-Fe pyroxene system near one atmosphere, Fig. 5.12, indicate that with increasing temperature the field in which pigeonite is stable expands toward more Mg-rich compositions and encompasses a broader range of compositions. Fig. 5.13 gives an estimate for the minimum temperature stability of pigeonite relative to augite + orthopyroxene as a function of Fe/(Fe + Mg) (X_{Fe}) (Lindsley, 1983). The curve has been constructed using data from Ross and Heubner (1979), Podpora and Lindsley (1979) and Lindsley and Andersen (1983). The elevation of the curve above that for the pure Ca-Mg-Fe system for $X_{Fe} < 0.5$ reflects the stabilisation of augite and orthopyroxene relative to pigeonite by non-quadrilateral components. More Fe-rich pyroxenes have fewer of the non-quadrilateral components with the result that the minimum stability of pigeonite approaches that of the pure system. The dashed portion of the curve emphasises that the actual temperature depends on the proportion of non-quadrilateral components in the pigeonite (Lindsley, 1983). This thermometer is particularly useful in instances where pigeonite is the only pyroxene to form, for example in some of the Springbok units, and it can also be

Fig. 5.11 Lindsley (1983) Pyroxene Thermometer at 1 atm.

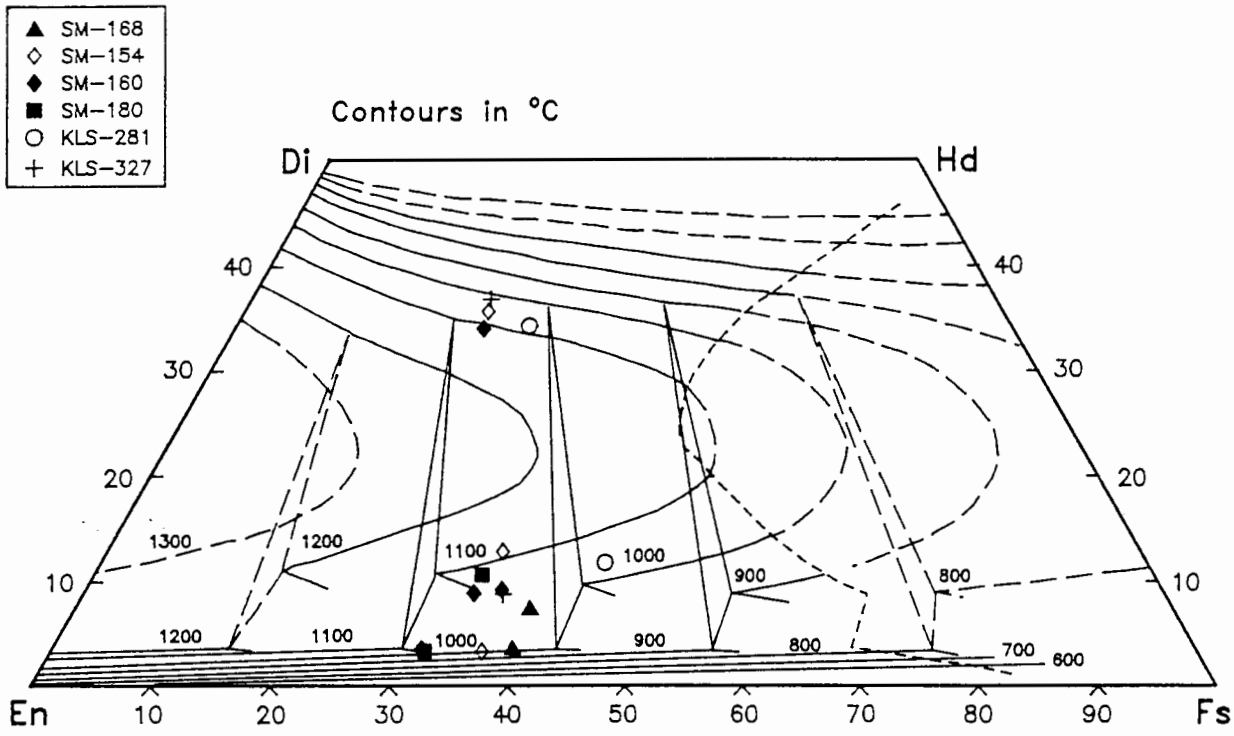

Table 5.5 Temperatures obtained for quartz latite pyroxenes using the graphical thermometer in Figure 5.11.

Sample Number	Pyroxene Phase	Temperature °C (±50 °C)	Average Temperature °C
SM–168	Hyp	1000	1015
	Pig	1030	
SM–154	Hyp	1000	1060
	Pig	1110	
	Aug	1070	
SM–160	Hyp	1050	1070
	Pig	1070	
	Pig	1050	
	Aug	1110	
SM–180	Hyp	1000	1040
	Pig	1080	
KLS–281	Pig	1030	1060
	Aug	1090	
KLS–327	Pig	1050	1040
	Aug	1030	

Fig. 5.12 Ca–Mg–Fe Pyroxene phase relations at and near one atmosphere.

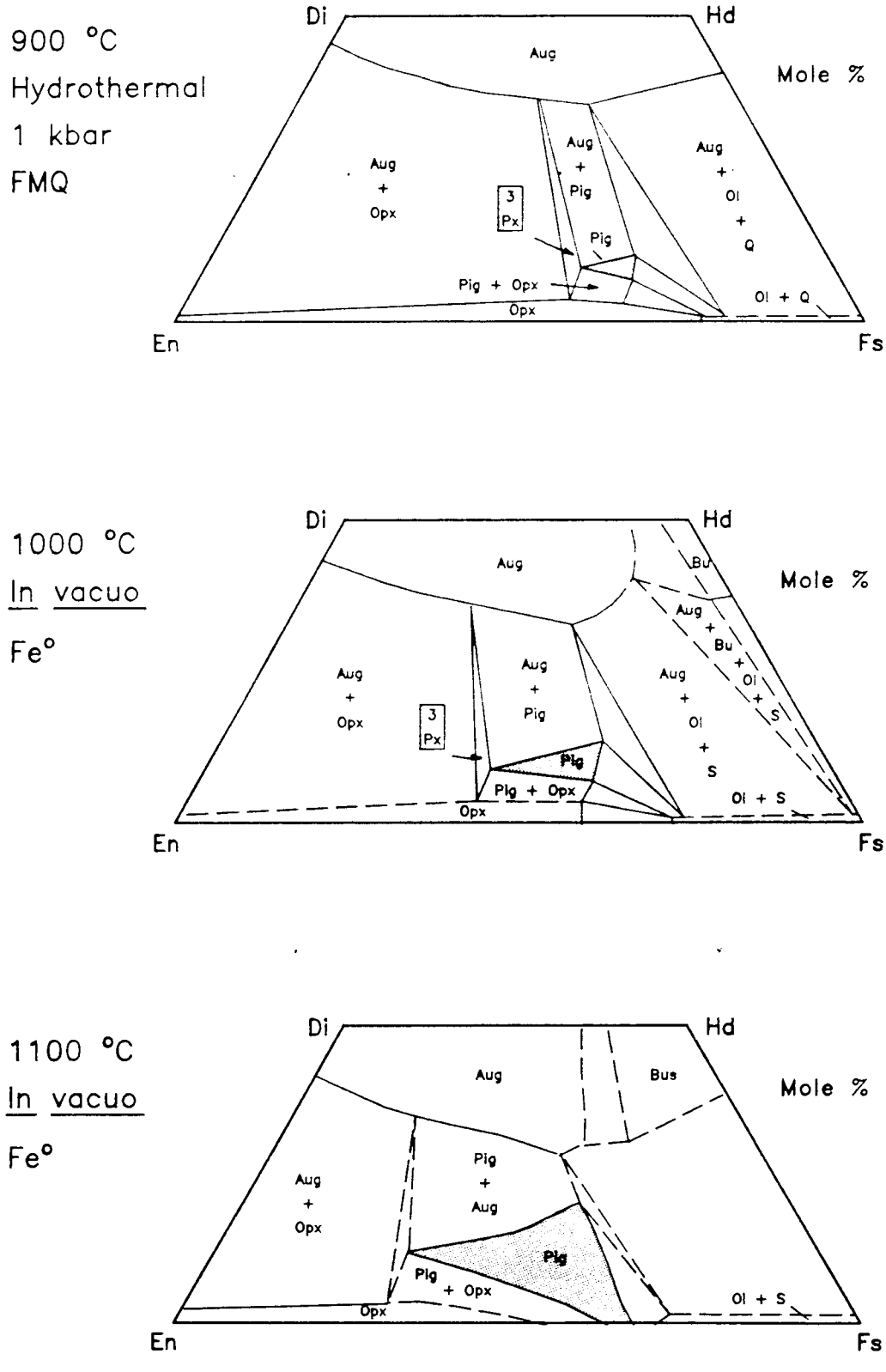

Adapted from Lindsley (1983).

Fig. 5.13 Minimum Stability of Natural Pigeonite at Low Pressures.

(After Lindsley; 1983, Figure 13)

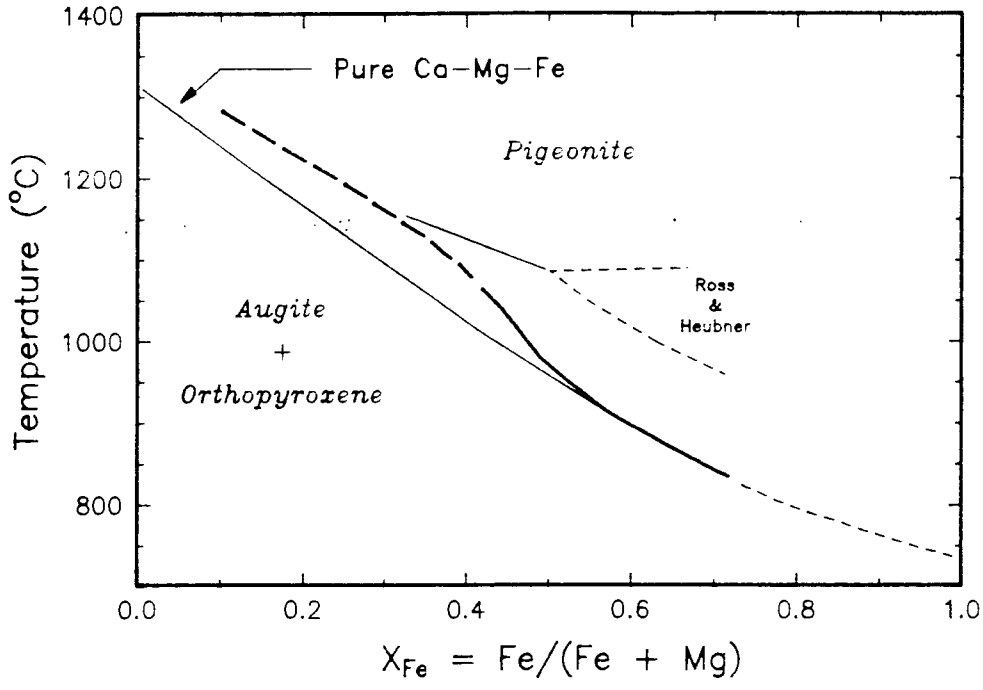

Table 5.6 Temperatures obtained for quartz latite pigeonite phenocrysts using Fig. 5.13.

Sample Number	Average X_{Fe}/ sample	Temp (°C)	Sample Number	X_{Fe} individual phenocryst *	Temp (°C)
SM–017	0.500	970	SM–168	0.420	1065
SM–208	0.491	975	SM–154	0.390	1090
SM–172	0.494	970	SM–160(1)	0.365	1115
KLS–051	0.433	1050	SM–160(2)	0.393	1090
SM–179	0.334	1140	SM–180	0.370	1110
KLS–327	0.383	1100	KLS–281	0.487	980
			KLS–327	0.390	1090

* X_{Fe} values for the pigeonite phenocrysts in Table 5.5.

used to confirm temperatures obtained from the graphical two-pyroxene thermometer (Lindsley, 1983).

Application of this thermometer to pigeonites from the Etendeka quartz latites yields temperatures of 970 - 1140 °C (Table 5.6). Table 5.6 indicates the average X_{Fe} values of pigeonite analyses in individual samples as well as the X_{Fe} values of pigeonites used to estimate temperatures from the graphical thermometer (Fig. 5.11). A comparison of the temperatures obtained by the two methods are generally in good agreement (±50 °C). However, this is not unexpected since the minimum stability of pigeonite in the pure Ca-Mg-Fe system is one of the factors used by Lindsley to construct his thermometer. The amounts of non-quadrilateral components in the Etendeka quartz latite pyroxenes are comparable to those in the pyroxenes of Ross and Heubner (1979), suggesting that the temperatures estimated from the dashed portion of the curve (X_{Fe} 0.32 - 0.42) are not unreasonable.

5.5.3 Plagioclase Thermometry

Partitioning of mineral components (An and Ab) between coexisting crystals and melt forms the basis of this thermometer. Recent studies of the thermodynamic behavior of silicate melts have been aimed at understanding the interaction of minerals and complex natural melts. One of the main aims of such thermodynamic modeling is to predict the activities of various mineral components in a melt from its chemical composition. In crystals there is a simple correspondence between activity and composition, but in silicate melts this correspondence does not exist. Quasi-crystalline (Burnham, 1975 and 1981) and regular solution (Ghiorso and Carmichael, 1980 and Ghiorso *et al.*, 1983) models are quite successful in describing mineral-melt equilibria and divide the melt into mineral-like components which are chosen to resemble molecular species thought to exist in silicate liquids. Glazner (1984) indicated that "the main difficulty in using a classic thermodynamic approach to model melt activities lies in defining the mole fractions of mineral components such as An, Fo and Qtz in the melt" predominantly because schemes allotting oxides to mineral components tend to be arbitrary. Glazner (1984) takes an empirical approach to model such activities using an equation of the form:

$$\ln a_j^m = f(X_1, X_2 \ldots X_n)$$

Where the X_i are mole fractions of the n oxide components in the melt and a_j^m is the activity of mineral component j in the melt which are fit to experimental data from the literature on crystal-melt equilibria in natural (basic to intermediate) systems. The mole fractions of these mineral components are not explicitly calculated and Glazner states that an advantage of this approach is that the fit coefficients show how the melt composition affects the activities of the melt components without any assumption as to the melt speciation. The Glazner thermometer takes the form:

$$T\ ^\circ C = a + bk_j + ck_j^2$$

Where:

a, b and c are constants for a particular component.

$k = \ln a_j^m / a_j^s$

and

a_j^s is the activity of a mineral component j in a crystal which approximates to X_j^s - the mole fraction of that component.

a_j^m is the activity of a mineral component j in the melt which is computed by first determining the mole fractions of oxides present in the melt then applying a correction coefficient to the oxide species found significant in the modelling of that particular component.

Application of this plagioclase thermometer (An and Ab) to several quartz latites yields the following temperatures (°C):

Sample	Anorthite	Albite	Quartz Latite Unit
SM-179	1203	1093	Lower
SM-193	1395	1131	Tafelberg
SM-192	1538	1159	
SM-172	1302	1151	Upper Springbok

The effect of subtracting the modal % of plagioclase from the whole rock composition to gain a more accurate estimate of the melt composition was found to be insignificant.

Three whole rock compositions for the Lower Tafelberg quartz latite were used with a single plagioclase analysis ($An_{64}Ab_{34}Or_2$) from sample SM-179 in order to determine the effect of whole rock composition on temperature. Note that this sample (SM-179) is a pitchstone with relatively unaltered plagioclase phenocrysts, whereas the other samples (SM-192 and SM-193) are completely devitrified with severely altered phenocrysts. The use of a single plagioclase composition is justified on the grounds that there is very little compositional variation within the immobile element chemistry of the Lower Tafelberg quartz latite (Milner and Duncan, 1987). The Upper Springbok sample (SM-172) provided a means of comparison with the pyroxene thermometer (subsection 5.5.2). Several points arising from the application of the plagioclase thermometer to the quartz latites can be summarised as follows:

(1) Most of the temperatures obtained are considerably higher than those obtained using pyroxene (e.g. SM-172 pigeonite 975 °C) and appear to be rather unrealistic. Poor correlation between the An and Ab thermometers may indicate whole rock/crystal disequilibrium.

(2) The closest An/Ab temperature pair is obtained for SM-179 (1100 - 1200 °C), but the significance of these temperatures is questionable considering the large range of values obtained. However, it is interesting to note that quenched pigeonite microlites in this sample give a minimum stability temperature of 1140 °C (Table 5.6). Sparse plagioclase (<3 %) and Ti-magnetite (<0.4 %) crystals are the only phenocrysts present (no pyroxene) (see Appendix 1). The plagioclase represents the most anorthitic analysed in the quartz latites and the Ti-magnetites contains the highest concentrations of Al_2O_3, both of which indicate high crystallisation temperatures. It is suggested that temperatures of 1100 - 1200 °C for the crystallisation of this plagioclase probably represent an upper limit for the eruption temperature.

(3) Temperatures for the Lower Tafelberg samples vary considerably (1538 - 1093°C) which is thought to be the result of whole rock/crystal disequilibrium induced by post-eruptive alteration processes (Milner and Duncan, 1987). The whole rock compositions of these samples vary with

respect to CaO (3.07 - 1.42 wt%), Na_2O (3.26 - 2.80 wt%) and K_2O (3.22 - 5.07 wt%). In the calculation of mineral activities, particularly An, K_2O appears to make a considerable contribution to the function of the mineral activity equation, with larger concentrations of K_2O increasing the activity of An in the melt and hence the temperatures derived. Although this type of approach to mineral/melt equilibria is only of limited use as a geothermometer for the quartz latites, it does highlight the problem in determining the "true" eruptive composition of the quartz latites. It may be possible to use this type of approach in conjunction with mineral compositions to place some constraints on the primary melt composition.

It is further recognised that the intermediate to acid compositions of the quartz latites fall on the outer limits of the calibration range for this thermometer which undoubtedly adds further uncertainty to the temperature estimates obtained.

5.6 SUMMARY

(1) Quartz latite samples from individual units generally exhibit narrow ranges in phenocryst compositions and zonation is only weakly developed. Notable exceptions include the phenocryst-rich Sarusas sample SM-110 and the Beacon Tafelberg sample SM-007 which show up to 10 - 20 mole % variation in the anorthite content of plagioclase (Table 5.2). Note that in the latter sample plagioclase occurs as "large" microphenocrysts which are often overgrown by groundmass K-feldspar.

(2) Compositional variations of plagioclase (Fig. 5.1a) and augite (Fig.5.4b) between three of the Sarusas samples (KLS-327, SM-115 and SM-110) are consistent with a model relating them by a crystal fractionation process. A fourth sample in this suite, SM-112, does not appear to be part of this trend.

A decrease in the An content of plagioclase with increasing stratigraphic height in the Tafelberg and Interbedded Coastal quartz latite sequence (Fig. 5.1b) mimics a conventional fractionation trend. However, this is not consistent with whole rock geochemistry which becomes less evolved higher in the sequence.

(3) In the southern Etendeka quartz latites the compositions of pyroxene (Mg-number 50 - 70) and plagioclase (An_{50} - An_{65}) phenocrysts appear relatively unevolved with regard to the whole rock compositions. It is interesting to note that many of the basaltic lavas of the Etendeka, particularly the more evolved varieties (55 - 57 wt % SiO_2), apparently have more fractionated mineral compositions than the quartz latites (Erlank *et al.*, 1984; Fig. 12). This supports the conclusions of Erlank *et al.* (1984) that the quartz latites were not derived by continuous fractionation from the basaltic lavas.

(4) The composition of Ti-magnetites in the quartz latites is thought to be dominantly controlled by fO_2. High values of fO_2 promote the early crystallisation of magnetite and of ulvospinel-poor compositions. Early crystallisation of magnetite, coupled with high liquidus temperatures, is thought to stabilise relatively Mg-rich pyroxenes, and it is interesting to note that the most Mg-rich pyroxenes coexist with the most ulvospinel-poor magnetites.

(5) Poor totals obtained for microprobe determinations of Ti-magnetites can be attributed to the oxidation of magnetite to maghemite, a cation-deficient spinel.

(6) Geothermometry indicates high temperatures of crystallisation and the summary below shows the temperature ranges for samples from various groups of quartz latite in order of decreasing temperature:

Etendeka quartz latites		Temperature °C
Lower Tafelberg	(SM-179)	1140[2] - 1200[3](?)
Lower Coastal Interbedded		
	(SM-160)	1070[1] - 1115[2]
	(SM-154)	1060[1] - 1090[2]
	(SM-180)	1040[1] - 1110[2]
Upper Springbok (hypersthene bearing)	(SM-168)	1015[1] - 1065[2]

Upper Coastal Interbedded		
	(KLS-281)	980^2 - 1060^1
Upper Springbok (pigeonite bearing)	(SM-172)	~ 970^2
Lower Springbok	(SM-017)	~ 970^2
	(SM-208)	~ 975^2

Sarusas latite

	(KLS-327)	1040^1 - 1100^2

Superscripts indicate the method of temperature estimation:
1 - Graphical two-pyroxene thermometer (Fig. 5.11) - see Table 5.5.
2 - Minimum stability of pigeonite (Fig. 5.13) - see Table 5.6.
3 - Plagioclase thermometry.

These temperatures are significantly higher than those usually envisaged for acidic melts, and indicates that the quartz latite magmas were relatively dry (H_2O-undersaturated). Similar temperature estimates have also been obtained for rhyolites showing outcrop characteristics similar to those displayed by the quartz latites, Bonnichsen and Kauffman (1987), Ekren *et al.* (1984) and Bellieni *et al.* (1984).

CHAPTER 6

GEOCHEMISTRY OF THE ETENDEKA FORMATION QUARTZ LATITES

6.1 INTRODUCTION

The Etendeka Project database currently contains whole rock, major and trace element, data for 492 samples, 89 of which have previously been published (Erlank *et al.*, 1984). It contains analyses of 199 quartz latite and 12 latite samples, of which 183 are new analyses produced during this study. All the quartz latite and latite whole rock data are given in Appendix 2 (Tables 1 - 24 on microfiche). Most were obtained using conventional XRF techniques at the Geochemistry Department of the University of Cape Town, and a summary of the analytical methods and conditions are outlined in Appendix 2. The sources of rare earth and isotopic data are also indicated in Appendix 2.

The whole rock data displayed in the tables and diagrams of this thesis have been recalculated to 100 % on a H_2O^-(loss at 110 °C)-free basis, with all iron as FeO (unless stated otherwise). It is important to note that the data are not recalculated on a volatile(LOI)-free basis. The data are presented in this way because it will be shown that the high LOI (loss on ignition at 850 °C) values encountered in the pitchstones are the result of post eruptive alkali-ion:water exchange reactions and are not simply the result of hydration and the addition of water (Section 6.3). In some of the pitchstones up to 2.5 wt% K_2O has exchanged with H_2O and in such cases a simple volatile-free normalisation procedure would be incorrect, yielding results for the other oxides and elements with a +2.5 % error.

In this Chapter the composition of the Etendeka quartz latites and their classification is compared with that of other felsic volcanics. Compositional variations displayed by the quartz latites are outlined, and the role of magmatic and secondary alteration processes in these variations is assessed. An important use of the new geochemical data has been the correlation of major quartz latite units within the southern Etendeka enabling the construction of a stratigraphic model for the lavas in this region (Milner and Duncan, 1987). Much of what is covered by this Chapter is intended to supplement the findings of Milner and Duncan (1987), and to avoid unnecessary duplication this work is frequently referenced. A copy of Milner and Duncan (1987) is bound at the back of this thesis.

6.2 CLASSIFICATION

The nomenclature used in this study to classify the Etendeka volcanics is essentially the same as that proposed by Erlank *et al.* (1984). Fig. 6.1 shows all the currently available data for the extrusives on the K_2O *vs.* SiO_2 classification scheme of Peccerillo and Taylor (1976). Erlank *et al.* (1984) referred to low- and high-SiO_2 lavas of the basic suite (open and filled circles, Fig. 6.1) as "basalts" and "evolved basalts" respectively, rather than use terms such as basaltic andesite and andesite which they felt had strong tectonic and petrogenetic connotations. The terms "basalt" and "evolved basalt" also serve to emphasise the continuous nature of the chemical, petrographic and mineralogical features of the suite. Lavas with intermediate silica contents (58 - 63 wt% SiO_2) and high K_2O (4.0 - 5.5 wt%) are termed "latite" and plot in the appropriate field in Fig. 6.1. The acid extrusives (65 - 70 wt% SiO_2) have been termed "quartz latite" (>3.0 wt% K_2O) and "high-K dacite" (<3.0 wt% K_2O) (Erlank *et al.*, 1984). With the much larger data set now available it is clear that all the samples with K_2O contents less than 3.5 wt% are pitchstones. Alteration studies (Milner and Duncan, 1987 and Section 6.3) have shown that the lower K_2O content of the pitchstones is apparently due to low temperature hydration and ion exchange of the glassy mesostasis in these rocks. As the division of the felsic volcanics into quartz latite and high-K dacite by Erlank *et al.* (1984) is now believed to be a consequence of post-eruptive alteration the latter term has been dropped and the term quartz latite applied to all the felsic volcanics.

6.2.1 Quartz Latite - a comparison with other rhyolite and rhyodacite compositions

The term "quartz latite" and its application to the felsic volcanics of the Etendeka requires a brief review, particularly since compositionally similar rock types from the Lebombo, southern Africa (Cleverly *et al.*, 1984) and Paraná, Brazil (Bellieni *et al.*, 1984) have been called rhyodacites and rhyolites. These authors used the classification schemes of Streckeisen (1979) and De La Roche *et al.* (1980) respectively. Erlank *et al.* (1984) applied a similar reasoning to their naming of the Etendeka quartz latites as they did with the basic lavas, wanting to avoid terms such as dacite and rhyodacite which are generally associated with calc-alkaline suites. The occurrence of felsic volcanics with compositions similar to those of the

Fig. 6.1 Classification of Etendeka Volcanic Rocks using the SiO_2 vs. K_2O diagram of Peccerillo and Taylor (1976)

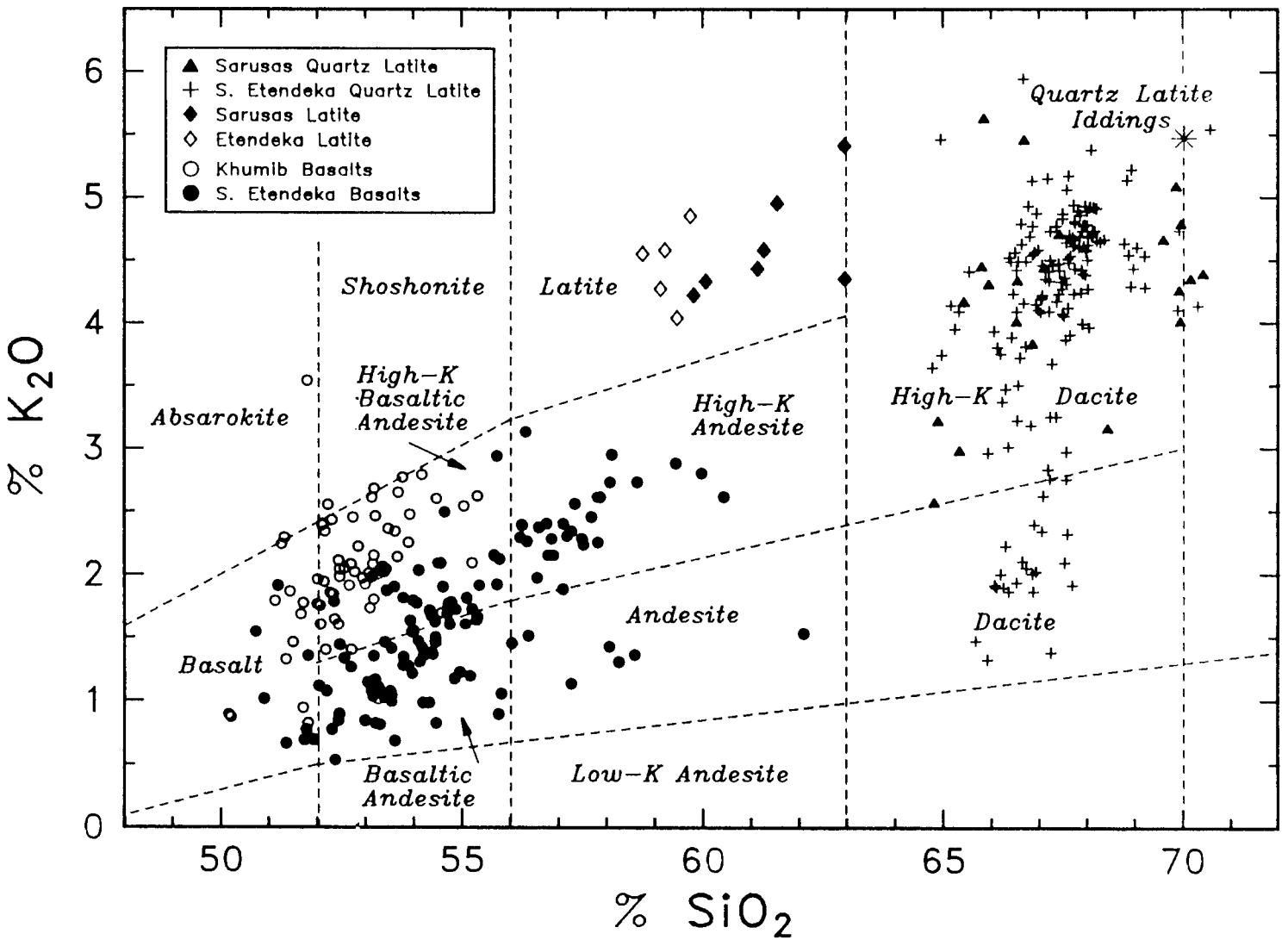

Etendeka quartz latites are only rarely reported from areas outside the Karoo and Paraná Igneous provinces. Ekren *et al.* (1984) report similar compositions, also termed quartz latite, from the Owyhee Plateau, south-western Idaho (see Table 6.1 for comparative analyses), and similar compositions are reported from the British Tertiary Province (Ridley, 1971) although these have not been classified as such and are merely referred to as felsites and pitchstones.

On the normative Q-A-P classification scheme (not shown) of Streckeisen (1979) the majority of Etendeka quartz latite analyses plot in the lower left-hand part of the "rhyodacite" quadrant and the latites, which plot in the appropriate field in Fig. 6.1, cluster within the "quartz latite" field.

A comparison of the major element compositions of the Etendeka quartz latites with average compositions for acid volcanics from Le Maitre (1976) and Taylor and McLennan (1985) in Table 6.1 and with the data compilations of Ewart (1979) indicate the following:

(1) Rhyolites, particularly those from bimodal mafic-silicic associations, have higher SiO_2 (73 - 77 wt%) and Na_2O (3.4 - 4.7 wt%) and lower TiO_2 (0.1 - 0.45 wt%), FeO* (1.0 - 3.3 wt%) and MgO (0.08 - 0.40 wt%) compared to the Etendeka quartz latites [SiO_2 (65 - 70 wt%), Na_2O (2.5 - 4.0 wt%), TiO_2 (0.8 - 1.4 wt%), FeO* (4.5 - 8.0 wt%) and MgO (0.5 - 1.8 wt%).]

(2) Rhyodacite compositions (66 - 69 wt% SiO_2) show significantly higher Al_2O_3 (15 - 16 wt%), lower FeO* (<4.5 wt%) and $Na_2O > K_2O$ compared to the quartz latites [Al_2O_3 (12 - 13 wt%), FeO* (4.5 - 8.0 wt%) and $Na_2O < K_2O$.]

(3) Dacites commonly have higher Al_2O_3 (~ 16 wt%), $Na_2O > K_2O$ and contain less SiO_2 and FeO* than the quartz latites.

Thus it would appear that the compositions of the Etendeka quartz latites are different from that generally accepted for rhyodacites and rhyolites, a conclusion supported by A. Ewart (pers. comm. to A. Erlank, 1980). Although it would be desirable to achieve some sort of consistency in the naming of the Karoo-Paraná felsic volcanics the author does not feel justified in changing the nomenclature of the Etendeka volcanics, particularly as this would lead to confusion with the earlier work of Erlank *et al.* (1984). It is also noteworthy that in terrains, such as the Owyhee Plateau, south-western Idaho,

TABLE 6.1

The composition of Etendeka Quartz Latite compared with published data for other felsic volcanics.

Analysis	(1)	(2)	(3)	(4)	(5)	(6)	(7)
SiO_2	68.98	69.28	71.13	68.99	73.40	67.69	66.30
TiO_2	0.86	0.88	0.50	0.87	0.30	0.60	0.67
Al_2O_3	13.02	13.35	12.73	13.72	13.50	15.57	15.90
FeO*	5.39	5.42	5.74	5.33	2.21	4.02	4.40
MnO	0.09	0.09	0.10	-	-	-	-
MgO	1.22	1.17	0.35	0.99	0.50	1.68	1.76
CaO	2.47	3.49	1.48	3.05	2.00	3.36	4.32
Na_2O	2.88	3.45	3.18	3.09	3.74	3.91	3.97
K_2O	4.80	2.56	4.64	3.79	4.24	3.17	2.57
P_2O_5	0.29	0.30	0.14	0.17	-	-	-

Analysis Number

(1) Etendeka Quartz Latite (devitrified) Lower Tafelberg and Lower Interbedded Coastal (n = 67)#.

(2) Etendeka Quartz Latite (pitchstone) Lower Tafelberg and Lower Interbedded Coastal (n = 17)#.

(3) Jozini Rhyolite (Lebombo Monocline, Karoo; n = 47) (Cleverly *et al.*, 1984).

(4) Quartz Latite (pitchstone) Owyhee Mountains, Idaho (Ekren *et al.*, 1984).

(5) Average Rhyolite (orogenic) (Taylor and McLennan, 1985).

(6) Average Rhyodacite (Le Maitre, 1976).

(7) Average Dacite (orogenic) (Taylor and McLennan, 1985).

Data recalculated to 100 % volatile free for comparitive purposes.
Total Fe as FeO*.

#Note LOI is normally quoted in this study - see Section 6.3 for a discussion of possible erupted compositions.

where rhyolites (*sensu stricto*) occur with less silicic tuffs and lavas (with compositions similar to the Etendeka quartz latites) the term "quartz latite" has been used in preference to the term rhyodacite (Ekren *et al.*, 1984).

6.3 QUARTZ LATITE ALTERATION

Comparison of pitchstone and devitrified quartz latite compositions from similar sample localities within individual flow units (Milner and Duncan, 1987, Table 1) revealed differences for a number of oxides and elements, particularly K_2O, LOI, CaO, Na_2O and Cs. Differences in K_2O and LOI are attributed to a loss of K_2O in the pitchstones due to low-temperature hydration and ion exchange (K^+ for H_3O^+) reactions affecting the glassy mesostasis of these rocks. In contrast, the pitchstones are enriched in CaO and Na_2O relative to the devitrified quartz latites. This feature is thought to have resulted from the alteration of plagioclase in the devitrified quartz latites and the subsequent removal of these elements from the system (Milner and Duncan, 1987).

In order to show clearly what significant compositional differences exist between pitchstone and devitrified quartz latite a statistical approach has been used. Milner and Duncan (1987) show that the southern Etendeka quartz latites can be divided into several geochemically distinct "groups" using certain immobile elements as discriminants. Each "group" represents samples either from individual quartz latite units (e.g. the Upper Springbok quartz latite) or from several units (e.g. the Lower Interbedded Coastal quartz latites) which exhibit very similar field and petrographic characteristics. The uniformity of composition (discussed in Section 6.4) displayed by each group means that pitchstone and devitrified quartz latite analyses from a particular group can be pooled to form two separate populations. Statistical differences between these populations can be readily identified assuming that both populations started with equivalent compositions. A justification of this approach is demonstrated by the strikingly similar mean values of relatively immobile elements such as Ti, Al, Fe, P, Ba, Zr, V and Y (Table 6.2). In Fig. 6.2 compositional differences between pitchstone and devitrified quartz latite for three groups of quartz latites are expressed as a relative percentage of the pitchstone mean. In Fig. 6.2 vertical lines indicate those elements for which the mean values for pitchstones and devitrified quartz latite differ statistically at the 95 %

TABLE 6.2

A comparison of the average composition of pitchstone and devitrified quartz latite from the Lower Tafelberg and Lower Interbedded Coastal units.

	Pitchstone (n = 17)	S.D.	Devitrified (n = 67)	S.D.
SiO_2	67.04	0.55	68.12	0.70
TiO_2	0.85	0.02	0.85	0.02
Al_2O_3	12.92	0.12	12.86	0.25
FeO*	5.23	0.10	5.32	0.11
MnO	0.09	0.01	0.09	0.02
MgO	1.13	0.12	1.20	0.24
CaO	3.38	0.21	2.44	0.36
Na_2O	3.34	0.47	2.84	0.39
K_2O	2.48	0.56	4.74	0.43
P_2O_5	0.29	0.02	0.29	0.01
LOI	3.24	0.84	1.26	0.32
Cs	19.2	13.0	5.1	1.3
Rb	194	65.4	181	12.7
Ba	632	28.3	630	44.2
Sr	176	23.0	133	20.0
Th	14.7	1.3	15.1	2.1
U	4.7	1.1	4.7	1.2
Zr	268	4.8	266	6.8
Nb	24.2	1.0	23.4	1.0
Cr	4.4	2.4	4.3	2.0
V	53.8	6.6	54.6	8.8
Sc	17.8	1.3	18.2	1.0
Ni	2.4	0.8	2.7	0.9
Co	11.4	1.0	12.1	1.1
Pb	24.2	2.7	24.3	3.0
Zn	75.6	3.6	72.5	4.5
Cu	33.0	6.6	30.5	6.0
Y	40.6	2.6	41.1	2.5
La	44.1	4.3	42.3	1.8
Ce	89.2	4.6	87.0	2.8
Nd	48.2	1.5	47.6	3.3

NOTE:
Fig. 6.2(a) gives a graphical representation of the differences exhibited by this data.

Fig. 6.2 Pitchstone and Devitrified Quartz Latite Differences.

Vertical bars indicate those elements for which the mean values for pitchstones and devitrified quartz latites differ statistically at the 95 % confidence level. Positive values indicate greater concentrations in the pitchstones.

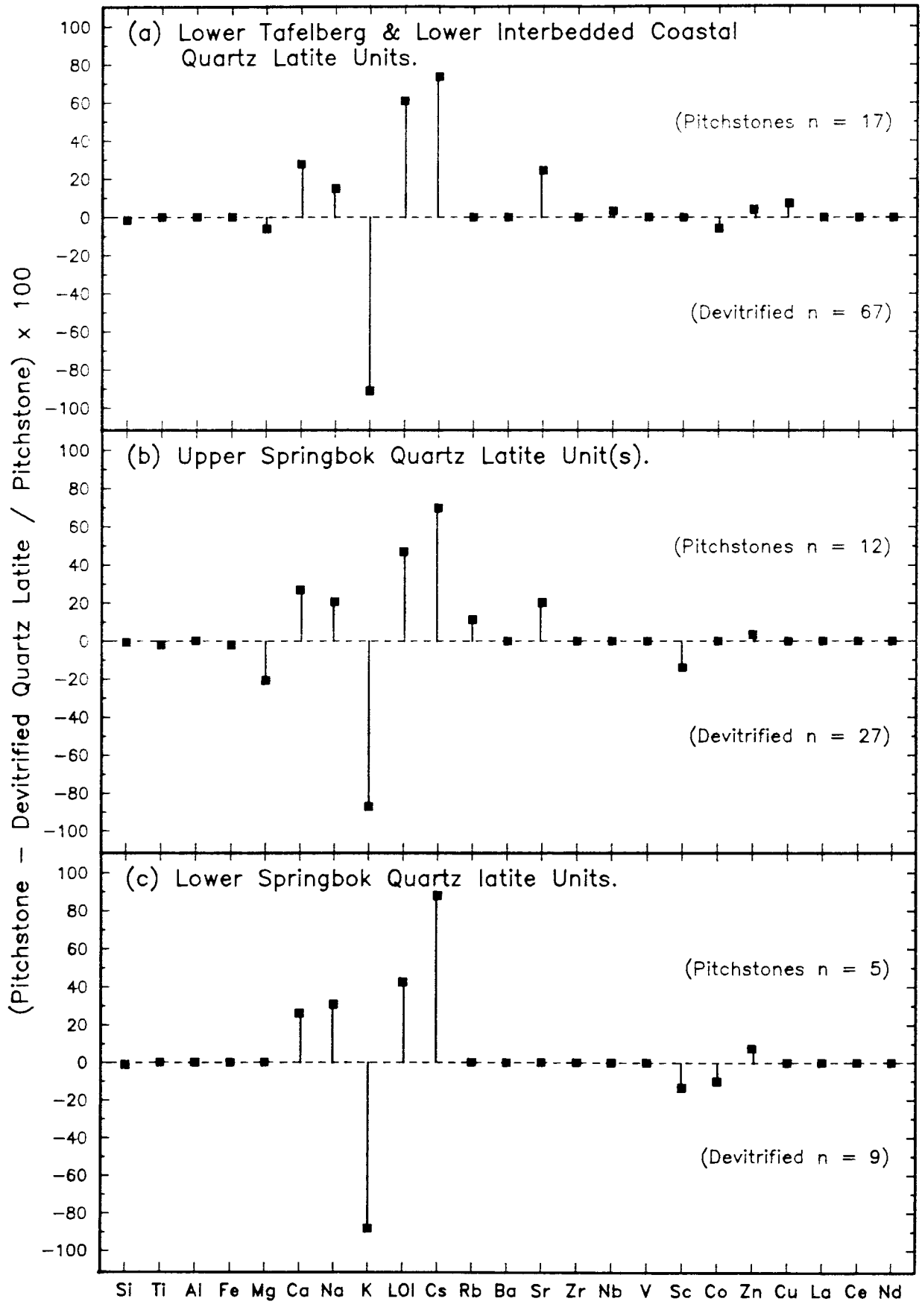

confidence level. The statistical significance of such differences were assessed using two-sample t-tests calculated using the P3D routine of the BMDP statistical software package (Dixon *et al.*, 1981). P3D calculates both t-pooled and t-separate statistics which assume equality and inequality of variance respectively. In most cases the variances were equal at the 95 % confidence level (using Lavene's W test) enabling the more powerful t-pooled statistic to be used.

Elements which showed statistically significant differences between pitchstones and devitrified quartz latites in more than one of the three graphs in Fig. 6.2 are Si, Mg, Ca, Na, K, LOI, Cs, Sr, Sc, Co and Zn. The most significant of these are Ca, Na, K, LOI, Cs and Sr. Two important features can be noted from Fig. 6.2. Firstly, the apparent "decoupling" of the alkalis (Na, K, Rb and Cs) with some alkali elements showing relative "enrichment" in the pitchstones and others showing relative depletion or little difference. Secondly, the roughly equivalent relative "enrichment" of Ca, Na and Sr in the pitchstones. K, Rb and Cs can be viewed slightly differently from Na because they do not form essential components of the primary mineralogy present in the pitchstones and must reside in the interstitial glass. Why Rb and Cs behave so differently from K is unknown. Hydration and ion exchange reactions are dependent upon temperature, pH, Eh, salinity and composition of pore solutions (Fisher and Schmincke, 1984) and will also presumably depend upon differential rates of ionic diffusion in the glass. Unfortunately few, if any, of these parameters are known. Furthermore it is not known whether the higher concentrations of Cs in the pitchstones are due to some kind of enrichment (possibly during hydration), or whether they represent primary concentrations, which would suggest preferential loss of Cs from the devitrified quartz latites.

Recent $\delta^{18}O$ (‰) data on mineral separates and whole rocks for two pitchstone samples (SM-115 and SM-168, Harris *et al.*, 1988) indicate considerable oxygen isotopic disequilibrium:

	Plagioclase	Cpx	Whole Rock	Average Difference
SM-115	6.62	6.64	16.59	9.96
SM-168	10.94	10.63	17.88	7.09

Taylor (1968) and Cerling *et al.* (1985) have reported similar, if not greater (up to 20 ‰), shifts in the oxygen isotopic composition of hydrated

obsidians indicating that the hydrated glasses had not simply absorbed H_2O but must have exchanged with large quantities of it. Cerling *et al.* (1985) calculated hydration temperatures of 45 - 65 °C, assuming an exchange with meteoric water (0 to -3 ‰) and glass-water fractionation factors approaching that of albite. Similar calculations using the quartz latites (Harris *et al.*, 1988) yield maximum temperatures of 100 °C with infinite water:rock ratios. Since the water:rock ratio must be less than infinity the corresponding temperatures must be lower in order to explain the observed fractionation effects.

Semi-quantitative microprobe analyses of interstitial glass in the pitchstones have shown low concentrations of CaO (< 0.35 wt%) relative to whole rock values (~ 3.4 wt%), indicating that the majority of CaO must reside in crystalline phases (plagioclase and pyroxene). Considering the unaltered nature of the phenocrysts and microphenocrysts in the pitchstones compared to those in the devitrified quartz latites (Chapter 3), it is likely that the higher concentration of CaO in the pitchstones is a primary feature. The variation of Na and Sr between pitchstone and devitrified quartz latite is roughly proportional to that of Ca (Fig. 6.2), and can be correlated with the altered nature of the plagioclase in the devitrified samples. Since both the pitchstones and the devitrified quartz latites must have experienced similar environments (e.g. depth of burial, fluid circulation, etc..) subsequent to the initial cooling of the flow, it seems likely that the alteration of plagioclase and pyroxene took place during the slow cooling and devitrification of the central portions of the flow unit, and was probably contemporaneous with the high temperature oxidation of Ti-magnetite (Section 3.4). Fluids responsible for the zeolite mineralisation observed in the amygdaloidal flow tops of some of the quartz latites may have derived Na and Ca from within the host flow. Erlank *et al.* (1984) have reported that zeolite minerals hosted by quartz latites contained substantial concentrations of Sr (3000 - 6000 ppm), and the $^{87}Sr/^{86}Sr$ initial ratios of amygdale zeolite and calcite are similar to that of the host rock, further suggesting that these minerals derived some of their components from the quartz latite host.

From the preceding discussion it would appear that neither the pitchstone nor the devitrified quartz latites are truly representative of primary erupted compositions. It is tentatively suggested that the erupted composition can be estimated by taking the average pitchstone composition (excluding K_2O and

LOI), and substituting a K_2O content similar to that for average devitrified quartz latite. The development of alkali-feldspar during the slow cooling and devitrification of the flow interior is thought to have prevented the loss of K from the latter. The result of doing this for the Lower Tafelberg and Lower Interbedded Coastal quartz latites can be seen below:

	Mean Devitrified QL	Mean Pitchstone QL	? Theoretical Composition
SiO2	68.12	67.04	67.04
TiO2	0.85	0.85	0.85
Al2O3	12.86	12.92	12.92
FeO*	5.32	5.24	5.24
MnO	0.09	0.09	0.09
MgO	1.20	1.13	1.13
CaO	2.44	3.38	3.38
Na2O	2.84	3.34	3.34
K2O	4.74	2.48	4.74
P2O5	0.29	0.29	0.29
LOI	1.26	3.23	0.98
TOTAL	100.00	100.00	100.00

Notice that after summing the major oxides, the residual from 100 % (effectively LOI) is about 1 %, which is consistent with the anhydrous mineralogy observed. Admittedly this is only a rough estimation of the erupted composition, and there is particular uncertainty with regard to Na_2O, which shows variable concentrations in both pitchstones and devitrified quartz latites. The same procedure can also be carried out for the quartz latites in other groups.

6.4 WITHIN UNIT VARIATION

Detailed studies of many ash-flow deposits have revealed systematic variations in composition, both vertically and laterally within individual units (Hildreth, 1979; Smith and Bailey, 1966; Williams, 1944 and Ritchey, 1980) and it has been suggested that virtually all pyroclastic eruptions exceeding 1 km^3 are compositionally zoned (Fisher and Schmincke, 1984). In order to evaluate

the extent to which the Etendeka quartz latites show compositional zonation several stratigraphic sections and lateral traverses were sampled. Using elements relatively unaffected by the alteration outlined above, Milner and Duncan (1987) demonstrate that the Lower Tafelberg unit exhibits a remarkably uniform composition, both vertically, through a 70 m section of the flow at Wêreldsend (see Plate 3.4), and laterally over a distance of 140 km (Milner and Duncan, Figures 5 and 6).

An additional serial stratigraphic section through the Lower Tafelberg at the Dunes locality (Fig. 2.3), further emphasises the compositional uniformity of this flow unit. Table 6.3 presents the range, mean and standard deviation (with analytical errors) for selected elements in samples collected from the main bulk of the flow, which is approximately 200 m thick at this locality. A comparison of the sample standard deviation with the analytical errors (Table 6.3) shows that there is hardly any compositional variation in this section. [Note that the analytical errors quoted are those calculated from XRFS counting statistics alone, without the additional errors introduced during sampling and sample preparation!]

Investigation of serial variations within the Springbok quartz latites has not been carried out in as much detail as it has for the Lower Tafelberg unit. However, at certain localities several samples were collected in order to monitor the possibility of within flow variation. Table 6.4 presents data for selected elements for samples from the Upper and Lower Springbok quartz latites at Awahab (Fig. 2.6) and for a short section in what is thought to be the uppermost flow of the Upper Springbok unit at Trig. 26 (Fig. 2.7b). In addition, Table 6.5 presents the range, mean and standard deviation (with analytical errors) of a suite of basal pitchstones from the Upper Springbok unit. These were sampled at the limits of the main outcrop and encompass an area of approximately 2700 km^2. Inspection this data reveals only small degrees of variation in individual vertical and lateral suites. A reasonable correspondence also exists between the compositions of all the Upper Springbok samples (Tables 6.4 and 6.5) despite the possibility that this may be a composite unit consisting of several flows.

The simple reconnaissance sampling of the Sarusas quartz latite units does not permit the problem of within flow variation to be addressed and it is not known whether they are compositionally zoned.

TABLE 6.3

Serial section data for the Lower Tafelberg quartz latite at the Dunes locality (n = 11).

	Min.	Max.	Mean	S.D.	Analytical Error (1 S.D.)
SiO_2	67.19	70.32	68.15	0.85	0.30
TiO_2	0.81	0.85	0.85	0.01	0.02
Al_2O_3	12.33	13.09	12.84	0.24	0.12
FeO*	5.18	5.50	5.39	0.10	0.10
MgO	0.99	1.28	1.17	0.09	0.09
Zr	258	274	270	4.76	0.70
Nb	21.6	23.8	22.9	0.76	0.58
Zn	70.6	80.3	74.8	2.83	0.48
Cu	24.9	34.0	28.3	2.95	0.53
Y	39.2	43.3	41.5	1.01	0.68
La	38.3	43.3	41.3	1.35	0.87

TABLE 6.5

Basal pitchstones from the Upper Springbok quartz latite, sample localities encompass an area of 2700 km^2 (n = 7).

	Min.	Max.	Mean	S.D.	Analytical Error (1 S.D.)
SiO_2	66.36	66.88	66.61	0.16	0.30
TiO_2	0.90	0.93	0.92	0.01	0.02
Al_2O_3	12.79	13.01	12.90	0.10	0.12
FeO*	5.92	6.15	6.02	0.09	0.10
MgO	0.86	1.12	1.01	0.12	0.08
Zr	265	277	274	3.89	0.88
Nb	22.1	23.3	22.8	0.49	0.60
Zn	79.7	84.8	81.7	1.68	0.50
Cu	14.6	18.6	16.1	1.36	0.52
Y	42.3	44.1	43.6	0.79	0.83
La	42.9	47.9	45.7	1.69	0.92

TABLE 6.4

A comparison of quartz latite samples taken from three sections through the Springbok quartz latite units.

[A] Lower Springbok

Sample	(1) SM-212	(2) SM-212A	(3) SM-212B
Rel. Ht. (m)	0	10	25
SiO_2	66.30	66.81	67.05
TiO_2	1.01	1.01	1.04
Al_2O_3	12.77	12.73	13.03
FeO*	6.74	6.70	6.64
MgO	.98	1.11	.91
Zr	294	294	300
Nb	25	28	27
Zn	89	90	81
Cu	19.1	18.7	19.7
Y	48	50	46
La	46	46	47

[B] Upper Springbok

Sample	(4) SM-220	(5) SM-220A	(6) SM-220B	(7) SM-220C	(8) SM-184	(9) SM-185	(10) SM-186	(11) SM-187
Rel. Ht. (m)	0	20	100	180	0	26	40	56
SiO_2	66.65	67.07	66.68	67.47	67.04	67.07	66.63	67.86
TiO_2	0.91	0.93	0.92	0.92	0.92	0.90	0.91	0.91
Al_2O_3	12.79	12.97	12.84	12.72	13.07	12.84	13.17	12.78
FeO*	5.96	6.03	6.04	6.03	6.02	5.91	6.06	5.98
MgO	1.09	1.41	1.46	1.69	0.93	0.88	1.18	1.18
Zr	265	270	262	264	275	272	273	271
Nb	22	23	22	22	23	23	23	23
Zn	81	81	76	77	79	86	85	79
Cu	14.6	14.7	14.7	19.6	16.8	15.6	15.1	16.4
Y	44	42	45	40	43	45	43	44
La	43	43	44	44	45	44	46	46

Analysis Number

1 - 3 Lower-most quartz latite unit at Awahab.

4 - 7 Upper-most quartz latite unit at Awahab.

8 - 11 Upper part of the Upper Springbok quartz latite at Trig. 26.

6.5 COMPOSITIONAL DIFFERENCES BETWEEN QUARTZ LATITE GROUPS

6.5.1 Southern Etendeka Quartz Latites

The identification and geochemical characterisation of groups of quartz latites in the southern Etendeka is covered in some detail by Milner and Duncan (1987). Despite the overall compositional uniformity displayed by these quartz latites, elements such as Fe, Ti and Cu are effective in discriminating between various groups (Milner and Duncan, Figures 7 and 8). Statistical treatment of the data using discriminant function analysis enhanced the distinction between groups of quartz latites defined using Fe, Ti and Cu and enabled the classification of "unknown" samples (i.e. those which could not be defined stratigraphically) into one of the groups used to define a particular discriminant function. Five geochemically distinct groups have been identified and these consist of the following quartz latite units:

(1) Lower Springbok
(2) Upper Springbok
(3) Lower and Middle Tafelberg and Lower Interbedded Coastal
(4) Upper Tafelberg and Middle Interbedded Coastal
(5) Tafelberg Beacon and Upper Interbedded Coastal

Table 6.6 presents the average chemical composition of quartz latite in each of these groups. The average composition of the Tafelberg latite is also included.

The use of Cu as a discriminant (Milner and Duncan, 1987) may be criticised because of its mobility under certain conditions of alteration and hydrothermal activity. Cu occurs as discrete concentrations in individual quartz latite groups, and highly uniform Cu concentrations occur within individual units over large distances (Section 6.3). It is also noteworthy that quartz latites from relatively "Cu-poor" and "Cu-rich" groups occur in the same stratigraphic sequence sometimes lying in direct contact with one another. These features require any secondary process to be both pervasive and uniform within individual units over hundreds of kilometres whilst at the same time having a selective intensity in different units over only a few tens of metres. A process of this nature is considered highly unlikely and therefore the use of Cu as a discriminant element does not appear unreasonable.

6.5.1.1 Stratigraphic Interpretation

The implied stratigraphic correlation of quartz latite units in the groups outlined above, particularly the Tafelberg and Interbedded Coastal units, is

TABLE 6.6

Average whole rock compositions of quartz latites and latites from the southern Etendeka.

(Major elements - weight % oxide. Trace elements - p.p.m.)

Analysis	(1)	(2)	(3)	(4)	(5)	(6)
SiO_2	66.61	66.93	67.90	67.39	66.00	59.26
TiO_2	1.01	.93	.85	.94	1.17	2.29
Al_2O_3	12.73	12.95	12.87	12.88	12.68	13.88
FeO*	6.66	6.13	5.30	5.72	7.04	10.11
MnO	.11	.10	.09	.11	.12	.13
MgO	1.03	1.16	1.19	1.31	1.60	1.69
CaO	2.84	2.82	2.63	3.03	2.94	4.20
Na_2O	2.89	2.87	2.94	3.00	3.17	2.53
K_2O	3.89	3.81	4.28	4.22	3.81	4.45
P_2O_5	.31	.28	.29	.28	.37	.44
LOI	1.93	2.01	1.66	1.13	1.10	1.02
Total	100.00	100.00	100.00	100.00	100.00	100.00
Cs	20.4	8.9	8.8	4.6	4.8	1.1
Rb	177	181	183	167	149	149
Ba	720	682	631	602	580	1100
Sr	156	152	142	132	130	206
Th	14.0	15.6	15.1	14.2	13.2	19.1
U	5.7	5.3	4.7	4.5	4.4	2.0
Zr	295	275	267	259	298	444
Nb	24.2	22.4	23.6	22.7	24.1	25.4
Cr	4.7	5.0	4.3	4.8	4.5	13.3
V	44.6	49.0	54.4	78.2	68.3	61.8
Sc	19.8	18.8	18.1	20.0	19.8	20.2
Ni	2.5	2.6	2.6	4.1	2.0	5.4
Co	14.6	12.8	11.9	14.2	16.2	24.4
Pb	24.2	24.7	24.3	23.2	19.7	29.8
Zn	84.1	79.6	73.1	71.2	86.8	142
Cu	18.7	16.9	31.0	69.2	111	20.3
Y	46.2	42.6	41.0	38.9	52.0	57.8
La	46.5	46.5	42.6	41.9	41.8	71.6
Ce	97.5	92.0	87.4	84.0	87.0	147
Nd	53.7	49.5	47.7	44.2	49.9	74.8
$\delta^{18}O$	15.00	16.10	13.39	14.08	12.69	12.54
ϵ_{Sr}	204.3	223.8	229.5	200.1	125.7	153.5

Analysis Number

(1) Lower Springbok Quartz Latites (n = 15).
(2) Upper Springbok Quartz Latites (n = 39).
(3) Lower Tafelberg and Lower Interbedded Coastal Quartz Latites (n = 84).
(4) Upper Tafelberg and Middle Interbedded Coastal Quartz Latites (n = 14).
(5) Beacon Tafelberg and Upper Interbedded Coastal Quartz Latites (n = 13).
(6) Tafelberg Latite (n = 5).

Averages (1), (2) and (3) include analyses of both pitchstone and devitrified quartz latite. Data normalised to 100 %, H_2O^- free. Total Fe as FeO*.
The isotope data in this table are for a limited number of samples only.

illustrated in Milner and Duncan, Table 2, and is supported by the petrographic evidence presented in Table 3.4. Based on these correlations a reconstruction of the lava succession has been proposed (Milner and Duncan, Figure 11), whereby a thick succession of quartz latites in the west thins and is intercalated with basaltic units in the east. A Comparison of the schematic sections in Milner and Duncan, Figure 11 with the scaled cross section in Fig. 2.4a yields a more realistic perspective of the lava succession.

6.5.2 Sarusas Quartz Latites and Latites

The Sarusas quartz latites and latites crop out in a narrow coastal belt which extends from just north of the Hoarusib River to Cape Fria (Fig. 2.1). Exposure is generally poor and a detailed evaluation of the outcrop characteristics and stratigraphic relationships of these volcanics could not be made during the two brief visits to the area. Fig. 6.1 clearly shows that the Sarusas suite can be divided into latite and quartz latite compositions. Figs. 6.3 and 6.4 indicate the relatively trace element enriched character of these lavas compared to those of the southern Etendeka and serve to discriminate between different groups of quartz latite within the Sarusas suite.

The Sarusas quartz latites can be divided into two groups based on their major element compositions and these groups have been termed the Sarusas a-type and b-type quartz latites. A comparison of the average composition of these types (Table 6.7) shows that the b-type quartz latites are less evolved with lower SiO_2 and higher TiO_2, FeO and MgO than the a-type quartz latites, and that they are enriched in trace elements such as Zr, Nb, Ce, Ba and Sr relative to the a-type samples (Figs. 6.3 and 6.4). The a-type quartz latites can be subdivided into two groups based on their trace element composition (Figs. 6.3 and 6.4). One of these subgroups is compositionally similar to the quartz latites of the southern Etendeka, but can be distinguished from the latter by its lower TiO_2 and higher Zr and Nb.

A traverse from west to east at Sarusas (Fig. 2.1) encountered three units of the b-type quartz latite overlain by two units of the a-type variety (the more enriched subgroup). These in turn give way to at least one more unit of the b-type quartz latite, although it is not known whether this unit forms an upper part to the sequence, or whether it is a unit from the lower part of the sequence which has been repeated by faulting.

Fig. 6.3 Plot of TiO_2, Ba and Sr vs FeO* for the Sarusas Volcanic Suite. Minor symbols indicate the composition of the southern Etendeka quartz latites and latite for comparison

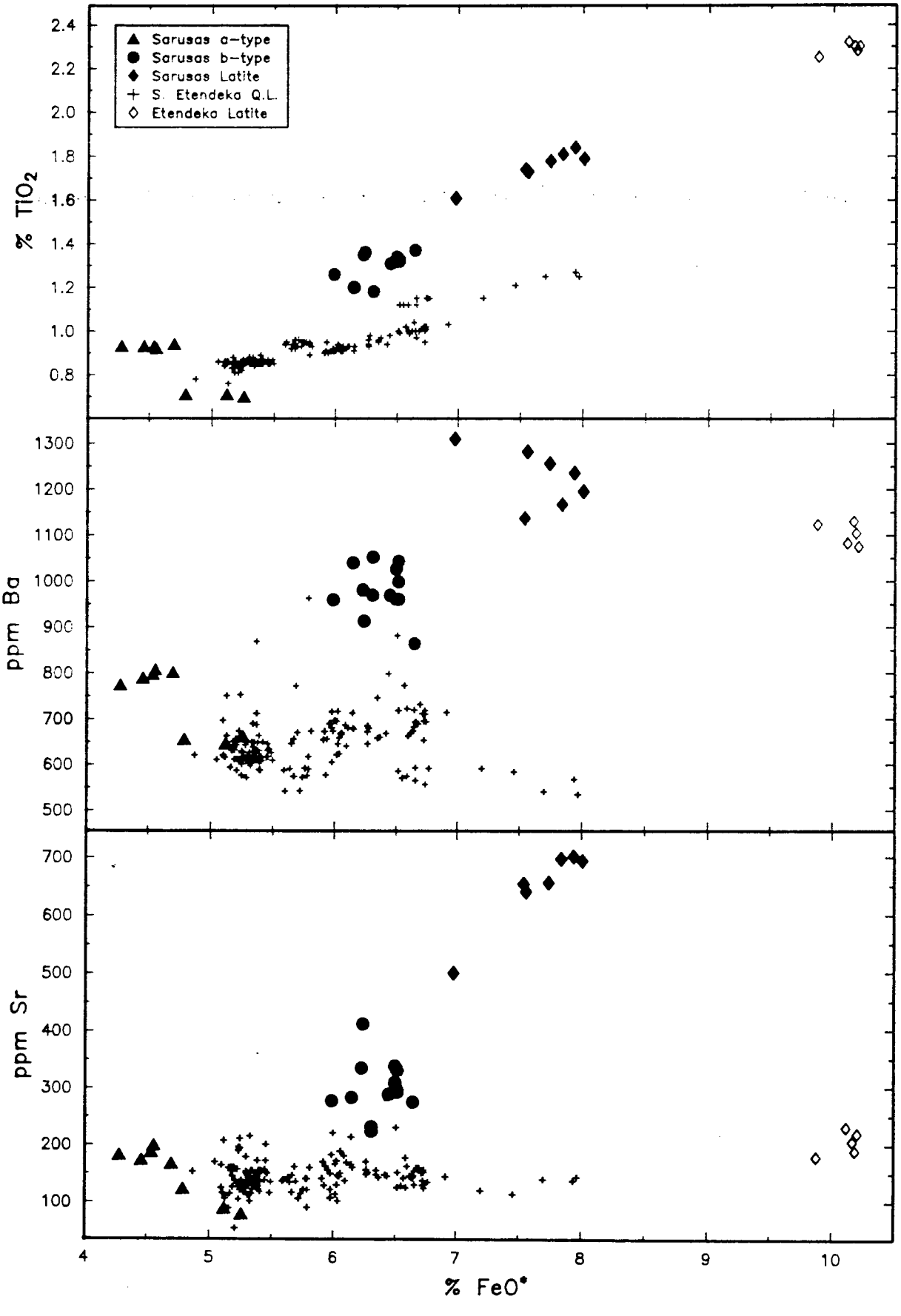

Fig. 6.4 Plot of Zr, Nb and Ce vs FeO* for the Sarusas Volcanic Suite. Minor symbols indicate the composition of southern Etendeka quartz latites and latite for comparison

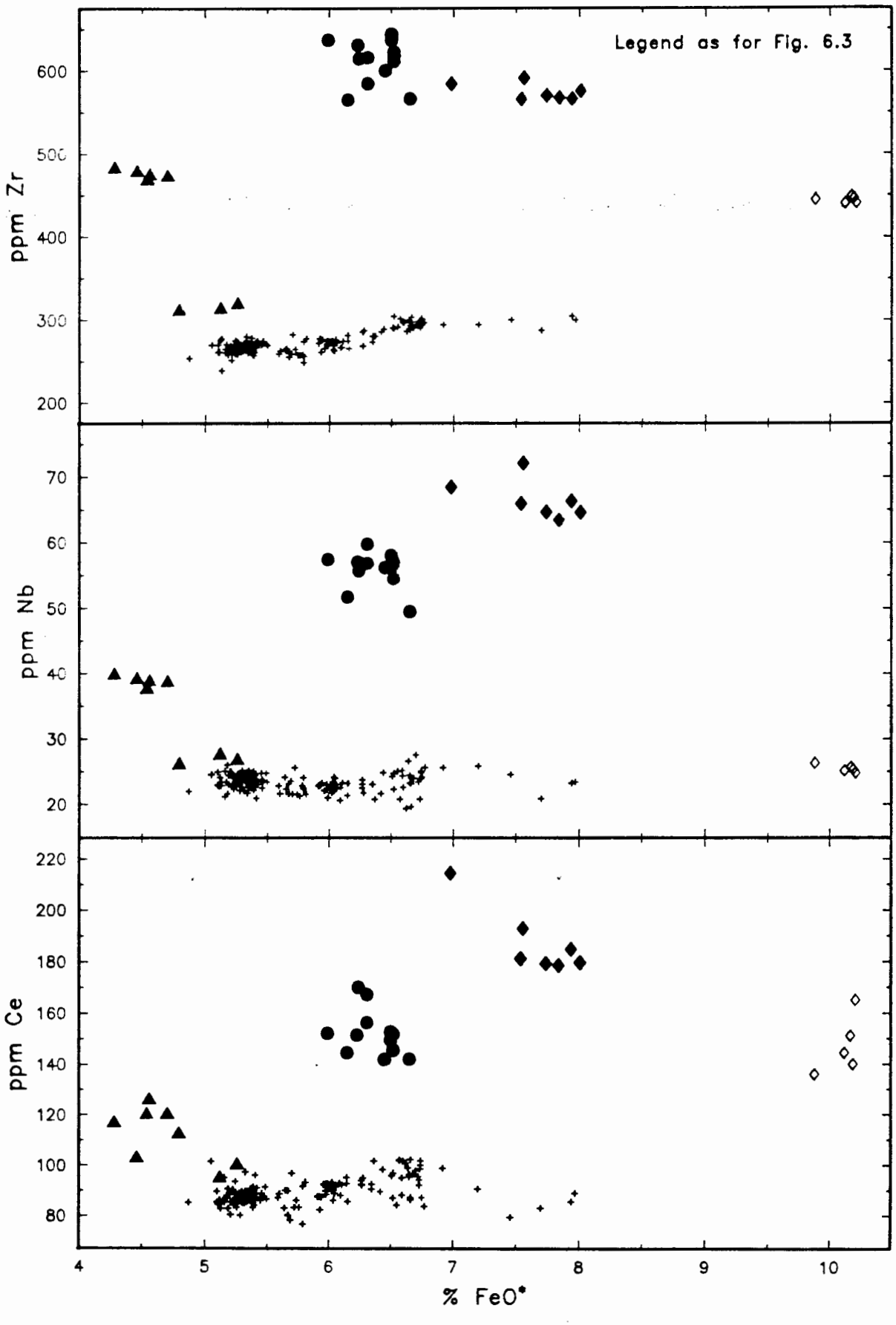

TABLE 6.7

Average whole rock composition of quartz latites and latites from the Sarusas region of the northern Etendeka.

(Major elements - weight % oxide. Trace elements - p.p.m.)

Analysis	(1)	(2)	(3)	(4)
SiO_2	69.78	69.81	66.10	61.39
TiO_2	.93	.71	1.30	1.76
Al_2O_3	12.78	12.43	12.84	14.09
FeO*	4.51	5.06	6.38	7.66
MnO	.12	.10	.14	.12
MgO	.79	.76	1.28	1.59
CaO	2.43	1.98	2.56	3.45
Na_2O	3.27	2.95	3.55	3.46
K_2O	4.03	4.85	4.16	4.61
P_2O_5	.27	.22	.39	.62
LOI	1.08	1.12	1.32	1.25
Total	100.00	100.00	100.00	100.00
Cs	4.9	8.4	4.9	4.2
Rb	158	200	120	121
Ba	793	653	979	1225
Sr	181	96.5	299	648
Th	13.3	18.9	11.5	14.2
U	-	3.3	5.2	-
Zr	477	316	611	574
Nb	39.0	26.9	55.9	66.5
Cr	-	3.2	10.0	2.5
V	29.4	16.4	15.5	57.1
Sc	14.3	18.4	12.7	12.2
Ni	-	3.2	2.5	2.4
Co	5.9	7.0	6.8	16.0
Pb	15.3	33.6	12.2	16.6
Zn	72.7	70.0	107	115
Cu	43.0	24.5	14.4	25.1
Y	61.7	52.3	64.2	52.4
La	53.4	52.3	69.2	88.0
Ce	117	103	151	187
Nd	68.2	55.1	89.6	109
$\delta^{18}O$	12.43	-	15.36	11.19
ϵ_{Sr}	83.9	-	35.2	38.3

Analysis Number

(1) Sarusas (a) Quartz Latite (n = 5).
(2) Sarusas (a) Quartz Latite (less enriched group) (n = 3).
(3) Sarusas (b) Quartz Latite (n = 13).
(4) Sarusas Latite (n = 7)

Averages (1) and (3) include analyses of both pitchstone and devitrified quartz latite.

Data normalised to 100 %, H_2O^- free. Total Fe as FeO. The isotope data in this table are for a limited number of samples only.

A brief mention of the Sarusas Latites is made here because they have not been previously documented. Latite units have been encountered at two localities. Two units occur north of the Sechomib River and one south-east of Rocky Point (Fig. 2.1), thus showing a more widespread occurrence than the single unit at Tafelberg in the southern Etendeka. Samples from the two units north of the Sechomib river form a tight cluster in Figs. 6.3 and 6.4, the outlying point representing a sample from Rocky Point. Note that the compositional characteristics of these latites (Table 6.7) are different from those of the Tafelberg latite (Table 6.6).

6.5.3 The southern Etendeka and Sarusas quartz latites: a comparison

One of the most striking features of the basaltic volcanics of the Karoo and Paraná Igneous Provinces are the presence of "enriched" and "normal" basalts which predominate in the northern and southern parts of each Province respectively. This geochemical anomaly, initially recognised in the Lebombo and Serowe district of Botswana (Fig. 1.2) and in the Paraná of Brazil (Cox *et al.*, 1967; Cox, 1983 and Bellieni *et al.*, 1984) has also been recognised in the Etendeka (Duncan, 1987). Division of the Etendeka volcanics into "enriched" (northern) and "normal" (southern) areas can also be extended to the quartz latites. The Sarusas quartz latite units show notable enrichments in Ba, Sr, Nb, Zr, P, Ti, Y and LREE relative to the southern Etendeka units. Similar compositional differences have also been recognised between the felsic volcanics of the northern and southern parts of the Paraná (Bellieni *et al.*, 1986). Elements which show enrichments in the Khumib basalts and Sarusas quartz latites are essentially similar (Fig. 6.5 and 6.6), although the overall enrichment in the quartz latites is less than it is in the basalts. It is interesting that strongly incompatible elements such as K, Rb and Th do not follow the general pattern of relative enrichment in the north, although the Khumib basalts as a whole are slightly enriched in K_2O (Fig. 6.1).

Isotopic studies have also revealed differences between "normal" and "enriched" lavas. The southern Etendeka basalts (Albin- and Tafelberg-type) show wide-ranging initial $^{87}Sr/^{86}Sr$ ratios (0.7081 - 0.7135) (Bristow *et al.*, 1984), whilst the Khumib basalts show a more restricted range with lower initial $^{87}Sr/^{86}Sr$ ratios (0.7051 - 0.7088) (Duncan *et al.*, in prep.). Similarly the southern Etendeka quartz latites have relatively high $^{87}Sr/^{86}Sr$ initial ratios (0.7131 - 0.7218) compared to the Sarusas latites

Fig. 6.5 Comparison of the average composition of southern Etendeka and Sarusas b–type quartz latites.

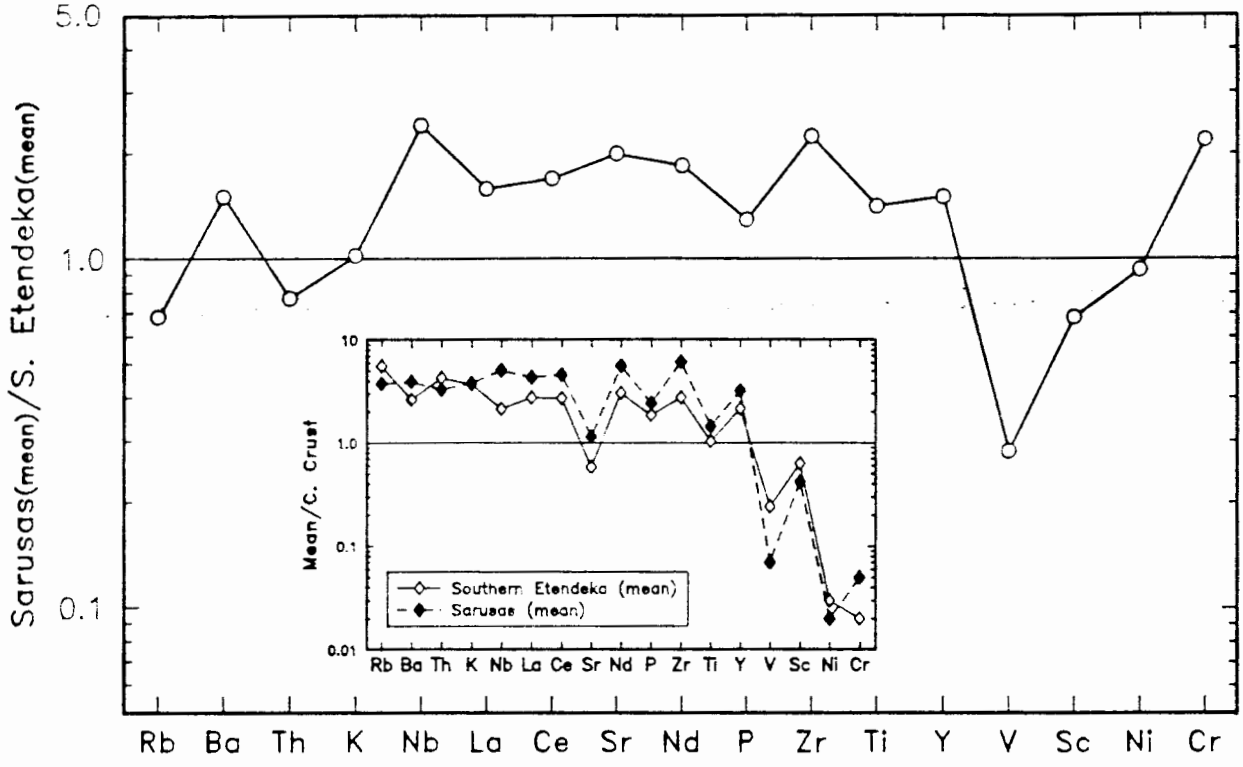

Values for continental crust are those quoted by Taylor and McLennan (1985) for bulk continental crust.

Fig. 6.6 Comparison of Tafelberg– and Khumib–type basalt samples with similar major element chemistries.

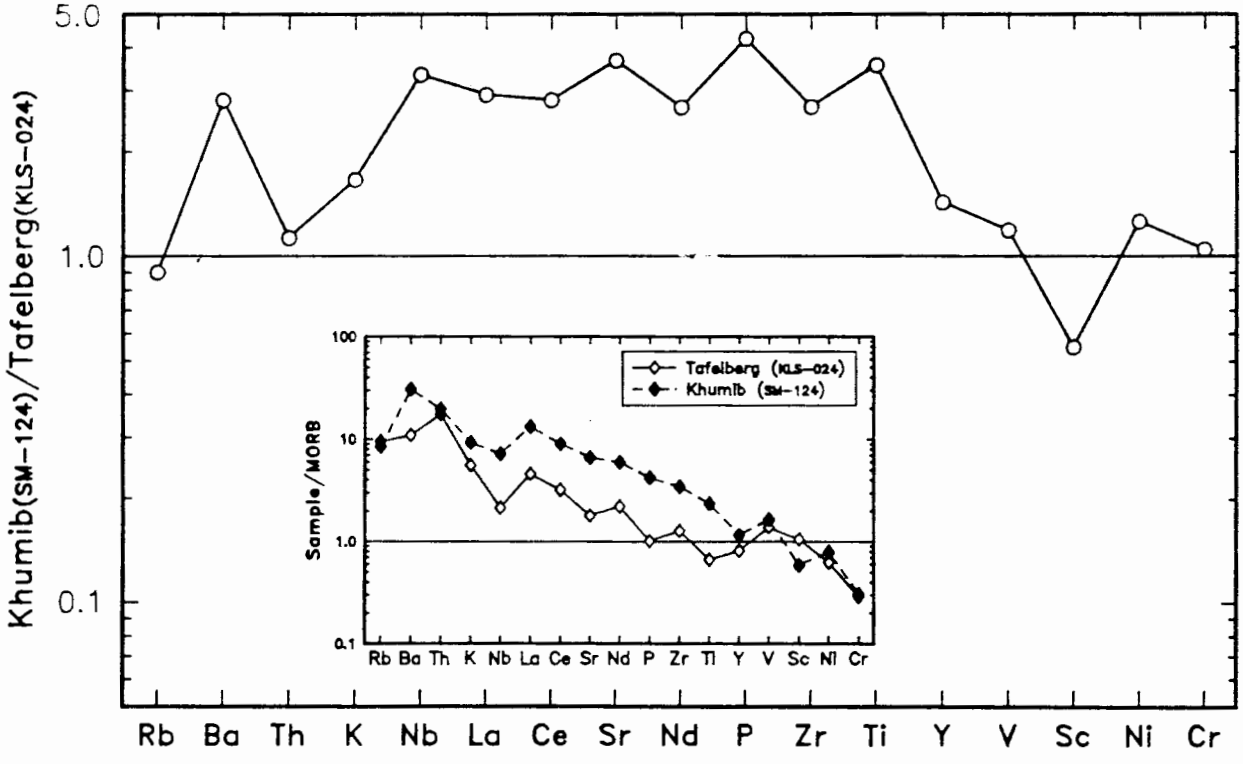

MORB composition from Pearce (1982) with additional estimated values for La(3.0), Nd(8.5) and V(190) ppm.

and quartz latites (0.7066 - 0.7105). The limited oxygen isotope data for mineral separates from the quartz latites (Section 6.3) are also interesting in the light of these Sr isotopic differences. If one accepts the average of plagioclase and pyroxene $\delta^{18}O$ values as indicative of the original (pre-alteration) $\delta^{18}O$ value of the total rock, then the Sarusas quartz latite sample (SM-115) exhibits $\delta^{18}O$ values of approximately + 6.63 ‰, a value commonly associated with mantle derived material (Kyser, 1986). Conversely a value calculated in the same way for the southern Etendeka quartz latite sample (SM-168) $\delta^{18}O$ = + 10.79 ‰, is more typical of material derived from the crust.

6.6 SUMMARY

(1) The quartz latites of the Etendeka from part of a tri-modal suite, coexisting with basaltic and minor latitic lavas.

(2) Etendeka quartz latites display compositions which have not been widely reported in the literature for felsic volcanics outside the Karoo and Paraná Igneous Provinces.

(3) Pitchstone and devitrified quartz latites have been affected by alteration. The combination of low concentrations of K_2O and high LOI, coupled with significant enrichment in ^{18}O of the whole rock relative to mineral separates, implies a low temperature hydration event. The apparent loss of CaO, Na_2O and Sr in the devitrified quartz latites is related to the alteration of plagioclase (and pyroxene). This alteration is believed to have occurred during the much slower cooling of these samples, shortly after eruption, and may have been contemporaneous with the zeolite-calcite-silica mineralisation which occurs in many of the flow tops.

(4) The extremely uniform composition displayed by individual quartz latite units in the southern Etendeka indicates that their magma reservoirs were not compositionally zoned.

(5) Small, but significant, variations of certain element abundances and the use of discriminant function analysis has allowed the characterisation of 5 groups of quartz latites which can be correlated over much of the Etendeka area.

(6) A stratigraphic model for the Etendeka Formation in the southern Etendeka is proposed on the basis of these correlations, and it is envisaged that the thick sequence of quartz latites in the west thins and is intercalated with basaltic units in the east.

(7) Three geochemically distinct groups of quartz latite and one latitic group are recognised among the Sarusas units. The latites and b-type quartz latites are enriched in Ba, Sr, Nb, Zr, P, Ti, Y and LREE compared to the southern Etendeka quartz latite units. Thus the geochemical discontinuity displayed by the basalts from northern and southern areas of the Karoo and Paraná Igneous Provinces is also displayed by quartz latites from northern and southern parts of the Etendeka.

CHAPTER 7

PETROGENESIS OF THE ETENDEKA FORMATION QUARTZ LATITES

7.1 INTRODUCTION

In this chapter an attempt is made to place some constraints on the petrogenesis of the Etendeka Formation quartz latites. Isotopic evidence (Erlank *et al.*, 1984) strongly suggests that the southern Etendeka quartz latites were derived either wholly or in part by crustal anatexis, which probably occurred as a result of contemporaneous basaltic magmatism. What is not clear, however, is whether the quartz latites evolved by differentiation and crustal contamination of a basaltic precursor; a model which has been proposed for rhyolitic volcanics in the Paraná (Bellieni *et al.*, 1984; Hawkesworth *et al.*, 1987); or whether they represent crustal melts which have undergone comparatively little mixing or interaction with basaltic magma, a model suggested for extensional terrains by Hildreth (1981) and supported by experimental studies (Huppert and Sparks, 1987), which predict negligible mixing between lower density crustal melts and underlying hotter, denser basaltic melts. The principle aim of this chapter, therefore, is to investigate the possible processes involved in the generation of quartz latite magmas and of their compositional variation, and to evaluate the extent to which basalt or latite magmas were involved in their petrogenesis. The strategy adopted here is to make a comprehensive study of the magmatic processes which may have affected the quartz latites of the Tafelberg/Interbedded Coastal succession (reconstructed in Fig. 11b, Milner and Duncan, 1987), which exhibit coherent variations in bulk chemistry and mineralogy with stratigraphic height. This is followed by a somewhat briefer treatment of similar processes affecting the Springbok and Sarusas quartz latites. Finally, the generation of quartz latite magma by partial melting and the possible source compositions involved in such a process are discussed. In an attempt to condense the material presented in this chapter a summary of the magmatic processes, modelling procedures and model parameters considered herein are outlined in Sections 7.2 and 7.3.

7.2 PETROGENETIC MODELS

The processes by which the Etendeka formation quartz latites may have been derived, or are related to other magma types, are considered as follows:

(1) **Magma Mixing** or **Simple Assimilation** considers simple mixing of magmas or the bulk assimilation of country rock by a magma. Quantitative models have been calculated using the general mixing equations of Langmuir *et al.* (1978).

(2) **Fractional Crystallisation (FC)** considers the effects of simple closed-system crystallisation and continuous removal of liquidus phases from the melt. Quantitative modelling of this process involves the use of a least squares mixing approximation, GENMIX (Le Maitre, 1981), in conjunction with observed rock and mineral compositions to obtain a solution for the major elements. The fractionating phases, their proportions and the degree of fractionation (F) estimated from these calculations were then used to predict trace element concentrations in the derivative melt using the well-known Rayleigh fractionation equations (e.g. Arth, 1976).

(3) **Assimilation-Fractional Crystallisation (AFC)** considers the evolution of a magma affected by simultaneous fractional crystallisation and wall rock assimilation. A modified version of GENMIX and an unpublished algorithm (A.R. Duncan, pers. comm.) has been used in conjunction with observed rock, mineral and assumed assimilant compositions to yield a quantitative solution for the major elements. The equations of De Paolo (1981) were used in conjunction with the F and r (mass assimilated/mass crystallised) values derived from the least squares approximation to predict the trace element and isotopic composition of the fractionated liquid.

(4) **Partial Melting** has been considered in an attempt to identify likely source composition and mineralogies, and also the effect that different degrees of partial melting of the source may have on the quartz latite composition. The calculation of melting modes (proportions of possible source minerals constituting the melt) was carried out using a least squares approximation modified from Bryan *et al.* (1969).

Calculations of the quantitative magma mixing, fractional crystallisation and AFC models discussed in this chapter were carried out using the computer program DARTS, programmed and maintained by A.R. Duncan and R.J. Sweeney (Cape Town) and developed in collaboration with A. Ewart (Queensland). DARTS, which

contains an impressive options menu, allows the "fine tuning" of model parameters and rapid evaluation of numerous models.

7.3 MODEL PARAMETERS

In order to permit a fairly brief discussion of the various petrogenetic models investigated in this study it is necessary to outline the choice of end-member compositions which define, or are thought to contribute to a particular trend, and of the general assumptions made regarding differentiation pathways and the partitioning of trace elements between crystals and liquid.

7.3.1 Whole rock compositions

7.3.1.1 End-member compositions

The quartz latites of the Tafelberg and Interbedded Coastal succession are characterised by a progression towards more mafic whole rock compositions and lower ϵ_{Sr} values higher in the sequence (compare analyses 3, 4 and 5 in Table 6.6). Fe shows the most significant major element variation and can be used as an "index of variation" defining what might be regarded as an evolutionary trend from more mafic samples containing higher FeO, TiO_2 and MgO and lower SiO_2 and K_2O to more evolved samples with lower FeO, TiO_2 and MgO and higher SiO_2 and K_2O. FeO* can also be used as a variation index for the basaltic rocks but it is important to note that in this instance the concentration of Fe increases rather than decreases with fractionation (the classic "tholeiite trend").

If the major rock types of the Etendeka Formation are all related by some sort of differentiation process then it is likely to progress in the following manner, encompassing three main stages:

(I) Basalt to Evolved Basalt (10 ---> 13 % FeO*)

(II) Evolved Basalt to most-mafic quartz latite (13 ---> 8 % FeO*)

(III) Most-mafic quartz latite to least-mafic quartz latite (8 ---> 5 % FeO*)

Stage (I) is covered in considerable detail by Erlank *et al.* (1984) and since it is not directly concerned with the quartz latite petrogenesis it is not discussed further here. In order to reduce lengthy descriptive terminology when

referring to trends and their typical end-member compositions specific samples can be regarded as being representative of the following:

(1) Evolved basalt - **SM-045**

(2) Most-mafic quartz latite - **SM-164**

(3) Least-mafic quartz latite - **KLS-083**

The major, trace element and isotopic composition of these samples are given in Table 7.1. To avoid modelling variations which are due to secondary alteration both quartz latite end-members are of devitrified material (see discussion in Chapter 6). The majority of analyses plotted on the various diagrams are also of devitrified quartz latite.

7.3.1.2 Assimilants and possible source rock compositions

The basement geology of north-western Namibia is outlined in Chapter 2 and consists of a variety of lithologies (schist, amphibolite, granite, etc..). The identification of a representative upper crustal composition is difficult and the nature and composition of the lower crust in this area is unknown. For these reasons the crustal compositions used in petrogenetic models are the averages of Taylor and McLennan (1985) given in Table 7.1. The Sr-isotopic characteristics of the basement rocks also vary considerably. Damara granites and sediments are essentially bimodal with regard to ϵ_{Sr} (at 121 Ma), with average values of 40 for some of the Salem granitic rocks and 500 for the Kuiseb Schists and other assorted granites (data recalculated from Hawkesworth *et al.*, 1983). Some of the older basement granites and migmatites have ϵ_{Sr} (at 121 Ma) greater than 1000 (Bristow *et al.*, 1984).

7.3.2 Mineral compositions

The mineral compositions used in the FC and AFC models that follow are given in Table 7.2. Models involving the generation of SM-164 from SM-045 were carried out using plagioclase, augite, pigeonite and Ti-magnetite compositions determined in an evolved Tafelberg-type basalt (KLS-054) (data from Erlank *et al.*, 1984; microfiche data base). Mineral data for models involving SM-164 and KLS-083 are phenocryst compositions from two Upper Interbedded Coastal quartz latite samples (SM-161 and KLS-281).

TABLE 7.1

End-member, assimilant and source rock compositions used in the petrogenetic modelling of the southern Etendeka quartz latites.

	(1) SM-045	(2) SM-164	(2) SM-162	(3) KLS-083	(4) UCRUST	(5) BCRUST	(6) LCRUST
SiO_2	54.87	64.78	65.69	68.79	66.00	57.30	54.40
TiO_2	1.78	1.27	1.11	0.85	0.50	0.90	1.00
Al_2O_3	13.44	12.71	12.61	12.74	15.20	15.90	16.10
FeO*	13.01	7.94	6.44	5.11	4.50	9.10	10.60
MnO	0.19	0.10	0.09	0.10	0.00	0.00	0.00
MgO	3.95	1.74	1.42	1.13	2.20	5.30	6.30
CaO	7.72	3.19	2.84	2.46	4.20	7.40	8.50
Na_2O	3.05	2.98	3.08	2.99	3.90	3.10	2.80
K_2O	1.72	3.64	4.04	4.63	3.40	1.10	0.34
P_2O_5	0.27	0.40	0.39	0.27	0.20	0.10	0.10
Total	100.00	98.75	97.71	99.07	100.10	100.20	100.14
Rb	51.0	144	156	189	112	32.0	5.3
Ba	488	567	578	616	550	250	150
Sr	273	138	124	116	350	260	230
Zr	207	305	300	261	190	100	70.0
Nb	23.4	23.0	24.0	23.0	25.0	11.0	6.0
Cr	15.2	-	-	9.1	35.0	185	235
V	458	58.0	55.0	45.0	60.0	230	285
Sc	35.4	22.0	19.1	17.7	11.0	30.0	36.0
Ni	27.8	-	-	-	20.0	105	135
Co	45.2	17.6	15.0	9.5	10.0	29.0	35.0
Zn	118	99.0	87.0	66.0	71.0	80.0	83.0
Cu	123	113	166	29.0	25.0	75.0	90.0
Y	38.7	54.0	52.0	34.0	22.0	20.0	19.0
La	32.1	39.0	39.0	41.0	30.0	16.0	11.0
Ce	60.8	85.0	86.0	84.0	64.0	33.0	23.0
Nd	34.0	51.0	51.0	40.0	26.0	16.0	12.7
ϵ_{Sr}	120.0	121.0	-	236.0	-	-	-

End-member compositions:

(1) "Evolved Basalt" - ϵ_{Sr} (at 121 Ma) inferred from data of Erlank *et al.* (1984)
(2) Upper Interbedded Coastal quartz latites.
(3) Lower Tafelberg quartz latite.

Contaminants and possible source rock compostions:

(4) Average Upper Crust.
(5) Average Bulk Crust.
(6) Average Lower Crust.

(2) - (3) Not normalised volatile-free.
(4) - (6) Crustal averages from Taylor and McLennan (1985).

TABLE 7.2

(a) **Mineral composition data used in the Stage (II) models.**

	Plagio-clase	Augite N°1	Augite N°2	Pigeonite	Titano-magnetite
SiO_2	56.74	51.31	50.46	49.76	0.00
TiO_2	0.00	0.60	0.78	0.51	21.59
Al_2O_3	27.05	1.53	1.56	0.74	1.66
FeO*	0.77	19.67	17.20	29.15	73.53
MnO	0.00	0.42	0.35	0.60	0.43
MgO	0.07	10.83	12.91	13.57	0.23
CaO	8.51	15.35	16.50	5.62	0.00
Na_2O	6.12	0.29	0.24	0.06	0.00
K_2O	0.74	0.00	0.00	0.00	0.00
P_2O_5	0.00	0.00	0.00	0.00	0.00
Total	100.00	100.00	100.00	100.00	100.00

Microprobe data from Erlank *et al.* (1984) for "evolved basalt" sample KLS-054.

(b) **Mineral composition data used in the Stage III models.**

	Plagio-clase N°1	Plagio-clase N°2	Pigeonite	Titano-magnetite
SiO_2	56.38	56.28	50.60	0.46
TiO_2	0.00	0.00	0.34	21.62
Al_2O_3	27.46	26.69	0.66	1.25
FeO*	0.90	1.02	27.55	72.41
MnO	0.00	0.00	0.90	1.48
MgO	0.09	0.10	15.00	0.24
CaO	9.85	10.72	4.89	0.04
Na_2O	5.24	4.77	0.07	0.00
K_2O	0.43	0.43	0.00	0.00
P_2O_5	0.00	0.00	0.00	0.00
Total	100.00	100.00	100.00	100.00

Plagioclase compositions from Upper Interbedded Coastal quartz latite sample SM-161. Pigeonite and titanomagnetite compositions from Upper Interbedded Coastal quartz latite sample KLS-281.

The composition of phases such as apatite and zircon, and of those phases used in least squares approximations of the melting mode, were calculated from the mineral formulae.

7.3.3 Crystal-liquid distribution coefficients

The distribution coefficients used in quantitative trace element modelling are given in Table 7.3. Most trace elements, with the exception of Zr which is an essential constituent of zircon, are assumed to behave in accordance with Henry's law; which states that for dilute solutions elemental activity coefficients have a constant value which is independent of concentration. Therefore a Kd is simply defined as the elemental concentration ratio between equilibrated crystals of a specific phase and the liquid. Kd values do, however, vary as a function of bulk composition and it is necessary to change Kd values for models which span large ranges in composition. Thus slightly different Kd values are used in modelling the Stage (II) and Stage (III) trends (Tables 7.3a and 7.3b respectively).

7.4 THE ROLE OF MAGMATIC PROCESSES IN THE PETROGENESIS OF THE SOUTHERN ETENDEKA QUARTZ LATITES.

7.4.1 Introduction

The purpose of this section is to investigate the extent to which the compositional variations displayed by the southern Etendeka quartz latites can be explained by processes such as magma mixing, fractional crystallisation and AFC, and to see what genetic relationships there are, if any, between the basaltic lavas and the quartz latites.

7.4.2 Stage II models

In their petrogenetic modelling of the Etendeka basaltic volcanics Erlank *et al.* (1984) showed that:

(1) The trace element and Sr- and Nd-isotopic characteristics of the Etendeka volcanics precluded the derivation of the basaltic lava - latite - quartz latite suite by any simple closed system model, e.g. partial melting of an isotopically homogeneous source or fractionation of a homogeneous parental magma.

(2) The data preclude any simple mixing relationship between quartz latite and

TABLE 7.3

(a) **Partition coefficient data used to calculate trace element concentration in the Stage II FC and AFC models.**

	Plagio-clase	Clino-pyroxene	Titano-magnetite	Apatite
Rb	0.1000	0.0130	0.0040	0.0100
Ba	0.3000	0.0800	0.4000	0.0100
Sr	1.8000	0.0700	0.5000	50.3500
Zr	0.0370	0.2000	0.6500	0.0300
Nb	0.1000	0.3900	1.0000	0.0100
Cr	0.1780	43.2590	59.8700	0.0100
V	0.0200	1.1000	20.0000	0.0600
Sc	0.0250	10.0000	3.2880	0.2000
Ni	0.2170	5.7250	9.6000	0.0100
Co	0.0510	5.3600	20.0000	0.0100
Zn	0.2160	6.0000	10.0000	0.0100
Cu	0.3000	0.4500	5.4700	0.2800
Y	0.1000	0.5800	1.0000	185.0000
La	0.2450	0.3540	0.4790	34.0000
Ce	0.2000	0.5190	0.5670	37.0000
Nd	0.1620	1.2230	0.7650	108.0000

(b) **Partition coefficient data used to calculate trace element concentration in the Stage III FC and AFC models, and in the modelling of partial melting processes.**

	Plagio-clase	Alkali-Feldpar	Quartz	Clino-pyroxene	Ortho-pyroxene	Titano-magnetite
Rb	0.0320	0.7500	0.0090	0.0900	0.0100	0.0040
Ba	0.5000	7.2820	0.0320	0.0240	0.0380	0.4000
Sr	4.4040	6.2230	0.0010	0.0670	0.0300	0.1000
Zr	0.2000	0.1500	0.0800	0.2950	0.0430	0.2950
Nb	0.0300	0.0060	0.0010	1.0000	0.3000	3.0000
Cr	0.1780	0.5600	0.0010	43.2590	42.0920	59.8780
V	0.4600	0.5500	0.0010	2.0000	1.4250	20.0000
Sc	0.0250	0.0500	0.0100	10.0000	4.8430	3.2880
Ni	0.2170	1.8200	0.0010	5.7250	16.9500	9.6000
Co	0.0510	0.6100	0.0010	5.3600	10.5200	20.0000
Zn	0.2160	0.1000	0.0010	6.0000	3.2340	10.0000
Cu	0.2470	1.0000	0.0010	5.0000	0.5530	10.0000
Y	0.0400	0.0060	0.0010	0.5800	0.4000	1.2000
La	0.2450	0.1550	0.0140	0.3540	0.4220	0.9000
Ce	0.2700	0.0450	0.0200	0.5000	0.1500	1.1000
Nd	0.2000	0.0250	0.0120	1.2000	0.2200	1.6500
Eu	2.1000	1.1000	0.0300	1.3000	0.1800	0.5000
Yb	0.0500	0.0070	0.0100	1.5000	0.8000	1.1000

continued....

Table 7.3(b) continued....

	Ilmenite	Apatite	Biotite	Horn-blende
Rb	0.0100	0.0100	3.8670	0.0700
Ba	0.0100	0.0100	6.2300	0.1600
Sr	0.0100	50.3500	0.1450	0.6300
Zr	3.0000	0.0300	2.3300	0.4350
Nb	10.0000	0.0100	3.1000	0.4750
Cr	10.0000	0.0100	11.4800	64.6670
V	10.0000	0.0600	50.0000	21.4500
Sc	2.3000	0.2000	10.8030	11.5200
Ni	10.0000	0.0100	1.2200	10.3500
Co	10.0000	0.0100	27.7500	11.9770
Zn	75.0000	0.0100	15.3500	7.8130
Cu	5.0000	0.2800	2.9000	1.6000
Y	0.1000	185.0000	0.9900	4.0150
La	7.1000	34.0000	0.2000	0.1890
Ce	7.8000	40.0000	0.3300	1.5000
Nd	7.6000	60.0000	0.0300	4.0000
Eu	2.5000	30.0000	0.2500	5.0000
Yb	4.1000	20.0000	0.4200	8.5000

Data for REE heavier than La for the silicates from Hanson (1978).
Data for REE for oxides from Nash and Crecraft (1985).
All other data are derived from a database of both published and unpublished partition coefficients complied by A. Ewart and A.R. Duncan (Duncan, pers. comm., 1986).

less-evolved basalt.

(3) The most likely model of magma mixing between Tafelberg basalt and quartz latite, one which requires mixing followed by a proportional amount of fractional crystallisation, could also be ruled out on the basis of inconsistent incompatible trace element enrichment trends.

Thus it would appear that no simple genetic relationship exists between the basaltic lavas and the quartz latites. However, the new data presented in this study necessitates a re-evaluation of some of the processes investigated by Erlank *et al*, (1984). Despite the new data it is important to point out that FC and AFC models still remain difficult to reconcile with the paucity of samples with compositions intermediate between the two end members (SM-045 and SM-164), and with the well defined bimodal SiO_2 distribution (Fig. 6.1).

7.4.2.1 Fractional crystallisation

Distinct Sr-isotopic differences between quartz latites and basaltic lavas was one of the arguments used by Erlank *et al.* (1984) to preclude the derivation of the basalt - quartz latite suite by simple closed system fractionation. New Sr-isotopic data for the more-mafic Upper Interbedded Coastal quartz latites suggests that this group is characterised by relatively low ϵ_{Sr} (121 - 130) compared to the other groups of quartz latite (ϵ_{Sr} = 199 - 240, data recalculated from Bristow *et al.*, 1984). The Sr-isotopic characteristics of the more mafic quartz latites are similar to those of the evolved basaltic lavas (ϵ_{Sr} = 77 - 127) necessitating a re-evaluation of a fractional crystallisation process (see Fig. 7.1 for the disposition of available Sr-isotope data).

Table 7.4(a) shows the optimum (lowest residual sum of squares) least squares mixing model between SM-045 and SM-164 obtained using a typical evolved basaltic phase assemblage. The results of modelling for selected trace elements using this major element solution are presented in Figs. 7.2 - 7.6 (plots A and C in each case). The model shows a poor fit for many of the trace elements (V, Y, Zr, Ba, Cu and Sr). High Kds for elements such as Y, Nb and V in titanomagnetite and apatite, and Sr in plagioclase (Table 7.3a) contribute a significant component to the bulk D of the fractionating mineral assemblage thus providing a strong control on behavior of these elements. Published Kd data for apatite and titanomagnetite, in particular, are scarce and rather varied, permitting considerable latitude in the choice of values. Because the degree of

Fig 7.1 Plot of $\mathcal{E}_{Sr}$ *vs.* FeO*.

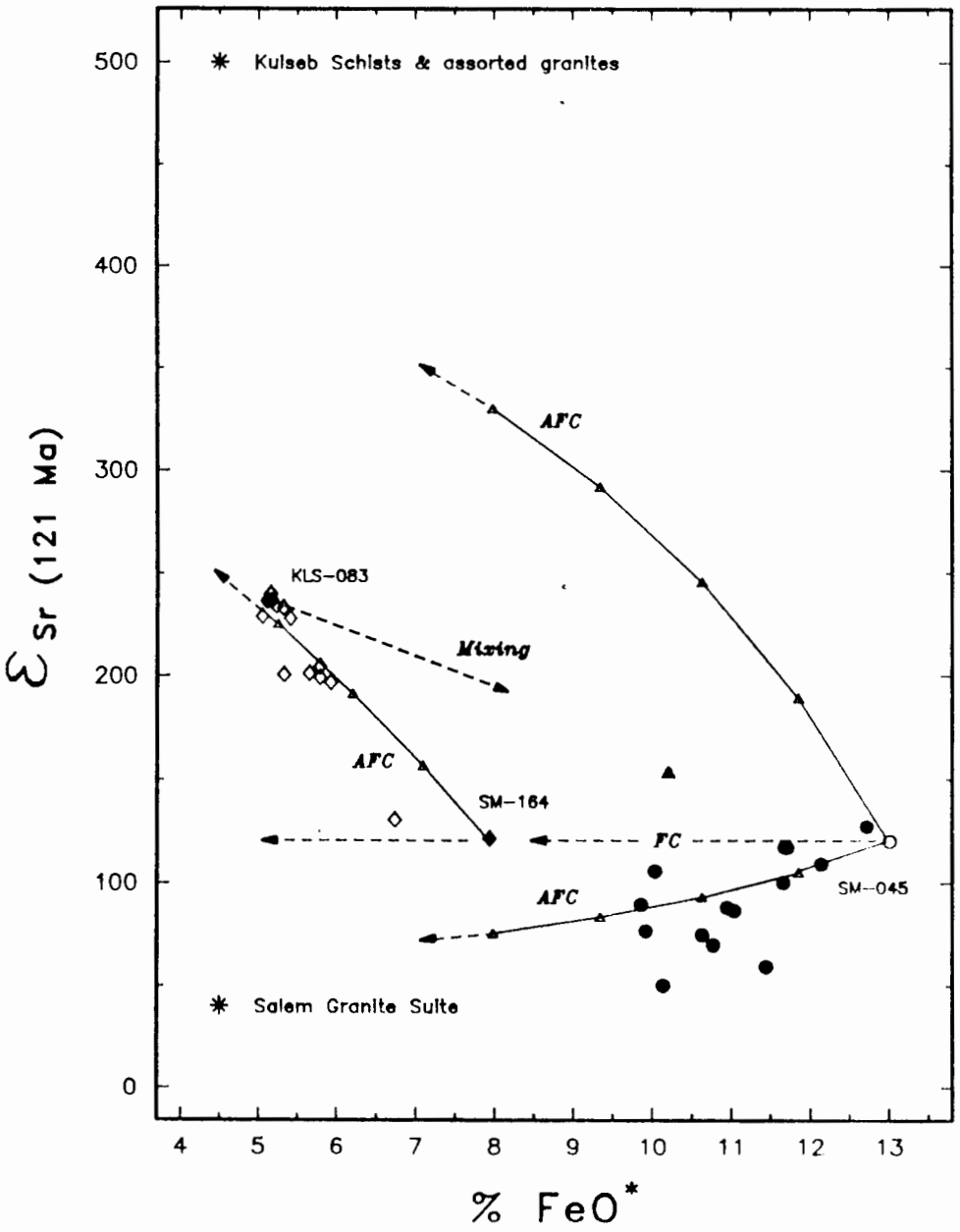

Legend for Figs. 7.1 – 7.6

- ✳ Average Upper Crust (Taylor & McLennan, 1985)
- ◆ Quartz Latite End Members (KLS-083 & SM-164)
- ○ Evolved Basalt Composition (SM-045)
- ◇ Tafelberg and Interbedded Coastal Quartz Latites
- ▲ Tafelberg Latite
- □ Highly Evolved "Basaltic" Lavas
- ● Tafelberg-type Basalts

See text for details of FC and AFC models

In Figs. 7.2 – 7.6 ...
Plots A and C show Stage (II) models
Plots B and D show Stage (III) models

Symbols on model trajectories indicate increments of F:

Stage (II)	AFC	= 0.025 F
	FC	= 0.100 F
Stage (III)	AFC	= 0.025 F
	FC	= 0.025 F

NB $\mathcal{E}_{Sr}$ values of typical Damara rocks have been used in conjunction with Taylor and McLennan's average upper crust to yield the possible assimilant compositions on this diagram.

Fig. 7.2 Plots of TiO_2 and V *vs.* FeO*.

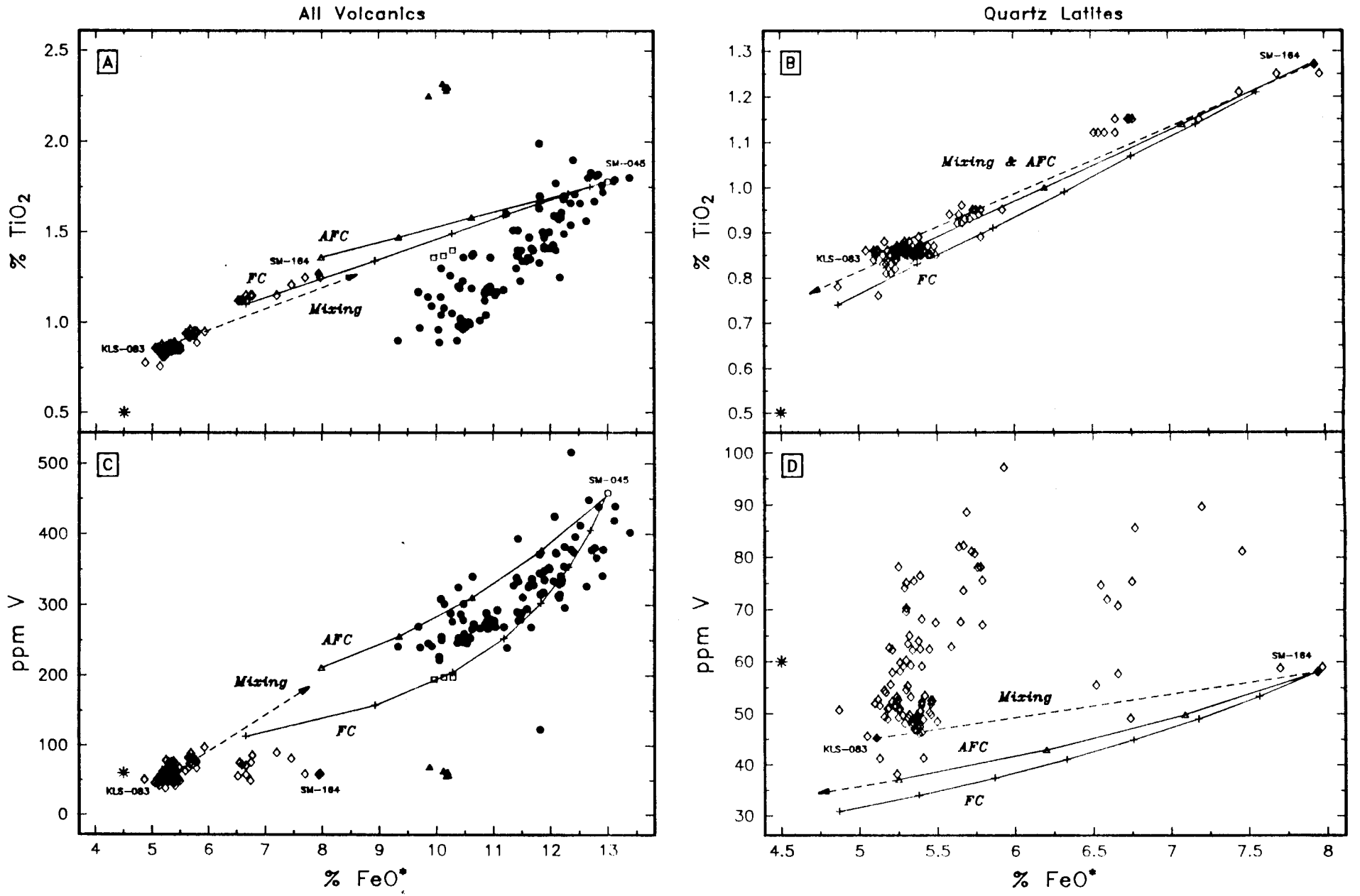

Fig. 7.3 Plots of P_2O_5 and Y *vs.* FeO*.

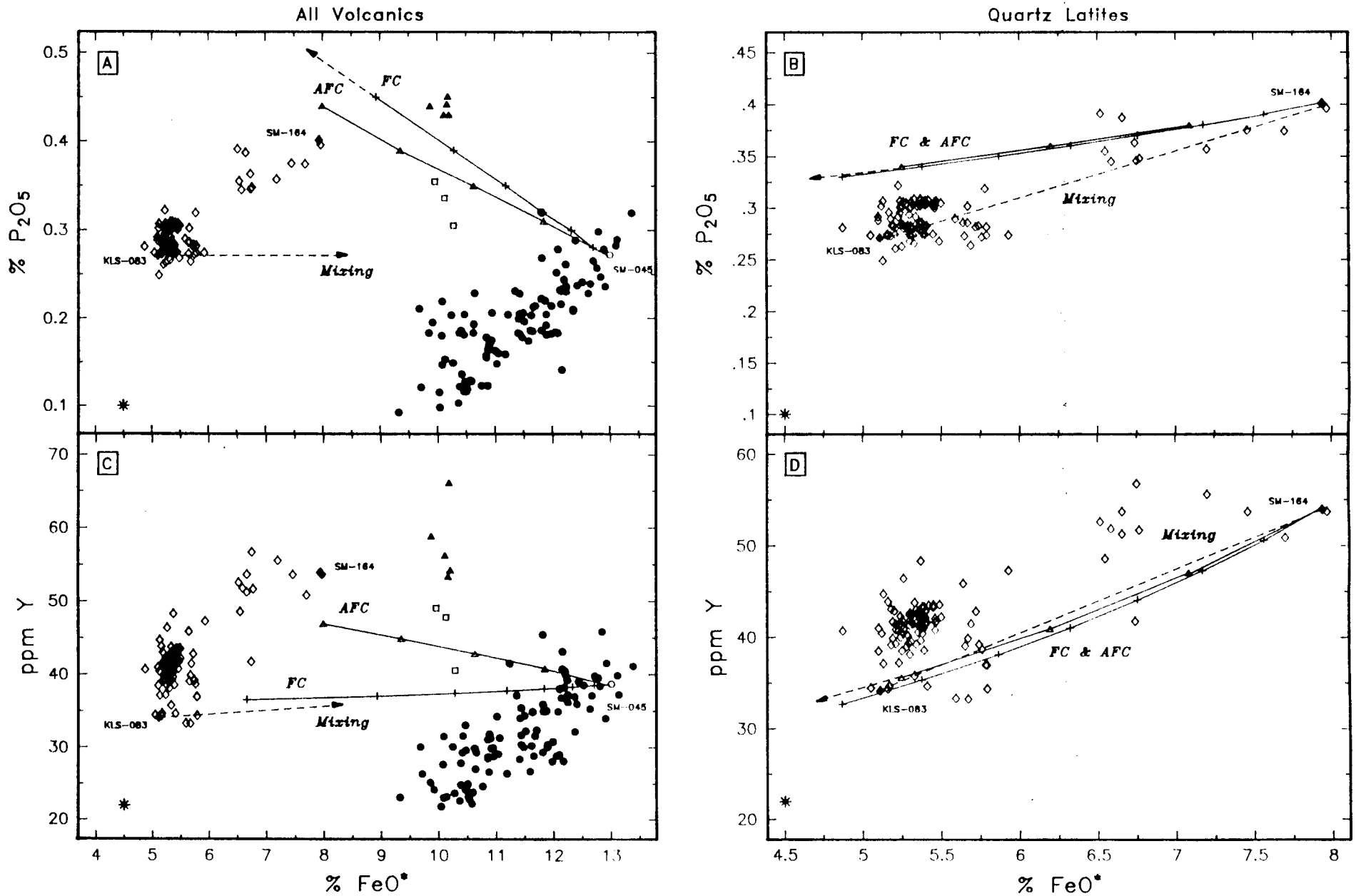

Fig. 7.4 Plots of Zr and Nb *vs.* FeO*.

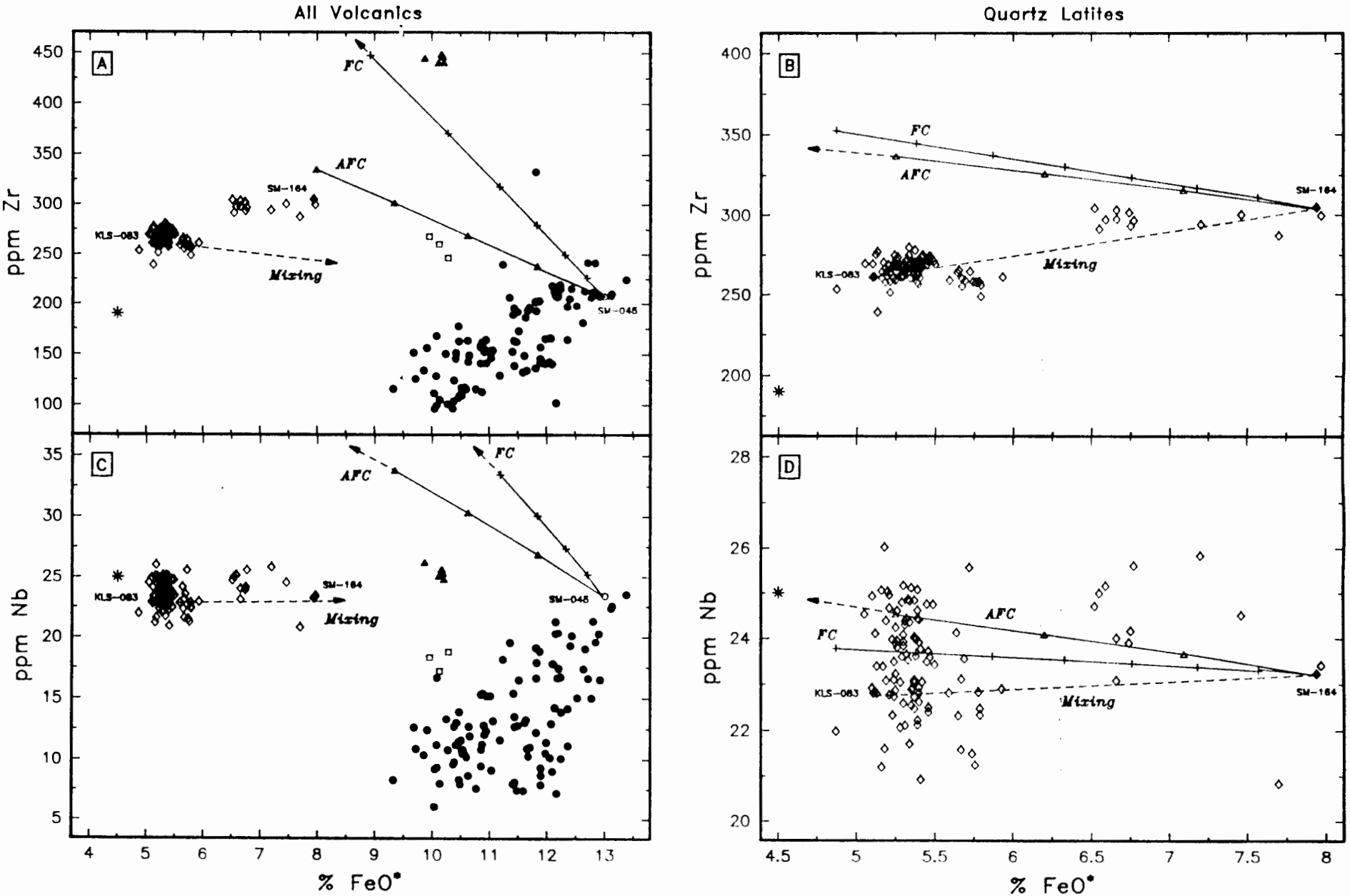

Fig. 7.5 Plots of Ba and Cu *vs.* FeO*.

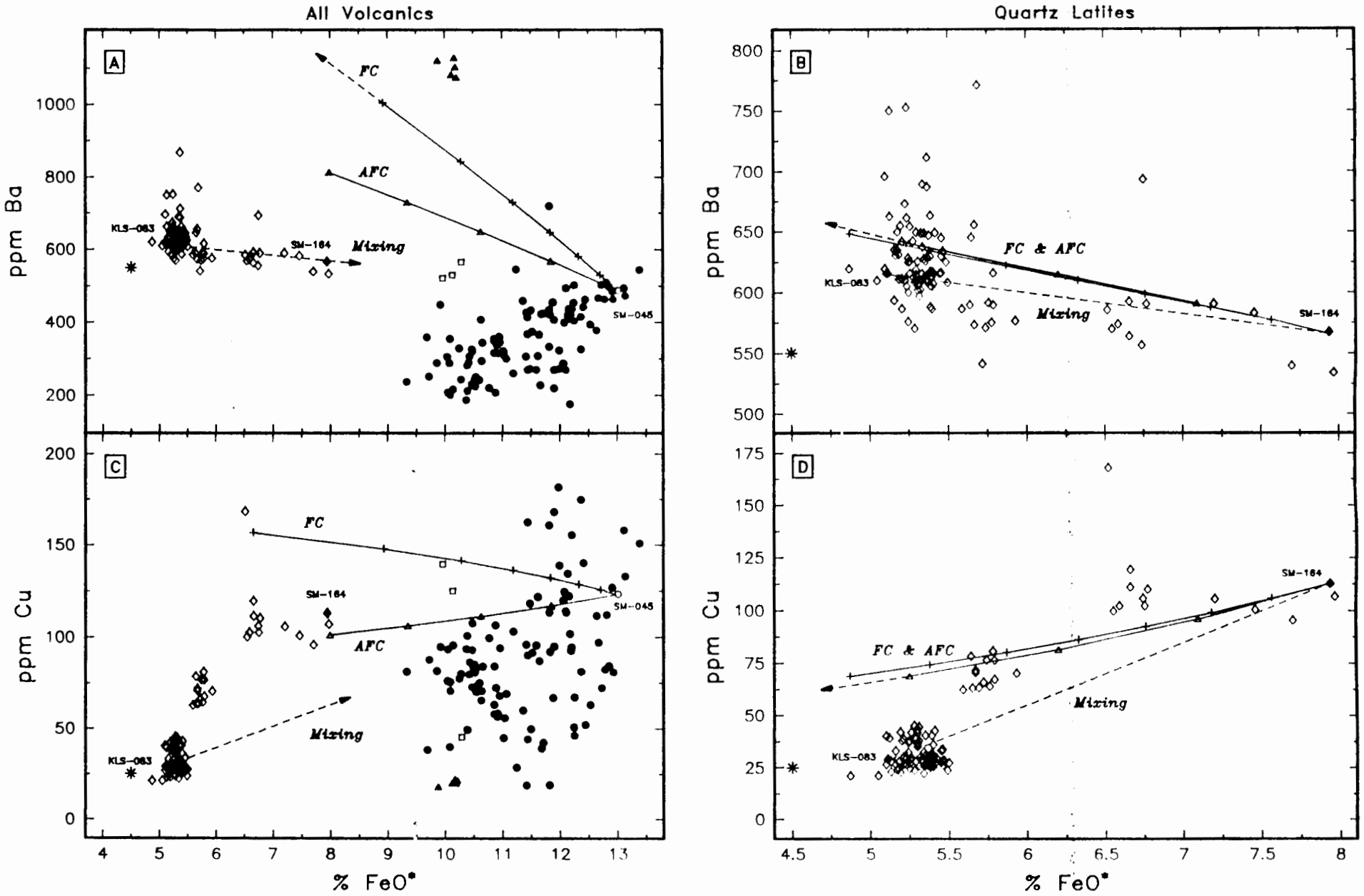

Fig. 7.6 Plots of Rb and Sr *vs.* FeO*.

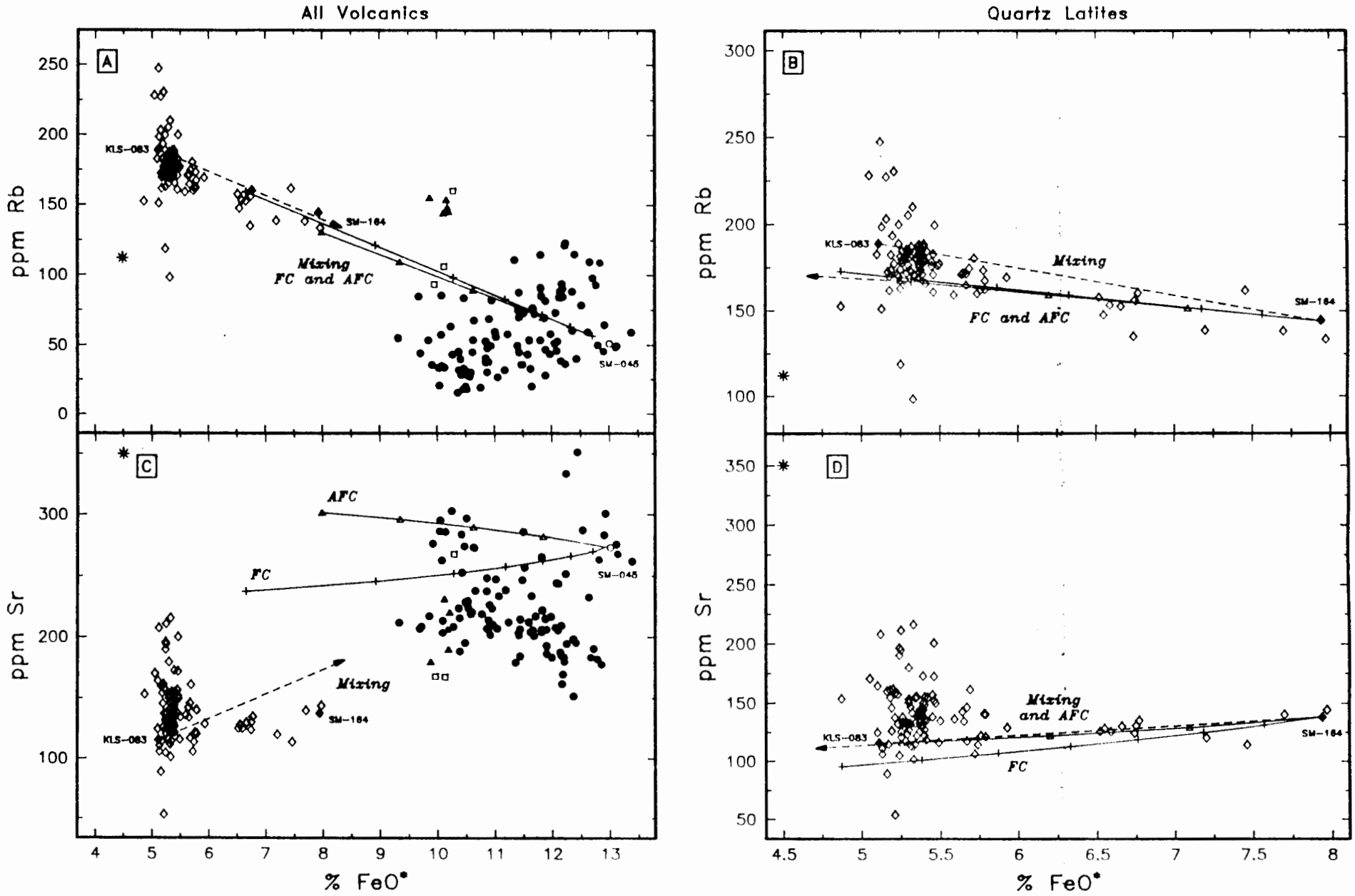

TABLE 7.4

STAGE (II) MAGMATIC MODELS

(a) Least Squares Mixing Solution (GENMIX) for closed system fractional crystallisation model.

	TARGET COMPOSITION (SM-164)			STARTING COMPOSITION (SM-045)	
	Actual	Estimated	Difference	Fractionating Phases	Proportions Wt%
SiO_2	64.78	64.90	0.12	Plagioclase	48.01
TiO_2	1.27	1.26	-0.01	Augite #1	29.08
Al_2O_3	12.71	12.94	0.23	Augite #2	5.46
FeO*	7.94	8.15	0.21	Pigeonite	8.72
MnO	0.10	0.12	0.02	Ti-magnetite	8.38
MgO	1.74	1.92	0.18	Apatite	0.36
CaO	3.19	3.41	0.22		
Na_2O	2.98	3.07	0.09	F-value = 0.36	
K_2O	3.64	4.15	0.51		
P_2O_5	0.40	0.49	0.09		
				Augite N°1 = En_{33}	
Total	98.75	100.39		Augite N°2 = En_{38}	

Residual Sum of Squares = 0.469

(b) Least Squares Mixing Solutions (GENMIX) for Assimilation-Fractional Crystallisation models.

Model (i)

	TARGET COMPOSITION (SM-164)			STARTING COMPOSTION (SM-045)	
	Actual	**Estimated**	**Difference**	**Fractionating Phases**	**Proportions Wt%**
SiO_2	64.78	64.91	0.13	Plagioclase	55.83
TiO_2	1.27	1.37	0.10	Augite #1	10.94
Al_2O_3	12.71	12.84	0.13	Augite #2	19.56
FeO*	7.94	8.11	0.17	Pigeonite	9.37
MnO	0.10	0.06	-0.04	Ti-magnetite	4.31
MgO	1.74	1.90	0.16		
CaO	3.19	3.36	0.17		
Na_2O	2.98	3.27	0.29	**F-value = 0.90**	
K_2O	3.64	3.91	0.27	**r-value (Ma/Mc) = 0.86**	
P_2O_5	0.40	0.44	0.04		
				Assimilant = Average Upper Crust	
Total	98.75	100.16			

Residual Sum of Squares = 0.284

continued...

Table 7.4(b) continued...

Model (ii)

	TARGET COMPOSITION (SM-164)			STARTING COMPOSTION (SM-045)	
	Actual	Estimated	Difference	Fractionating Phases	Proportions Wt%
SiO_2	64.78	64.93	0.15	Plagioclase	59.02
TiO_2	1.27	1.37	0.10	Augite #2	27.93
Al_2O_3	12.71	12.84	0.13	Pigeonite	10.33
FeO*	7.94	8.13	0.19	Ti-magnetite	2.71
MnO	0.10	0.05	-0.05		
MgO	1.74	1.87	0.13		
CaO	3.19	3.37	0.18		
Na_2O	2.98	3.31	0.33	F-value = 1.61	
K_2O	3.64	3.85	0.21	r-value (Ma/Mc) = 1.22	
P_2O_5	0.40	0.39	-0.01		
				Assimilant = Average Upper Crust	
Total	98.75	100.12			

Residual Sum of Squares = 0.292

fractionation is large (~ 65 % crystallisation) quite modest changes in the Kds for various elements may be sufficient to yield satisfactory solutions for these elements. Likewise a slight adjustment of the fractionating assemblage to include slightly more apatite and small amounts of zircon would improve the model for P and Zr. The results obtained when modelling Rb and Ba are important in the evaluation of this model. Both of these elements are incompatible in terms of the fractionating assemblage with bulk D's << 1, resulting in an enrichment of these elements by a factor of 2 - 2.5 relative to SM-045. Whilst this results in a reasonable solution for Rb (Fig. 7.6A) it yields a Ba concentration which is almost twice as much as that observed in SM-164 (Fig. 7.5A), thus providing reasonable grounds for the rejection of this model.

7.4.2.2 Assimilation Fractional Crystallisation.

Differentiation of low-Ti basalt accompanied by crustal contamination is a model proposed by Hawkesworth *et al.* (1987) to account for the genesis of basalt to "rhyolite" compositions of the Paraná Volcanics. Evaluation of a similar model for the Etendeka Volcanics by Erlank *et al.* (1984) indicated that AFC could not reasonably explain the variation within the basaltic suite, let alone account for the generation of quartz latite. In the light of these differences of opinion the role of an AFC process in the generation of the quartz latites from a basaltic precursor is re-evaluated.

Least squares modelling of the major element composition of derivative liquids imposes important constraints on F (the fraction of liquid remaining) and r (mass assimilated/mass crystallised). The values of F and r are, however, sensitive to the composition of the assimilant and to the bulk composition of the fractionating assemblage, the latter can be demonstrated by comparing models (i) and (ii) in Table 7.4b. The main difference between the two models is the addition of a slightly more magnesian augite to the fractionating assemblage in model (i). Although the residual sum of squares for both models is approximately equal, model (i) is more realistic in terms of F and r, as model (ii) requires more assimilation than fractionation (r > 1) with a net increase in the amount of liquid present (F > 1). In simple AFC models the upper limit of r is dependent upon the temperature of the assimilated material and probably varies from 0.3 at 150 °C to about 1.0 at 1000 °C in regions of active volcanism and high heat flow (De Paolo, 1981).

The results of AFC calculations for various trace elements and ϵ_{Sr} using the parameters for model (i) are illustrated in Figs. 7.1 - 7.6 (plots A and C in each case). The failure of this AFC model to account for the evolution of the quartz latites from the evolved basic lava is best illustrated by V, Nb, Ba and Sr. Increasing the Kd values for these elements, in line with those encountered in more evolved rock-types (e.g. 63 - 68 % SiO_2, Table 7.3(b)) in order to reduce their overall enrichment in the melt does not have any marked effect because the degree of fractionation is quite small (10%). The Sr-isotopic evolution of an AFC model is dependent upon the Sr contents and Sr-isotopic characteristics of the assimilant. If one uses Sr-isotopic ratios typical of Damaran upper crustal rocks with AFC model (i) the results are divergent from typical quartz latite values (Fig. 7.1). The roughly equivalent Sr-isotopic ratios of SM-164 and evolved basalt requires the assimilant to have the same isotopic signature.

7.4.3 Stage III models

7.4.3.1 Magma mixing

The mixing of less evolved basaltic magma with quartz latite cannot account for the trends observed in the basaltic suite, particularly in view of the trends displayed by TiO_2 and V *vs.* FeO* (Fig. 7.2) (Erlank *et al.*, 1984). However, it is conceivable that mixing between evolved quartz latite (KLS-083) and a basaltic magma may have generated the KLS-083/SM-164 trend. For many major and trace elements the quartz latite compositional trend lies on, or close to, a mixing line between KLS-083 and evolved basalt (SM-045). However, the variation of ϵ_{Sr} and elements such as V, P, Y, Zr and Cu (Figs. 7.1 - 7.6) is not consistent with such a mixing relationship. Mixing between KLS-083 and latite which might be inferred from data for P and Y in Fig. 7.3 is not consistent with data for Ba and Cu (Fig. 7.5).

Rejection of basaltic or latitic magmas as possible components in a mixing relationship leaves the possibility that the quartz latite trend might be the result of mixing between two quartz latite magma types (SM-164 and KLS-083), or of assimilation of crustal material by SM-164. Although the data for many elements lie quite close to mixing lines between SM-164 and KLS-083, Figs. 7.1 - 7.5 (B and D in each case) illustrate significant scatter from such lines for relatively immobile elements such as P, Y, Zr and Cu. A mixing relationship (not shown) between SM-164 and average upper crust is unsatisfactory for

elements such as Mg, K, Rb, Sr, and Zr. In addition, the contribution of crustal material required to generate KLS-083 from SM-164 would be some 75 - 80 %, which presents significant thermal problems in the assimilation process.

7.4.3.2 Magmatic differentiation processes

Before discussing specific fractional crystallisation and AFC models it is important to point out that serious limitations are placed on such differentiation processes by the mineral chemistry of the quartz latites. The differentiation of a magma whether by fractional crystallisation or AFC should be characterised by a coherent evolution of liquidus phase compositions, with a progression towards more albitic plagioclase and more Fe-rich pyroxenes, such as that observed with the evolution of the Etendeka basaltic lavas (Erlank *et al.*, 1984). Plagioclase phenocrysts in quartz latites from the Tafelberg/Interbedded Coastal succession are increasingly anorthitic in the least mafic quartz latites from the lower part of the succession (Fig. 5.1b). Increasing anorthite content and concomitant iron enrichment in plagioclase (Fig. 5.3) must almost certainly be related to higher temperatures of crystallisation, a feature supported to some extent by pyroxene geothermometry (summarised in section 5.6). Since crystallisation and differentiation of a magma necessarily defines a "down-temperature path" it follows that neither fractional crystallisation nor AFC could be responsible for the apparent "evolution" in the whole rock compositions of the Stage (III) trend.

The possibility that a differentiation process operated in the opposite direction (i.e. from least-mafic to most-mafic) is highly unlikely since fractionation of the observed phase assemblage would drive the liquid composition in the wrong direction. The assimilation of material more basic than the melt is also considered unlikely. The amount of heat required to assimilate basic material would accelerate the crystallisation of plagioclase, pyroxene and titanomagnetite which would tend to maintain the liquid composition rather than make it more mafic. Moreover, unless the assimilation of basic material was wholesale, for instance by the stoping of large blocks of material into the magma chamber, heating of basic material would almost certainly yield minimum melts of similar, or more felsic, composition to the quartz latites.

As the conclusions reached from the mineral chemistry must be regarded as probabilities not certainties, the following two sections will briefly evaluate FC and AFC modelling of the Stage III trend.

7.4.3.3 Fractional crystallisation

Table 7.5a presents a least squares mixing approximation for the major element modelling of this process, with the results of trace element modelling shown in Figs. 7.2 - 7.6 (plots B and D in each case). As noted previously significant latitude in the choice of Kd values (Table 7.3b) for certain elements allows for sufficient flexibility such that a model involving 16 % fractionation can account for the variation shown by many trace elements; although it is readily apparent that the data often show considerable scatter from the model trajectory. Sr-isotopic characteristics (Fig. 7.1) of the various groups of quartz latite which constitute the trend argue strongly against fractional crystallisation.

Although this may be the conclusion for the entire Tafelberg/Interbedded Coastal quartz latite trend it is noteworthy that the Upper Interbedded Coastal quartz latites, which represent approximately half the FeO* variation within this trend, appear to show only small variations in ϵ_{Sr} (121 - 130) therefore allowing the presence of some fractional crystallisation in this sequence. Least squares mixing approximations between samples within this subtrend (Table 7.6a) show that 8 % crystallisation of a plagioclase (43%), pigeonite (40%), Ti-magnetite (17%) and trace apatite assemblage is sufficient for its generation. Note that only two samples from the Upper Interbedded Coastal quartz latite trend have been analysed for Sr-isotopes and additional data are required to substantiate this model.

7.4.3.4 Assimilation Fractional Crystallisation.

The results of least squares major element modelling and the calculated F and r values for this stage are presented in Table 7.5b, and the calculated trajectories for selected trace elements and Sr-isotope compositions illustrated in Figs. 7.1 - 7.6 (B and D in each case). Because of the relatively small degrees of fractionation (~ 8%) and an assimilant composition similar in many respects to KLS-083 the major and trace element solutions are very similar to those obtained for the fractional crystallisation model and similar observations apply. A serious discrepancy in both FC and AFC models occurs for Zr (Fig.7.4b), however the presence of a very small amount of zircon in the fractionating assemblage would be sufficient to prevent the increases in Zr calculated for both models. A notable improvement on the FC model however, is the reasonable approximation of ϵ_{Sr} in the AFC model derivative liquid (ϵ_{Sr} = 230) to the Sr-isotopic composition of KLS-083 (ϵ_{Sr} = 236), see

TABLE 7.5

STAGE (III) MAGMATIC MODELS

(a) Least Squares Mixing Solution (GENMIX) for closed system fractional crystallisation model.

	TARGET COMPOSITION (KLS-083)			STARTING COMPOSITION (SM-164)	
	Actual	Estimated	Difference	Fractionating Phases	Proportions Wt%
SiO_2	68.79	68.82	0.03	Plagioclase N°1	45.71
TiO_2	0.85	0.79	-0.06	Pigeonite	35.76
Al_2O_3	12.74	12.69	-0.05	Ti-magnetite	16.61
FeO*	5.11	5.13	0.02	Apatite	1.72
MnO	0.10	0.01	-0.09		
MgO	1.13	1.02	-0.11		
CaO	2.46	2.41	-0.05		
Na_2O	2.99	3.09	0.10	F-value = 0.84	
K_2O	4.63	4.31	-0.32		
P_2O_5	0.27	0.35	0.07		
Total	99.07	98.60			

Residual Sum of Squares = 0.149

(b) Least Squares Mixing Solution (GENMIX) for Assimilation-Fractional Crystallisation model.

	TARGET COMPOSITION (KLS-083)			STARTING COMPOSTION (SM-164)	
	Actual	Estimated	Difference	Fractionating Phases	Proportions Wt%
SiO_2	68.79	68.81	0.02	Plagioclase N°1	51.46
TiO_2	0.85	0.83	-0.02	Pigeonite	34.38
Al_2O_3	12.74	12.68	-0.06	Ti-magnetite	12.82
FeO*	5.11	5.12	0.01	Apatite	1.34
MnO	0.10	0.00	-0.10		
MgO	1.13	1.06	-0.07		
CaO	2.46	2.40	-0.06		
Na_2O	2.99	3.15	0.16	**F-value = 0.92**	
K_2O	4.63	4.33	-0.30	**r-value (Ma/Mc) = 0.60**	
P_2O_5	0.27	0.34	0.07		
				Assimilant = Average Upper Crust	
Total	99.07	98.73			

Residual Sum of Squares = 0.141

TABLE 7.6

(a) UPPER INTERBEDDED COASTAL QUARTZ LATITE TREND

Least Squares Mixing Solution (GENMIX) for closed system fractional crystallisation model.

	TARGET COMPOSITION (SM-162)			STARTING COMPOSITION (SM-164)	
	Actual	Estimated	Difference	Fractionating Phases	Proportions Wt%
SiO_2	66.54	66.57	0.03	Plagioclase N°2	43.30
TiO_2	1.12	1.05	-0.07	Pigeonite	39.76
Al_2O_3	12.77	12.77	0.00	Ti-magnetite	16.72
FeO*	6.52	6.56	0.04	Apatite	0.22
MnO	0.09	0.06	-0.03		
MgO	1.44	1.36	-0.08		
CaO	2.88	2.88	0.00		
Na_2O	3.12	3.06	-0.06	F-value = 0.92	
K_2O	4.09	3.95	-0.14		
P_2O_5	0.39	0.43	0.04		
Total	98.96	98.68			

Residual Sum of Squares = 0.041

(b) SPRINGBOK QUARTZ LATITE TREND

Least Squares Mixing Solution (GENMIX) for closed system fractional crystallisation model.

	TARGET COMPOSITION (SM-220A)			STARTING COMPOSTION (SM-015)	
	Actual	**Estimated**	**Difference**	**Fractionating Phases**	**Proportions Wt%**
SiO_2	67.07	67.08	0.01	Pigeonite	53.63
TiO_2	0.93	0.90	-0.03	Ti-magnetite	40.54
Al_2O_3	12.97	12.86	-0.11	Apatite	5.83
FeO*	6.04	6.04	0.00		
MgO	1.41	1.33	-0.08		
P_2O_5	0.28	0.26	-0.02		
				F-value = 0.98	
Total	88.70	88.47			

Residual Sum of Squares = 0.019

CaO, Na_2O and K_2O are excluded from this mixing solution since they are affected by post-eruptive alteration.

continued....

Table 7.6(b) continued...

Whole rock and mineral compositions used in this least squares mixing calculation.

	WHOLE ROCK		MINERAL	
	SM-015	SM-220A	Pigeonite	Ti-magnetite
SiO_2	66.38	67.07	51.24	0.10
TiO_2	1.02	0.93	0.32	19.82
Al_2O_3	12.66	12.97	0.78	2.54
FeO	6.72	6.04	26.15	73.49
MnO	0.11	0.10	0.81	0.44
MgO	1.46	1.41	15.60	0.80
CaO	2.95	2.65	5.04	-
Na_2O	2.32	2.66	0.07	-
K_2O	4.52	4.20	-	-
P_2O_5	0.30	0.28	-	-
Total	98.44	98.31	100.01	97.19

The composition of apatite was calculated from its mineral formula.

Fig. 7.1.

7.4.4 Springbok quartz latites

The quartz latites of the Upper and Lower Springbok units exhibit limited compositional variation (see Table 6.6). Typically the Lower Springbok units are characterised by higher concentrations of TiO_2, FeO*, P_2O_5 and Zr, and to a lesser extent Y, Ba, Ce and Nd. Differences in ϵ_{Sr} (Table 6.6) may also be significant although the data are few, consisting of a single determination for a Lower Springbok unit (ϵ_{Sr} = 204) and three determinations for the Upper Springbok unit (ϵ_{Sr} = 214 - 239). Apart from the hypersthene-bearing variant of the Upper Springbok unit these quartz latites are mineralogically indistinguishable from one another.

In broad terms the Springbok quartz latites are compositionally similar to the Tafelberg and Interbedded units, so that arguments regarding their derivation from the basaltic lavas are the same as those discussed for the latter. Least squares mixing approximations (Table 7.6b) indicate that much of the immobile major element variation exhibited by the Springbok quartz latites can be accounted for by very small degrees of fractional crystallisation (1.5 - 2 %) of a pigeonite (54 %), Ti-magnetite (40 %) and apatite (6 %) assemblage (whole rock and mineral compositions given in Table 7.6b). Fractionation of this assemblage is sufficient to account for the small (~ 5 ppm), but consistent, differences in Y, Ce and Nd, and fractionation of trace amounts of zircon could account for the variation in Zr.

7.4.5 Summary

Geochemical modelling of the Stage II trend indicates that the quartz latites of the Tafelberg/Interbedded Coastal succession cannot be related to the evolved basaltic lavas by processes such as magma mixing, FC and AFC. AFC models could account for the Stage III variation trend in the Tafelberg/Interbedded Coastal quartz latites themselves, but a fractional crystallisation model can be rejected on Sr-isotopic grounds. Both FC and AFC models for this variation trend appear to be precluded by mineral composition data, which indicate increased liquidus temperatures in the compositionally more evolved quartz latites.

Trends defined by small variations in the composition of the Springbok and Upper Interbedded Coastal quartz latites show limited variations in ϵ_{Sr}, and such trends can be accounted for by small degrees of fractional crystallisation. Note that magmatic differentiation within individual groups of quartz latites does not suffer the mineralogical constraints encountered when modelling between different groups.

The ability to distinguish accurately between different groups of quartz latite which make up the Tafelberg and Interbedded Coastal succession (Milner and Duncan, 1987) indicates a clustering of compositions rather than smooth trends expected from mixing or differentiation processes. This feature, coupled with the mineral composition data and the inadequacy of the main FC and AFC models tested above, suggests that the overall composition of the quartz latites and the variations they show are controlled to a large extent by characteristics of the source, e.g. the source composition, its mineralogy, and the degree of melting (discussed in Section 7.7).

7.5 SARUSAS QUARTZ LATITES AND LATITES

The Sarusas acid rocks have been divided into three main groups on the basis of their whole rock composition (Subsection 6.5.2) and in this section a brief discussion of the magmatic processes which might relate them is presented. Detailed investigations to see whether the Sarusas acid volcanics can be related to the "enriched" Khumib-type basalts by magmatic differentiation (FC or AFC) have not been made, as such relationships are considered unlikely. The degree of differentiation shown by the basalts is much smaller than that shown by the Tafelberg-type basalts and consequently the compositional gap between the basalts and the latites and quartz latites is significantly greater and more clearly defined than it is in the southern Etendeka (e.g. Fig. 6.1).

Inconsistent major and trace element enrichment trends between the basalts and the latites also rule out models relating them by magmatic differentiation. The concentration of Al_2O_3 and Sr in the basalts and latites are roughly equivalent whilst the CaO concentration in the latter is significantly lower. In order to reconcile these variations by magmatic differentiation the fractionating assemblage would have to be dominated by clinopyroxene rather than plagioclase. This is considered highly unlikely because modelling of the

variation within the basaltic suite (Duncan *et al.*, in prep.) implies the fractionation of plagioclase and clinopyroxene in approximately equal proportions, together with minor olivine. Furthermore, plagioclase is the dominant phenocryst phase in the latites (Table 3.1, KLS-311 and KLS-327). Similar arguments involving a relationship between the basalts and quartz latites can also be made. For example, lower concentrations of P_2O_5 in the quartz latites (0.22 - 0.39 %) relative to the basalts (0.35 - 0.68 %) would infer apatite fractionation. This is commonly accompanied by Y depletion as the Kd for Y in apatite is high (~185). However, the concentration of Y in the quartz latites (52 - 62 ppm) is considerably higher than it is in the Khumib basalts (30 - 46 ppm).

The latites and b-type quartz latites have similar isotopic characteristics (ϵ_{Sr} = 22 - 45 and 20 - 50 respectively) and show trends in plagioclase and pyroxene compositions (Figs. 5.1c and 5.4b) which are consistent with fractional crystallisation or AFC from latite to quartz latite, providing the assimilant has a similar ϵ_{Sr}. However, such processes can be ruled out on the basis of inconsistent enrichment and depletion patterns shown by both major and trace elements. Some of these inconsistencies are summarised below:

(1) Ba is depleted in the quartz latites relative to the latite (Fig. 6.3). It is impossible to decrease Ba concentrations by fractionating the observed latite phase assemblage of plagioclase, augite, pigeonite, titanomagnetite and ilmenite. There is no evidence for the crystallisation of alkali-feldspar.

(2) K and Rb should be significantly increased in concentration by fractionation of the liquidus phases present (Table 6.7 analyses 3 and 4). This is not observed and the concentrations of these elements in both latites and b-type quartz latites are roughly equivalent; with the exception of much lower K_2O in three samples of hydrated quartz latite pitchstone.

(3) Cr is enriched in the quartz latites (up to 14 ppm) compared to the latites (< 2.5 ppm). Unless fractionation is accompanied by assimilation of Cr-bearing material the crystallisation of ferro-magnesian and Fe-Ti oxide minerals should cause the Cr contents to decrease.

(4) Lower concentrations of P_2O_5 in the quartz latites would also infer apatite fractionation if they are derived from the latite. However, the quartz latites show enrichments in Y which are greater than those observed

for more incompatible elements such as Rb, Ba and Th (Table 6.7).

The a-type quartz latites, which have the least mafic bulk compositions (Table 6.7, compare analyses 1 and 2 with analysis 3), have plagioclase and augite compositions which are distinctly more mafic than those of the b-type quartz latites and latites (Figs. 5.1c and 5.4b) indicating that they had higher temperatures of crystallisation than the latter. Limited data on the composition of titanomagnetite in these quartz latites show that it is relatively ulvospinel-poor (Usp_{40}) compared to the other acid volcanics (Usp_{60-70}), indicating crystallisation under conditions of higher fO_2. Note that the a-type quartz latites show features in common with the Lower Tafelberg and Lower Interbedded Coastal quartz latites. It is considered highly unlikely that the a-type quartz latites are related to the other Sarusas acid volcanics by magmatic differentiation. This conclusion is supported by major and trace element data, and by higher ϵ_{Sr} values (Table 6.7 and Figs. 6.3 and 6.4). For example, the Ba concentration in the a-type quartz latites is considerably less than it is in the b-type quartz latites. Again it is not possible to decrease the Ba concentration by fractionating the observed b-type quartz latite phase assemblage and there is no evidence for the crystallisation of alkali-feldspar.

The trends observed within the Sarusas felsic volcanics cannot be generated by simple mixing with either one another or with the basaltic lavas. It is suggested that like the quartz latites of the southern Etendeka the different groups within the Sarusas acid suite are unrelated by processes of magmatic differentiation and mixing, and that they probably represent different batches of magma whose compositions are controlled by the composition and degree of melting of the source.

7.6 DERIVATION OF QUARTZ LATITE BY ANATEXIS

7.6.1 Introduction

While different isotopic and trace element characteristics of the southern Etendeka and Sarusas quartz latites argue strongly for different source compositions, very similar major element compositions (Tables 6.6 and 6.7) and their close relationship in space and time strongly suggest that they were generated by a similar process. The Sr-, Pb- and O-isotopic characteristics of

the southern Etendeka quartz latites (Erlank *et al.*, 1984 and Erlank, data unpublished) show that they are clearly crustal in origin. However, the low ϵ_{Sr}, low $\delta^{18}O$ (6‰ for mineral separates, Harris *et al.*, 1988) and trace element enriched character of the Sarusas latites and b-type quartz latites (Table 6.7) suggest that they may be closely linked to the "enriched" Khumib basalts in some way. Cleverly *et al.* (1984) proposed that the partial melting of underplated basaltic material could have provided a source for some of the Lebombo rhyolites and this model may also be applicable to the northern Etendeka. This section discusses the generation of the southern Etendeka quartz latites from typical crustal compositions and investigates the possibility that the Sarusas quartz latites were derived by the partial melting of underplated Khumib basalt. Modelling of the southern Etendeka quartz latites in this section makes use of the theoretical quartz latite composition presented in Chapter 6, as it is the best available estimate of the composition of a typical quartz latite magma. In broad terms the quartz latites can be regarded as being essentially granodioritic in composition.

7.6.2 Crustal melting

Wyllie (1977) indicated that considerable variations of Na/K/Si ratios are possible in H_2O-undersaturated liquids generated at crustal temperatures and pressures. At low pressures the first liquids resulting from the anatexis of crustal materials are granitic in composition, only becoming more granodioritic as the temperature and degree of partial melting increases. At higher pressures however, the first liquids produced are generally more granodioritic in composition (Wyllie, 1977). In order to melt the mafic mineral components essential to the composition of these liquids temperatures of up to 1100°C are required, even with a fairly "generous" allowance of 2 wt% dissolved H_2O (Wyllie, 1977). Two important conclusions from the present study are that the quartz latites represent hot (1000 - 1100°C), relatively dry (< 1 wt% volatiles) liquids. Fig. 7.7 presents the CIPW norm of the theoretical quartz latite composition and shows its position in terms of the dry Qz-Ab-Or system. The quartz latite composition plots above the 10 kb liquidus surface and towards a more Or-rich composition than the minimum for the pure system at this pressure. However, the studies of Winkler *et al.*, (1975) and (1977) have shown that in low-temperature, H_2O-saturated Qz-Ab-Or-An systems the isobaric cotectic moves towards more Or-rich compositions with increasing An content.

Fig. 7.7 Effect of pressure on the liquidus field boundaries in the system Qz–Ab–Or (H_2O) after Wyllie, 1977.

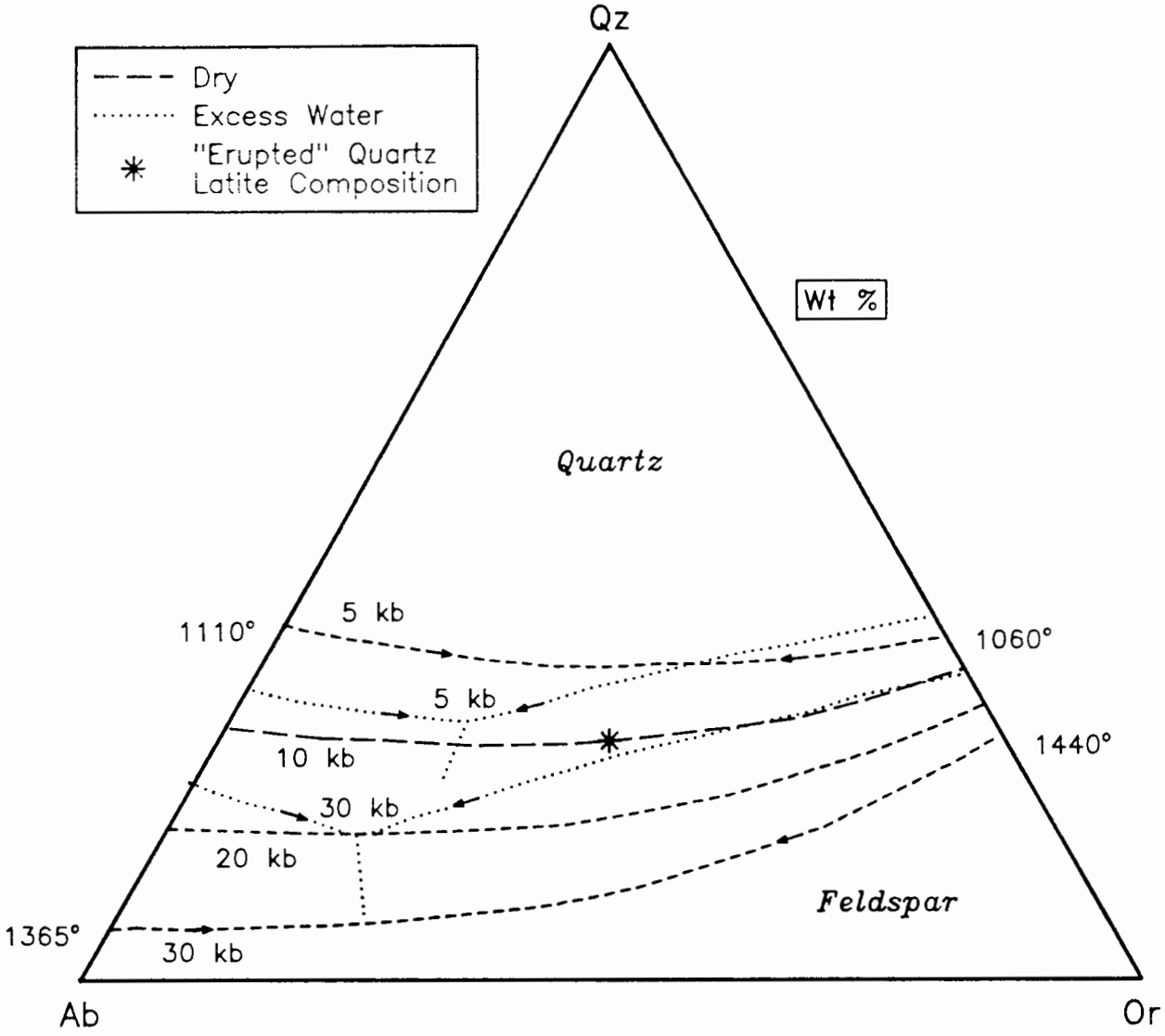

The "erupted" quartz latite composition represents an estimate of the Lower Tafelberg/Lower Interbedded Coastal quartz latite compositions prior to alteration (see Chapter 6). The normative mineralogy is given below:

CIPW norm (wt %)		Qz–Ab–Or	
Qz	19.40	Qz	25.64
Or	28.01	Ab	37.35
Ab	28.26	Or	37.01
An	6.26		
Di	7.38		100.00
Hy	7.42		
Ilm	1.61		
Ap	0.69		

Assuming that increasing the An contents in a high-temperature, H_2O-undersaturated system has a similar effect, the 6 wt% normative An in quartz latite is probably sufficient to displace its composition from the pure Qz-Ab-Or minimum. Note that the experimentally determined temperatures in the dry Qz-Ab-Or system are comparable to the liquidus temperatures envisaged for quartz latite. These experimental studies indicate that the maximum pressure of quartz latite generation is 8 - 10 kb and that at these pressures such a liquid would be a first generated, or minimum composition. At lower pressures the generation of quartz latite magma requires much higher degrees of partial melting, with melting initially producing liquids of granitic composition.

7.6.3 Southern Etendeka quartz latites

If the quartz latites were generated in a single-stage melting process what constraints can be placed on the source composition and mineralogy using minor and trace elements? Assuming that the melt is in equilibrium with the residual mineral phases until separation of the melt and residue (i.e. batch or equilibrium melting), the concentration of a trace element in the melt relative to its concentration in the source (C_l/C_o), for a particular weight fraction of melt (F), is given by:

$$C_l/C_o = 1 / [D (1 - F) + F] \quad .. (1)$$

Where D is the bulk mineral/melt distribution coefficient for the minerals in the residue at the time of removal of the melt:

$$D = \Sigma(Kd.X) \quad .. (2)$$

Where Kd is the distribution coefficient for an element in a mineral and X the proportion of that mineral in the residue.

Figs. 7.8 and 7.9 show trace element and REE patterns for various quartz latite samples and group averages normalised to average compositions of the bulk and lower crust (Taylor and McLennan, 1985) which are regarded as possible source compositions. Also plotted in the REE diagrams is the Tafelberg latite for comparison. Such diagrams illustrate the enrichment and depletion of certain elements relative to concentrations in a putative source. The maximum amount of quartz latite which can be generated from these source compositions

Fig. 7.8 Southern Etendeka quartz latite data normalised against bulk crust.

Bulk crust and chondrite values from Taylor and McLennan (1985)

·····■····· = average values for an 18–24 % partial melt extract from bulk crust

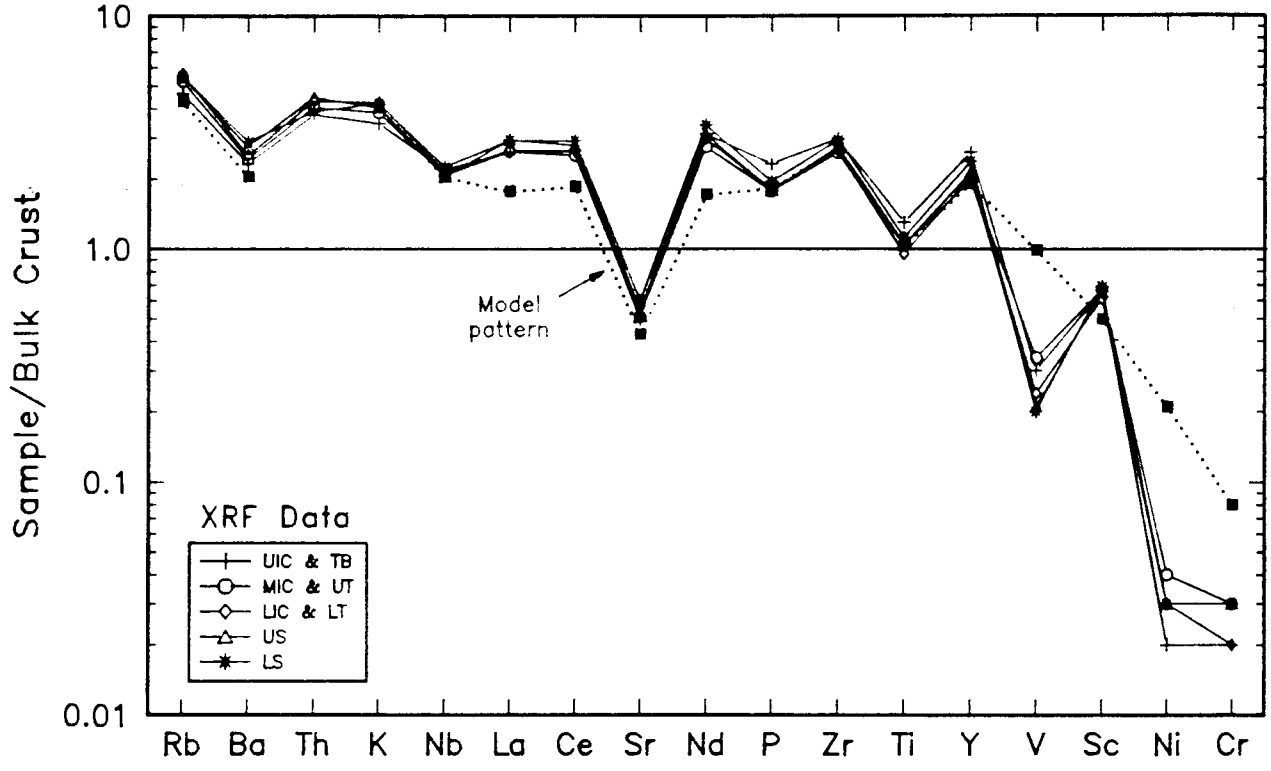

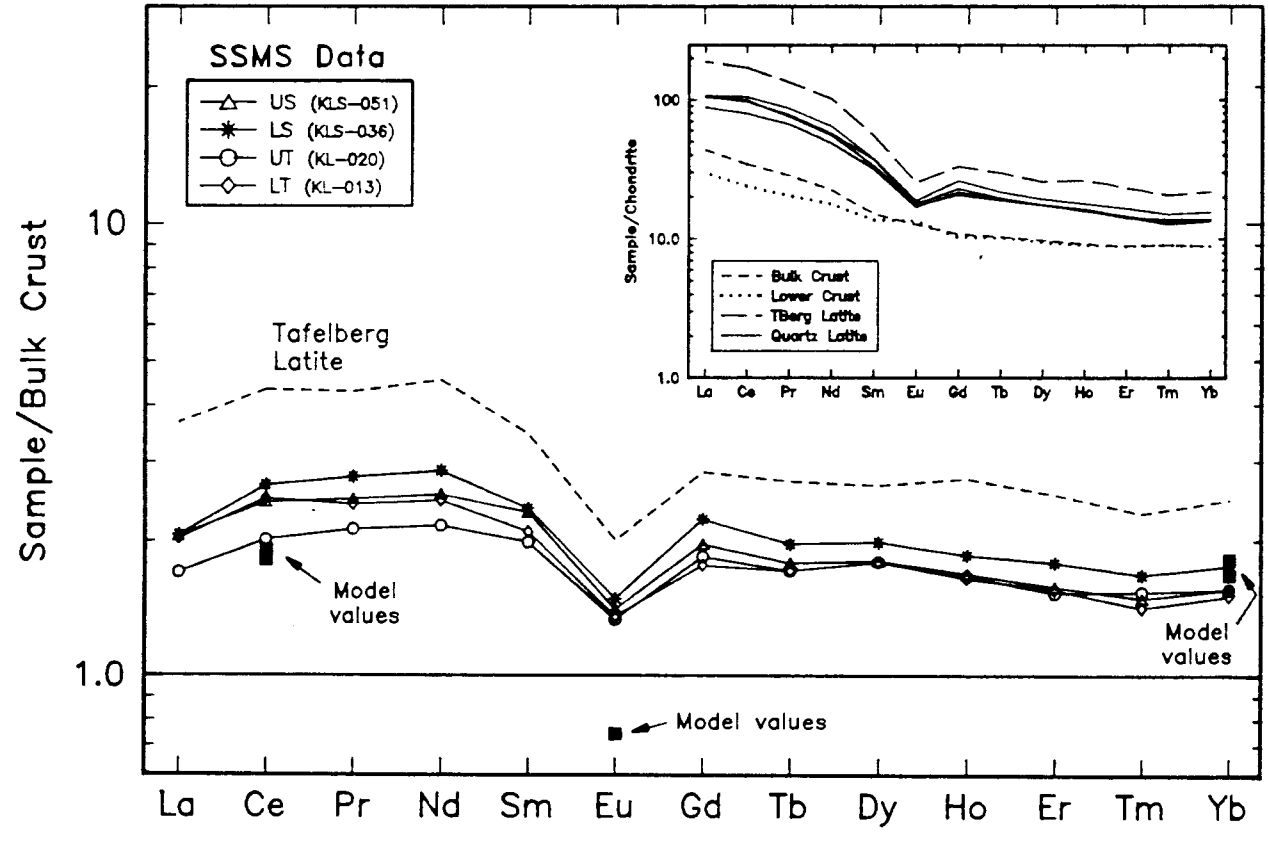

Fig. 7.9 Southern Etendeka quartz latite data normalised against lower crust.

Lower crust and chondrite values from Taylor and McLennan (1985)

···■··· = average values for a 3.3–7.0 % partial melt extract from lower crust

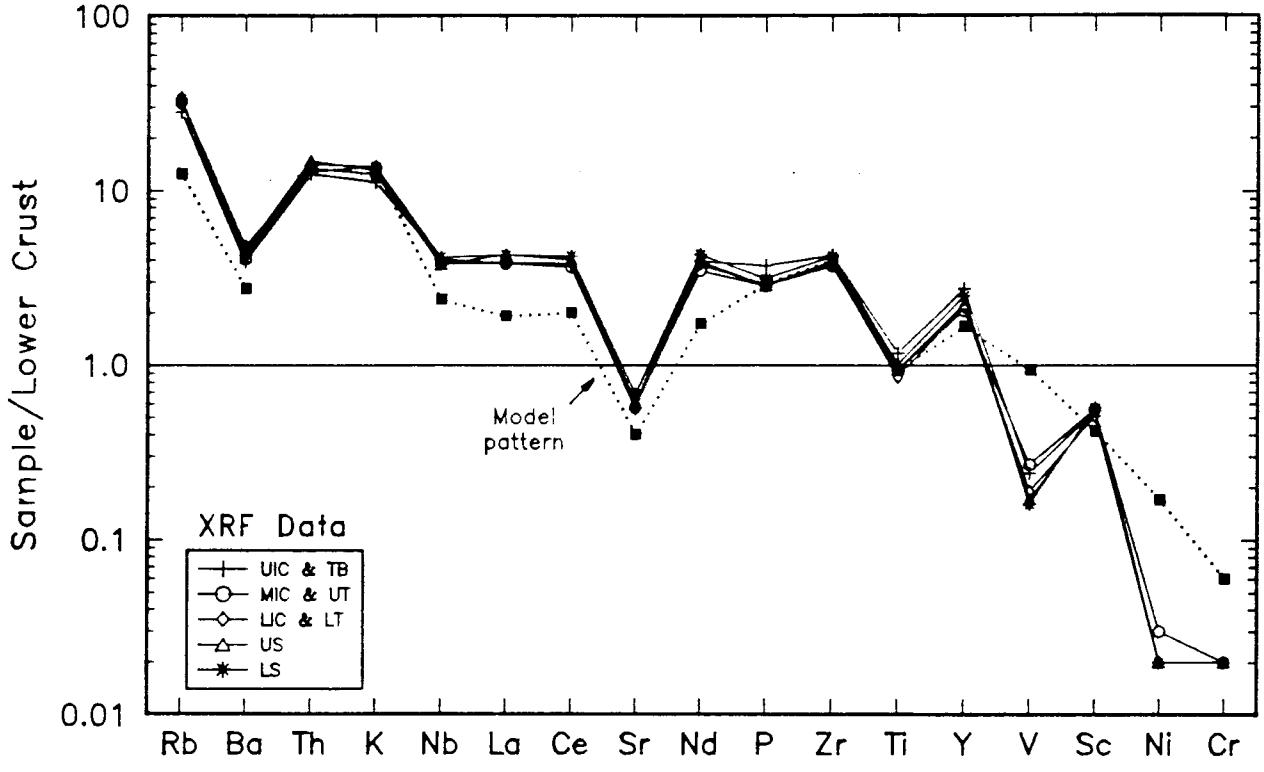

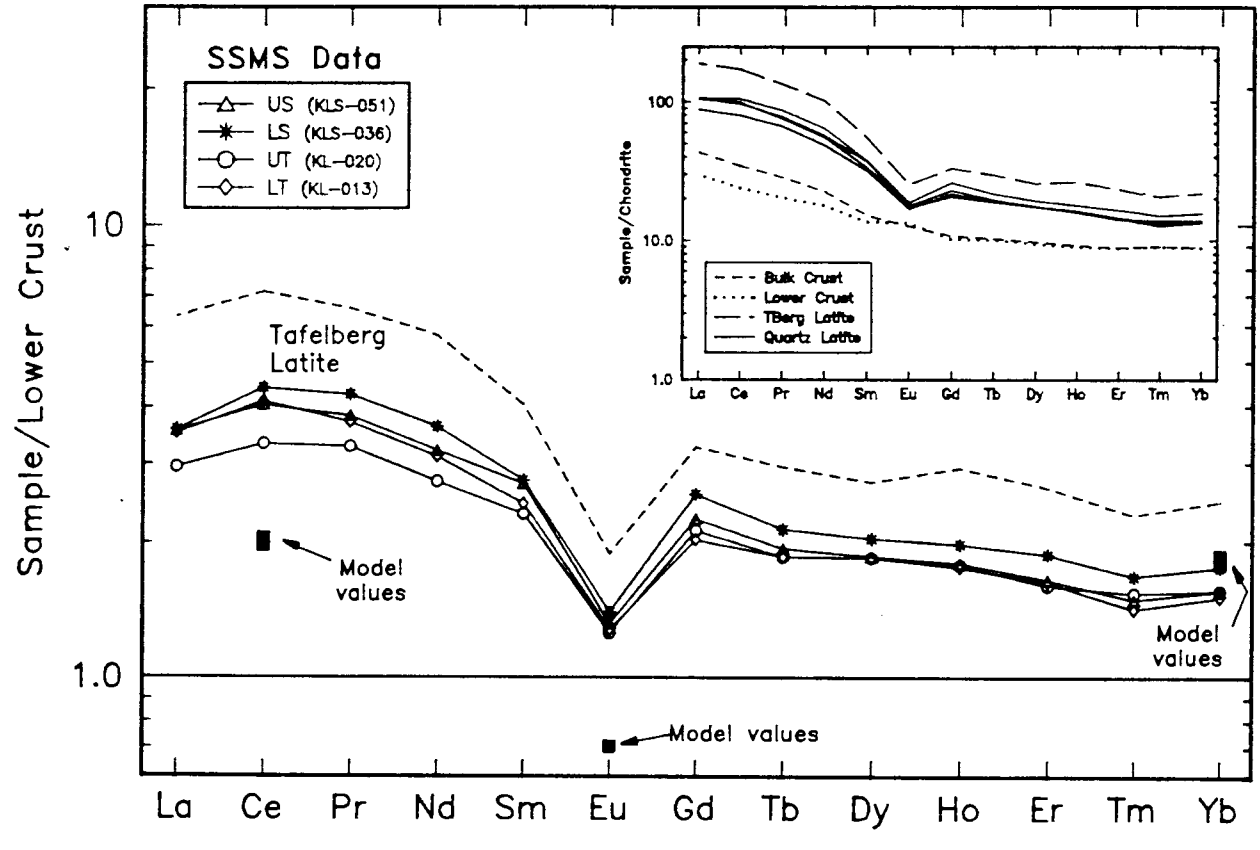

can be estimated as the point at which all the K_2O enters the melt. Similarly the minimum degree of partial melting can be estimated by assuming that Rb is a completely incompatible element (D = 0); because from equation (1) as D approaches zero then C_l/C_o approaches 1/F, thus giving a minimum measure of F (amount of melting) for the assumed source Rb concentration. Using this approach the amount of melting required to generate quartz latite from these compositions can be bracketed at 18 - 24 % for the bulk crustal composition and 3 - 7 % for the lower crustal composition. For most elements D is greater than zero and in order to calculate this parameter and the concentration of an element in the melt it is necessary to know the types and proportions of minerals in both the starting material and the restite. This information can be estimated using a least squares mixing approximation (after Bryan *et al.*, 1969) to calculate a melting mode, which is the proportion of source minerals which constitute the melt composition. The melting mode is subtracted from the source mineralogy to yield the restite:

$$Restite_i = [Source_i - (F * Melt_i)] / 1 - F \quad .. (3)$$

where: i = mineral phase

Table 7.7 shows the restite mineralogy calculated for the range of melting conditions envisaged for each source composition for an anhydrous Qz-Or-Ab-An-Opx-Cpx-Ilm-Ap assemblage. Because minerals such as pyroxenes partition Fe and Mg between the melt and the restite during melting an allowance must be made for this in the mixing model (Cox *et al.*, 1984). This has been done by adding FeO and MgO together in the quartz latite composition and in the putative source minerals. Initially this was the only simplifying assumption made regarding the differential partitioning of major elements between melt and residue, and plagioclase was assumed to melt stoichiometrically as the studies of Johannes (1983) indicate; i.e. that "metastable" or non-equilibrium melting of plagioclase results from kinetic restraints on the reaction. However, this approach resulted in poor mixing solutions for Na_2O, Al_2O_3 and SiO_2 and plagioclase was subsequently treated as individual mineral components, Ab and An. An additional assumption that small amounts of Or occur as discrete K-feldspar, rather than existing in solid solution with plagioclase also makes the modelling exercise easier. Although this affects the bulk D for elements such as Ba, which has a much higher Kd in K-feldspar than in plagioclase (see

TABLE 7.7

Restite compositions generated by extracting varying amounts of the melting mode from putative source compositions.

(a) Bulk Crust (Weight %)

Chemical Composition		Phases	Source Norm	Melting Mode	Restite ~ 18% melting	Restite ~ 23% melting
SiO_2	57.2	Quartz	6.13	18.38	3.44	2.47
TiO_2	0.9	K-Feldspar	6.50	28.22	1.73	0.01
Al_2O_3	15.9	Albite	26.26	28.42	25.79	25.61
FeO	9.1	Anorthite	26.50	6.41	30.61	32.18
MgO	5.3	Opx (En 50)	24.73	7.60	28.49	29.85
CaO	7.4	Cpx (Di 50)	8.18	8.68	8.07	8.03
Na_2O	3.1	Ilmenite	1.71	1.62	1.73	1.74
K_2O	1.1	Apatite	0.23	0.68	0.13	0.10
P_2O_5	0.1					
		Restite plagioclase composition Mole %			An 53	An 54

(b) Lower Crust (Weight %)

Chemical Composition		Phases	Source Norm	Melting Mode	Restite ~ 3.3% melting	Restite ~ 7% melting
SiO_2	54.3	Quartz	3.74	18.38	3.24	2.64
TiO_2	1.0	K-Feldspar	2.00	28.22	1.10	0.03
Al_2O_3	16.1	Albite	23.76	28.42	23.60	23.41
FeO	10.6	Anorthite	30.23	6.41	31.05	32.02
MgO	6.3	Opx (En 50)	28.89	7.60	29.62	30.49
CaO	8.5	Cpx (Di 50)	9.25	8.68	9.27	9.29
Na_2O	2.8	Ilmenite	1.90	1.62	1.91	1.92
K_2O	0.34	Apatite	0.23	0.68	0.21	0.20
P_2O_5	0.1					
		Restite plagioclase composition Mole %			An 55	An 57

Source compositions for the Bulk and Lower crust are from Taylor and McLennan (1985), with a nominal 0.1 % P_2O_5 added to each composition.

Table 7.3b), the amount of K-feldspar present is insignificant in terms of the overall D. The plagioclase compositions of the calculated restites in Table 7.7 range from An_{53} to An_{57}. Comparison of these values with those for phenocrysts in the quartz latites (Fig. 5.1) is encouraging because under equilibrium conditions initial crystallisation of the melt should yield phase compositions equivalent to that of the restite. Note that if the K-bearing phase in the source rock was biotite rather than K-feldspar, this would not greatly affect the melt composition because as temperature rises and dehydration occurs, biotite reacts with quartz and plagioclase to yield K-feldspar (which melts) and orthopyroxene (± garnet and corderite) (Clemens and Vielzeuf, 1987), thus generating the same restite as the anhydrous assemblage. Table 7.8a presents the bulk D's of selected trace elements calculated for the restite assemblages in Table 7.7, and Table 7.8b compares typical trace element concentrations observed in quartz latite with those calculated using equation (1) for melts in equilibrium with restite at various degrees of partial melting. The calculated trace element patterns for the melts from each source composition are compared with the observed quartz latite trace elements patterns in Figs. 7.8 and 7.9. On balance, melting the bulk crustal composition to generate quartz latite provides a better solution than using that of the lower crust, as demonstrated by Ba, Sr, Nb and REEs. Elements such as Ni and Cr are difficult to model because of the their large, poorly constrained, Kds for orthopyroxene and clinopyroxene. An important feature indicated by this modelling is that the quartz latites have a significantly smaller Eu anomaly than expected from calculation. The calculated anomaly cannot be reduced sufficiently by choosing more favorable Kd values or by changing the likely restite mineralogy; for example, a hydrated restite containing amphibole would only exacerbate the problem, as the Kds for Sr and Eu in amphibole are larger than for pyroxene. Furthermore, processes such as fractional crystallisation involving plagioclase, acting upon the melt subsequent to its removal from the restite would further increase the anomaly. Thus it appears likely that the quartz latite source is characterised by a positive Eu anomaly which largely offsets the calculated anomaly; such a feature may have been inherited from an earlier partial melting event.

The strong similarity of the trace element patterns of the main groups of quartz latite from the southern Etendeka (e.g. Fig.7.8) suggest that they were generated from very similar source materials with similar degrees of partial melting. The LREE depleted nature of the Upper Tafelberg sample (KL-020) and

TABLE 7.8

Bulk D and trace element concentration data calculated for models involving the extraction of varying amounts melt from average compositions of the bulk and lower crust.

(a) Restite/Liquid Bulk distribution coefficients

	BULK CRUST		LOWER CRUST	
	18% melting	23% melting	3.3% melting	7.0% melting
Rb	0.04	0.03	0.04	0.03
Ba	0.42	0.30	0.37	0.29
Nb	0.36	0.36	0.39	0.39
La	0.46	0.45	0.50	0.50
Ce	0.42	0.42	0.47	0.47
Sr	2.67	2.61	2.60	2.56
Nd	0.48	0.47	0.56	0.56
Zr	0.21	0.21	0.21	0.21
Y	0.43	0.38	0.59	0.57
V	1.00	1.02	1.06	1.07
Sc	2.24	2.30	2.42	2.46
Cr	15.77	16.31	16.77	17.14
Ni	5.62	5.82	5.88	6.01
Eu	1.44	1.45	1.45	1.45
Yb	0.47	0.48	0.52	0.53

(b) Trace element concentrations in the melt (ppm).

	BULK CRUST		LOWER CRUST		
	18% melting	23% melting	3.3% melting	7.0% melting	Average Quartz latite
Rb	149	127	76.0	56.1	183
Ba	478	543	384	441	630
Nb	23.1	21.7	14.6	13.9	23.6
La	28.8	27.6	21.3	20.6	42.6
Ce	62.7	59.7	46.9	45.1	87.4
Sr	109	117	90.0	94.0	135
Nd	27.8	27.0	22.2	21.6	47.7
Zr	286	257	299	263	267
Y	38.0	38.4	31.7	31.7	41.0
V	228	225	270	268	54.4
Sc	15.0	15.0	15.1	15.1	18.1
Cr	15.8	15.8	14.0	14.0	4.5
Ni	22.0	22.0	23.0	24.0	2.6
Eu	0.81	0.81	0.82	0.82	(1.48)
Yb	3.98	3.67	4.10	3.92	(3.30)

Average quartz latite values are for the Lower Tafelberg - Lower Interbedded Coastal quartz latite group (Table 6.5); values in parentheses are for sample KL-013 (Erlank *et al.*, 1984) which is the only Lower Tafelberg quartz latite sample for which Eu and Yb data are available.

the slightly incompatible trace element depleted patterns of the Upper Interbedded Coastal and Beacon Tafelberg group, coupled with their less evolved major element compositions, suggest that they have been generated by slightly higher degrees of partial melting. The largely uniform compositions of the southern Etendeka quartz latites suggests that they represent "minimum" compositions generated by melting at relatively high pressures. Assuming the sufficient heat is available the amount of melt produced depends on the source composition. From the fairly simplistic trace element modelling outlined above an 18 - 24 % partial melt of an intermediate (bulk) crustal composition produces more favorable results than smaller degrees of melting of a more basic crustal composition. It is interesting to note that the isobaric T-X_{H2O} rock-H_2O diagrams of Wyllie (1977) indicate that a tonalitic source composition (similar to bulk crust) at 10 kb with < 1 wt% H_2O yields approximately 20 % melt at between 1000 and 1100 °C. Furthermore, it is thought that between 20 - 35 % melting is required for the efficient segregation of melt, and its ascent, from the restite (Clemens and Vielzeuf, 1987). Geophysical data from northern and central Namibia (Van Zijl and De Beer, 1983; and Green, 1983) indicate that the thickness of the continental crust in this region at the present time is 36 - 55 km (average ~ 40 km). Pressures of 8 - 10 kb (30 - 35 km) envisaged for the generation of quartz latite as a minimum melt places the source region for these rocks at the base of, or within the lower portion of the crust. Melting is probably induced by the ponding of hot basaltic magma at these levels due to a contrast in density with the overlying crust. Basement rocks of Damara age can be largely rejected as possible source rocks on isotopic and compositional (too felsic) grounds. Furthermore, much of the Damara sequence in northern Namibia is quite thin (3 - 4 km, Miller, 1983). The Sr-isotopic composition of the quartz latites can also be rationalised in terms of a pre-Damara (2.0 Ga old) basement source. The Sr-isotopic composition of the Kuiseb schist (530 Ma) and the Donkerhuk s-type granite (520 Ma) (Hawkesworth and Marlow, 1983; Haack *et al.*, 1983) have initial ratios of 0.710 - 0.720. These rocks are thought to have been derived from the pre-Damara basement and therefore reflect its isotopic composition at 520 - 530 Ma. Recalculated initial ratios of this pre-Damara source material at 121 Ma using the Rb/Sr ratio of bulk continental crust (Taylor and McLennan, 1985) yields a range of values, 0.713 - 0.723, which closely match the initial ratios of the southern Etendeka quartz latites. Furthermore, the average $\delta^{18}O$ value (11.18) of the Donkerhuk granites (Haack *et al.*, 1985) is in close agreement with the average $\delta^{18}O$ values of

minerals separated from the southern Etendeka quartz latites ($\delta^{18}O$ = 10.79, Harris *et al.*, 1988), indicating that they may have been derived from a similar source. Indeed partial melting of old basement to generate some of the s-type Damara granites may have produced the positive Eu anomaly required in the quartz latite source.

The Tafelberg latite which has a more mafic major element composition relative to the quartz latites (Table 6.6) is significantly more enriched in Ba, Sr, Zr and REEs, clearly indicating that they cannot have been derived from the same source material. Studies of the Salem Granitic Suite (550 Ma) at Otjosondjou, 160 km ESE of Tafelberg (Miller, 1973) show the presence of diorites and monzonites which have high concentrations of Ba (1100 - 1500 ppm), Sr (700 - 900 ppm) and Zr (200 - 600 ppm). It is possible that the Tafelberg latite may have been derived from this material or have a similar source region.

7.6.4 Sarusas quartz latites

The major element compositions of the Sarusas quartz latites (Table 6.7) are very similar to those of the southern Etendeka quartz latites (Table 6.6) and it is likely that they are also minimum melts derived under similar T/P conditions to the latter. The similarity in trace element enrichment trends between the Sarusas quartz latites (b-type) and the Khumib basalts (Figs. 6.5 and 6.6) suggest that they may be linked in some way. The trace element enriched character of the quartz latites may have been inherited from the Khumib basalts, and it is possible that underplated (crystallised) basaltic magma was subsequently remelted to produce quartz latite. Alternatively, if one accepts that the trace element enriched character of the Khumib basalts relative to the basalts of the southern Etendeka is due to some kind of enrichment process of their mantle source regions (Sweeney, 1988), then it is conceivable that this process may also have affected the lower crust and the source regions of the Sarusas quartz latites.

Fig. 7.10a shows the trace element patterns for the Sarusas latites and quartz latites normalised to average Khumib basalt and shows the pattern for average southern Etendeka quartz latite for comparison. Variations in the trace element, Sr-isotopic and mineralogical characteristics between the Sarusas a-type and b-type quartz latites precludes their derivation from a common source, indeed the Sr-isotopic data ($\epsilon_{Sr} > 35$) indicate that neither type of

Fig. 7.10 Sarusas felsic volcanics normalised against average Khumib basalt.

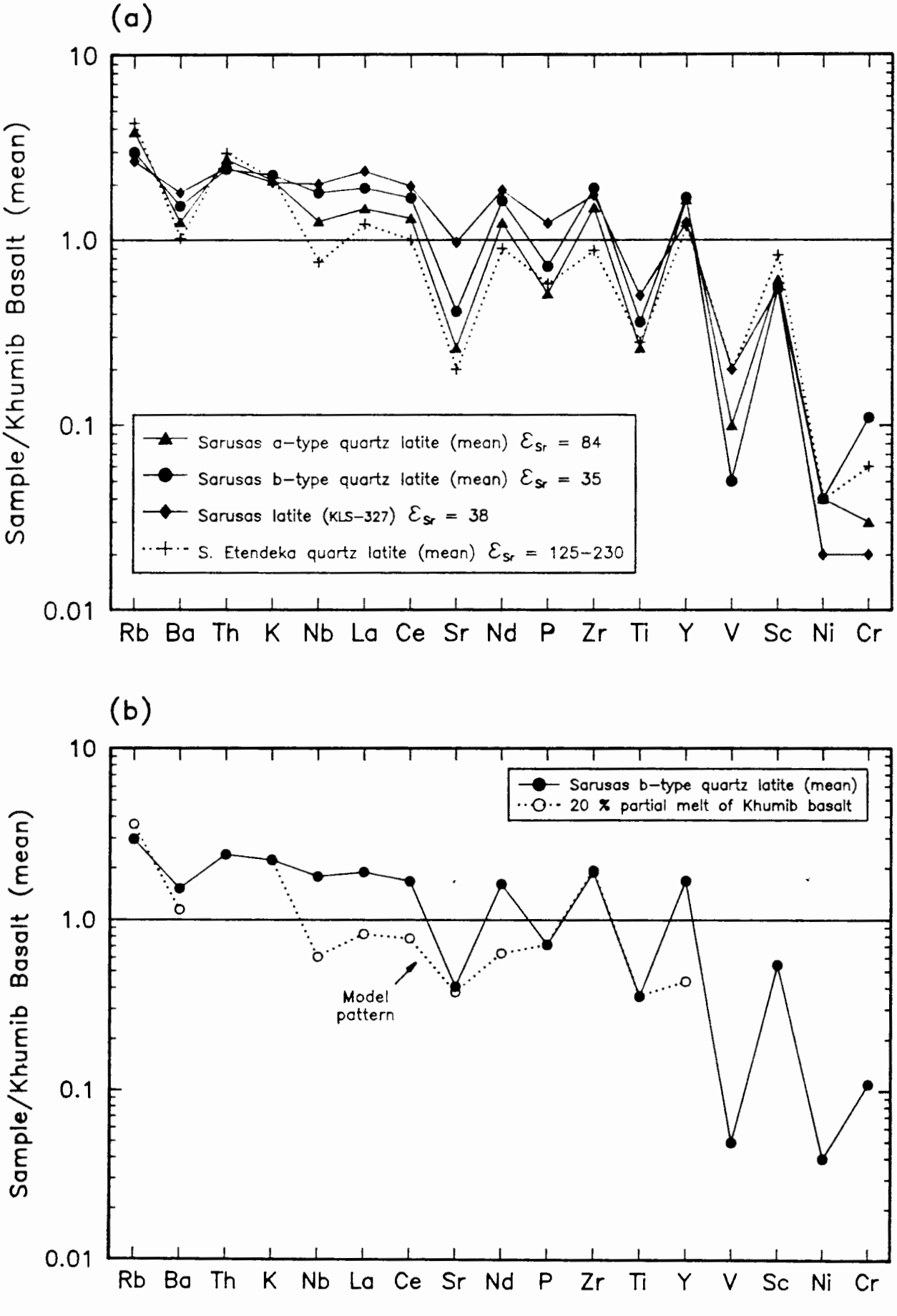

quartz latite could have been derived directly from Khumib-type basalt (average ϵ_{Sr} = 10; Erlank, unpublished data) without some degree of crustal contamination. It is possible that the melting of underplated basalt and adjacent lower crustal granulite could yield a quartz latite of mixed source origin, which would help to explain the elevated ϵ_{Sr} values. If one accepts that the southern Etendeka quartz latites are typical of melting lower crustal (mafic to intermediate) granulite in the area then the trace element patterns in Fig 7.10a would indicate a larger proportion of melted granulite in the Sarusas a-type quartz latite.

Setting aside the Sr-isotopic constraints a model can be tested to see if the trace element pattern of the b-type (least radiogenic) quartz latites can be generated by the partial melting of a source composition similar to that of average Khumib basalt. The approach taken here is similar to that taken in the partial melt modelling of the southern Etendeka quartz latites, and involves the calculation of a melting mode (using a least squares approximation) and of a restite for a particular degree of melting (equation 3). In order to calculate the melting mode it was first necessary to estimate the composition of the b-type quartz latite before it was affected by post-eruptive alteration. This was done using pitchstone and devitrified quartz latite compositions in the same way as they were used to estimate the theoretical composition of the Lower Tafelberg/Lower Interbedded Coastal in Section 6.3. The maximum amount of quartz latite that can be produced from the basaltic source composition is approximately 20 %, after which quartz becomes exhausted. It is interesting to note that highly incompatible elements such as Rb and Th show relatively small degrees of enrichment over the other trace elements (Fig. 7.10a) suggesting that the degree of partial melting is greater than 20 %. Note that if one assumes D_{Rb} = 0 equation (1) reduces to 1/F, so that if C_l/C_o = 3.0 (Fig. 7.10a) the degree of partial melting should be of the order of 33 %.

Table 7.9 shows the chemical composition of the source and the theoretical Sarusas b-type quartz latite, and the proportions of various minerals in the source, melting mode and a restite calculated after 20 % melting. The trace element pattern calculated for the melt extract (calculated using equations (1) and (2) and the Kd values in Table 7.3b) is compared with the trace element pattern of average b-type quartz latite in Fig. 7.10b. The calculated melt composition shows a poor correspondence with the b-type quartz latite for elements such as Ba, Nb, La, Ce, Nd and Y. The chief control over these

TABLE 7.9

Calculated mineral proportions in a restite generated by the extraction of 20% of the Sarusas b-type quartz latite melting mode from the normative mineralogy of average Khumib basalt.

CHEMICAL COMPOSITIONS

	Basalt Source	b-type QL
SiO_2	52.78	65.37
TiO_2	3.55	1.34
Al_2O_3	13.42	12.97
FeO	11.62	6.44
MnO	0.16	0.16
MgO	5.02	1.20
CaO	8.11	3.32
Na_2O	2.78	4.22
K_2O	2.02	4.56
P_2O_5	0.53	0.40

MINERAL PROPORTIONS

	Source Norm	Melting Mode	Restite ~ 20% melting
Quartz	2.35	11.95	0.02
K-Feldspar	11.94	26.76	8.34
Albite	23.52	35.46	20.63
Anorthite	18.17	2.97	21.84
Opx (En 50)	20.53	7.96	23.57
Cpx (Wo 50)	15.51	11.12	16.56
Ilmenite	6.74	2.53	7.76
Apatite	1.26	1.24	1.27

The basalt Source composition is the average composition of Khumib basalt. The data was collected during the course of a collaborative programme in this department.

The Sarusas b-type quartz latite composition was estimated using pitchstone and devitrified quartz latite analyses - see text for detail.

elements (except Ba) is the presence of significant amounts of ilmenite and apatite in the restite (Table 7.8), which have relatively large Kds for such elements (Table 7.3b). The model could be improved significantly by lowering the Kd values for these elements, however, there are no Kd data in the literature to support this.

The modelling carried out above, coupled with the Sr-isotopic data suggest that the Sarusas b-type quartz latites are not related to the Khumib basalts by a simple partial melting process. The possibility of a mixed underplated basalt/lower crustal granulite source would not significantly alter the calculated trace element trend. This is because the trace element pattern of a possible lower crustal melt (e.g. average southern Etendeka quartz latite, Fig. 7.10a) is similar to that of the calculated trend (Fig. 7.10b). The need to invoke partial melting of underplated basalt as a mechanism to produce the Sarusas quartz latites but not for the southern Etendeka quartz latites also presents severe geodynamic problems. A simpler model in terms of the geodynamics and the generation of the different Sarusas magma-types is the partial melting of heterogeneously enriched lower crust. It is possible that this enrichment was due to a metasomatic event which may also have affected the basalt source regions at greater depths, resulting in similar trace element enrichment trends. Further speculation with regard to the petrogenesis of all the "enriched" rock types in the northern Etendeka must await more detailed modelling and isotope studies which are beyond the scope of this thesis.

7.7 CONCLUSIONS

(1) Geochemical modelling indicates that the southern Etendeka quartz latites are not related to the Tafelberg-type basalts by fractional crystallisation, AFC or magma mixing. The basalts show fractionation trends which are clearly divergent from the quartz latites. This feature coupled with the well defined composition gap and the elevated ϵ_{Sr} of the quartz latites can be taken as evidence that the quartz latites are crustal melts.

(2) Phenocryst compositions indicate that magmatic differentiation could not be responsible for the apparent "evolution" in the whole rock compositions within the Tafelberg/Interbedded Coastal quartz latite trend. Furthermore, the Sr-isotopic variation displayed by the Tafelberg/Interbedded Coastal

quartz latites precludes the generation of this trend by fractional crystallisation, although the compositional variation alone could be explained by AFC involving an average upper crustal composition with an ϵ_{Sr} value of 500.

(3) Limited compositional variation in the Springbok and Upper Interbedded Coastal quartz latites can be accounted for by limited fractional crystallisation of the observed phenocryst phase assemblages.

(4) The Sarusas latites and quartz latites can not be related to one another, or to the "enriched" Khumib basalts, by processes such as fractional crystallisation, AFC and magma mixing.

(5) The major element composition of the quartz latites is consistent with their generation as minimum melts under H_2O-undersaturated conditions at pressures of 8 - 10 kb. Partial melting is thought to have occurred at the base of, or within, the lower crust as a result of high heat flow induced by continental rifting and contemporaneous basaltic magmatism.

(6) Trace element modelling of the southern Etendeka quartz latites suggests that they are probably produced by 18 - 20 % partial melting of an intermediate source composition, which approximates to the bulk crustal average of Taylor and McLennan (1985). Sr- and O-isotopic data are consistent with their derivation from *ca.* 2.0 Ga old pre-Damara basement.

(7) The source characteristics of the Sarusas quartz latites are more equivocal. Simple trace element modelling suggests that these quartz latites are not the products of partial melting of underplated Khumib basalt as might be implied from their trace element and isotopic characteristics. Furthermore, it seems ad hoc to invoke the partial melting of underplated basaltic material to produce the Sarusas quartz latites but not the southern Etendeka quartz latites. If one accepts that the Khumib basalts were derived from enriched sub-continental mantle, then it is possible that such enrichment process(es) also affected the source regions of the quartz latites at or near the base of the Continental crust in this region.

CHAPTER 8

EMPLACEMENT AND COOLING HISTORY OF THE ETENDEKA QUARTZ LATITES

8.1 INTRODUCTION

Silicic volcanism may produce a wide variety of deposits from blocky lava flows to pyroclastic tuffs. Rhyolite lavas, which are normally highly viscous, commonly form domes of limited extent above and around the volcanic vent. Violent, explosive activity results in fallout and pyroclastic flow deposits which are volumetrically the most significant expression of acid volcanism. Air-fall tuff deposits resulting from the fallout of tephra from eruption clouds or the highly inflated tops of ash flows are unwelded and often well-bedded. Pyroclastic flows resulting from eruption column collapse, boiling over, or dome collapse yield a variety of ash flow (ignimbrite) and base surge deposits with varying degrees of compaction and welding. Complete welding and re-mobilisation of extensive ash-flows can result in rocks which can be easily confused with large silicic lava flows. The Etendeka quartz latites display features common to both rhyolite lavas and ignimbrites and are believed to be high temperature ash-flows or rheoignimbrites which underwent en masse lava-like flowage following their deposition but prior to their final cooling (Milner, 1986). This chapter draws on information presented in previous chapters and discusses the emplacement of quartz latite flow units and the generation of their characteristic features.

8.2 IDENTIFICATION OF LAVAS AND ASH-FLOWS

"Typical" rhyolite lavas are more easily defined than ash-flow tuffs due to the broad spectrum of textural features exhibited by the latter. Ash-flow tuffs have volumes spanning several orders of magnitude (0.001 - 3000 km^3) and show significant variations in the degree of compaction and welding, with transitions from completely undeformed shards, typical of air-fall tuffs, to essentially homogeneous vitrophyre, typical of glassy rhyolitic lavas. Comprehensive reviews of ash-flows and their associated deposits are given by Ross and Smith (1961), Chapin and Elston (1979) and Fisher and Schmincke (1984). Broad comparative features of acid lavas and ash-flow tuffs, and of features displayed by the southern Etendeka quartz latites are presented below:

ASH-FLOW TUFFS	ACID LAVAS
** Extensive sheet form	Limited extent
** Planar flow contacts	Irregular contacts
** Pyroclastic character	** Auto-brecciated
** Welded/Non-welded	** Contorted banding
** Glassy/Devitrified	** Glassy/Devitrified

** Characteristics exhibited by the Etendeka quartz latites.

Despite the flow banding and flow folding (Plates 2.15 - 2.17) and brecciation (Plates 2.20 - 2.22) more commonly associated with rhyolite lavas, it is considered that the extensive sheet-like form (often exceeding 2500 km^2) and the pyroclastic features (Chapter 4) provide evidence that the Etendeka quartz latites are ignimbritic in origin. The most convincing pyroclastic textures are the fiammé from the Lower Tafelberg unit (Plates 4.27 - 4.28) and a variety of welding and compaction features observed in the Gemini quartz latite unit (Plates 4.5 - 4.16). Even if one invokes lavas with low bulk viscosities to account for their widespread character (Twist, 1984; Bonnichsen and Kauffman, 1987), rhyolite lavas do not usually exhibit features that can be confused with the pyroclastic features reported here.

Extensive Cenozoic silicic units in south-western Idaho and adjacent areas of Nevada and Oregon show many features in common with the Etendeka quartz latites. These volcanics which originate from eruptive centres in the south-western part of the Snake River Plain, have been variously interpreted as high temperature lava-like ash-flows (Ekren *et al.*, 1984) and/or as large volume rhyolite lavas (Bonnichsen and Kauffman, 1987). The latter authors present several criteria for distinguishing between lavas and ash-flows of this nature, and it is useful to compare some of their rhyolite lava criteria with features observed in the Etendeka quartz latites (quotes from Bonnichsen and Kauffman in *italics*):

(1) *Absence of bubble-wall shards, pumice fragments and lithic fragments, especially foreign rock types within the rhyolite*. Many of the photomicrographs in Chapter 4 illustrate shard- and globule-like textures, and fragments and blocks of pumice are not uncommon, particularly in the

upper parts of quartz latite flow units (Chapter 2). Basalt clasts are also present in the basal zones of some units (Plates 2.25 - 2.26) and quartzite xenoliths occur throughout the Upper Springbok unit (Plate 2.33).

(2) *A paucity or lack of parallel flow marks that record primary flow azimuths and of laterally extensive lithophysal horizons within or at the base of flows*. Elongate, flattened vesicles which constitute "flow marks" (Bonnichsen and Citron, 1982) are a common feature in the Etendeka quartz latites, particularly the Springbok units (Fig. 2.11). Lithophysae, which are angular to spherical gas cavities (Bonnichsen and Citron, 1982), are probably represented in the quartz latites by partially or completely mineralised amygdales which commonly occur in the upper parts of the flow.

(3) *Lobate marginal zones with blunt terminations and crumble breccia*. Features such as these have yet to be identified in the Etendeka, although a re-investigation of the apparent termination of the upper of the Lower Springbok units at Fonteine may be considered in the light of Bonnichsen and Kauffman (1987). These authors also indicate that the flow margins of their rhyolite lavas are seldom less than 25 m thick. Quartz latites such as the Lower Springbok and Gemini units on the other hand maintain fairly constant thicknesses of 30 m or less over large areas, a feature inconsistent with abrupt terminations.

(4) *Complexly deformed contact between basal glassy zone and overlying devitrified central zone of the flow and evidence, such as folds, of en masse flowage within the basal vitrophyre*. Contacts between basal pitchstones and devitrified quartz latite are commonly planar (Plates 2.18 - 2.19). Some signs of en masse flowage are occasionally observed in pitchstone (Plate 2.17).

(5) *Presence of extensive vitrophyre in the upper zone of the sheet, which may contain abundant "red and black breccia"*. Extensive pitchstone horizons are not observed in the upper flow zones of the quartz latite units and pitchstone is generally confined to thin bands and lenses. The "red and black breccia" described by Bonnichsen and Kauffman (1987) consists of equant blocks of vitrophyre in a matrix of red, oxidised vitrophyre fragments which have been welded. The breccia is thought to have resulted from the breaking up of glassy rhyolite either by the jostling movement of the underlying flow or explosive steam venting. Although few vitrophyre

breccias of this nature have been observed in the Etendeka some of the breccias in the quartz latite upper zone may have been generated by similar mechanisms. While such breccias do not provide strong evidence that the quartz latites are lavas, they do suggest lava-like motion at some stage.

It should be noted that the rhyolites described by Bonnichsen and Kauffman (1987) have a smaller areal coverage (< 1000 km^2) than the quartz latites (> 2500 km^2) and appear to be confined to a topographic basin created by subsidence related to the eruption of the Cougar Point tuff which underlies these rhyolites (Bonnichsen, 1982). No such confinement of the lavas in the Etendeka has been identified.

A review of the literature concerning the rhyolites of south western Idaho suggests that magmas of essentially similar composition and temperature are erupted by both lava-flow and ash-flow mechanisms (Bonnichsen and Citron, 1982); however, Bonnichsen and Kauffman (1987) caution that some voluminous, high temperature ash-flow tuffs may become so totally welded that they develop the same types of structures observed in lava flows, such that all evidence of their pyroclastic origin is destroyed. It is postulated that this is effectively what has happened to the Etendeka quartz latites.

8.3 RHEOIGNIMBRITES

Reversion from ash-flow to liquid flow or rheomorphism was first recognised in peralkaline ash-flow units. Peralkaline froth flows (McCall, 1962) and globule lavas (Johnson, 1968) in the East African rift were independently reinterpreted as densely welded ash-flow tuffs (Schmincke, 1974) and as globule ignimbrites (Hay *et al.*, 1979). Although such flows differ quite markedly from most calc-alkaline ash-flow tuffs, being quite thin (< 30 m) with fairly small volumes (< 10 km^3), they are of particular interest here because their primary structures indicate laminar creep, such as the extreme stretching of pumice blocks and lapilli, and include pronounced lineations on parting planes and folds ranging from millimetres to several metres in wave length (Schmincke, 1974). Schmincke attributes these and other textural features to the generally lower viscosity and higher temperature of peralkaline magmas which results in a high degree of welding and homogenisation in dense particulate ash flows.

The viscosity of a silicate liquid is dependent upon its composition, volatile content and temperature. Empirical models for the calculation of viscosity (Bottinga and Weill, 1972 and Shaw, 1972) have been used to compare the erupted viscosity of the quartz latites with other volcanic rocks (Fig. 8.1, data calculated using Shaw's approximation). Viscosity was calculated using Shaw (1972) despite indications by Urbain *et al.* (1982) that Bottinga and Weill (1972) is in fact more accurate. Two different viscosity values could be calculated using Bottinga and Weill (1972) because the quartz latite X_{SiO2} values fall at about the cutoff for two sets of constants used in their calculation. The Shaw (1972) method, apart from being less cumbersome and quicker to calculate, yielded viscosity estimates between the two sets of values obtained using the Bottinga and Weill method.

Schmincke (1974) indicates that high alkalis and iron and low alumina contents are important factors in lowering the viscosity of peralkaline magmas relative to calc-alkaline magmas and this may also be true to some extent for the quartz latites (see Section 6.2 for a comparison with other rhyolite/dacite compositions). The most important factor controlling viscosity does, however, appear to be temperature. In Fig. 8.1 the eruption temperatures of various lava types have been estimated, viz. quartz latite (1050 °C), basalt (1150 - 1200 °C), rhyolite (800 °C) and pantellerite (950 °C), in order to compare their typical erupted viscosities. High eruptive temperatures envisaged for the quartz latites (1000 - 1100 °C; Chapter 5) lowers their viscosity relative to lower temperature rhyolites by several orders of magnitude. At 1050 °C the calculated viscosity of quartz latite magma (1 % H_2O) is approximately 10^5 Poise, which is at the lower end of the range of values calculated for peralkaline magmas (1 % H_2O) at 950 °C (Schmincke, 1974). The quartz latites therefore probably had very similar physical properties to the peralkaline magmas which have been described as rheomorphic ash flows (Schmincke, 1974). Whether such viscosities are low enough to permit the quartz latite magma to flow as lava for great distances (up to 130 km) over essentially flat lying terrain is open for debate. Note that basaltic lavas which may form widespread sheet-like flows are considerably less viscous (10^2 - $<10^4$ Poise) than quartz latite (Fig. 8.1).

Important textural evidence supporting a rheoignimbritic origin for the quartz latite units comes from the Gemini quartz latite unit (SM-229 locality; Fig. 2.3). A single outcrop of this unit shows widely varying degrees of shard

Fig. 8.1 Estimates of erupted viscosity.*

* Does not account for the effects of crystallisation or vesiculation.
Notice the significant affect of H_2O on lowering viscosity.

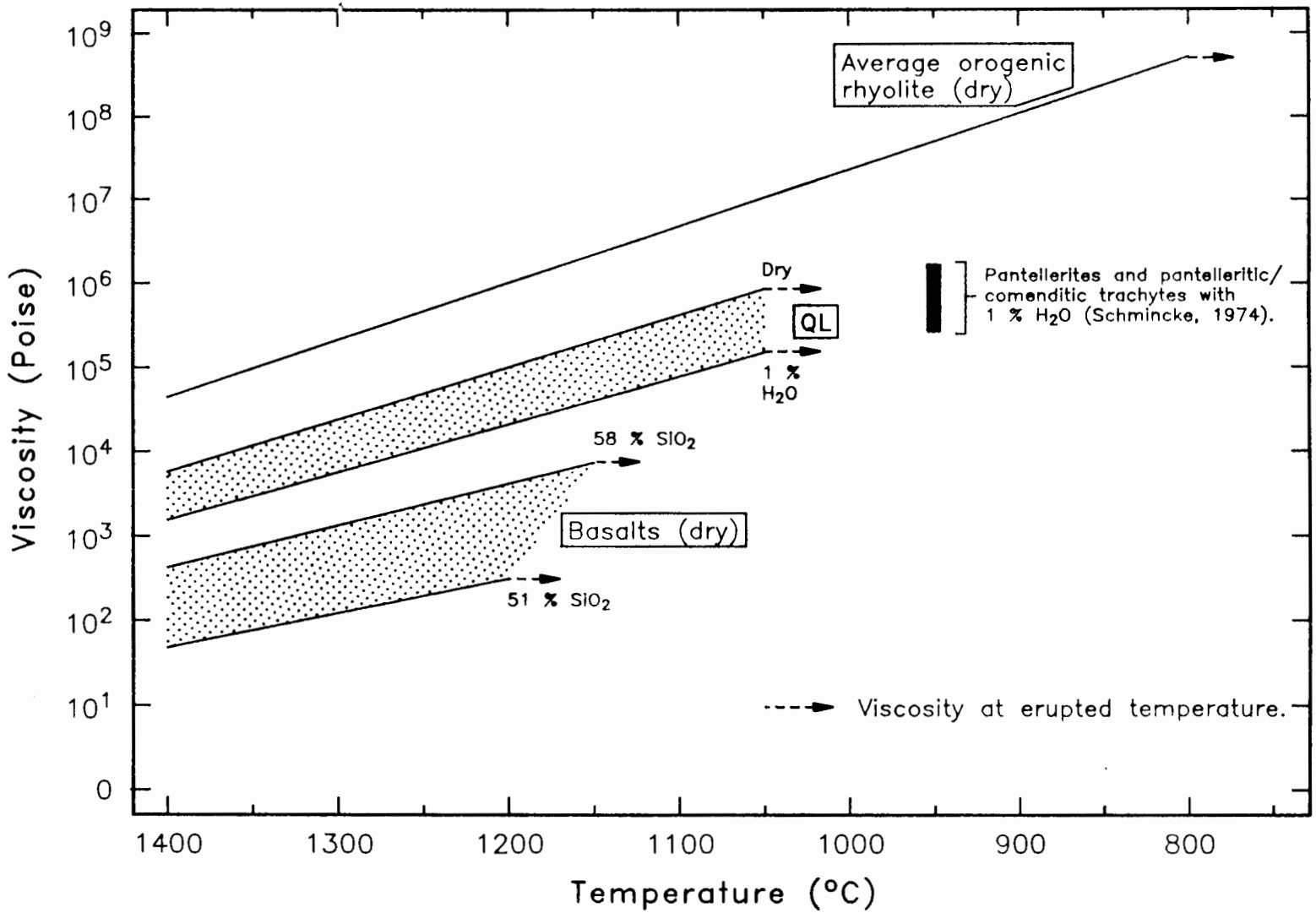

preservation and the progressive welding, compaction and rheomorphism of what is interpreted as primary tephra (ash and pumice lapilli) is illustrated in a series of photomicrographs (Plates 4.5 - 4.16; see captions for detail). It is suggested that the Gemini flow unit is either the product of a relatively small eruption or is the distal margin of a much larger flow. Fairly rapid heat loss from such a thin unit (15 - 20 m) probably prevented thorough welding, rheomorphism and devitrification of the ash flow, thus preserving features intermediate in the development of a quartz latite flow unit.

8.4 ASH FLOWS - ERUPTIVE MECHANISMS

8.4.1 Introduction

The origin of pyroclastic flows is controversial and limited observations of "small" volcanic eruptions in recent times have led to the proposal of a number of mechanisms (see Fisher and Schmincke, 1984). Currently favored mechanisms for the production of ash flows, rather than block flows, lahars, etc., include the "boiling over" of rapidly vesiculating magma from a crater lip and the gravitational collapse of a vertical eruption column ("column collapse") (Smith, 1960; Sparks and Wilson, 1976; Sparks *et al.*, 1978). It is also possible that a combination of both types of lava emission may occur during the course of a single eruption. Sparks and Wilson (1976) consider that an eruption column consists of two components which may generate ash-flow and air-fall deposits respectively; (1) a lower, gas thrust component, which results from the decompression of gas and (2) an upper, convective thrust component, which occurs when air entrained in the gas thrust phase is heated thereby reducing the density of the column such that it behaves as a thermally convective plume. If the absorption and heating of atmospheric air is low, or if there is a sudden reduction in the gas velocity or an increase in the vent radius, the column may become gravitationally unstable and collapse, thus generating ash flows. Furthermore, once collapse begins the column is protected from air mixing so that re-instatement of Plinian activity is difficult without a break in activity, decrease in vent diameter or a major increase in the gas velocity (Sparks *et al.*, 1978). The development of gas thrust and convective thrust regimes, and hence the nature of the resultant pyroclastic deposits, depends on a complex interplay of several parameters, which include magma gas content, gas composition and gas velocity, the volume and rate of lava emission and the

radius of the vent. Sparks and Wilson (1976) indicate a correspondence between the temperature and degree of welding of an ash flow and the amount of associated air-fall deposits. Magmas with high water contents and high gas velocities favour the formation of Plinian eruptions resulting in low temperature air-fall tuffs and non-welded ignimbrites. Eruptions from wider vents and/or of magmas with low water contents (< 1%) or high proportions of CO_2 form much denser dispersions which significantly reduce atmospheric mixing and concomitant cooling. This results in more strongly welded ash-flow tuffs and a paucity of air-fall deposits. The height attained by the eruption column before it collapses ultimately controls the lateral distance the ash flow travels from the vent. Initial eruption velocities of 400 - 600 m/s may generate gas thrust zones of 1.5 - 4.5 km in height (Sparks and Wilson, 1976) and Sparks (1976) indicate that ignimbrites may travel 10 - 25 times the column collapse height from their source. Thus an eruption column which collapses from a height of 4.5 km could generate an ash-flow tuff with a radius of between 45 - 110 km, the precise distance traveled depending on the fluidised nature of the ash flow and the terrain traversed.

8.4.2 Eruption of an Etendeka quartz latite ash flow

The large volume, lateral extent and complete welding of the Etendeka quartz latites makes it very difficult to envisage the type and scale of the eruptions which produced them. The paucity of air-fall deposits in the Etendeka Formation suggest that such eruptions did not have a plinian phase, in agreement with the observations of Sparks and Wilson (1976). The apparent mobility and volume of the hot, dry quartz latite ash flows is problematic for both "column collapse" and "boiling over" eruptive mechanisms. Sparks *et al.* (1978) suggest that flows produced under conditions of high emplacement temperatures should not be particularly mobile because the same conditions produced low initial velocities and volume rates of production. However, the minimum distance traveled by the Lower Tafelberg quartz latite (i.e. unidirectional thinning without vent or fissure identification) is approximately 130 km and requires that the minimum column collapse height must have been between 5 and 13 km. Conditions of optimum flow mobility required by collapse from 5 km would probably lead to too much cooling and it is thought the densely welded quartz latite ash flows must have descended from much greater heights. In order to increase the collapse height and reduce the proportion of atmospheric mixing and

heat loss, such eruptions require very high volume rates of production and large vent diameters. Ekren *et al.* (1984) suggest that eruption velocities of 1 km/s and column collapse heights of 15 km are required to generate the extensive lava-like ash-flow tuffs of south-western Idaho. It is highly unlikely that a simple "boiling over" or outwelling of the quartz latite ash flow from a vent or fissure would produce sufficient initial velocity for the flow to cover such large distances.

8.5 OUTFLOW AND RHEOMORPHISM OF THE QUARTZ LATITE ASH FLOW

The quartz latites of the Etendeka Formation represent the products of hot (1000 - 1100 °C), dense, rheomorphic ash-flows or rheoignimbrites. Initially the eruption cloud consisted of a fluidised suspension of near molten shards or droplets of fairly low viscosity. Fluidisation plays a major role in extending the run-out of most ash-flow sheets (Sheridan, 1979) and results from the exsolution of gases from tephra within the flow or by the heating and expansion of air engulfed at the flow front. Lapilli and blocks may be transported in the eruption cloud by matrix strength, turbulence, buoyancy, grain-dispersive forces or other mechanisms (Sheridan, 1979). Pumice clasts lighter than the matrix would work their way to the surface of the flow and hence explain the presence of pumice block breccia (Fig. 2.12) and the higher proportion of pumice fragments in the ashy matrix of breccias in the upper parts of the quartz latite flow units. Intense welding of tephra within the ash-flow occurs with the gradual deflation of the fluidised cloud. Shear strain deformation resulting from the continued motion of the welded ash-flow (rheomorphism) produces laminar flow features which may become folded or contorted, such features are common in the upper part of the quartz latite basal zone (Fig. 2.12). More rapidly quenched parts of the flow could be easily disrupted by continued motion of the flow interior causing breccias to form. Breccias are more strongly developed at the base of the quartz latite flows rather than at the top, probably due to more effective contact chilling with the ground surface. Vesicles resulting from exsolved volatiles trapped at this stage become highly stretched in the direction of flow and it is thought that clasts exhibiting a flattened amygdaloidal fabric resulted from brecciation of such material. The matrix of flow-base breccias consists of ash and lapilli (Plates 4.1 - 4.2) which is probably of both cognate and juvenile origin (Table 4.1). It is tentatively

suggested that in the matrix material illustrated in Plates 4.1 - 4.2 the rounded, yellowish fragments with deformed vesicles formed in a similar fashion to the larger clasts, but that the dark brown angular fragments with nearly spherical vesicles represent primary particulate matter which was quenched from the eruption cloud. Re-incorporation of breccia clasts into flow banded, or massive quartz latite (Plate 2.21) may have occurred either by physical mixing or by the progressive welding and rheomorphism of the ash matrix between the clasts, a feature illustrated in Plates 4.17 - 4.21. Relatively rapid quenching and only partial homogenisation in some instances preserve rare, but unequivocal, fiammé textures (Plates 4.27 and 4.28).

Migration of volatiles towards the upper parts of the flow during the final stages of emplacement are thought to have resulted in lithophysae subsequently mineralised to form amygdales. Schmincke (1974) suggested that rapid welding of dense ash flows inhibits the complete degassing of the collapsed ash flow resulting in the formation of spherical (secondary) vesicles within collapsed ash and pumice particles and of the larger gas cavities which form beneath tightly welded layers. Similar features are observed in the quartz latites with small spherical vesicles in strongly welded vitrophyre (Plate 4.25) and flattened fiammé (Plate 4.28), and abundant amygdales in the upper portions of many units (Fig. 2.12).

The presence of devitrification textures (Plates 3.1 - 3.3) in most felsitic or lithoidal quartz latite indicates that the quartz latite units were probably glassy throughout shortly after emplacement. However, thorough devitrification of the units occurred as they cooled and pitchstone is only preserved where cooling was most rapid at the base, top and distal parts of the flow. Glass results from the super-cooling of a liquid to a temperature below that at which it would normally start to crystallise. Although the transformation of a super-cooled liquid to a glass is largely dependent on the cooling rate the temperature at which this transformation takes place (T_g), is commonly defined in the glass industry as the temperature at which the viscosity of a super-cooled liquid exceeds 10^{13} Poise (Carmichael, 1979). Naturally occurring anhydrous silicic lavas have yielded glass transformation temperatures as high as 800 °C (Bacon, 1977) so it is possible that the quartz latites were completely glassy whilst remaining relatively hot. Devitrification of glass occurs rapidly at high temperatures promoting granophyric crystallisation, which may be further enhanced by the degassing of volatiles retained by the ash flow

(Schmincke, 1974). Granophyric textures are more strongly developed in the central parts of the quartz latite units (Plate 3.5), which coupled with the grainsize distribution of plagioclase microphenocrysts and high temperature (> 600 °C) oxidation textures in titanomagnetite (Plate 3.6), indicate that the interior of the flow remained hot for some time after flow emplacement (Subsection 3.5.3). Alteration of pyroxenes and plagioclase, common in most devitrified samples, probably result from reactions at fairly high temperature (600 - 800 °C) involving volatiles degassed from the flow. Bonnichsen and Citron (1982) indicate that devitrification of the Cougar Point tuff generally involved strong oxidation which altered mafic minerals and imparted a red colouration to the devitrified tuff. A profile of titanomagnetite oxidation textures in the Lower Tafelberg quartz latite (Plate 3.6) shows that the most intense oxidation occurs in the upper and lower parts of the flow with the centre remaining relatively unaffected. This indicates that the alteration of pyroxene throughout the devitrified parts of the flow is not merely a function of oxidation and further suggests that little air was engulfed by the quartz latite ash flow during its eruption.

Devitrification is accompanied by a decrease in volume which is accommodated by the formation of joints. Bonnichsen and Citron (1982) and Bonnichsen and Kauffman (1987) document in some detail the types of jointing present in welded tuffs and rhyolite lavas. These authors suggest that devitrification and contemporaneous jointing began before the final stages of emplacement with sub-horizontal sheeting joints forming in response to flow stresses. Vertical, columnar or shrinkage joints observed in the main zone of the flow result from final cooling and contraction of the flow.

8.6 ALTERATION ZONES

Alteration zones in the Lower Tafelberg quartz latite are often characterised by post-depositional hydraulic fracturing and brecciation (Chapter 2). This probably results from the emplacement of the ash flow over wet ground or small areas of open water. Vapourisation of this water would cause relatively rapid cooling in the unit above increasing the likelihood that primary eutaxitic, fiammé and flow banding features are preserved; explosive volatile release would lead to fracturing and secondary brecciation (Plates 2.36 and 2.37). The orangy-red colouration of the rock in these zones is indicative

of strong oxidising conditions. At Tafelberg the style of alteration in the Lower Tafelberg quartz latite differs slightly from that seen west of the ABFZ as it contains more pitchstone and abundant vesicles. It is possible that volatile interaction was less well developed in this zone and that volatiles introduced to the base of the flow migrated upwards in the form of vesicles rather than resulting in explosive fracturing. The deformed and elongate nature of such vesicles suggests that the flow was still mobile at this stage. This zone probably cooled more rapidly than unaffected parts of the flow and as a result contains more vesicular pitchstone, much of which has altered to a yellow, friable rock characteristic of fairly low temperature alteration. The localised nature of alteration zones and their confinement to individual units is consistent with the proposed model and suggests that the activity within these zones was relatively short lived.

8.7 QUARTZ LATITE ERUPTIVE CENTRES

Little is known of the precise locality of the vents from which the Etendeka quartz latites erupted, or of the nature of these vents (central or fissure). Although little flow directional data have been collected during this study, the directions in which the units thicken provide some clues as to their vent areas. The south-westward thickening of the Lower Tafelberg quartz latite unit, and of the Tafelberg/Interbedded Coastal quartz latite succession as a whole, suggests that the vents for these units lie to the west of the present coast line. Whether such vents lie on the continental shelf or within the Paraná Basin, Brazil, is unknown. The Lower Springbok quartz latite units thicken in a south or south-easterly direction towards the Brandberg and Messum Complexes (Fig. 2.1). Flow-banding and vesicle elongation directions measured at several localities in the Upper Springbok unit also suggest that it may have come from the south.

Voluminous ash-flow tuffs can often be related to calderas and many workers believe them to have erupted either from central vents or from ring fractures associated with caldera formation. Fissures which form perpendicular to the main stress direction during continental extension are commonly exploited by basaltic magmas forming dolerite dykes, and it is possible that acidic magmas could be erupted from depth along similar fissures without being related to central high level intrusions. For example, Bristow (1985) considers that the

Jozini rhyolites were produced by the outwelling of dense (degassed) pyroclastic flows from large fissures, and suggests that the rhyolitic dykes and elongate granophyre plutons in the Lebombo may represent the original volcanic feeder sites. Furthermore, extensive rhyolite lavas in south-western Idaho are also thought to have erupted from fissures (Bonnichsen and Kauffman, 1987). However, Landsat images of the lavas and basement in north-western Namibia show no sign of dykes or elongate plutons which could have acted as feeders for quartz latite fissure eruptions and no intrusive rocks of quartz latite composition have been encountered in the Etendeka region.

The late-Karoo subvolcanic complexes of Brandberg, Messum and Cape Cross (Fig. 2.1), which are interpreted as caldera structures (Korn and Martin, 1954 and Martin *et al*, 1960) provide ideal sites from which some of the Etendeka quartz latites may have been erupted. However, the predominantly alkaline to peralkaline composition of these intrusions indicates that any relationship with the quartz latites is not as simple as their apparent coincidence in space and time. Although the precise relationships between the Etendeka volcanics and the Brandberg, Messum and Cape Cross complexes have yet to be established, the thickening of the Lower Springbok quartz latite units towards Brandberg and Messum suggests that there may be a link between these complexes and the quartz latites. This is also supported by an occurrence of quartz monzonite (compositionally similar to quartz latite) on the north side of the Brandberg massif (M. Diehl, pers. comm., 1987). The alkaline intrusive complexes of Erongo and Paresis, which lie 230 km south-east and 220 km east of the Etendeka respectively, both have acidic volcanics compositionally similar to the Etendeka quartz latites associated with them (Siedner, 1965; Blumel *et al*, 1979). The Erongo complex, which is interpreted as a caldera collapse structure, consists of intrusive granites and granodiorites, with intracaldera basalts and ash-flow tuffs (F. Piranjo, pers. comm., 1987). Many of the ash-flow tuffs are texturally similar to the Etendeka quartz latites, and are typically highly welded with vitrophyre horizons, some exposures show excellent eutaxitic and fiammé textures (personal inspection by the author). In view of the large distances involved it is highly unlikely that either the Erongo or Paresis complexes represent the centres from which the Etendeka quartz latites were erupted. However, these examples do indicate that volcanics very similar to the Etendeka quartz latites were erupted from central complexes and were subsequently intruded by more alkaline magmas. It is possible therefore that the Brandberg and Messum plutons represent resurgent magmatism which intruded

the eruption centres of the Springbok quartz latites. Resurgence of the Brandberg, which intrudes an unknown thickness of lavas to stratigraphic levels much higher than the Springbok units, may have destroyed an earlier centre, and its present margins may represent the old caldera ring faults.

The apparent lack of calderas associated with some of the Idaho rhyolites led Ekren *et al.* (1984) to suggest deep, possibly lower crustal, magma chambers which precluded caldera collapse. Similar deep-seated eruptions may have given rise to the Etendeka quartz latites, a possibility supported by their high eruptive temperatures and postulated lower crustal source regions (Chapter 7). Note that a centre of this nature, with little surface expression, could easily be obscured by a subsequent intrusion.

8.8 CONCLUSIONS

(1) The quartz latites exhibit features common to both acid lavas and ash-flow tuffs. Despite the flow banding, flow folding and brecciation more commonly associated with rhyolite lavas, it is considered that the extensive sheet-like form and the pyroclastic features provide evidence that the quartz latites are ignimbritic in origin.

(2) Rheomorphism and en masse lava-like flow, appears to have occurred during the final emplacement of the Etendeka quartz latite ash flows. This may explain the often completely welded, homogeneous textures encountered at most outcrops. This also results in laminar features which may become folded, and rapidly quenched parts of the flow may be disrupted at this stage causing breccias to form. The rheomorphic character of the quartz latites can be attributed to high temperatures of eruption (1000 - 1100 °C) which lowers their viscosity relative to lower temperature rhyolites by several orders of magnitude.

(3) The apparent mobility of the quartz latite ash flows suggests that they resulted from the gravitational collapse of eruption columns with heights in excess of 5 km. High volume rates of magma production and/or large vent diameters probably reduced the proportion of atmospheric mixing and heat loss, helping to explain the strongly welded character of the quartz latites and the lack of associated air-fall ash.

(4) Thorough devitrification of the quartz latite unit occurred shortly after emplacement whilst the interior of the flow remained quite hot (600 - 800 °C). Devitrification was accompanied by the crystallisation of granophyre and the alteration plagioclase, pyroxene and titanomagnetite.

(5) Localised zones of alteration, often characterised by post-depositional brecciation and hydraulic fracturing, are indicative of some kind of hydrothermal activity with explosive volatile release. These zones probably result from the emplacement of the hot ash flow over wet ground or small areas of open water.

(6) The nature and precise locality of the Etendeka quartz latite eruptive centres is unknown. The quartz latites of the Tafelberg and Interbedded Coastal succession thicken towards the south-west and were probably erupted from centres to the west of the present coast line. However, the Springbok quartz latites thicken in a southerly direction and there is a strong possibility that they may be associated with the intrusive complexes of Brandberg, Messum and/or Cape Cross.

CHAPTER 9

SYNTHESIS

9.1 CONCLUSIONS

This chapter summarises the findings of this study and includes a brief discussion on the geodynamics of the Etendeka volcanics and their relationship to continental break up. A final section indicates areas where future research would be valuable.

The main conclusions regarding the nature and origin of the Etendeka quartz latites are presented below:

(1) The quartz latites occur as voluminous (80 - 800 km^3), widespread (up to 4500 km^2) sheet-like units which form a significant (> 25 %) proportion of the Etendeka lava sequence. They are sparsely (< 10%) porphyritic with phenocrysts of plagioclase, pyroxene and titanomagnetite which are evenly distributed throughout the flow units. Major element compositions are very similar in different groups of quartz latites and individual units have extremely uniform compositions both vertically and laterally. High temperatures (1000 - 1100 °C) and low water contents (< 1%) in the quartz latites are suggested by high pyroxene equilibration temperatures, An-rich plagioclase compositions, sparse phenocrysts and an absence of hydrous phases.

(2) The southern Etendeka quartz latites are interpreted as minimum, or first generated, partial melts of mid- to lower-crustal material of basic to intermediate composition. Melting occurred at depths of 30 - 35 km (8 - 10 kb) and was probably induced by the underplating or ponding of basalt within the lower crust. The major and trace element and isotopic (Sr and O) composition of the southern Etendeka quartz latites indicates that they underwent little mixing or interaction with basaltic magma, and precludes their derivation from a basaltic precursor, either by simple closed system fractional crystallisation or by differentiation and crustal contamination.

Phenocryst compositions indicate that magmatic differentiation could not be responsible for the apparent "evolution" in the whole rock compositions within the Tafelberg/Interbedded Coastal quartz latite trend. However, limited compositional variations displayed by individual groups of quartz latite units, such as the Springbok and Upper Interbedded Coastal quartz latites, are probably

the result of small degrees of fractional crystallisation. It is suggested that the compositional differences between different groups of quartz latite units are largely due to slight variations in the composition of the source, its mineralogy and the degree of melting.

(3) The Sarusas quartz latites are interpreted as minimum partial melts produced under similar conditions to those which produced the southern Etendeka, quartz latites. Simple trace element modelling indicates that these quartz latites are not the product of partial melting of underplated Khumib-type basalt, as might be implied from their trace element and isotopic characteristics. It is suggested that the trace element "enriched" character of the Sarusas quartz latites may have been inherited from an enrichment of their lower crustal source regions, possibly by processes similar to those which are thought to have affected the mantle source regions of the Khumib basalts.

(4) The compositional homogeneity of the quartz latites, coupled with their high temperature and low viscosity, suggests that rapid convection and mixing prevented the evolution of a thermally and compositionally stratified magma chamber prior to eruption.

(5) The quartz latites are considered to have erupted as dense, high-temperature ash flows which underwent en masse lava-like flowage during their final emplacement (i.e. they are rheoignimbrites). A combination of high eruption temperatures and calculated viscosities of 10^5 Poise (comparatively low for magmas involved in pyroclastic eruptions) help to explain the often completely welded, homogeneous textures encountered at most outcrops. The extraordinary mobility of the quartz latite ash flows suggests that they descended from high eruption columns (possibly 10 - 13 km high) which were generated by very high volume rates of magma eruption.

(6) Post-depositional cooling was accompanied by devitrification, joint formation and localised phreatic activity. Devitrification of the central portions of the flow occurred at high temperature (600 - 800 °C) and was accompanied by granophyric groundmass crystallisation and the alteration of plagioclase and pyroxene. Titanomagnetite oxidation textures indicate increased temperatures towards the centre of the flow, and are most strongly developed in the upper and lower portions of the flow. The central part of the flow is relatively unoxidised.

(7) The composition of both pitchstone and devitrified quartz latite have been affected by secondary alteration. A combination of low concentrations of K_2O, high LOI and gross $^{18}O/^{16}O$ disequilibrium between whole rock/mineral pairs in the pitchstone implies a low-temperature (~ 50 °C) hydration event. The apparent loss of CaO, Na_2O and Sr in the devitrified quartz latites is related to the alteration of plagioclase and pyroxene, probably at quite high temperatures.

9.2 CONCLUDING REMARKS

Despite the interbedding of quartz latites with basalt throughout the Etendeka-Paraná lava succession, there is a tendency for the proportion of quartz latite to increase not only in the upper part of the succession (Bellieni *et al.*, 1984 and 1986), but also towards the continental margins (Milner and Duncan, 1987; Bellieni *et al.*, 1986). This distribution suggests that there was a progressive build up to quartz latite magmatism and that this magmatism was more strongly developed in the central part of the South Atlantic rift zone.

A model depicting the possible relationship between the Etendeka-Paraná volcanism and continental break up is illustrated in Fig. 9.1. Extension and the upwelling of hot, asthenospheric material induces partial melting in the lithospheric mantle generating basaltic magma. This basaltic liquid migrates upwards, both penetrating the crust to be erupted as lavas and ponding at the base of the crust to cause partial melting and the generation of quartz latite melt. At the onset of volcanism the crust is relatively cool and is easily penetrated by basaltic magma, hence the lower portion of the succession is dominated by basaltic lavas. However, as heating and partial melting of the lower crust intensifies, an increase in the density contrast between the basaltic liquid and the overlying continental crust causes a larger degree of underplating. This in turn results in large scale melting of the lower crust and the eruption of proportionately more quartz latite magma. The paucity of basalt in sequences such as the Interbedded Coastal succession may be due to a combination of preferential underplating and an inability to propagate dykes and fissures through the partially molten quartz latite source regions. Contemporaneous basaltic volcanism does however, occur at the margins of the silicic centres, thereby explaining the interfingering of basalt and quartz latite units in the reconstruction of Milner and Duncan (1987).

Fig. 9.1 Schematic model relating the Etendeka and Parana magmatism to continental rifting.

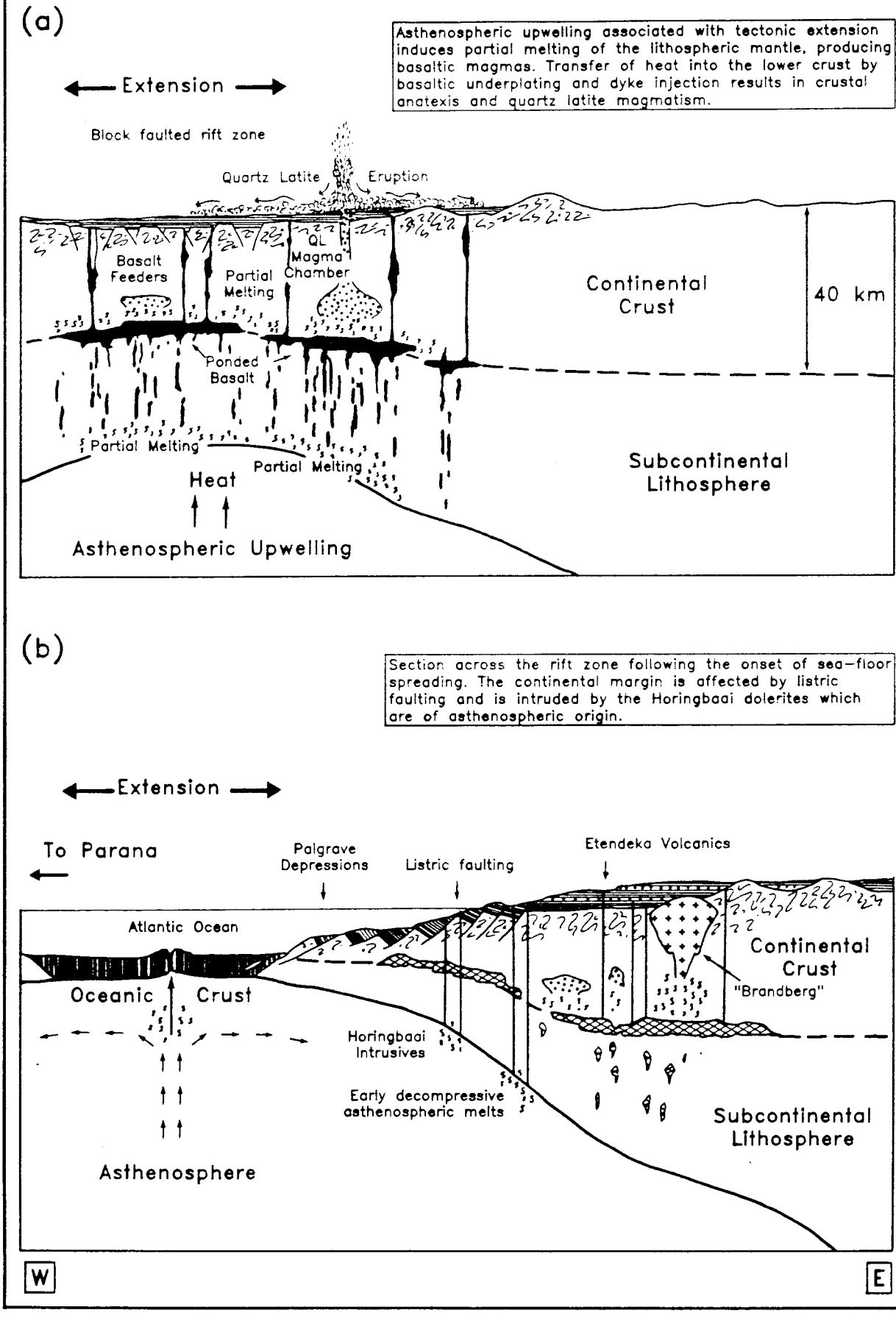

Continental break-up, with the development of listric faulting along the margin of the new continent, is accompanied by a change to more asthenospheric magmatism in the rift zone, with the late-stage emplacement of the basic Horingbaai intrusives (Erlank *et al.*, 1984) and the onset of plate separation. Continental magmatism becomes more alkaline in character with the intrusion of alkali granite (e.g. Brandberg), syenite (e.g. Okonjeje) and carbonatite (e.g. Okorusu), some of which may have intruded earlier quartz latite eruptive centres.

9.3 FUTURE RESEARCH

The opportunities for future research in the Etendeka region are considerable and investigations should be carried out to further constrain the nature of magmatism associated with continental break-up and of the processes which have affected the volcanics. The following key areas of research requiring attention have been identified:

(1) Determination of the precise nature and origin of the composite basalt-quartz latite "cooling unit" in the Springbok succession (section 2.5).

(2) The distribution and stratigraphy of the Gobobosebberge lavas (Fig. 2.1) and a geochemical characterisation and comparison of the quartz latites which are known to occur in this lava sequence with those which crop out in the southern Etendeka (Fig. 2.2).

(3) The geological, geochemical and geochronological relationships between the Etendeka volcanics and the late-Karoo complexes (e.g. Brandberg and Messum) which intrude them.

(4) A study of quartz latite flow directions and isopachs in order to get a better indication of the locality of their eruptive centres.

(5) Quantitative modelling of the secondary alteration processes affecting the lavas. Particular attention should be paid to the geochemical and mineralogical changes during the alteration of pitchstone and to the origin of the secondary quartz-zeolite-calcite mineralisation.

(6) More detailed isotopic and modelling studies of the Sarusas acid volcanics

in order to try and define their source characteristics more clearly. In particular to investigate the possibility that these volcanics were derived from a lower crust which had been metasomatically enriched.

(7) A detailed comparison of the Etendeka and Paraná stratigraphies and an attempt to make direct geochemical correlations using the techniques employed in this thesis. Although data for the Paraná have become available in the last few years, this comparison is beyond the scope of this thesis.

REFERENCES CITED

AHRENDT, H., BEHR, H.J., CLAUER, N., and WEBER, K. (1983). K/Ar age determinations of the northern Damara branch and their implications for the structural and metamorphic evolution of the Damara Orogen, South West Africa/Namibia. *Spec. Publ. Geol. Soc. S. Afr.*, 11, 299 - 306.

AKIMOTO, S. and KATSURA, T. (1959). Magneto-chemical study of the generalised titanomagnetite in volcanic rocks. *J. Geomag. Geoelectricity*, 3, 69 - 90.

ALBEE, A.L. and RAY, L. (1970). Correction factors for electron probe microanalysis of silicates, oxides, carbonates, phosphates and sulphates. *Anal. Chem.*, 42, 1408 - 1414.

ALLSOPP, H.L., BRISTOW, J.W., LOGAN, C.T., EALES, H.V., and ERLANK, A.J. (1984a). Rb-Sr geochronology of three Karoo-related intrusive complexes. *Spec. Publ. Geol. Soc. S. Afr.*, 13, 281 - 287.

-----, MANTON, W.I., BRISTOW, J.W., and ERLANK, A.J. (1984b). Rb-Sr geochronology of Karoo felsic volcanics. *Spec. Publ. Geol. Soc. S. Afr.*, 13, 273 - 280.

ARTH, J.G. (1976). Behaviour of trace elements during magmatic processes - a summary of theoretical models and their applications. *J. Res. U.S. Geol. Surv.*, 4, 41 - 47.

BACON, C.R. (1977). High temperature heat content and heat capacity of silicate glasses: Experimental determination and a model for calculation. *Amer. J. Sci.*, **277**, 109 - 135.

BELLIENI, G., BROTZU, P., COMIN-CHIARAMONTI, P., ERNESTO, M., MELFI, A., PACCA, I.G., and PICCIRILLO, E.M. (1984). Flood basalt to rhyolite suites in the southern Paraná Plateau (Brazil): Palaeomagnetism, petrogenesis and geodynamic implications. *J. Petrology*, **25**, 579 - 618.

-----, COMIN-CHIARAMONTI, P., MARQUES, L.S., MELFI, A.J., NARDY, A.J.R., PAPATRECHAS, C., PICCIRILLO, E.M., ROISENBERG, A., and STOLFA, D. (1986). Petrogenetic aspects of acid and basaltic lavas from the Paraná Plateau (Brazil): Geological, mineralogical and petrochemical relationships. *J. Petrology*, **27**, 915 - 944.

BERGH, H.W. (1987). Underlying fracture zone nature of Astrid ridge off Antarctica's Queen Maud Land. *J. Geophys. Res.*, **21**, 475 - 484.

BENCE, A.E. and ALBEE, A.L. (1969). Empirical correction factors for the electron microanalysis of silicates and oxides. *J. Geol.*, **76**, 382 - 403.

BETTON, P.J. (1978). Geochemistry of Karoo volcanic rocks in Swaziland. *D. Phil. Thesis (unpubl.), Univ. Oxford*, 287pp.

BLÜMEL, W.-D., EMMERMANN, R. and HÜSER, K. (1979). Der Erongo. Geowissenschaftliche Beschreibung und Deutung eines Südwestafrikanischen Vulkankomplexes. *Scient. Res. SWA Ser., S.W.Afrika Scient. Soc.*, **16**, 140pp.

BONNICHSEN, B. (1982). The Bruneau-Jarbridge eruptive center, south-western Idaho. *In* BONNICHSEN, B., and BRECKENRIDGE, R.M. (eds.). Cenozoic geology of Idaho: Idaho Bureau of Mines and Geology Bulletin, **26**, 237 - 254.

-----, and CITRON, G.P. (1982). The Cougar Point Tuff, south-western Idaho and vicinity. *In* BONNICHSEN, B., and BRECKENRIDGE, R.M. (eds.). Cenozoic geology of Idaho: Idaho Bureau of Mines and Geology Bulletin, **26**, 255 - 281.

-----, and KAUFFMAN, D.F. (1987). Physical features of rhyolite lava flows in the Snake River Plain volcanic province, south-western Idaho. *Geol. Soc. Amer. Spec. Paper*, **212**, 119 - 145.

BORTHWICK, J. and HARMON, R.S. (1982). A note regarding ClF_3 as an alternative to BrF_5 for oxygen isotope analysis. *Geochim. Cosmochim. Acta*, **46**, 1665 - 1668.

BOTTINGA, Y. and WEILL, D.F. (1972). The viscosity of magmatic silicate liquids: A model for calculation. *Amer. J. Sci.*, **272**, 438 - 475.

BREMNER, J.M. (1977). Sediments on the continental margin off South West Africa between latitudes 17° and 25° S. *Ph.D. Thesis (unpubl.), Univ. Cape Town*, 300pp.

BRISTOW, J.W. (1985). The Jozini Rhyolites: A new type of pyroclastic rock. *Univ. Natal. Geol. Dept. Spec. Publ.*, **1**, 31 - 37.

-----, ALLSOPP, H.L., ERLANK, A.J., MARSH, J.S. and ARMSTRONG, R.A. (1984). Strontium isotope characterisation of Karoo volcanic rocks. *Spec. Publ. Geol. Soc. S. Afr.*, **13**, 295 - 329.

----- and CLEVERLY, R.W. (1979). Volcanology of the Lebombo rhyolites. *Geocongr. 79, Geol. Soc. S. Afr.*, 60 - 63.

BRYAN, W.B., FINGER, L.W. and CHAYES, F. (1969). Estimating proportions in petrologic mixing equations by least squares approximation. *Science*, **163**, 926 - 927.

BUDDINGTON, A.E. and LINDSLEY, D.H. (1964). Iron-titanium oxide minerals and synthetic equivalents. *J. Petrology*, **5**, 310 - 357.

BURGER, A.J., CLIFFORD, T.N. and MILLER, R.McG. (1976). Zircon U-Pb ages of the Franzfontein Granitic Suite, northern South West Africa. *Precambrian Res.*, **3**, 415 - 431.

BURNHAM, C.W. (1975). Water and Magmas: a mixing model. *Geochim. Cosmochim. Acta*, **39**, 1077 - 1084.

----- (1981). The nature of multicomponent aluminosilicate melts. *In* RICKARD, D.T. and WICKMAN, F.E. (eds). Chemistry and geochemistry of solutions at high-temperatures and pressures. *Phys. Chem. Earth*, **13/14**, 187 - 229.

CARMICHAEL, I.S.E. (1979). Glass and the glassy rocks. *In* YODER, H.S., Jr., (ed). The evolution of the igneous rocks. Princeton Univ. Press, Princeton, N.J., 233 - 244.

CERLING, T.E., BROWN, F.H. and BOWMAN, J.R. (1985). Low temperature alteration of volcanic glass: Hydration, Na, K, ^{18}O and Ar mobility. *Chem. Geol.*, **52**, 281 - 293.

CHAPIN, C.E. and ELSTON, W.E. (eds.) (1979). Ash-Flow Tuffs. *Geol. Soc. Amer. Sp. Paper*, **180**, pp211.

CLAYTON, R.N. and MAYEDA, T.K. (1963). The use of bromine pentafluoride in the extraction of oxygen from oxides and silicates for isotope analysis. *Geochim. Cosmochim. Acta*, **27**, 43 - 52.

CLEMENS, J.D. and VIELZEUF, D. (1987). Constraints on melting and magma production in the crust. *Earth Planet. Sci. Lett.*, **86**, 287 - 306.

CLEVERLY, R.W. (1977). The structural and magmatic evolution of the Lebombo Monocline, southern Africa, with particular referrence to Swaziland. *D. Phil. Thesis (unpubl.), Univ. Oxford*, 316pp.

-----, BETTON, P.J. and BRISTOW, J.W. (1984). Geochemistry and petrogenesis of the Lebombo rhyolites. *Spec. Publ. Geol. Soc. S. Afr.*, **13**, 171 - 194.

----- and BRISTOW, J.W. (1979). Revised volcanic stratigraphy of the Lebombo Monocline. *Trans. Geol. Soc. S. Afr.*, **82**, 227 - 230.

COX, K.G. (1983). The Karoo Province of southern Africa: Origin of trace element enrichement patterns. *In* HAWKESWORTH, C.J. and NORRY, M.J. (eds). Continental basalts and mantle xenoliths. Shiva, UK, 139 - 157, 272pp.

-----, DUNCAN, A.R., BRISTOW, J.W., TAYLOR, S.R. and ERLANK, A.J. (1984). Petrogenesis of the basic rocks of the Lebombo. *Spec. Publ. Geol. Soc. S. Afr.*, **13**, 149 - 169.

-----, JOHNSON, R.L., MONKMAN, L.J., STILLMAN, C.J. and VAIL, J.R. (1965). The geology of the Nuanetsi igneous province. *Phil. Trans. R. Soc. Lond.*, **257**, 71 - 218.

-----, MACDONALD, R. and HORNUNG, G. (1967). Geochemical and petrographic provinces in the Karoo basalts of southern Africa. *Amer. Mineral.*, **52**, 1451 - 1474.

DA SILVA, A.T.S.F., TORQUATO, J.R. and KANASHITA, K. (1975). Algunas dadas geocronologicos pelo metodo K/Ar du regiao de vila Piava Couceiro, Quitengres e Chicomba (Angola). *Bulm. Servs. Geol. Min. Angola*, **24**, 29 - 46.

DE CARUALLIO, H. (1970). Contribution à la géo-chronologie du sudouest de 1'Angola. *Bulm. Servs. Geol. Min.. Angola,* **19**, 23 - 35.

DEER, W.A., HOWIE, R.A. and ZUSSMAN, J. (1963). Rock forming minerals. Vol. 4, Framework Silicates. John Wiley and Sons, Inc., New York. 435pp.

-----, HOWIE, R.A. and ZUSSMAN, J. (1966). An introduction to the rock forming minerals. Longman, London. 528pp

DE LA ROCHE, H., LETERRIER, J., GRANDCLAUDE, P. and MARCHAL, M. (1980). A classification of volcanic and plutonic rocks using R_1 - R_2 diagram and

major-element analyses. Its relationship with current nomenclature. *Chem. Geol.*, **29**, 183 - 210.

DE PAOLO, D.J. (1981). Trace element and isotopic effects of combined wall-rock assimilation and fractional crystallisation. *Earth Planet. Sci. lett.*, **53**, 189 - 202.

DE WIT, M.J., JEFFREY, M., BERGH, H.W. and NICOLAYSEN, L.O. (1988). Geological map of sectors of Gondwanaland (Reconstituted to their disposition ~ 150 Ma). *American Association of Petroleum Geologists and the University of Witwatersrand.*

DIXON, W.J., BROWN, M.B., ENGELMAN, L., FRANE, J.W., HILL, M.A., JENNRICH, R.I. and TOPOREK, J.D. (1981). BMDP statistical software. *Univ. of California Press, Berkeley,* 785pp.

DUNCAN, A.R. (1987). The Karoo Igneous Province - a problem area for inferring tectonic setting from basalt geochemistry. *J. Volcanol. Geotherm. Res.*, **32**, 13 - 34.

-----, ERLANK, A.J. and MARSH, J.S. (1984). Regional geochemistry of the Karoo Igneous Province. *Spec. Publ. Geol. Soc. S. Afr.*, **13**, 355 - 388.

-----, ERLANK, A.J. and BETTON, P.J. (1984a). Appendix 1. Analytical techniques and database descriptions. *Spec. Publ. Geol. Soc. S. Afr.*, **13**, 389 - 395.

EALES, H.V., MARSH, J.S. and COX, K.G. (1984). The Karoo Igneous Province: An introduction. *Spec. Publ. Geol. Soc. S. Afr.*, **13**, 1 - 26.

EKREN, E.B., McINTYRE, D.H. and BENNETT, E.H. (1984). High-temperature large-volume, lavalike ash-flow tuffs without calderas in southwestern Idaho. *Prof. Pap. US. Geol. Surv.*, **1272**, 1 - 73.

ERLANK, A.J. (ed) (1984). Petrogenesis of the volcanic rocks of the Karoo Province. *Spec. Publ. Geol. Soc. S. Afr.*, **13**, 395pp.

-----, MARSH, J.S., DUNCAN, A.R., MILLER, R.McG., HAWKESWORTH, C.J., BETTON, P.J., and REX, D.C. (1984). Geochemistry and petrogenesis of the Etendeka volcanic rocks from SWA/Namibia. *Spec. Publ. Geol. Soc. S. Afr.*, **13**, 195 - 245.

EWART, A. (1979). A review of the mineralogy and chemistry of Tertiary-Recent

dacitic, latitic, rhyolitic and related salic volcanic rocks. *In* BARKER, F. (ed). Trondjemites, dacites and related rocks. Elsevier, New York, 13 - 121.

FISHER, R.V. and SCHMINCKE, H.-U. (1984). Pyroclastic rocks. Springer-Verlag, Berlin, 472pp.

FITCH, F.J. and MILLER, J.A. (1984). Dating Karoo igneous rocks by the conventional K-Ar and $^{40}Ar/^{39}Ar$ age spectrum methods. *Spec. Publ. Geol. Soc. S. Afr.*, **13**, 247 - 266.

FRETS, D.C. (1969). Geology and structure of the Huab-Welwitschia area, South West Africa. *Precambrian Res. Unit, Bull. 5*, Univ. Cape Town, 235pp.

GHIORSO, M.S. and CARMICHAEL, I.S.E. (1980). A regular solution model for metaluminous silicate liquids: Applications to geothermometry, immiscibility and the source regions of basic magma. *Contib. Minerl. Petrol.*, **71** 323 - 342.

-----, CARMICHAEL, I.S.E., RIVERS, M.L. and SACK, R.O. (1983). The Gibbs free energy of mixing of natural silicate liquids; an expanded regular solution approximation for the calculation of magmatic intensive variables. *Contrib. Mineral. Petrol.*, **84**, 107 - 145.

GIDSKEHAUG, A., CREER, K.M. and MITCHELL, J.G. (1975). Palaeomagnetism and K/Ar ages of the South West African basalts and their bearing on the time of initial rifting of the South Atlantic. *Geophys. J. R. astr. Soc.*, **42**, 1 - 20.

GLAZNER, A.F. (1984). Activities of olivine and plagioclase components in silicate melts and their application to geothermometry. *Contrib. Mineral. Petrol.*, **88**, 260 - 268.

GREEN, R.W.E. (1983). Seismic refraction observations in the Damaran Orogen and flanking craton and their bearing on deep-seated processes in the orogen. *Spec. Publ. Geol. Soc. S. Afr.*, **11**, 355 - 367.

HAACK, U., HOEFS, J. and GOHN, E. (1983). Genesis of Damaran granites in the light of Rb/Sr and $d^{18}O$ data. *In* MARTIN, H. and EDER, F.W. (eds). Intracontinental fold belts. Springer-Verlag, Berlin, 847 - 872.

HAGGERTY, S.E. (1976). Oxidation of opaque mineral oxides in basalts.

Reviews in Mineralogy, 3, Hg1 - Hg100.

----- (1976). Opaque mineral oxides in terrestrial igneous rocks. *Reviews in Mineralogy*, 3, Hg101 - Hg300.

HANSON, G.N. (1978). The application of trace elements to the petrogenesis of igneous rocks of granitic composition. *Earth Planet. Sci. Lett.*, **38**, 26 - 43.

HARMER, R.H., EGLINGTON, B.M., FARROW, D., BUTCHER, A.R., AURET, J.M., STANDER, Y.Y. and GROSSER, E. (1986). Manual of laboratory procedures for isotope analysis. Geochronology Division, National Physical Research Laboratory, CSIR, PRETORIA.

HARRIS, C. SMITH, H.S., MILNER, S.C., ERLANK, A.J., DUNCAN, A.R. and MARSH, J.S. (1988). Evidence of gross oxygen isotope disequilibrium in Karoo lavas of the Etendeka Formation of Namibia. *Paper submitted for publication*.

HAWKESWORTH, C.J., GLEDHILL, A.R., RODDICK, J.C., MILLER, R.McG. and KRÖNER, A. (1983). Rb-Sr and $^{40}Ar/^{39}Ar$ studies bearing on models for the thermal evolution of the Damara belt, Namibia. *Spec. Publ. Geol. Soc. S. Afr.*, 11, 323 - 338.

-----, MANTOVANI, M.S.M., PEATE, D., WRIGHT, D.W., PALACZ, Z. and van CALSTEREN, P.W. (1987). Magmatic processes in the Paraná. *Terra Cognita*, 7, 611.

-----, MARSH, J.S., DUNCAN, A.R., ERLANK, A.J. and NORRY, M.J. (1984). The role of Continental lithosphere in the generation of the Karoo volcanic rocks: Evidence from combined Nd- and Sr-isotopic studies. *Spec. Publ. Geol. Soc. S. Afr.*, **13**, 341 - 354.

----- and MARLOW, A.G. (1983). Isotopic evolution of the Damara orogenic belt. *Spec. Publ. Geol. Soc. S. Afr.*, **11**, 397 - 407.

HAY, R.L., HILDRETH, W. and LAMBE, R.N. (1979). Globule ignimbrite of Mount Suswa, Kenya. *Geol. Soc. Amer. Sp. Paper*, **180**, 167 - 175.

HEUBNER, J.S. (1980). Pyroxene phase equilibria at low pressure. *Reviews in Mineralogy*, 7, 213 - 280.

HILDRETH, W. (1979). The Bishop Tuff: Evidence for the origin of compositional

zonation in magma chambers. *Geol. Soc. Amer. Sp. Paper,* **180**, 43 - 75.

----- (1981). Gradients in silicic magma chambers: Implications for lithospheric magmatism. *J. Geophys. Res.*, **86**, 10153 - 10192.

HODGSON, F.D.I. (1970). The geology of the Karroo system in the southern Kaokoveld, South West Africa. *Proceedings and papers of the second Gondwana syposium*, 233 - 235.

----- and BOTHA, B.J.V. (1976). Notes on the Cretaceous volcanism in the area north-west of the Doros Complex, South West Africa. *Ann. Geol. Surv. Dep. Min. S. Afr.*, **11**, 135 - 136.

HUPPERT, H.E. and SPARKS, R.S.J. (1987). The fluid dynamics of crustal melting by injection of basaltic sills (abstract). *R. Soc. Lond./Edinburgh., Conference on "The Origin of Granites"*, 49.

JOHANNES, W. (1983). Metastable melting in granite and related systems. *In* ATHERTON, M.D. and GRIBBLE, C.D. (eds). Migmatites, melting and metamorphism. Shiva, UK, 326pp, 27 - 36.

JOHNSON, R.W. (1968). Volcanic globule rock from Mount Suswa, Kenya. *Geol. Soc. Amer. Bull.*, **79**, 647 - 652.

KORN, H. and MARTIN, H. (1954). The Messum Igneous Complex in South West Africa. *Trans. Geol. Soc. S. Afr.*, **57**, 83 - 124.

KYSER, T.K. (1986). Stable isotope variations in the mantle. *Reviews in Mineralogy*, **16**, 141 - 164.

LANGMUIR, C.H., VOCKE, R.D. Jr, HANSON, G.N. and HART, S.R. (1978). A general mixing equqtion with applications to Icelandic basalts. *Earth Planet. Sci. Lett.*, **37**, 380 - 392.

LE MAITRE, R.W. (1976). The chemical variability of some common igneous rocks. *J. Petrology*, **17**, 589 - 598.

----- (1981). GENMIX - A generalised petrological mixing model program. *Comp. Geosciences*, **7**, 229 - 247.

LINDSLEY, D.H. (1976). The crystal chemistry and structure of oxide minerals as exemplified by the Fe-Ti oxides. *Reviews in Mineralogy*, **3**, L1 - L52.

----- (1983). Pyroxene thermometry. *Amer. Mineral.*, **68**, 477 - 493.

----- and ANDERSEN, D.J. (1983). A two-pyroxene thermometer. *Proceedings of the 13th Lunar and Planetary Science Conference. Part 2. J. Geophys. Res.*, **88** supplement, A887 - A906.

LIPMAN, P.W. (1971). Iron-Titanium oxide phenocrysts in compositionally zoned ash-flow sheets from southern Nevada. *J. Geol.*, **79**, 438 - 456.

MARSH, J.S. and EALES, H.V. (1984). The chemistry and petrogenesis of igneous rocks of the Karoo central area, southern Africa. *Spec. Publ. Geol. Soc. S. Afr.*, **13**, 27 - 67.

MARTIN, H. (1973). The Atlantic matgin of southern Africa between latitude 17° south and the Cape of Good Hope. *In* NAIRN, A.E.M. and STEHLI, F.G. (eds). The ocean basins and margins, 1. The South Atlantic. Plenum Publ. Co., New York, 277 - 300.

-----, MATHIAS, M. and SIMPSON, E.S.W. (1960). The Damaraland sub-volcanic ring complexes in South West Africa. *Rep. Int. Geol. Cong. XXI Sess.*, **13**, 156 - 174.

McCALL, G.J.H. (1964). Froth flows in Kenya. *Geol. Rundsch.*, **54**, 1148 - 1195.

MILLER, R.McG. (1973). The Salem granite suite, South West Africa: Genesis by partial melting of Khomas schist. *Mem. Geol. Surv. S. Afr.*, **64**, 106pp.

----- (1983). The Pan-African Damara Orogen of South West Africa/Namibia. *Spec. Publ. Geol. Soc. S. Afr.*, **11**, 431 - 515.

----- (1988). Geological Map 2013 - Cape Cross, scale 1:250000. *Geol. Surv. S.W. Africa/Namibia.*

MILNER, S.C. (1986). The geological and volcanological features of the quartz latites of the Etendeka Formation. *Communs. Geol. Surv. S.W. Africa/Namibia*, **2**, 109 - 116.

----- and DUNCAN, A.R. (1987). Geochemical characterisation of quartz latite units in the Etendeka Formation. *Communs. Geol. Surv. S.W. Africa/Namibia*, **3**, (in press).

NAKAMURA, Y. and KUSHIRO, I. (1970). Equilibrium relations of hypersthene, pigeonite and augite in crystallizing magmas: Microprobe study of a pigeonite andesite from Wieselberg, Germany. *Amer. Mineral.*, **55**, 1999

- 2015.

NASH, P.W. and CRECRAFT, H.R. (1985). Partition coefficients for trace elements in silicic magmas. *Geochim. Cosmochim. Acta*, **49**, 2309 - 2322.

NORRISH, K. and HUTTON, J.T. (1969). An accurate X-ray spectrographic method for the analysis of a wide range of geological samples. *Geochim. Cosmochim. Acta.*, **33**, 431 - 453.

PEARCE, J.A. (1982). Trace element characteristics of lavas from destructive plate boundaries. *In* THORPE, R.S.(Ed). Andesites. Wiley & Sons, New York, N.Y., 525 - 548.

PECCERILLO, A. and TAYLOR, S.R. (1976) Geochemistry of Eocene calc-alkaline volcanic rocks from the Kastamonu area, northern Turkey. *Contrib. Mineral.Petrol.*, **58**, 63 - 81.

PODPORA, C. and LINDSLEY, D.H. (1979). Fe-rich pigeonites: Minimum temperatures of stability in the Ca-Mg-Fe quadrilateral (abstract). *EOS, (Trans. Amer. Geophys. Union)*, **60**, 420 - 421.

REUNING, E. (1929). Differentiation der Karroo-eruptiva im Südlichen Kaokofeld, Südwestafrika. *Cmpte. Rendu. Int. Geol. Congr.*, Vol II, **15**, 28 - 35.

----- and MARTIN, H. (1957). Die Par-Karroo-landschaft, die Karroo-sedimente und Karroo-eruptivgesteine des Südlichen Kaokofelds im Südwestafrika. *Neues. Jahrb. Minerl. Geol. Palaont.*, **91**, 193 - 212.

RIDLEY, I. (1971). The petrology of some volcanic rocks from the British Tertiary Province: The Islands of Rhum, Eigg, Canna and Muck. *Contrib. Mineral. Petrol.*, **32**, 251 - 266.

RITCHEY, J.L. (1980). Divergent magmas at Crater Lake, Oregon: Products of fractional crystallization and vertical zoning in a shallow water-undersaturated chamber. *J. Volcanol. Geotherm. Res.*, **7**, 373 - 386.

ROBINSON, P. (1980). The composition space of terrestrial pyroxenes - internal and external limits. *Reviews in Mineralogy*, **7**, 419 - 490.

ROSS, C.S. and SMITH, R.L. (1961). Ash-flow tuffs: their origin, geologic relations, and identification. *U.S. Geol. Surv. Prof. Paper*, **366**, 1 -

77.

ROSS, M. and HUEBNER, J.S. (1979). Temperature-composition relationships between naturally occurring augite, pigeonite and orthopyroxene at one bar pressure. *Amer. Mineral.*, **64**, 1133 - 1155.

SACS (SOUTH AFRICAN COMMITTEE FOR STRATIGRAPHY) (1980). Stratigraphy of South Africa. Part 1 (comp. L.E. KENT). Lithostratigraphy of the Republic of South Africa, South West Africa/Namibia, and the Republics of Bophuthatswana, Transkei and Venda. *Handbk. Geol. Surv. S. Afr.*, **8**, 690pp.

SCHMINCKE, H.-U. (1974). Volcanological aspects of peralkaline silicic welded ash-flow tuffs. *Bull. Volcanol.*, **38**, 594 - 636.

SCOTESE, C.R., LAWVER, L.A. and BERGH, H. (1988). *Tectonophysics*, (in press).

SEGOUFIN, J. (1978). Anomalies magnetique Mesozoiques dans le bassin de Mozambique. *C. R. Acad. Sci. Paris, Ser. D.*, **287**, 109 - 112.

SHAW, H.R. (1972). Viscosities of magmatic silicate liquids: an empirical method of prediction. *Amer. J. Sci.*, **272**, 870 - 893.

SHERIDAN, M.F. (1979). Emplacement of pyroclastic flows: a review. *Geol. Soc. Amer. Sp. Paper*, **180**, 125 - 136.

SIEDNER, G. (1965). Geochemical features of a strongly fractionated alkali igneous suite. *Geochim. Cosmochim. Acta*, **29**, 113 - 137.

----- and MILLER, J.A. (1968). K-Ar age determinations on basaltic rocks from South West Africa and their bearing on continental drift. *Earth Planet. Sci. Lett.*, **4**, 451 - 458.

----- and MITCHELL, J.G. (1976). Episodic Mesozoic volcanism in Namibia and Brazil: A K-Ar isochron study bearing on the opening of the South Atlantic. *Earth Planet. Sci. Lett.*, **30**, 292 - 302.

SMITH, J.V. (1983). Some chemical properties of feldspars. *Reviews in Mineralogy*, **2**, 281 - 296.

SMITH, R.L. (1960). Ash-flows. *Geol. Soc. Amer. Bull.*, **71**, 795 - 842.

----- and BAILEY, R.A. (1966). The Bandelier Tuff: A study of ash-flow eruption cycles from zoned magma chambers. *Bull. Volcanol.*, **29**, 83 - 104.

SPARKS, R.S.J. (1976). Grain size variations in ignimbrites and implications for the transport of pyroclastic flows. *Sedimentology*, **23**, 147 - 188.

----- and WILSON, L. (1976). A model for the formation of ignimbrite by gravitational column collapse. *J. Geol. Soc. Lond.*, **132**, 441 - 451.

-----, WILSON, L. and HULME, G. (1978). Theoretical modeling of the generation, movement and emplacement of pyroclastic flows by column collapse. *J. Geophys. Res.*, **83**, 1727 - 1739.

SPENCER, K.J. and LINDSLEY, D.H. (1981). A solution model for coexisting iron-titanium oxides. *American Mineralogist*, **66**, 1189 - 1201.

STORMER, J.C. (1983). The effects of recalculation on estimates of temperature and oxygen fugacity from analyses of multicomponent iron-titanium oxides. *American Mineralogist*, **68**, 586 - 594.

STRECKEISEN, A.L. (1979). Classification and nomenclature of volcanic rocks, lamprophyres, carbonatites and melilitic rocks: recomendations and suggestions of the IUGS Subcommision on the systematics of Igneous rocks. *Geology*, **7**, 331 - 335.

SWEENEY, R.J. (1988). Geochemistry of the Sabie River Basalt Formation in the central Lebombo, Karoo Igneous Province. *Ph.D. (submitted) Univ. Cape Town*, Vol 1, pp309.

TAYLOR, H.P. (1968). The oxygen isotope geochemistry of igneous rocks. *Contrib. Mineral. Petrol.*, **19**, 1 - 71.

TAYLOR, S.R. and McLENNAN, S.M. (1985). The continental crust: Its composition and evolution. Blackwell, Oxford, U.K., 312pp.

TWIST, D. (1984). Emplacement of voluminous silica lavas in the Bushveld Complex. *Abstr. 97th* annual meet. Geol. Soc. Amer., p679.

URBAIN, G., BOTTINGA, Y. and RICHET, P. (1982). Viscosity of liquid silica, silicates and alumino-silicates. *Geochim. Cosmochim. Acta*, **46**, 1061 - 1072.

VAN ZIJL, J.S.V. and DE BEER, J.H. (1983). Electrical structure of the Damara Orogen and its tectonic significance. *Spec. Publ. Geol. Soc. S. Afr.*, 11, 369 - 379.

WERNICKE, B. and BURCHFIEL, B.C. (1982). Modes of extensional tectonics. *J. Struct. Geol.*, **4**, 105 - 115.

WILLIAMS, H. (1942). The geology of Crater Lake National Park. *Carnegie Inst. Wash. Publ.*, **540**, 1 - 162.

WINKLER, H.G.F., BOESE, M. and MARCOPOULOS, T. (1975). Low-temperature granitic melts. *Neues. Jahrb. Minerl. Monatsh.*, **H.6**, 245 - 268.

-----, DAS, B.K. and BREITBART, R. (1977). Further data of low-temperature melts existing on the quartz + plagioclase + liquid + vapour isobaric cotectic surface within the system Qz-Ab-Or-An-H_2O. *Neues. Jahrb. Mineral. Monatsh.*, **H.6**, 241 - 247

WYLLIE, P.J. (1977). Crustal anatexis: An experimental review. *Tectonophysics*, **43**, 41 - 71.

APPENDIX 1

PETROGRAPHIC TYPE EXAMPLES

[A] INTRODUCTION

This appendix presents detailed petrographic descriptions of the principle types of quartz latites and latites documented in Chapter 3. The southern Etendeka quartz latites are described separately from the Sarusas quartz latites and latites and are subdivided into the groups outlined in Table 3.4. Where possible, representative examples of pitchstone and devitrified quartz latite are described for each group.

The bracketed figures in millimetres are approximations of mineral grain size, and in the case of lath or bladed shaped crystals refer to the long axis measurement. Percentage data refer to the approximate crystal content (volume %) and have been taken from Table 3.1, where point count data is presented for all the samples described below.

The terms magnetite and titanomagnetite are used interchangeably, although, the latter has been reserved for those samples where a positive identification has been made in reflected light.

[B] ETENDEKA QUARTZ LATITES

[B.1] Lower Springbok

SM-212 Is a porphyritic (~9 %) pitchstone with phenocrysts of plagioclase, pigeonite and titanomagnetite enclosed in a microlitic glass. The phenocrysts are gently rounded and commonly occur in glomeroporphyritic aggregates around which a flow banded texture is developed. Phenocrysts within the glomeroporphyritic aggregates often show an interlocking texture, with only those crystals on the outer edges of the aggregate showing good crystal faces. The plagioclase phenocrysts (0.2 - 4.5 mm) are blocky, subhedral crystals and may be weakly zoned, twinning is generally simple. Larger plagioclase phenocrysts are often sieve textured and may show repeated twinning. Fractured or broken crystals are occasionally observed. Pigeonite forms subhedral to anhedral grains (0.1 - 1.2 mm) which sometimes show simple twinning. Titanomagnetite occurs as subhedral to anhedral (0.1 - 0.5 mm) crystals which are essentially unaltered. Microlites (<0.03 mm) in the glass consist of magnetite, clinopyroxene and feldspar, the latter pair showing weak polarisation colours. Flow banding in the groundmass is caused by differences in abundance of microlites, the darker bands being particularly rich in a dusty opaque material. Accessory apatite occurs as sparse euhedral crystals often enclosed by the main phenocryst phases. Very little alteration is observed, although there is a slight rusty-brown discolouration of the glass around sparse vesicles and near the crystal aggregates.

SM-212A This sample is the devitrified equivalent of SM-212 with partially altered phenocrysts of plagioclase, pigeonite and magnetite set in a brown cryptocrystalline groundmass. Plagioclase shows considerable

alteration, taking on a rather turbid appearance. Pigeonite is altered to an amorphous green-brown material along cracks leaving cores of fresh pigeonite. Microlites of plagioclase and some opaque material can be recognised in the rather stained groundmass and faint grey polarising areas (~0.03 mm) probably represent the development of quartz and alkali-feldspar.

[B.2] Upper Springbok

SM-168 Is a porphyritic to microporphyritic pitchstone. Phenocrysts (~8 %) of plagioclase, hypersthene, pigeonite and titanomagnetite commonly form glomeroporphyritic clusters. The intergrowth of phenocrysts in such clusters is not as well developed as that observed in SM-212. Plagioclase phenocrysts (0.25 - 3.0 mm) form blocky subhedral to euhedral crystals with fairly sharp crystal faces. The majority of these phenocrysts exhibit simple twinning although repeated twinning is occasionally observed, particularly in sieve-textured crystals. Compositional zonation in plagioclase phenocrysts is slight. Phenocrysts of hypersthene (0.3 - 1.5 mm) have a blocky, subhedral morphology and are characteristically rimmed by pigeonite. These pigeonite coronas are commonly complete, but are notably absent where hypersthene is closely intergrown with plagioclase or magnetite. Pigeonite phenocrysts occur as sparse, subhedral to euhedral grains (0.2 - 1.0 mm). Phenocrysts of titanomagnetite occur as subhedral to anhedral grains (0.25 - 0.5 mm) which are gently rounded and show little sign of alteration. Microphenocrysts (~19 %) of plagioclase, clinopyroxene and titanomagnetite are evenly distributed throughout the rock. Plagioclase forms stubby subhedral to euhedral laths (0.1 - 0.3 mm) and clinopyroxene occurs as grains and laths (0.05 - 0.3 mm) with a pigeonitic composition (Chapter 5). Titanomagnetite occurs as subhedral equant grains (<0.05 mm) which are unaltered. The microlitic glassy groundmass shows incipient devitrification with the development of buff-coloured, slightly anisotropic spots (~0.25 mm).

SM-172 Is a porphyritic to microporphyritic pitchstone, similar to SM-168, with phenocrysts (~12 %) of plagioclase, pigeonite and titanomagnetite enclosed in a banded microlitic glass. The phenocrysts are slightly rounded and commonly form glomeroporphyritic aggregates (Plate 3.1c). Plagioclase phenocrysts (0.25 - 2.5 mm) generally have a blocky, subhedral to eu-hedral habit, although large (8.0 mm), complicated sieve-textured aggregates are also observed. Twinning is normally simple although repeated twinning is common in sieve textured crystals. Pigeonite phenocrysts (0.2 - 1.0 mm) occur as blocky, occasionally tabular, subhedral crystals. Phenocrysts of titanomagnetite (0.1 - 0.7 mm) form subhedral grains and are essentially unaltered. Microphenocrysts (~14 %) of plagioclase, clinopyroxene and titanomagnetite are similar in nature to those discussed for SM-168. Banding in the groundmass is due to a varying abundance of microphenocrysts and microlites (Plate 3.1c). Buff coloured spots in the glass indicate incipient devitrification and are more common where the microphenocryst and microlite density is greatest. Glass within the glomeroporphyritic aggregates and the sieve textured plagioclase crystals is often a buff to brown colour and has distinctive acicular microlites with few microphenocrysts.

SM-220A This sample is a devitrified equivalent of the two pitchstone samples described above and has a granophyric to micrographic textured groundmass and severely altered phenocrysts and microphenocrysts of plagioclase, pyroxene and magnetite. Plagioclase has a turbid appearance and most of the pyroxene is pseudomorphed by serpentine, carbonate and zeolite, although sparse relatively unaltered pigeonite phenocrysts are observed. Magnetite commonly shows diffuse oxidised rims. The microphenocrysts tend to be obscured by the groundmass texture. The groundmass is composed of a delicate, rather turbid intergrowth of quartz and alkali-feldspar.

[B.3] Lower Tafelberg

SM-179 Is a sparsely porphyritic (~3 %) pitchstone with phenocrysts of plagioclase and titanomagnetite in a densely microlitic glass. Abrupt changes in microlite orientation and density, and broken plagioclase crystals against such boundaries indicate that this is probably a welded clastic rock. Plagioclase phenocrysts (0.1 - 0.5 mm) occur as blocky, euhedral simply twinned crystals with clearly defined crystal faces. Occasional repeatedly-twinned, sieve-textured plagioclase crystals also occur and a single large (8.0 mm), zoned and broken plagioclase crystal has also been observed. Titanomagnetite phenocrysts (0.075 - 0.3 mm) occur as subhedral, gently rounded grains. In reflected light they have a fairly uniform composition, although some of the larger phenocrysts have a lobate texture mimicking the fracture pattern which is indicative of incipient maghemitisation. Microlites of pyroxene and feldspar vary between 0.05 and 0.5 mm in length and are of the order 0.02 mm wide; equant grains of an opaque phase are less than 0.01 mm in diameter. A modal analysis of the groundmass gives microlite abundances of 20 % pyroxene, 9 % feldspar and 4.5 % opaque. Alteration in the glass is only observed along small fractures and round sparse quartz amygdales where it shows an orange-brown coloured staining.

SM-196 Is sparsely porphyritic to moderately microporphyritic with a devitrified groundmass. Phenocrysts (~3 %) of altered plagioclase and titanomagnetite tend to occur in small glomeroporphyritic clusters. Microphenocrysts (~13 %) of plagioclase, clinopyroxene and titanomagnetite occur in the groundmass and are evenly distributed throughout. Plagioclase phenocrysts (0.25 - 1.0 mm) occur as blocky subhedral to euhedral crystals and show moderate alteration to sericite and carbonate. Phenocrysts of titanomagnetite (0.15 - 0.6 mm) occur as subhedral grains with red oxidised rims. In reflected light these titanomagnetites are partially altered to hematite and show incipient oxidation exsolution of ilmenite lamellae (Plate 3.6). Plagioclase microphenocrysts (0.05 - 0.2 mm) have a subhedral to euhedral, stubby lath shaped morphology and are occasionally altered. Microphenocrysts of clinopyroxene occur as equant grains (0.05 - 0.1 mm) and slightly longer bladed crystals (<0.3 mm) which often exhibit a greenish alteration. Titanomagnetite microphenocrysts (0.025 - 0.05 mm) occur as subhedral equant grains, and are altered in a similar manner to the phenocrysts. The groundmass consists of brown spherulitic masses which exhibit a radial arrangement of opaque needle-like fibres at their outer margins; under crossed polars the spherulites have an indistinct radial anisotropy. Between these spherulitic areas, a granophyric intergrowth

of quartz and alkali-feldspar is developed.

[B.4] Middle Tafelberg

SM-060 Is a porphyritic to microporphyritic seriate textured pitchstone with a densely microlitic, sparsely vesicular, glassy groundmass. Phenocrysts of plagioclase, hypersthene and titanomagnetite occasionally form glomeroporphyritic aggregates with interlocking textures. Microphenocrysts are of plagioclase, clinopyroxene and titanomagnetite. Plagioclase (~6 %) occurs as euhedral, blocky phenocrysts and microphenocryst laths with a continuous range of sizes (0.2 - 1.5 mm). Twinning is generally simple. Hypersthene phenocrysts (0.5 %) have a subhedral to euhedral, blocky to bladed morphology (0.1 - 3.5 mm). Long bladed crystals often partially or completely enclose small plagioclase and titanomagnetite phenocrysts. Titanomagnetite phenocrysts(0.2 - 0.4 mm) occur as unaltered, subhedral grains. Microphenocrysts of clinopyroxene (~3 %) occur as subhedral grains and laths (0.1 - 0.3 mm). Titanomagnetite microphenocrysts occur as subhedral to euhedral grains (<0.05 mm), which occasionally show signs of maghemitisation along cracks. Bladed crystals of all kinds exhibit a crude sub-trachytic texture. The groundmass is composed of a dense mat of branching, dark, non-polarising microlites which are uniformly distributed and show no preferred orientation. Glass alteration is slight and only occurs along fractures leading to and from quartz and zeolite amygdales.

[B.5] Upper Tafelberg

SM-059 Is non-porphyritic and consists of microphenocrysts (~22 %) of plagioclase, clinopyroxene and magnetite in a devitrified groundmass. Microphenocrysts of plagioclase (0.2 - 1.0 mm) occur as stubby, subhedral to euhedral laths which are evenly distribution throughout the groundmass. Clinopyroxene microphenocrysts (0.1 - 0.5 mm) occur as subhedral to anhedral grains and laths which frequently show a murky greenish alteration. Microphenocrysts of magnetite (0.05 - 0.15 mm) occur as equant grains. The groundmass is chiefly composed of a dark brown cryptocrystalline material which exhibits a faint patchy, radial anisotropy. Areas interstitial to this material are occupied by a turbid intergrowth of quartz and alkali-feldspar which comprises 10 - 15 % of the groundmass.

[B.6] Tafelberg Beacon

SM-007 Is non-porphyritic and consists of microphenocrysts (~23 %) of plagioclase, clinopyroxene and titanomagnetite in a devitrified cryptocrystalline to granophyric groundmass. The microphenocrysts exhibit a poorly developed intergranular texture, and despite an overall uniform distribution they are not strongly represented in the granophyric areas. Microphenocrysts of plagioclase (0.1 - 0.5 mm) occur as subhedral to euhedral stubby lath shaped crystals which show simple twinning and slight alteration. Plagioclase crystals commonly exhibit a zoned extinction pattern which often propogates into the anhedral alkali-feldspar crystals of the groundmass granophyre. Clinopyroxene

microphenocrysts occur as subhedral to anhedral grains and bladed crystals (0.1 - 0.3 mm). Titanomagnetite occurs as equant, subhedral grains (0.05 - 0.1 mm) with partially oxidised rims. In reflected light both homogeneous unaltered titanomagnetite and magnetite with exsolved ilmenite lamellae can be observed. The groundmass consists of a network of brownish-green cryptocrystalline material with interstitial areas of granophyre (Plate 3.2c). The cryptocrystalline material defines an anastomosing spherulitic texture which shows a patchy, sometimes radial anisotropy. The granophyric texture appears to post date and overprint the devitrification texture and consists of anhedral crystals (<0.5 mm) of quartz and alkali-feldspar. The latter tends to be turbid with included devitrified material.

[B.7] Lower Interbedded Coastal

SM-150 Is porphyritic to microporphyritic with a devitrified groundmass. Phenocrysts (~ 7 %) and microphenocrysts of plagioclase, pyroxene and magnetite are quite severely altered. The phenocrysts occur in glomeroporphyritic aggregates while the microphenocrysts are evenly distributed in the groundmass. Plagioclase phenocrysts (0.2 - 1.0 mm) occur as blocky euhedral crystals, where they are not intergrown in glomerophyric aggregates. Alteration is quite strong and often obscures simple twinning. Phenocrysts of pyroxene (0.2 - 3.0 mm) form subhedral, blocky to bladed crystals which are entirely pseudomorphed by a green clay mineral. The morphology of this altered pyroxene is consistent with that of hypersthene, which is observed in pitchstones from the same flow unit. Sparse, subhedral phenocrysts of magnetite (0.2 - 0.6 mm) occur as blocky grains with oxidised rims. Microphenocrysts of plagioclase (0.05 - 0.2 mm) occur as stubby laths which exhibit variable degrees of sericitisation. Clinopyroxene microphenocrysts (0.05 - 0.2 mm) occur as grains and laths which occasionally show a muddy-brown alteration. Equant, subhedral grains of magnetite (<0.05 mm) also show partial oxidation. The groundmass consists of buff-brown, cryptocrystalline spherulitic regions with a radial anisotropy, interspersed with a patchy, turbid intergrowth of quartz and alkali-feldspar.

SM-160 Is a sparsely porphyritic (~3 %) to moderately microporphyritic (~26 %) pitchstone. Subhedral to euhedral plagioclase phenocrysts (0.3 - 1.5 mm) have a range of dimensions which overlap with those of the microphenocrysts (0.1 - 0.4 mm), although they exhibit a blocky, rather than lath shaped morphology. Plagioclase phenocrysts, often occur in monomineralic aggregates, show simple twinning and weak zonation. Hypersthene phenocrysts occur as subhedral, grain to bladed shaped crystals (0.3 - 2.0 mm). Occasionally small acicular hypersthene crystals exhibit very thin clinopyroxene coronas. Microphenocrysts of clinopyroxene (0.1 - 0.4 mm) occur as subhedral grains and laths, and have augite to pigeonite compositions (Chapter 5). Titanomagnetite occurs as equant grains (<0.25 mm) which are maghemitised along curvilinear cracks. Glass with minute hair-like crystallites makes up the groundmass and shows incipient devitrification with sparse buff-coloured spots (<0.25 mm).

[B.8] Middle Interbedded Coastal

SM-103 Consists of microphenocrysts (~21 %) of plagioclase, clinopyroxene and magnetite set in a devitrified groundmass (Plate 3.1g). Quench-textured, partially sericitised, plagioclase is the dominant phase and exhibits a variety of skeletal and needle-like forms. Plagioclase laths commonly range between 0.1 and 0.3 mm long, although quenched needles range between 0.05 and 0.5 mm in length. Clinopyroxene microphenocrysts occur as subhedral grains (0.05 - 0.15 mm) and laths (<0.6 mm) and often show a green to brownish alteration. Magnetite occurs as equant, often euhedral, grains (<0.025 mm). The groundmass is composed of a brown, weakly anisotropic, cryptocrystalline material which partially obscures a myriad of curved and branched microlites.

[B.9] Upper Interbedded Coastal

SM-163 Consists of phenocrysts (~6 %) of plagioclase, augite and magnetite, and microphenocrysts of plagioclase enclosed in a devitrified groundmass. Plagioclase phenocrysts occur as subhedral, blocky to elongate crystals (0.25 - 2.0 mm) which may be gently rounded and exhibit both simple and repeated twinning. Plagioclase alteration is quite severe with the development of sericite(?) and a green chloritic(?) mineral. Predominantly unaltered augite phenocrysts have a subhedral to anhedral blocky to bladed habit (0.2 - 3.0 mm). They commonly show lobate embayments and in some instances partially or completely enclose small plagioclase phenocrysts. Sparse phenocrysts of magnetite (<0.75 mm) occur as rounded subhedral grains. Lath shaped microphenocrysts of plagioclase (0.05 - 0.1 mm) are all that can be recognised in the groundmass, which consists of a very dark brown cryptocrystalline material.

[C] SARUSAS QUARTZ LATITES AND LATITES

[C.1] Sarusas quartz latites

SM-110 Is strongly porphyritic (~20 %) with glomeroporphyritic aggregates of plagioclase, augite, pyroxene pseudomorphs, titanomagnetite and ilmenite set in a devitrified, sparsely vesicular (~4 %) groundmass. Plagioclase phenocrysts occur as blocky, subhedral to euhedral crystals (0.25 - 9.0 mm) and exhibit both simple and repeated twinning. Plagioclase is commonly zoned and frequently altered along cracks showing partial replacement by sericite(?) and carbonate. Augite occurs as subhedral to anhedral phenocrysts (0.2 - 1.0 mm). Serpentinised pyroxene pseudomorphs probably represent pigeonite. Opaque phenocrysts (Ti-Mt and Ilm) occur as rounded anhedral grains (0.1 - 1.0 mm) with diffuse oxidised rims, and show a variety of alteration textures in reflected light. The titanomagnetite exhibits fine- to coarse-grained trellis ilmenite and the host magnetite is largely replaced by hematite. In some grains magnetite with fine black needles of spinel (pleonaste-magnesioferrite$_{ss}$) can still be observed. Both phenocryst and trellis ilmenite show the development of fine rutile lenses. The

groundmass consists of quenched crystals of feldspar (<0.1 mm) enclosed in a granophyric intergrowth of quartz and alkali-feldspar, and a pale brown cryptocrystalline material with a patchy to radial anisotropism. Disseminated opaque material occurs throughout the groundmass, and is more abundant and has a larger grain size in the granophyric areas. Vesicles are partially or completely filled with chlorite and carbonate. Accessory apatite occurs as isolated euhedral grains and as inclusions in phenocrysts.

SM-115 Is a fresh porphyritic (~10 %) to microporphyritic (~7 %) pitchstone with crystals of plagioclase, augite, titanomagnetite and conspicuous accessory apatite which commonly form glomeroporphyritic aggregates. Plagioclase phenocrysts (0.4 - 3.5 mm) occur as euhedral, blocky, occasionally zoned crystals which exhibit both simple and repeated twinning. Phenocrysts and microphenocrysts of augite (0.1 - 1.25 mm) occur as blocky, subhedral to euhedral crystals which occasionally show lobate embayments. A large proportion of augite phenocrysts (>0.4 mm) have inclusions of euhedral apatite and more rarely magnetite. Titanomagnetite phenocrysts (0.1 - 0.8 mm) occur as subhedral grains and are generally unaltered. Microphenocrysts of plagioclase (0.05 - 0.2 mm) occur as sparse euhedral laths, and titanomagnetite occurs as equant grains (0.025 - 0.05 mm). The groundmass consists of a relatively fresh microlitic glass with a slight brownish discolouration along cracks and within glomeroporphyritic aggregates. Microlites (<0.01 mm) of plagioclase, clinopyroxene and magnetite are clearly identifiable.

KLS-315 Is essentially microporphyritic and is characterised by long acicular pyroxenes (~8.4 %) and quench needles of plagioclase (~8.0 %), the latter describing a sub-trachytic texture. Plagioclase occurs as elongate laths and needles up to 2.0 mm long and shows partial alteration. Pyroxene occurs as anhedral grains (0.1 - 0.3 mm) and as long acicular crystals commonly up to 1.0 - 3.0 mm long (more rarely 8.0 mm). The pyroxene is strongly oxidised and replaced by a serpentine-like material. Opaque microphenocrysts occur as equant grains (0.1 - 0.25 mm) which are predominantly titanomagnetite, although some composite grains of ilmenite and magnetite have been observed. Titanomagnetite shows varying degrees of alteration, with the exsolution of ilmenite lamellae and the oxidation magnetite to hematite. The groundmass is composed of a granophyric to micrographic intergrowth of quartz and alkali-feldspar which appears to overprint a turbid, pale brown devitrification texture.

[B.2] Sarusas Latites

KLS-327 Consists of phenocrysts (~7 %) of plagioclase, pigeonite augite, titanomagnetite and ilmenite set in a holocrystalline groundmass. The phenocrysts occur in glomeroporphyritic aggregates, where they are frequently accompanied by euhedral crystals of apatite (~0.5 %) up to 1.0 mm long. Plagioclase phenocrysts commonly occur as blocky, subhedral crystals (0.5 - 3.0 mm), although large (up to 12 mm long) anhedral, sieve textured crystals have also been observed. Plagioclase shows simple and repeated twinning, occasional zonation and incipient alteration along cracks. Pigeonite (0.25 - 2.0 mm) occurs as blocky, subhedral phenocrysts with characteristic cracks along which an opaque

alteration product is developed. In some instances pigeonite is mantled by augite. Phenocrysts of augite (0.25 - 1.0 mm) have a blocky, subhedral to euhedral morphology with few cracks and little alteration. Subhedral opaque phenocrysts (0.25 - 1.0 mm) of titanomagnetite and ilmenite impart a reddish oxidised stain to the surrounding groundmass. Composite grains of titanomagnetite and ilmenite are occasionally observed and are of a primary nature, rather than the result of oxidation exsolution. The groundmass has an even texture and consists of stubby, zoned laths of feldspar (anorthoclase) (0.05 - 0.15 mm), grains of pyroxene (<0.15 mm) and equant opaque grains (<0.05 mm) in a granophyric intergrowth of quartz and alkali-feldspar (<0.15 mm). Feldspar in the groundmass shows signs of sericitisation and the pyroxene is completely pseudomorphed by a greenish-brown material.

APPENDIX 2

ANALYTICAL TECHNIQUES AND DATA BASE DESCRIPTION

[A] INTRODUCTION

This appendix briefly outlines the methods employed during the analytical phase of this study and describes the presentation of whole rock and mineral data on the accompanying microfiche card.

X-ray Fluorescence (XRF), electron microprobe and oxygen isotope analyses of whole rock and mineral samples were carried out at the Geochemistry Department of the University of Cape Town (UCT). The sample preparation and analytical procedures commonly employed in this Department are covered in some detail by Duncan *et al.* (1984a), and are therefore not repeated at length here.

[B] SAMPLE PREPARATION

Samples were prepared for chemical analysis by splitting in a manual splitter, crushing in a jaw crusher with Mn-steel jaws and finally grinding to -300 powder in a carbon-steel grinding vessel on a Siebtechnik swing mill. Since the quartz latites were known to exhibit only limited compositional variation care was taken to process each sample in exactly the same way, in order to maintain some sort of consistency with regard to errors introduced during sample preparation. For example, grinding in a carbon-steel vessel is known to add approximately 0.1 % iron as a contaminant, and it was important to use the same grinding time for each sample.

[C] WHOLE ROCK ANALYSIS

X-ray Fluorescence Spectrometry

The major elements (except Na) were analysed using the procedure of Norrish and Hutton (1969) in which the sample powder is fused with a flux (Johnson-Matthey Spectroflux 105) to form glass disks. These disks were then analysed using the K-alpha line for each major element. Inter-element effects (except Na) were corrected by iterative calculations using the factors given in Norrish and Hutton (1969). An estimate of the precision, apparent accuracy and lower limits of detection for major element analysis at UCT are given in Duncan *et al.* (1984a), Table II. Volatile constituents (H_2O^- and loss on ignition, LOI) were determined by drying the sample at 110 °C (H_2O^-) and then by roasting the sample for 12 hours in a muffle furnace at 850 °C (LOI).

Na_2O and the trace elements were analysed on pressed powder briquettes (5g). The analytical techniques used (e.g. spectral lines, matrix corrections and interferences) are described by Duncan *et al.* (1984a), who also present estimates of precision and lower limits of detection at the 99 % confidence level.

Oxygen Isotope Determinations

Oxygen isotope analyses were carried out by H.S. Smith and N.P. Ikin who analysed whole rock samples, and by C. Harris who analysed both whole rock and mineral separate samples. Oxygen isotope ratios were determined on 10 mg of powder employing the oxygen liberation technique of Clayton and Mayeda (1963) except that ClF_3 was used instead of BrF_5 as reagent (Borthwick and Harmon, 1982). The liberated oxygen was converted to CO_2 using a heated carbon rod and run on a VG Isomass 602E mass spectrometer housed in the Department of Archaeology, UCT. All samples were run in duplicate and are reported in the delta notation; where $\delta X = (RX/Rstd - 1) \times 10^3$ ‰. All values are reported relative to the V-SMOW standard.

Radiogenic Isotope Analysis

Most of the Sr-isotope data quoted in this thesis are from the data base of Erlank *et al.* (1984). The source of this data and the methods of analysis employed are outlined by Bristow *et al.* (1984) and Hawkesworth *et al.* (1984). During this study new Sr-isotope data have been obtained for the following samples: SM-164, SM-150, SM-041, SM-115, SM110, SM-112, KLS-311 and KLS-327. These samples were analysed by R.J. Sweeney at the National Physical Research Laboratory (NPRL) of the Council for Scientific Research (CSIR). The procedures used were those currently in use at the NPRL and details of these procedures are given in Harmer *et al.* (1986) and Sweeney (1988).

Rare Earth Element (REE) Analysis

The REE data (Figs. 7.8 and 7.9) are from Erlank *et al.* (1984). These analyses were carried out by A.R. Duncan on a Spark Source Mass Spectrometer (SSMS) at the Research School of Earth Sciences, Australian National University. Additional elements analysed by SSMS include U, Th, Pb, Hf and Cs. Further details are provided by Duncan *et al.* (1984a).

[D] MINERAL ANALYSES

Compositions of individual minerals were determined on polished thin sections using a Cameca Camebax Microbeam Electron Microscope interfaced to a Digital PDP 11/23 microcomputer. The following instrumental conditions were used:

Beam Current	Plagioclase(20 nA), Pyroxene(40 nA), Magnetite(40 nA)
Accelerating Voltage	Plagioclase(15 KV), Pyroxene(25 KV), Magnetite(15 KV)
Analysing Crystals	TLAP for Na, Mg, Si and Al. LIF(200) for Fe and Mg. PET for Ca, K, Ti and Cr.
Detection	Flow counters with 10 % methane in argon gas mixture.

Beam Diameter 2 - 5 μm, but defocussed to 10 - 30 μm for plagioclase

Standards Used:

	Plagioclase	Pyroxene	Magnetite
Si	NUNI	DIOP	K-P
Ti	-	RUT	RUT
Al	NUNI	K-P	CHRO
Cr	-	CHRO	CHRO
Fe	K-H	K-P	ILMT
Mn	-	RHOD	RHOD
Mg	K-H	DIOP	CHRO
Ca	LACO	DIOP	K-P
Na	NUNI	K-H	-
K	OR-1	K-H	-

where:-

NUNI = Nunivak Is. Plagioclase
K-H = Kakanui Hornblende
LACO = Labradorite, Lake Co., Oregon
OR-1 = Orthoclase
DIOP = Diopside
K-P = Kakanui Pyrope
CHRO = Chromite 52NL11
RHOD = Rhodonite
ILMT = Ilmenite (Ilm.Mts., USSR)
RUT = Synthetic rutile

Counting times of 10 seconds on peaks and 5 seconds on each background on either side of the analyte peak were used. Data reduction was done "on line". Raw counts were corrected for dead-time losses and background, and the intensity-concentration relationship was calibrated using the standards listed above. Inter-element matrix effects for the analysis of pyroxene were corrected using the techniques of Bence and Albee (1968) and the α-factors of Albee and Ray (1970). Matrix corrections for plagioclase and magnetite were made using the ZAF technique. Typical 2σ counting errors and lower limits of detection (LLD) at the 99 % confidence limit on analyses of plagioclase, hypersthene and titanomagnetite are given below:

	Plagioclase			Hypersthene			Titanomagnetite		
OXIDE	**wt. %**	**LLD**	**2σ**	**wt. %**	**LLD**	**2σ**	**wt. %**	**LLD**	**2σ**
SiO2	53.70	0.06	0.35	52.31	0.04	0.24	0.11	0.04	0.03
TiO2	-	-	-	0.32	0.04	0.03	19.72	0.05	0.19
Al2O3	28.41	0.04	0.23	1.12	0.03	0.04	2.24	0.04	0.07
Cr2O3	-	-	-	-	-	-	0.18	0.05	0.04
FeO	1.18	0.10	0.14	20.77	0.07	0.34	72.33	0.10	0.70
MnO	-	-	-	0.68	0.06	0.08	0.68	0.08	0.09
MgO	0.13	0.03	0.25	22.72	0.03	0.17	1.61	0.03	0.06
CaO	12.26	0.04	0.19	1.77	0.03	0.05	-	-	-
Na2O	3.82	0.04	0.11	0.04	0.03	0.02	-	-	-
K2O	0.39	0.03	0.04	-	-	-	-	-	-

These estimates are the averages of 5 analyses of each phase from a particular sample with Plagioclase compositions from SM-160, Hypersthene compositions from SM-154 and titanomagnetite compositions from SM-115.

[E] WHOLE ROCK AND MINERAL DATA

A full listing of the Etendeka Formation quartz latite and latite whole rock and mineral data used in this study is given on the accompanying Microfiche card.

Whole rock data

The whole rock data presented include all the available quartz latite and latite analyses (206 samples) including 22 samples already published by Erlank *et al.* (1984). The majority (183) of the samples were collected, and analysed for major and trace elements by the author. Where all the REE data for a sample have been given they, and elements such as U, Th, Hf and Pb, have been analysed by SSMS; where only La, Ce and Nd are given they have been analysed by XRF. The "less than" symbols indicate that the concentration of that element was below the detection limit. The data are presented in two forms, firstly as the raw un-normalised data with all Fe as Fe_2O_3 and secondly as H_2O^--free data normalised to 100 with all Fe as FeO. Note that the data are not normalised on a LOI-free basis for reasons which are outlined in Chapter 6. The whole rock data are set out in Tables 1 - 24 and the samples are grouped according to the quartz latite or latite group to which they belong (e.g. Lower Springbok or Lower Tafelberg). An index of the contents of the Microfiche card can be found in the bottom right hand frame of the Microfiche card. A listing of the contents of each table and the first frame in which a particular table starts is given below:

RAW UN-NORMALISED DATA (All Fe as Fe_2O_3)

Table No	Contents	Frame No
1	Lower Springbok Quartz Latites	B1
2	Upper Springbok Quartz Latite(s)	D1
3	Albin and Gobobosebberge Quartz Latites	H1
4	Lower Tafelberg Quartz Latite	I1
5	Upper Tafelberg Quartz Latite	O1
6	Tafelberg Beacon Quartz Latite	P1
7	Lower Interbedded Coastal Quartz Latites	B2
8	Middle Interbedded Coastal Quartz Latites	E2
9	Upper Interbedded Coastal Quartz Latites	F2
10	Sarusas Quartz Latites	H2
11	Tafelberg Latite	K2
13	Sarusas Latite	L2

NORMALISED H_2O^--FREE DATA (all as FeO)

Table No	Contents	Frame No
13	Lower Springbok Quartz Latites	M2
14	Upper Springbok Quartz Latite(s)	O2
15	Albin and Gobobosebberge Quartz Latites	D3
16	Lower Tafelberg Quartz Latite	E3
17	Upper Tafelberg Quartz Latite	K3
18	Tafelberg Beacon Quartz Latite	L3
19	Lower Interbedded Coastal Quartz Latites	M3
20	Middle Interbedded Coastal Quartz Latites	P3
21	Upper Interbedded Coastal Quartz Latites	B4
22	Sarusas Quartz Latites	D4
23	Tafelberg Latite	G4
24	Sarusas Latite	I4

Mineral Chemistry Data

The mineral data are classified according to mineral type with Tables (25 -30) of analyses for plagioclase, pigeonite, hypersthene, augite, titanomagnetite and ilmenite. Up to 10 analyses appear on each Microfiche frame together with the calculated atomic proportions based on a selected number of oxygens in the mineral formula, and the end member compositions. A sample directory is given at the base of each frame which indicates the sample number, the type of unit to which the sample belongs (see abbreviations in Table 3.2), a crystal number (which is an arbitrary number allocated within each sample to allow recognition of multiple analyses of the same crystal) and position within the crystal (e.g. core, rim). A list of the mineral data tables, their contents and the first frame in which they start is given below:

MINERAL COMPOSITION DATA

Table No	Contents	Frame No
25	Plagioclase	I4
26	Pigeonite	M5
27	Hypersthene	E6
28	Augite	I6
29	Titanomagnetite	N6
30	Ilmenite	E7

APPENDIX 3

SAMPLE SITE LOCALITIES

This appendix gives the sample localities and lithology of the SM- samples collected during this study, and of the KLS- samples of Sarusas quartz latites and latites which have been discussed in this thesis. The latter samples were collected as part of a collaborative investigation on the Etendeka Formation lavas by members of this Department. The bracketed abbrevations indicate the type of quartz latite unit from which the sample was taken, a summary of the abbreviations used is given in Table 3.2.

Sample Number	Longtitude	Latitude	Lithology	Additional Comments
SM-001	~14° 04'30"	21° 50'00"	Basalt	
SM-002	~14° 04'30"	21° 50'00"	Basalt	Lagunenberg
SM-003	~14° 04'30"	21° 50'00"	Gabbro	Cape Cross
SM-004	13° 52'12"	21° 30'36"	Dolerite	
SM-005	~13° 52'30"	21° 32'45"	Dolerite	
SM-006	13° 27'36"	20° 26'38"	QL (LT)	
SM-007	14° 09'03"	20° 10'15"	QL (TB)	
SM-008	~13° 57'00"	21° 27'10"	QL (ALB)	
SM-009	~13° 57'00"	21° 27'10"	QL (ALB)	
SM-010	~13° 57'00"	21° 27'10"	QL (ALB)	
SM-011	13° 32'15"	20° 48'08"	QL (LT)	
SM-012	13° 34'33"	20° 46'26"	QL (LS)	
SM-013	13° 37'11"	20° 46'29"	Basalt	
SM-014	13° 40'01"	20° 45'18"	Basalt	
SM-015	13° 40'03"	20° 45'23"	QL (LS)	
SM-016	13° 37'12"	20° 47'04"	QL (LS)	
SM-017	13° 35'53"	20° 46'38"	QL (LS)	
SM-018	13° 37'24"	20° 40'39"	QL (US)	
SM-019	13° 34'35"	20° 40'54"	QL (US)	
SM-020	13° 34'40"	20° 36'59"	Basalt	
SM-021	13° 34'38"	20° 36'58"	QL (US)	
SM-022	13° 34'05"	20° 36'18"	QL (US)	
SM-023	13° 33'15"	20° 34'51"	QL (US)	
SM-024	13° 33'20"	20° 34'49"	QL (US)	
SM-025	13° 32'29"	20° 41'56"	Basalt	
SM-026	13° 32'17"	20° 43'30"	Basalt	
SM-027	13° 31'21"	20° 45'10"	QL (LT)	
SM-028	13° 20'23"	20° 36'20"	QL (LIC)	
SM-029	13° 20'45"	20° 36'42"	QL (LIC)	
SM-030	13° 20'30"	20° 37'17"	QL (LIC)	
SM-031	13° 20'55"	20° 37'48"	QL (LIC)	
SM-032	13° 26'19"	20° 29'12"	QL (LIC)	
SM-033	13° 25'21"	20° 34'08"	Basalt	
SM-034	13° 24'57"	20° 35'49"	QL (LIC)	
SM-035	13° 24'57"	20° 35'49"	Silicified breccia	
SM-036	13° 24'33"	20° 36'08"	QL (LIC)	
SM-037	13° 24'22"	20° 36'26"	QL (LT)	

SM-038	13° 25'57"	20° 35'28"	QL (UIC)	
SM-039	13° 26'00"	20° 36'21"	QL (UIC)	
SM-040	13° 25'44"	20° 36'33"	QL (UIC)	
SM-041	13° 25'40"	20° 36'36"	QL (MIC)	
SM-042	13° 25'30"	20° 32'14"	Dolerite	
SM-043	13° 25'17"	20° 30'32"	Silicified breccia	
SM-044	13° 26'06"	20° 32'30"	Basalt	
SM-045	13° 26'10"	20° 32'35"	Basalt	
SM-046	13° 26'23"	20° 32'22"	QL (LT)	
SM-047	13° 28'28"	20° 30'58"	QL (LIC)	
SM-048	13° 28'59"	20° 30'09"	QL (LT)	
SM-049	13° 27'38"	20° 28'01"	QL (LIC)	
SM-050	13° 30'16"	20° 24'05"	Basalt	
SM-051	13° 30'19"	20° 22'15"	Basalt	
SM-052	13° 30'28"	20° 22'15"	Basalt	
SM-053	13° 31'14"	20° 21'41"	Basalt	
SM-054	13° 31'14"	20° 21'41"	Basalt	
SM-055	13° 31'14"	20° 21'41"	Basalt	
SM-056	13° 45'03"	20° 15'43"	Basalt	
SM-057	13° 56'04"	20° 16'25"	QL (LT)	
SM-058	13° 56'12"	20° 16'25"	QL (US)	
SM-059	13° 59'56"	20° 13'41"	QL (UT)	
SM-060	13° 59'53"	20° 13'49"	QL (MT)	
SM-061	13° 31'02"	20° 30'02"	QL (US)	
SM-062	13° 37'15"	20° 46'07"	Basalt	
SM-063	13° 29'54"	20° 47'46"	Basalt	
SM-064	13° 27'33"	20° 43'31"	(?)	
SM-065	13° 26'49"	20° 32'14"	QL (LIC)	
SM-066	13° 27'18"	20° 29'01"	QL (LIC)	
SM-067	13° 28'14"	20° 32'08"	QL (LT)	
SM-068	13° 02'50"	20° 00'00"	QL	
SM-069	13° 45'36"	20° 23'57"	QL (LT)	
SM-070	13° 45'45"	20° 23'27"	QL (US)	
SM-071	13° 32'49"	20° 51'53"	QL (LT)	
SM-072	13° 32'36"	20° 50'53"	Basalt	
SM-073	13° 30'19"	20° 48'49"	QL (LIC)	
SM-074	13° 30'16"	20° 48'49"	Dolerite	
SM-075	13° 30'14"	20° 48'47"	QL (LIC)	
SM-076	13° 29'59"	20° 47'50"	QL (LIC)	
SM-077	13° 29'59"	20° 47'50"	QL (LIC)	
SM-078	13° 29'59"	20° 47'50"	QL (LIC)	
SM-079	13° 29'59"	20° 47'50"	QL (LIC)	
SM-080	13° 29'59"	20° 47'50"	QL (LIC)	
SM-081	13° 29'59"	20° 47'50"	QL (LIC)	
SM-082	13° 29'59"	20° 47'50"	QL (LIC)	
SM-083	13° 29'59"	20° 47'50"	QL (LIC)	Serial
SM-084	13° 29'59"	20° 47'50"	QL (LIC)	Section
SM-085	13° 29'59"	20° 47'50"	QL (LIC)	
SM-086	13° 29'59"	20° 47'50"	QL (LIC)	
SM-087	13° 29'59"	20° 47'50"	QL (LIC)	
SM-088	13° 29'59"	20° 47'50"	Basalt	
SM-089	13° 29'59"	20° 47'50"	Basalt(?)	
SM-090	13° 29'59"	20° 47'50"	Basalt	
SM-091	13° 29'59"	20° 47'50"	QL (LIC)	
SM-092	13° 29'59"	20° 47'50"	QL (LIC)	

SM-093	13° 30'07"	20° 48'00"	Dolerite	
SM-094	13° 27'46"	20° 43'34"	QL (LIC)	
SM-095	13° 28'07"	20° 43'46"	QL (LIC)	
SM-096	13° 28'17"	20° 43'46"	QL (LIC)	
SM-097	13° 28'20"	20° 43'38"	QL (LIC)	
SM-098	13° 28'24"	20° 43'42"	QL (LIC)	
SM-099	13° 28'27"	20° 43'22"	QL (LIC)	
SM-100	13° 28'29"	20° 43'27"	QL (?)	
SM-101	13° 28'32"	20° 43'20"	QL (MIC)	
SM-102	13° 30'16"	20° 48'02"	QL (LIC)	
SM-103	13° 28'33"	20° 43'14"	QL (MIC)	
SM-104	13° 28'40"	20° 43'15"	QL (MIC)	
SM-105	13° 28'33"	20° 42'30"	QL (UIC)	
SM-106	13° 27'33"	20° 43'31"	Basalt	
SM-107	13° 27'33"	20° 43'31"	QL (LT)	
SM-108	13° 27'33"	20° 43'31"	QL (LT)	
SM-109	13° 27'33"	20° 43'31"	QL (LT)	
SM-110	12° 22'31"	18° 46'37"	QL (SQL)	
SM-111	12° 22'34"	18° 46'35"	QL (SQL)	
SM-112	12° 23'19"	18° 46'13"	QL (SQL)	
SM-113	12° 23'04"	18° 46'14"	QL (SQL)	
SM-114	12° 23'03"	18° 46'33"	QL (SQL)	
SM-115	12° 23'40"	18° 46'09"	QL (SQL)	
SM-116	12° 22'30"	18° 45'14"	QL (SQL)	
SM-117	12° 22'08"	18° 43'35"	QL (SQL)	
SM-118	12° 19'47"	18° 40'56"	QL (SQL)	
SM-119	12° 26'12"	18° 50'19"	QL (SQL)	
SM-120	12° 26'15"	18° 50'53"	Basalt	Khumib Basalts
SM-121	12° 40'55"	18° 34'52"	Basalt	
SM-122	12° 41'00"	18° 34'58"	Basalt	
SM-123	12° 41'00"	18° 34'58"	Basalt	
SM-124	12° 41'00"	18° 34'58"	Basalt	
SM-125	12° 41'00"	18° 34'58"	Basalt	
SM-126	12° 41'00"	18° 34'58"	Basalt	
SM-127	12° 41'00"	18° 34'58"	Basalt	
SM-128	12° 41'03"	18° 34'58"	Basalt	
SM-129	12° 41'03"	18° 35'10"	Basalt	
SM-130	12° 41'08"	18° 35'10"	Basalt	
SM-131	12° 45'10"	18° 34'58"	Basalt	
SM-132	12° 45'02"	18° 34'58"	Basalt	
SM-133	12° 44'08"	18° 34'58"	Basalt	
SM-134	12° 28'41"	18° 59'53"	QL (SQL)	
SM-135	13° 27'33"	20° 43'31"	QL (LT)	
SM-136	13° 27'33"	20° 43'31"	QL (LT)	
SM-137	13° 27'33"	20° 43'31"	QL (LT)	Serial Section
SM-138	13° 27'33"	20° 43'31"	QL (LT)	
SM-139	13° 27'33"	20° 43'31"	QL (LT)	
SM-140	13° 27'33"	20° 43'31"	QL (LT)	
SM-141	13° 27'34"	20° 43'24"	QL (LT)	
SM-142	13° 27'46"	20° 43'15"	QL (LT)	
SM-143	13° 27'53"	20° 44'29"	QL (LT)	
SM-144	13° 27'44"	20° 44'04"	QL (LT)	
SM-145	13° 27'22"	20° 42'50"	QL (LT)	
SM-146	13° 27'12"	20° 42'19"	QL (LT)	
SM-147	13° 25'50"	20° 42'44"	QL (LT)	

SM-148	13° 25'13"	20° 40'55"	QL (LT)	
SM-149	13° 24'46"	20° 37'12"	Basalt	
SM-150	13° 23'54"	20° 34'51"	QL (LIC)	
SM-151	13° 23'28"	20° 33'58"	QL (LT)	
SM-152	13° 23'46"	20° 34'41"	QL (LIC)	
SM-153	13° 23'46"	20° 34'37"	Dolerite	
SM-154	13° 23'59"	20° 34'59"	QL (LIC)	
SM-155	13° 23'49"	20° 34'51"	QL (LIC)	
SM-156	13° 23'45"	20° 34'39"	QL (LT)	
SM-157	13° 24'10"	20° 33'51"	QL (LIC)	
SM-158	13° 24'51"	20° 35'48"	QL (LIC)	
SM-159	13° 24'42"	20° 35'44"	QL (LT)	
SM-160	13° 24'22"	20° 34'45"	QL (LIC)	
SM-161	13° 25'21"	20° 35'33"	QL (UIC)	
SM-162	13° 25'28"	20° 35'31"	QL (UIC)	
SM-163	13° 25'32"	20° 35'28"	QL (UIC)	
SM-164	13° 25'36"	20° 35'28"	QL (UIC)	
SM-165	13° 25'32"	20° 35'21"	QL (UIC)	
SM-166	13° 25'34"	20° 35'21"	Basalt	
SM-167	13° 36'10"	20° 33'48"	QL (US)	
SM-168	13° 36'13"	20° 34'01"	QL (US)	
SM-169	13° 40'44"	20° 35'46"	QL (US)	
SM-170	13° 40'41"	20° 35'25"	QL (US)	
SM-171	13° 40'41"	20° 35'19"	QL (US)	
SM-172	13° 40'41"	20° 35'08"	QL (US)	
SM-173	13° 37'12"	20° 37'35"	QL (US)	
SM-174	13° 41'41"	20° 39'09"	QL (US)	
SM-175	13° 36'44"	20° 42'31"	QL (US)	
SM-176	13° 34'37"	20° 40'57"	Basalt	
SM-177	13° 31'48"	20° 41'51"	QL (LT)	
SM-178	13° 29'16"	20° 27'24"	QL (LS)	
SM-179	13° 26'30"	20° 26'34"	QL (LT)	
SM-180	13° 26'58"	20° 26'27"	QL (LIC)	
SM-181	13° 27'12"	20° 29'01"	QL (LIC)	
SM-182	12° 58'30"	19° 51'50"	Dolerite	
SM-183	13° 38'02"	20° 31'09"	QL (US)	
SM-184	13° 38'05"	20° 31'07"	QL (US)	
SM-185	13° 38'07"	20° 31'09"	QL (US)	
SM-186	13° 38'09"	20° 31'11"	QL (US)	
SM-187	13° 38'11"	20° 31'14"	QL (US)	
SM-188	13° 38'57"	20° 24'35"	QL (LT)	
SM-189	13° 53'09"	20° 19'24"	Basalt	
SM-190	13° 54'09"	20° 20'11"	QL (LT)	
SM-191	13° 53'10"	20° 20'12"	QL (US)	
SM-192	13° 56'55"	20° 16'09"	QL (LT)	Wêreldsend Serial Section
SM-193	13° 56'55"	20° 16'09"	QL (LT)	
SM-194	13° 56'55"	20° 16'09"	QL (LT)	
SM-195	13° 56'55"	20° 16'09"	QL (LT)	
SM-196	13° 56'55"	20° 16'09"	QL (LT)	
SM-197	13° 56'55"	20° 16'09"	QL (LT)	
SM-198	13° 16'13"	13° 57'06"	QL (LT)	
SM-199	13° 16'13"	13° 57'06"	QL (LT)	
SM-200	13° 16'13"	13° 57'06"	QL (LT)	
SM-201	13° 57'38"	20° 20'00"	QL (US)	
SM-202	13° 57'38"	20° 17'40"	Dolerite	

SM-203	14° 04'52"	20° 17'44"	Basalt	
SM-204	14° 05'25"	20° 21'05"	QL (US)	
SM-205	14° 05'25"	20° 21'05"	QL (US)	
SM-206	14° 05'23"	20° 21'05"	Basalt	
SM-207	14° 05'23"	20° 21'05"	Basalt	
SM-208	14° 05'13"	20° 21'05"	QL (LS)	
SM-209	14° 07'14"	20° 56'02"	Turbidite	
SM-210	14° 07'04"	20° 48'42"	Basalt	
SM-211	14° 09'19"	20° 38'46"	Basalt	
SM-212	14° 09'19"	20° 38'43"	QL (LS)	
SM-213	14° 09'18"	20° 38'40"	Basalt	
SM-214	14° 09'18"	20° 38'40"	Dolerite	
SM-215	14° 09'17"	20° 38'37"	QL (LS)	
SM-216	14° 09'17"	20° 38'34"	Basalt	
SM-217	14° 09'17"	20° 38'34"	Basalt	
SM-218	14° 09'16"	20° 38'32"	Basalt	
SM-219	14° 09'16"	20° 38'32"	Basalt	
SM-220	14° 09'16"	20° 38'29"	QL (US)	
SM-220A	14° 09'16"	20° 38'29"	QL (US)	
SM-220B	14° 09'16"	20° 38'16"	QL (US)	
SM-220C	14° 09'23"	20° 38'13"	QL (US)	
SM-221A	14° 02'02"	20° 38'11"	QL (LS)	
SM-221B	14° 02'02"	20° 38'11"	QL (LS)	
SM-222A-F	13° 55'19"	20° 33'22"	QL (US)	Basal Contact
SM-223	14° 06'52"	20° 24'23"	QL (LS)	
SM-224	14° 06'45"	20° 24'11"	QL (LS)	
SM-225	14° 09'47"	20° 11'26"	Tafelberg Latite	
SM-226	14° 09'38"	20° 38'24"	Granite	
SM-227	14° 09'38"	20° 38'29"	Basalt	
SM-228	Float in Amis River, Brandberg.			
SM-229	13° 27'19"	20° 31'41"	QL (LIC)	
SM-230	14° 01'46"	20° 38'10"	QL (US)	
SM-231	14° 01'46"	20° 38'10"	QL (US)	
SM-232	14° 01'46"	20° 38'10"	QL (US)	
SM-233	14° 01'46"	20° 38'10"	QL (US)	
SM-234	14° 01'46"	20° 38'10"	(?) (US)	Basal
SM-235	14° 01'46"	20° 38'10"	(?) (US)	Contact
SM-236	14° 01'46"	20° 38'10"	(?) (US)	Zone
SM-237	14° 01'46"	20° 38'10"	(?) (US)	
SM-238	14° 01'46"	20° 38'10"	(?) (US)	
SM-239	14° 01'46"	20° 38'10"	(?) (US)	
SM-240	14° 01'46"	20° 38'10"	Basalt	

KLS-311	~12° 32'00"	19° 01'00"	Latite (SL)
KLS-313	~12° 32'00"	19° 01'00"	QL (SQL)
KLS-314	~12° 32'00"	19° 01'00"	QL (SQL)
KLS-315	~12° 32'00"	19° 01'00"	QL (SQL)
KLS-316	12° 23'27"	18° 43'32"	QL (SQL)
KLS-317	12° 18'24"	18° 40'02"	QL (SQL)
KLS-318	12° 17'33"	18° 39'52"	QL (SQL)
KLS-319	12° 16'25"	18° 38'37"	QL (SQL)

[Appendix 3]

KLS-326	12° 13'05"	18° 34'27"	Latite (SL)	Serial Section
KLS-327	12° 13'09"	18° 34'29"	Latite (SL)	
KLS-328	12° 13'16"	18° 34'40"	Latite (SL)	
KLS-329	12° 13'30"	18° 34'58"	Latite (SL)	
KLS-330	12° 13'37"	18° 35'10"	Latite (SL)	
KLS-331	12° 13'40"	18° 35'15"	Latite (SL)	
KLS-341	12° 01'33"	18° 28'28"	QL (SQL)	

Communs geol. Surv. S.W. Africa/Namibia, **2**, (1986), 109—116

THE GEOLOGICAL AND VOLCANOLOGICAL FEATURES OF THE QUARTZ LATITES OF THE ETENDEKA FORMATION

by

S.C. Milner

Department of Geochemistry
University of Cape Town
RONDEBOSCH
7700

ABSTRACT

The volcanic Etendeka Formation of S.W.A./Namibia consists predominantly of interbedded basalt and quartz latite units with an approximate age of 121 m.y. The quartz latites, which represent a significant proportion of the succession, exhibit characteristics common to both ignimbrites and lava flows. The local preservation of pyroclastic textures and broad areal extent of the units have led to the conclusion that these quartz latites are the products of high-temperature ash flows, which underwent *en masse* lava-like flowage following their deposition but prior to final cooling.

1. INTRODUCTION

The study area, situated in the Skeleton Coast Park and western Damaraland, is bounded by latitudes 21°00'S and 20°00'S and longitudes 13°15'E and 14°15'E (Fig. 1). Investigations have been confined to the volcanics of the Etedenka region, more specifically the acid rocks which crop out over a wide area within the southern Etendeka. The volcanic Etendeka Formation is the uppermost unit of the Karoo Sequence in S.W.A./Namibia and overlies discontinuous Karoo sediments and pre-Karoo basement. The basaltic rocks have yielded a K-Ar isochron age of 121 ± 2 m.y. (Siedner and Mitchell, 1976) and similar ages of approximately 125 m.y. were recently obtained by $^{39}Ar/^{40}Ar$ step heating analysis of three dolerites intruding Karoo sediments and the basaltic lavas near Cape Cross (Erlank *et al.*, in press).

The Etendeka Formation consists of a series of interbedded basalt (including both primitive and more evolved varieties) and quartz latite units, with some minor latite, which reach an observed maximum thickness of 900 m at Tafelberg (Erlank *et al.*, 1984). Although earlier workers have mentioned the presence of acidic rocks in the lava sequence, described as orthoclase porphyry (Reuning, 1929) or rhyolites (Korn and Martin, 1954; Martin *et al.*, 1960), they were ascribed only to the upper part of, or as a capping to the sequence. The widespread interbedded nature of the quartz latites has only recently become apparent (Erlank *et al.*, in press). The original maximum stratigraphic thickness of volcanics is unknown, although it is thought to have exceeded 2 km (Reuning and Martin, 1957).

The use of the term "quartz latite" to describe the acid volcanics of the Etedenka was first introduced by Erlank *et al.* (in press) to avoid the genetic implications of the term "dacite." Despite the absence of modal quartz, whole-rock chemical data fall within the field of quartz latites originally defined by Iddings (1913), and more recently by Ekren *et al.* (1984).

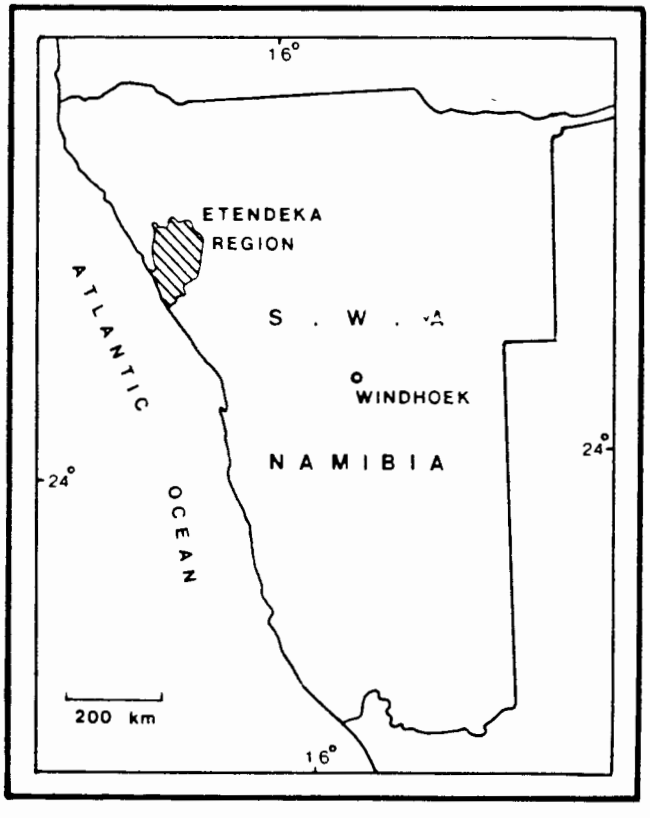

Fig. 1: Geographic locality of the Etendeka region in S.W.A./Namibia.

The descriptive information presented below shows that the quartz latites exhibit features common to both ignimbrites and lava flows and are similar in many respects to the rhyolites of the Lebombo (Bristow and Cleverly, 1979; Cleverly *et al.*, in press). Despite conflicting evidence, many workers on Karoo rhyolites in southern Africa have favoured an ignimbritic origin, although convincing macro- and micro-textural information has often not been available or apparent.

2. DETAILED GEOLOGY

The geology of the southern Etendeka volcanics is presented in Fig. 2. This illustrates the most detailed mapping of the Etendeka lava field currently available and covers approximately one third of the area of the main lava field.

2.1 Structure

The area mapped is divided into two structural regions by the Ambrosius Berg fault zone. This fault zone can be traced for a distance of 60 km north of Ambrosius Berg and constitutes a major structural break (Fig. 2).

West of the Ambrosius Berg fault zone the volcanics dip between 5° and 30° east and form a series of blocks which are bounded by faults parallel to the coast. Within single fault blocks the dip is normally constant and there is a general westward increase in the easterly dip. However, within certain fault blocks there are local unconformities which may have resulted from synvolcanic fault movements. Unfortunately, these faults are often obscured by superficial material in areas of low relief and are thus rarely detected.

To the east of the Ambrosius Berg fault zone the succession is characterised by predominantly flat-lying units with a slight westerly dip in the order of 1° or less. A fault with a trend parallel to the road north and south of Bergsig has lowered the volcanic sequence approximately 100 m to the west.

The difficulty in correlating stratigraphic units across the Ambrosius Berg fault zone, and the faulted nature of the coastal succession, imply that no overall stratigraphic column for the Etendeka volcanic succession can be readily compiled, although in local areas this has been possible as discussed below.

2.2 Quartz Latite Lithostratigraphy

The quartz latites are here divided into three main groups, the Springbok, Tafelberg and Interbedded Coastal varieties, which may be recognised in the field by differences in outcrop pattern and petrographic characteristics.

The Springbok group is composed of upper and lower members which are separated by approximately 90 m of basaltic lavas. The base of the lower member is situated between 150 and 180 m above the base of the Etendeka Formation, and appears to consist of a single unit between 10 and 20 m thick which crops out discontinuously over a wide area. The contact relationship of this unit with the underlying basalts is clearly transgressive and provides evidence, supported by a variation in unit thickness and stratigraphic height, for the existence of palaeorelief prior to its eruption. The upper Springbok member exhibits a maximum observable thickness of 270 m which thins out rapidly towards its northern contact, where it is overlain transgressively by flows of the Tafelberg group. Certain stratigraphic sections have allowed the recognition of three units within the upper member using criteria established for an idealised quartz latite unit. However, where this member thins beneath the Tafelberg lavas there is no evidence to support the presence of three units. It is tentatively suggested that the upper member was truncated by an erosional feature prior to the eruption of the Tafelberg group.

Outcrops of the more massive upper Springbok member are characterised by large, rounded, boulder-strewn hills which are in contrast to the trap-like outcrops of the Tafelberg volcanics. Both upper and lower members are characteristically feldspar phyric and range in colour from a rusty brown, devitrified rock to a black pitchstone.

Fig. 2 illustrates the large area over which the Springbok quartz latites occur. The upper member covers a present day area of some 1250 km² and it is evident from outliers to the south of the Huab River valley that this represents only a portion of the original area covered.

Upper and lower quartz latite members of the Tafelberg group are 85 m and 100 m thick, respectively, and are separated by approximately 320 m of basaltic material. At Tafelberg, the base of the lower member is about 340 m above the base of the Etendéka Formation. However, where the Tafelberg group overlies the upper Springbok member the intervening basalt wedge varies in thickness from 230—250 m in the west to zero near Driefontein. In the Driefontein area the lower Tafelberg member is truncated against the upper Springbok member.

The Tafelberg quartz latites are typically aphyric, devitrified and pink to grey in hand specimen with only occasional basal vitrophyre horizons. They tend to form significant topographic steps, or cliffs, which commonly exhibit a rough columnar joint pattern. Many of these features have been recognised in the quartz latite immediately west of the Ambrosius Berg fault zone, in particular where it is cut by the Koigab River. These features, together with similarities in chemistry, suggest that this outcrop should be cor-

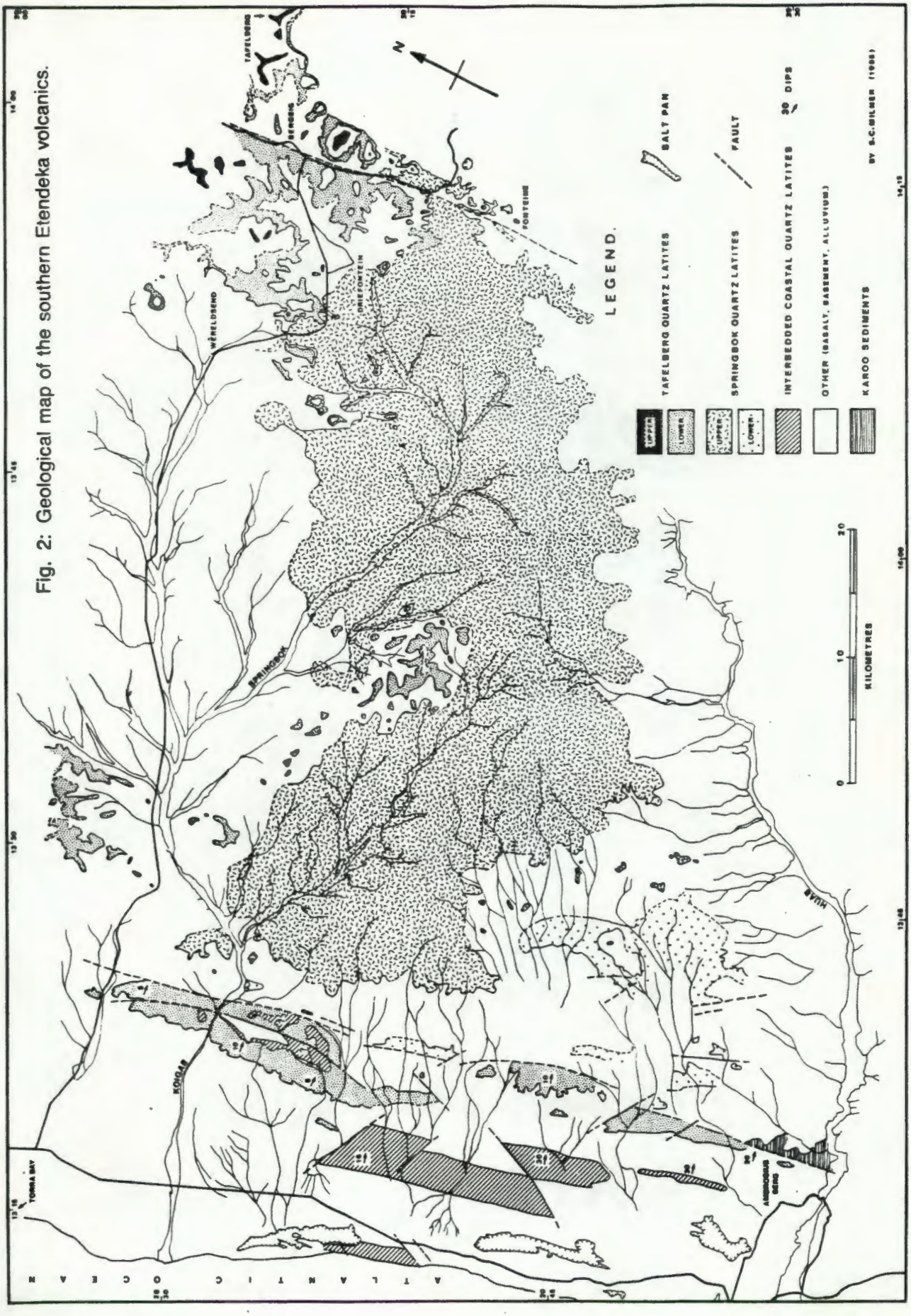

Fig. 2: Geological map of the southern Etendeka volcanics.

related with the lower Tafelberg quartz latite. South of the Koigab River this unit is overlain by two sparsely feldspar-phyric quartz latite units which are separated by approximately 60 m of basalt. This represents a considerable departure from the normal Tafelberg stratigraphy.

The quartz latites and basalts of the Tafelberg group exhibit a classic trap morphology. Individual flows, showing a constant thickness, can be traced for many kilometres and hill-top remnants of the lower Tafelberg quartz latite member have been mapped 70 km west of Tafelberg itself. Although the observed outcrop area of this lower member is not as great as that for the Springbok units, an area of 2 500 km² may have been covered within the limits of the outcrop remnants observed. In the northern Etendeka region the preserved extent of the upper Tafelberg quartz latite approaches 2 000 km², (R.McG. Miller, 1980, pers. comm.) and there is little doubt that these units form very extensive horizons.

The thickest individual accumulation of quartz latite units in the Etendeka area occurs in the coastal region west of the Ambrosius Berg fault zone. In this area a pile of quartz latite units, here termed the Interbedded Coastal group, have a maximum thickness of approximately 800 m and overlie an unknown thickness of basalt. The number of units observed varies from seven, encountered in a traverse across the southern end of the fault block, to eleven or more at the northern end, where the uppermost units are intercalated with basaltic material. The tilted and faulted nature of the coastal succession make it impossible to estimate the areal extent of these quartz latites. However, the lower units can be traced for up to 25 km along strike suggesting that these units covered a considerable area.

In outcrop both feldspar-phyric and aphyric varieties are observed and are predominantly devitrified and pink to grey in colour, although basal pitchstone zones are commonly encountered.

The overall position of the Interbedded Coastal quartz latites within the stratigraphic column is uncertain, as no equivalent formation has been recognised to the east of the Ambrosius Berg fault zone. The overall outcrop pattern for these units and the Koigab equivalent of the lower Tafelberg member suggest deposition within a fault-controlled depression or basin. In Fig. 2 the additional quartz latites in the region south of the Koigab are tentatively assigned to the Interbedded Coastal quartz latite group and may represent the interfingering of quartz latites from different volcanic centres.

The eruptive centres of the quartz latite volcanism are unknown. As yet no caldera related structures have been identified in the Etendeka region and no vent or acid dykes, which may have acted as feeders to the eruptions, have been observed. It is also interesting to note that no air-fall ash horizons, commonly associated with acid volcanism, have been seen.

3. THE QUARTZ LATITE UNIT

The terms flow unit, cooling unit and compound cooling unit are described by Fisher and Schmincke (1984). Briefly, the term flow unit is usually reserved for the product of a single pyroclastic eruption; this is in contrast to the cooling unit which occurs when several flows are erupted in rapid succession and cool as a single unit. The overall massive nature of the quartz latites in outcrop often precludes this distinction, hence the term "unit" has been used in preference to flow unit in this text.

A composite section of an idealised quartz latite flow unit is presented in Fig. 3 and brings together many important features common to the Etendeka quartz latites as a whole. It is important to note, however, that the development of many of the basal

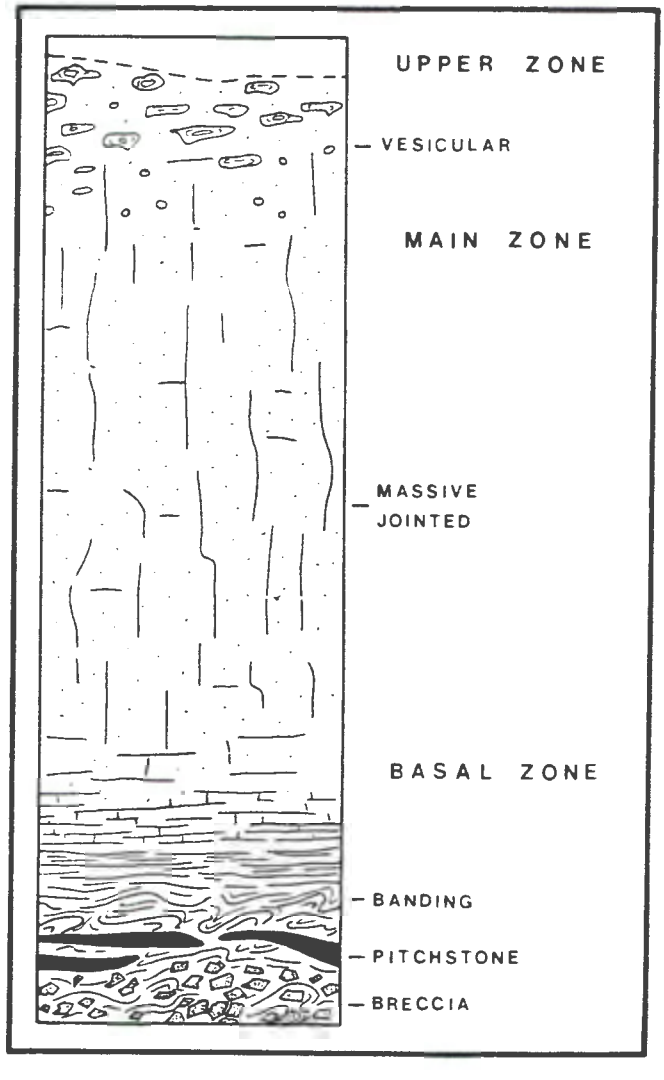

Fig. 3: Schematic section through an idealised Etendeka quartz latite flow unit.

features are in most cases localised and not common to all sections, although one or more of these features are usually present.

3.1 Basal Zone

The most informative portion of the unit is the base, where many features are preserved by rapid contact chilling with the ground surface. Banding, which is frequently contorted, a basal pitchstone, and a basal breccia are among the more important features observed.

3.1.1 Banding and Fiamme

In most cases the form of the observed banding has been enhanced by alteration which has differentially coloured the bands in shades of red, orange and grey. The alteration may have taken place shortly after deposition by late-stage phreatic or degassing events which may also have produced the breccia-filled pipes observed in some units. The banding typically occurs on a millimetre to decimetre scale. Near the base of the unit, normally within 2 or 3 m, the banding may be highly contorted both vertically and laterally. Towards the main body of the unit these contortions frequently give way to more laminar banding which often becomes associated with a strong centimetre-scale jointing in the same plane. There would appear to be a correlation between the presence of strongly contorted banding and an undulating topography prior to deposition. Quartz latites of the Tafelberg group rarely show contorted banding to any great degree, a feature attributed to their near planar contacts.

Thin sections from laminar banded regions near the base of flow units occasionally contain fiamme-like structures (see Fig. 5). These show textures consistent with pore space elimination and have frayed ends, a description not unlike that given for fiamme by Ross and Smith (1961).

3.1.2 Basal Pitchstone

Pitchstone occurs in irregular pods and bands, normally within 2 m of the base, and may show either sharp or gradational contacts with the devitrified portions of the unit. The exceptions to this are the very thick pitchstone horizons in the upper Springbok member which may be as much as 10 m thick. These particular pitchstones exhibit a lenticular fabric near the base similar to that observed in the brecciated material.

In thin section these pitchstones are for the most part homogeneous glass with varying amounts of phenocrysts. A typical example is shown in Fig. 4. In other examples from glassy, friable perlitic horizons, a texture composed of plastically moulded clasts of dark brown hydrated glass has been observed (Fig. 6). An almost identical photomicrograph is presented by Ross and Smith (1961, Fig. 39) which they describe as "a thoroughly welded glassy tuff with large pumice fragments that have collapsed and all the pore space eliminated . . .". This explanation is consistent with observations made of relict pores which occur as thin lines surrounded by slightly different coloured glass.

3.1.3 Basal Breccia

The breccia is composed of clasts of quartz latite, fragments of pumice and glass, and occasional fragmented feldspars. Figs. 7 and 8 depict a breccia with ignimbritic textures, where individual glassy fragments can be clearly seen filling interstitial areas between lithic and pumice-like clasts. Fig. 9 illustrates a similar texture although in this case the shards are more stretched out and the lithic fragments show some welding. The quartz latite clasts often have a lenticular nature resulting from the flattening and stretching of vesicles which have subsequently been filled with silica and zeolite.

3.2 Main Zone

The main body of a unit, in excess of 95 per cent of the whole, is characteristically massive and devitrified with little or no internal structure, although occasional horizontal laminations have been observed. The homogeneous nature of this central portion is borne out by petrographic studies, which normally reveal monotonous devitrification textures common to both phyric and aphyric varities alike. It is this type of quartz latite which is most commonly encountered in the field and although the exposure is good, little useful information may be gained as to the eruptive origin of the rock. In this respect, the main zone of the quartz latites resembles the central part of the rhyolite units of the Lebombo (Bristow and Cleverly, 1979).

3.3 Upper Zone

Flow tops, where they are still preserved, tend to be highly vesicular. Individual geodes with diameters of up to 40—50 cm have been observed and the cavities are filled with quartz, agate, zeolite and calcite and show a diversity of shapes from ovoid to complex flattened structures. The quartz latite in this portion of the flow tends to be highly altered and discoloured, a feature attributed to the passage of silica-, zeolite- and calcite-depositing solutions.

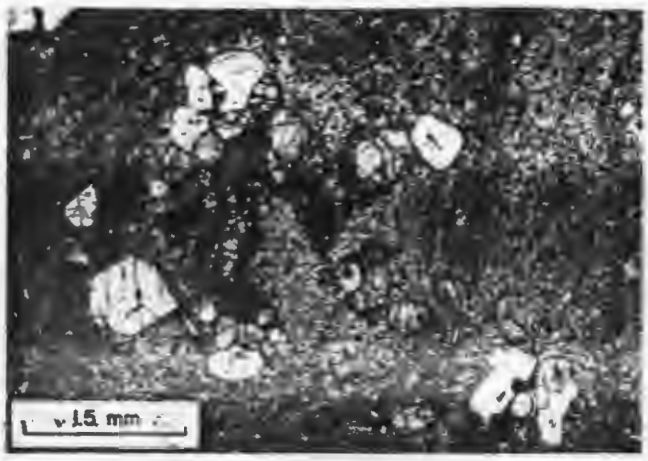

Fig. 4: Photomicrograph of a typical quartz latite pitchstone, showing a crystalline aggregate of plagiocalse, pigeonite and magnetite set in a microlitic glass (plane polarised light).

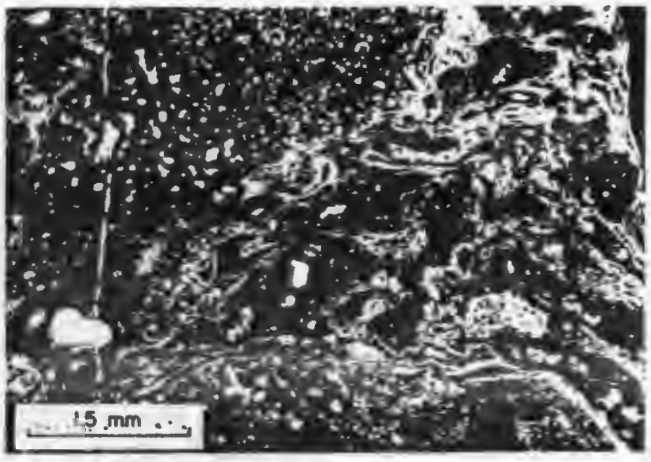

Fig. 7: Photomicrograph showing shards and pumice clasts infilling areas between lithic quartz latite fragments (plane polarised light).

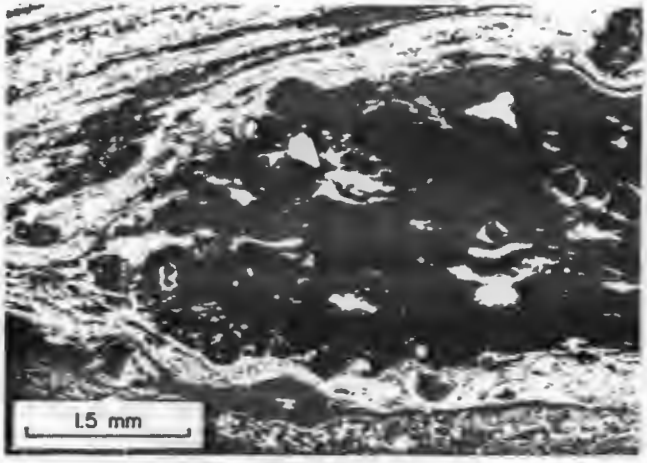

Fig. 5: Photomicrograph of a fiamme-like structure consisting of a flattened pumice with phenocrysts of plagioclase and magnetite (plane polarised light).

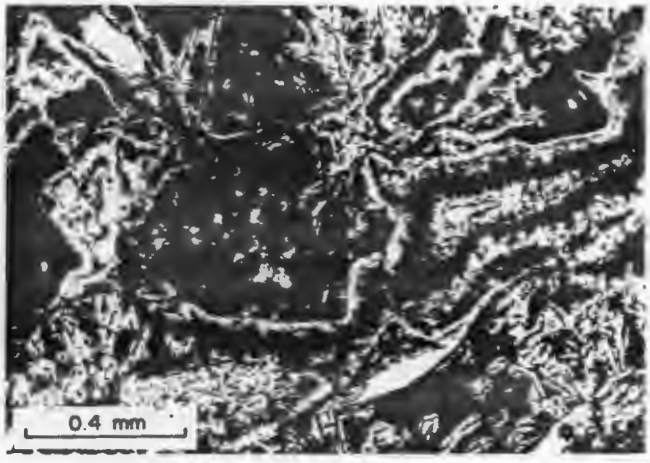

Fig. 8: A higher magnification photomicrograph of the textures illustrated in Fig. 7 shows the shards to be glassy with incipient microlites (plane polarised light).

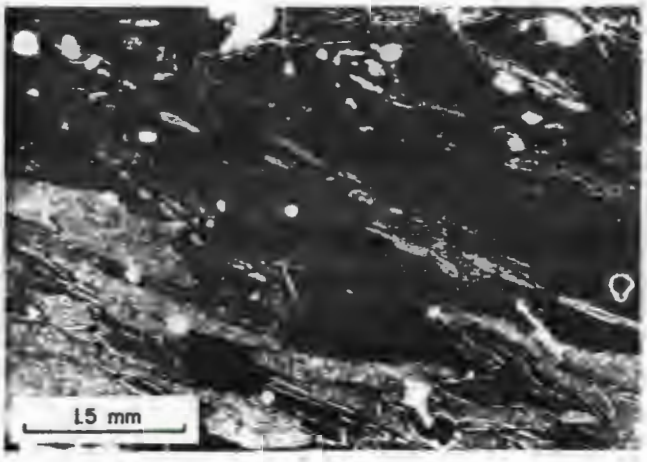

Fig. 6: Photomicrograph of a glassy perlitic pitchstone consisting of clasts of glass welded together (plane polarised light).

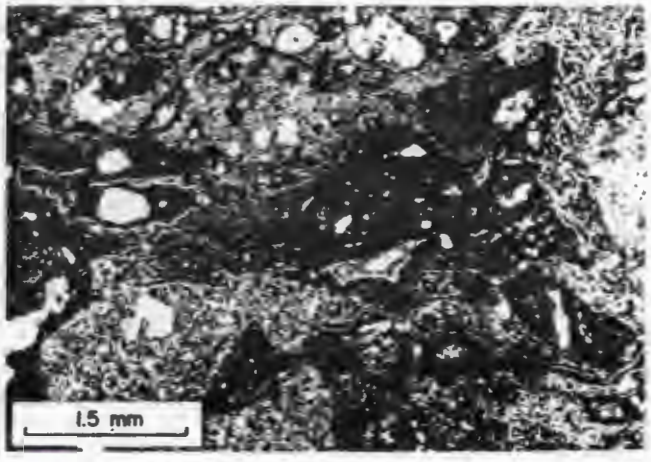

Fig. 9: Photomicrograph illustrating a more strongly welded and flattened fabric than that seen in Fig. 7 (plane polarised light).

4. DISCUSSION

The existence of the Etendeka quartz latites and other Karoo-age acid volcanics in southern Africa have long posed problems as to their volcanological history and emplacement mechanisms. For those unacquainted with the problems at hand, a brief summary of the main distinguishing features of lavas and ignimbrites is presented in Table 1 (after Bristow and Cleverly, 1979). Comparison with the Etendeka quartz latite reveals that they exhibit many features common to both ignimbrites and acid lavas.

TABLE 1. Comparative features of ignimbrites and acid lavas.

IGNIMBRITES	ACID LAVAS
** Extensive sheet form	Limited extent
** Planar flow contacts	Irregular contacts
** Pyroclastic character	** Autobrecciated
** Welded/Non-welded	** Contorted banding
** Glassy/Devitrified	** Glassy/Devitrified

** Characteristics exhibited by the Etendeka quartz latites.

Despite the contorted banding and brecciation, more commonly associated with rhyolite lavas, it is considered that the extensive sheet-like form and the pyroclastic features provide evidence that the quartz latites are ignimbritic in origin. Even if one invokes a lava with a low viscosity (e.g. Twist, 1984) to account for the extensive outcrop, rhyolite lavas do not usually exhibit features that can be confused with the pyroclastic textures reported here. Twist (1984) attributes low viscosity rheologies to high eruptive temperatures (900—1 100°C) and water contents of between 6 and 9 weight per cent. Such high water contents are unlikely in the Etendeka quartz latites as hydrous phases are rare.

It is therefore considered that the Etendeka quartz latites are the result of dense, high-temperature ash flows composed of a near molten suspension of material. In the final stages of emplacement, such flows still maintained sufficient heat and momentum to induce viscous lava-like flowage resulting in the observed banding. Ekren *et al.* (1984) described 10—16 m.y. old rhyolites from south-western Idaho, USA and suggested that they are principally high-temperature welded ash-flows which have characteristics indicative of viscous lava-like flowage. Many of the features they describe, such as the local preservation of pyroclastic textures, basal vitrophyres, brecciation and contorted banding, bear a strong resemblance to features seen in the Etendeka. The lava-like features, breccia and flow banding are explained by Ekren *et al.* (1984) in the following manner. The high-temperature, 'atypical' ash-flow tuff units are densely welded from bottom to top and have marked vitrophyre horizons at the base. The rapidly chilled lowermost portions of the flow could be easily disrupted by *en masse* movements of the still mobile overlying sheet causing a breccia to form. This explanation can be readily applied to previously described brecciated clasts with a lenticular fabric and the frequent occurrence of lenticular pitchstone at the base of some Etendeka quartz latite units.

Furthermore, Ekren *et al.* (1984) stated that mass-flow movements often occur when hot ash-flow material is deposited over irregular relief. More importantly, such movements occur over any terrain when the ash-flow is extremely hot and starts to coalesce to a viscous liquid while still moving away from the eruption column.

Eruption columns giving rise to pyroclastic deposits, as described by Sparks and Wilson (1976), consist of gas thrust and convective thrust regimes which give rise to ash-flow and air-fall tuffs respectively. Magma gas content, vent radius and the entrainment of atmospheric air are all said to have an effect on the products of such eruptions (Sparks and Wilson, 1976). Furthermore, these authors state that a hot dry magma will give rise to a dense eruptive column with minimal atmospheric interaction. This would result in a poorly developed convective thrust component and little air-fall ash associated with the resulting deposit. Ekren *et al.* (1984) appealed to this mechanism as a method of producing the Idaho rhyolites and suggested that large vent diameters would also minimise atmospheric mixing, ensuring that the ash-flow maintained a temperature high enough to produce the textures observed.

The apparent lack of calderas and the high temperature of the Idaho rhyolites has been attributed by Ekren *et al.* (1984) to deep, possibly lower crustal, magma chambers which precluded caldera collapse. Similar deep-seated eruptions could possibly have given rise to the Etendeka quartz latites and may explain the difficulty in identifying their eruption centres.

The above discussion has been used to strengthen the contention that the Etendeka quartz latites are ignimbritic in origin. In conclusion the areal extent of the Etendeka quartz latites is emphasised, particularly in the context of what appear to be large amounts of Karoo age quartz latite near Porto Alegre, in the southern Parana basin of South America (Bellieni *et al.*, 1984), as pre-drift Gondwanaland reconstructions show the juxtaposition of the Etendeka and Parana volcanics. A major input of thermal energy is required to generate extensive volumes of quartz latite over such large areas, accordingly future studies will consider the relationship between this thermal event and intercontinental rifting.

5. ACKNOWLEDGEMENTS

I am indebted to A.J. Erlank and A.R. Duncan for their supervision and constructive comments which

led to considerable improvements in the manuscript. I am also grateful to J.S. Marsh and the late P.J. Betton for many hours of helpful discussion.

6. REFERENCES

Bellieni, G., Comin Chiaramonti, P., Marques, L.S., Melfi, A.J., Piccirillo, E.M., Nardy, A.J.R. and Roisenberg, A. 1984. High- and low-TiO_2 flood basalts from the Parana Plateau (Brazil): Petrological and geochemical aspects bearing on their mantle origin. *Neues Jb. Miner. Abh.*, **150**, 273—306.

Bristow, J.W. and Cleverly, R.W. 1979. Volcanology of the Lebombo rhyolites. *Abstr. 18th Congr. geol. Soc. S. Afr.*, 60—63.

Cleverly, R.W., Betton, P.J. and Bristow, J.W. Geochemistry and petrogenesis of the Lebombo rhyolites. *Spec. Publ. geol. Soc. S. Afr.*, **13** (in press).

Ekren, E.B., McIntrye, D.H., Bennett, E.H. 1984. High temperature, large volume, lavalike ash-flow tuffs without calderas in southern Idaho. *Prof. Pap. U.S. geol. Surv.*, **1272**, 1—73.

Erlank, A.J., Marsh, J.S., Duncan, A.R., Miller, R.McG., Hawkesworth, C.J., Betton, P.J. and Rex, D.C. Geochemistry and petrogenesis of the Etendeka volcanic rocks from S.W.A./Namibia. *Spec. Publ. geol. Soc. S. Afr.*, **13** (in press).

Fisher, R.V. and Schmincke, H.-U. 1984. *Pyroclastic Rocks.* Springer-Verlag, Berlin, 195 pp.

Iddings, J.P. 1913. *Igneous rocks.* Vol. II. John Wiley and Sons, New York, 685 pp.

Korn, H. and Martin, H. 1954. The Messum Igneous Complex in South West Africa. *Trans. geol. Soc. S. Afr.*, **57**, 83—122.

Martin, H., Mathias, M. and Simpson, E.S.W. 1960. The Damaraland sub-volcanic ring complexes in South West Africa. *21st int. geol. Congr., Copenhagen*, **13**, 156—174.

Reuning, E. 1929. Differentiation der Karroo-Eruptiva in südlichen Kaokofeld, Südwestafrika. *C. r. 15th int. geol. Congr., Pretoria.*, **2**, 28—36.

Reuning, E. and Martin, H. 1957. Die Prä-Karroo-Landschaft, die Karroo-Sedimente und Karroo-Eruptivgesteine des südlichen Kaokofeldes in Südwestafrika. *Neues Jb. Miner. Geol. Paläont., Abh.*, **91**, 193—212.

Ross, C.S. and Smith, R.L. 1961. Ash-flow tuffs: Their origin, geologic relations, and identification. *Prof. Pap. U.S. geol. Surv.*, **366**, 1—77.

Siedner, G. and Mitchell, J. 1976. Episodic Mesozoic volcanism in Namibia and Brazil: A K-Ar isochron study bearing on the opening of the South Atlantic. *Earth Planet. Sci. Lett.*, **30** (2), 292—302.

Sparks, R.J.S. and Wilson, L. 1976. A model for the formation of ignimbrites by gravitational column collapse. *J. geol. Soc. Lond.*, **132**, 441—451.

Twist, D. 1984. Emplacement of voluminous silica lavas in the Bushveld Complex. *Abstr. 97th a. Meet. geol. Soc. Am.*, 679 pp.

Communs geol. Surv. S.W. Africa/Namibia, 3, *(1987) 83—90*

GEOCHEMICAL CHARACTERISATION OF QUARTZ LATITE UNITS IN THE ETENDEKA FORMATION

S.C. Milner and A.R. Duncan

Department of Geochemistry, University of Cape Town, Rondebosch 7700

ABSTRACT

Quartz latite units interbedded with basaltic lavas in the Etendeka Formation form extensive sheet-like deposits which are probably the product of high temperature ash-flows. Apart from some systematic differences between pitchstone and devitrified quartz latites, largely explained by low temperature alteration processes, individual quartz latite units exhibit remarkably uniform compositions. No significant lateral compositional variations within individual units are observed and compositional changes occur only in the uppermost parts of any particular unit. A regional stratigraphic correlation is difficult to establish due to local differences that may be attributed to palaeotopography and the faulted nature of the coastal region in the Etendeka. In this study geochemistry has been used as a primary criterion for the correlation of major quartz latite units within the southern Etendeka area.

1. INTRODUCTION

The geology of the Etendeka region in S.W.A/Namibia has been described in some detail by Erlank *et al.* (1984) and Milner (1986). In summary, the Etendeka Formation consists of a series of interbedded basalt and quartz latite units which overlie Karoo sediments and pre-Karoo basement. Detailed mapping of the southern Etendeka area (Milner, 1986) has shown that the quartz latites, which form extensive sheet-like deposits but rarely exhibit pyroclastic textures, are probably high-temperature ash flow tuffs. Three distinct groups of quartz latite units are recognised in the field by differences in outcrop pattern and petrographic character, namely the Springbok, Tafelberg and Interbedded Coastal groups. The term "unit" as used here can be considered synonymous with "cooling unit". It is not certain whether some cooling units contain multiple flow units, but this would seem likely in some areas on the basis of outcrop characteristics.

Recent field studies have resulted in a refinement of the stratigraphy defined by Milner (1986). A section through the Springbok group south of the Huab River has revealed the presence of a second lower Springbok quartz latite unit and two additional quartz latite units have been recognised in the Tafelberg group. The first of the additional Tafelberg quartz latites is a thin, sparsely porphyritic unit cropping out 15-20 m below the upper Tafelberg unit between Wereldsend and Bergsig, and will be referred to as the middle Tafelberg unit. The second is a separate unit above the main upper Tafelberg quartz latite which was sampled at Tafelberg beacon and will be referred to as the Tafelberg beacon unit. A regional stratigraphic column for the Etendeka Formation is not readily compiled using the field and petrographic data available because of local differences in stratigraphy and the faulted nature of the coastal region.

A total of 198 quartz latite samples have been analysed for 32 major and trace elements and it is now possible to attempt a chemical characterisation of individual quartz latite units. This characterisation enables a stratigraphic correlation of units where field and petrographic relationships are obscure. The effects of primary within-unit variation and secondary alteration have also been taken into consideration. In all of the diagrams the data presented were *not* recalculated to 100% on a volatile free basis.

2. CLASSIFICATION OF QUARTZ LATITES

Erlank *et al.* (1984) divided the acidic rocks of the Etendeka Formation into quartz latites and high K dacites on the basis of their relative SiO_2 and K_2O contents, according to the classification schemes proposed by MacKenzie and Chappell (1972) and Peccerillo and Taylor (1976). Only three of the Etendeka acidic rocks were classified as high-K dacites with markedly lower K_2O contents than the quartz latites. All the presently analysed Etendeka acidic rocks are plotted on a SiO_2 vs K_2O diagram (Fig. 1).

With the much larger data set that is now available it is clear that all samples with lower K_2O contents, and specifically those which plot in the dacite or high K-dacite fields, are pitchstones. Most of the acid rocks have a cryptocrystalline to microcrystalline groundmass in which devitrification textures are common and such rocks will be referred to in this paper as devitrified quartz latites.

The pitchstones whose compositions are shown in Fig. 1 are from a variety of localities and units. The pitchstones

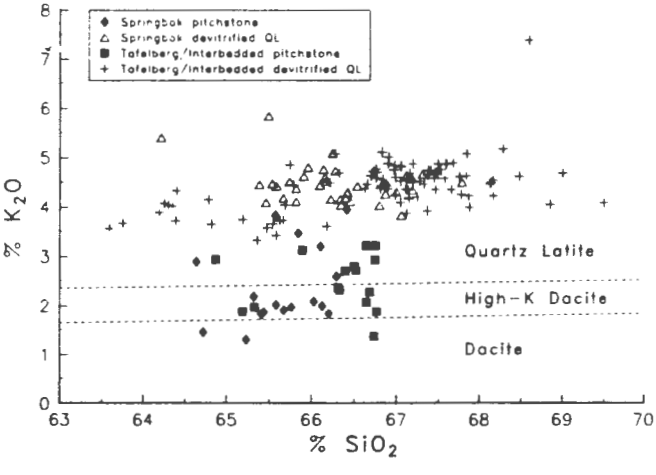

Fig. 1: K_2O-SiO_2 variations in acidic rocks (pitchstones and devitrified quartz latites) of the Etendeka Formation. The classification boundaries are from MacKenzie and Chappell (1972). The "Tafelberg/Interbedded devitrified QL" includes samples from all Tafelberg and all Interbedded Coastal quartz latite units.

generally crop out at the base of a unit (see Milner, 1986, Fig. 3) but there are rare instances where pitchstone also forms lenses or bands within the main body of a unit. Pitchstone and devitrified quartz latite are often found in close proximity at the same stratigraphic height near the base of a unit. No examples are known of a low-K (< 3.0 per cent K_2O) devitrified quartz latite in the Etendeka Formation. Therefore, it seems unlikely that the pitchstones represent a distinct magma type, or an eruptive product from a compositionally zoned magma chamber which was also the source of the devitrified quartz latites.

TABLE 1: A Comparison of individual pitchstone and devitrified quartz latite sample pairs.

	Upper Springbok		Lower Interbedded Coastal	
	Pitchstone Sample (SM23)	Divitrified Sample (SM21)	Pitchstone Sample (SM97)	Divitrified Sample (SM98)
SiO_2	65.68	66.42	66.34	67.68
TiO_2	0.91	0.92	0.84	0.86
Al_2O_3	12.63	12.61	12.81	12.98
Fe_2O_3*	6.65	6.89	5.72	5.82
MnO	0.11	0.15	0.11	0.08
MgO	1.11	1.50	0.97	1.15
CaO	3.73	2.58	3.15	2.35
Na_2O	3.27	2.50	3.54	2.83
K_2O	1.91	4.28	2.32	4.89
P_2O_5	0.27	0.27	0.28	0.28
H_2O-	0.64	0.36	0.25	0.13
LOI	3.12	1.39	3.45	1.11
TOTAL	100.03	99.87	99.75	100.16
Cs	28	< 5	19.5	< 5
Rb	196	166	191	184
Ba	657	638	648	612
Sr	186	147	160	132
Zr	269	265	266	267
Nb	22	23	25	24
V	65	67	55	60
Cu	14.4	13.4	38	42
Y	42	44	42	41
La	46	46	44	44
Ce	90	91	87	85
Nd	47	50	48	47

Fe_2O_3* - Total Fe reported as Fe_2O_3.
LOI - Loss of volatiles after roasting at 850°C

3. QUARTZ LATITE ALTERATION

Comparison of whole-rock data for pitchstone and devitrified quartz latite pairs from the upper Springbok and lower Interbedded Coastal groups are presented in Table 1. The samples in each pair, which were collected at similar locations and heights within each unit, show differences for a number of oxides and elements, but particularly for K_2O, LOI, CaO, Na_2O and Cs. The juxtaposition of sample sites suggests that these differences are not of a primary magmatic nature and may reflect secondary alteration processes. Elements considered relatively immobile during alteration support this conclusion, as illustrated by a plot of TiO_2 vs. LOI (Fig. 2). This figure also indicates that simple addition or subtraction of H_2O+ (the dominant component of LOI) cannot account for the compositional variations observed.

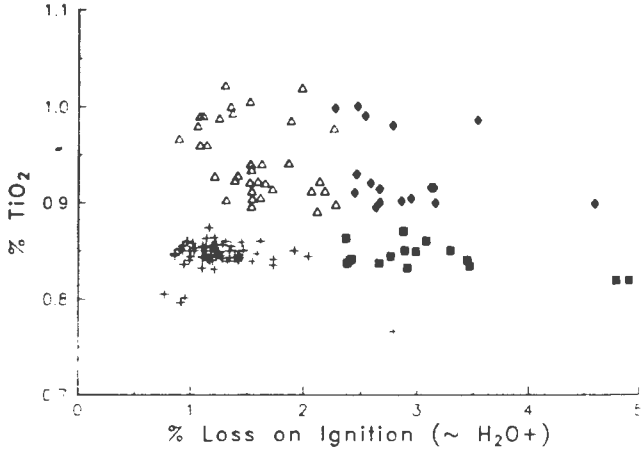

Fig. 2: Variation of LOI as a function of textural variety in acidic rocks of the Etendeka Formation. Note that pitchstones always show > 2.2 per cent LOI and that there is little difference in the TiO_2 content of pitchstones and devitrified quartz latites from the same units. See Fig. 1 for legend. Data for the upper Tafelberg, and the middle and upper Interbedded Coastal quartz latite units are not shown on this figure as no pitchstones from those units have been analysed.

Petrographically the pitchstones appear unaltered and it is tempting to regard their composition as that most closely representing the original quartz latite magma. However, they represent a small proportion of the quartz latite outcrop in the Etendeka area and it seems highly unlikely that the main volume of devitrified quartz latite, totalling several hundred cubic kilometres, could gain up to 2 wt per cent K_2O by post-eruptive alteration in a subaerial environment. Zielinski (1982), Jezek and Noble (1978) and Cerling *et al.* (1985) have documented alkali exchange and loss in volcanic glass and reported that a low temperature hydration of glass by ground water is accompanied by the exchange of Na^+ and K^+ with positive hydronium ions (H_3O^+) in the following reaction:

$$2H_2O + K^+ \text{ (Glass)} \rightarrow H_3O^+ \text{ (Glass)} + KOH$$

Cerling *et al.* (1985) stated that in peralkaline glasses "up to 40 per cent of the alkali cations (Na^+ and K^+) could be replaced by H^+ with no measurable change in the bulk composition of the glass or in the distribution of minor and trace elements, excepting other alkali ions such as Rb^+".

A plot of K_2O against LOI for the Etendeka samples exhibits a negative correlation, which is consistent with alkali loss during a hydration event (Fig. 3a). This relationship is more clearly illustrated by a plot of K_2O/LOI against LOI (Fig. 4). The relative magnitude of K_2O and LOI variations shown in Fig. 3a and the well-defined trend in Fig. 4 strongly suggest that H_2O+ is the principle exchange component for K^+ in the glass. It is surprising, however, that pitchstones and devitrified quartz latites do not show different concentrations of Rb and that pitchstones appear to have markedly higher concentrations of Na_2O and Cs than do the devitrified quartz latites (Table 1).

The higher concentration of CaO in the pitchstones relative to the divitrified quartz latites (Fig. 3b) is more difficult to explain. Since Al_2O_3 contents in the pitchstones and devitrified quartz latites do not differ significantly, differences in CaO cannot be ascribed to preferential concentration of plagioclase phenocrysts in the pitchstones. Plagioclase and pyroxene crystals in the pitchstones show little alteration compared to those in the devitrified quartz latites, which are often replaced by sericite, serpentine and minor carbonate. It seems likely that as a consequence of

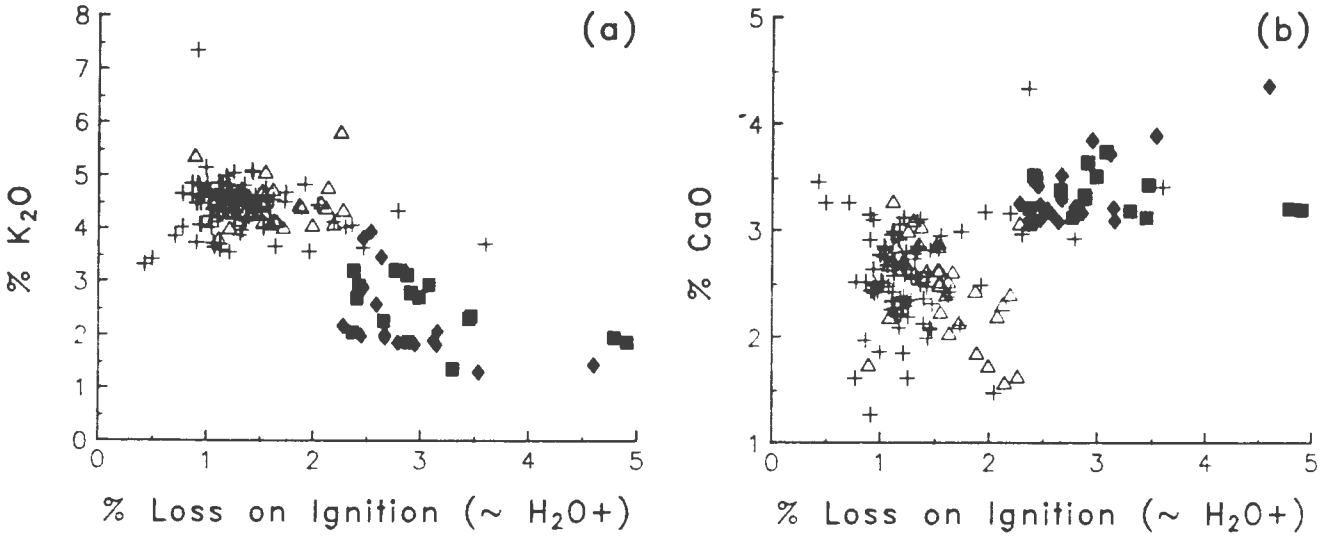

Fig. 3: Variation of K_2O and CaO as a function of the LOI of devitrified quartz latites and pitchstones from the Etendeka Formation. See Fig. 1 for legend.

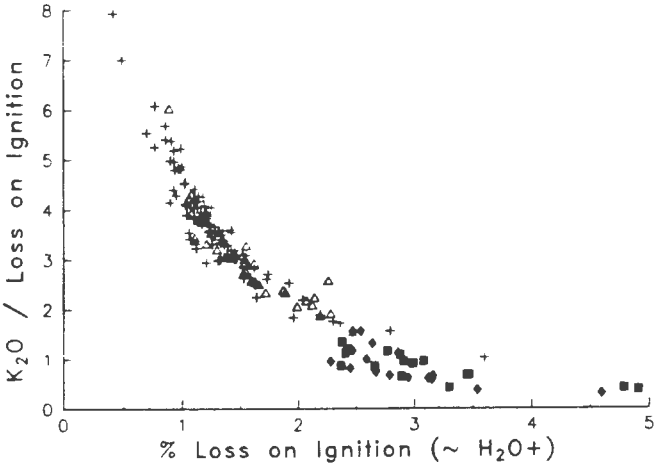

Fig. 4: Plot of the ratio K_2O/LOI against LOI for devitrified quartz latites and pitchstones from the Etendeka Formation. See Fig. 1 for legend.

this alteration process CaO, and possibly Na_2O, has been lost from the devitrified quartz latites.

In conclusion, the alkali and alkali earth elements are mobile in post-eruptive alteration processes and the concentrations of these elements are not representative of primary eruptive compositions. This is an important factor to consider in petrogenetic modelling and has serious implications for K-Ar and Rb-Sr age dating techniques.

4. WITHIN-UNIT VARIATION

Detailed studies of many ash flow deposits that are related to calderas show systematic mineralogical and chemical variations, as exemplified by the Bishop Tuff, California (Hildreth, 1979), the Bandelier Tuff, Valles Caldera, New Mexico, (Smith and Bailey, 1966) and the Mazama ash flow, Crater Lake, Oregon, (Williams, 1942; Ritchey, 1980). Vertical zonations within ash flows are often translated into lateral variations as the sheet thins away from its source area. It is necessary therefore to recognise such trends if successful correlations are to be made in distal or faulted portions of a succession. Processes leading to within-flow variation include sorting (which may involve crystal-glass fractionation during eruption and outflow), alteration, and pre-eruptive compositional gradients in magma chambers. Hildreth (1981) and Smith (1979) gave comprehensive accounts of the types of compositional zonations observed in ash-flow tuffs and suggested possible mechanisms for their formation.

Serial stratigraphic sections and lateral traverses were sampled in several localities in order to evaluate the extent to which the Etendeka quartz latites show vertical and lateral variations. The discussion below is specific to a single quartz latite unit but identical conclusions can be drawn from comparable studies made on other quartz latite units.

4.1 Vertical Variation

The evidence for vertical compositional variation within the quartz latite units can be illustrated using the lower Tafelberg unit as a type example. A 70 m section of this unit was sampled on the farm Wêreldsend, where the exposure is complete and readily accessible. Fig. 5 shows the variation of Fe_2O_3*, (total iron reported as Fe_2O_3) TiO_2, Zr and Cu with height from the base. These elements are not affected by the alteration processes discussed above and also show the greatest differences between different quartz latite groups and units (see Section 5). Within the main body of the unit (0-65 m) Fe_2O_3*, TiO_2, Zr and Cu show no systematic variation outside the limits of analytical error. However, the two uppermost samples show significant departures from the composition of the lower portions of the unit. This is probably due to high temperature alteration where the contorted, brecciated and amygdaloidal flow top is highly oxidised and contains abundant zeolite and secondary quartz.

4.2 Lateral Variation

The limited range of compositions exhibited within a vertical section allows the construction of a lateral traverse with samples that are not necessarily from the same stratigraphic level within an individual unit. A traverse of this nature was constructed for the lower Tafelberg unit from isolated hilltop remnants between Tafelberg in the east and the more tilted succession in the west. West of the Ambrosius Berg Fault Zone, where the lower Tafelberg unit is down-faulted, samples were collected along strike between the Torra Bay-Bergsig road and Ambrosius Berg (See Fig. 2 in Milner,

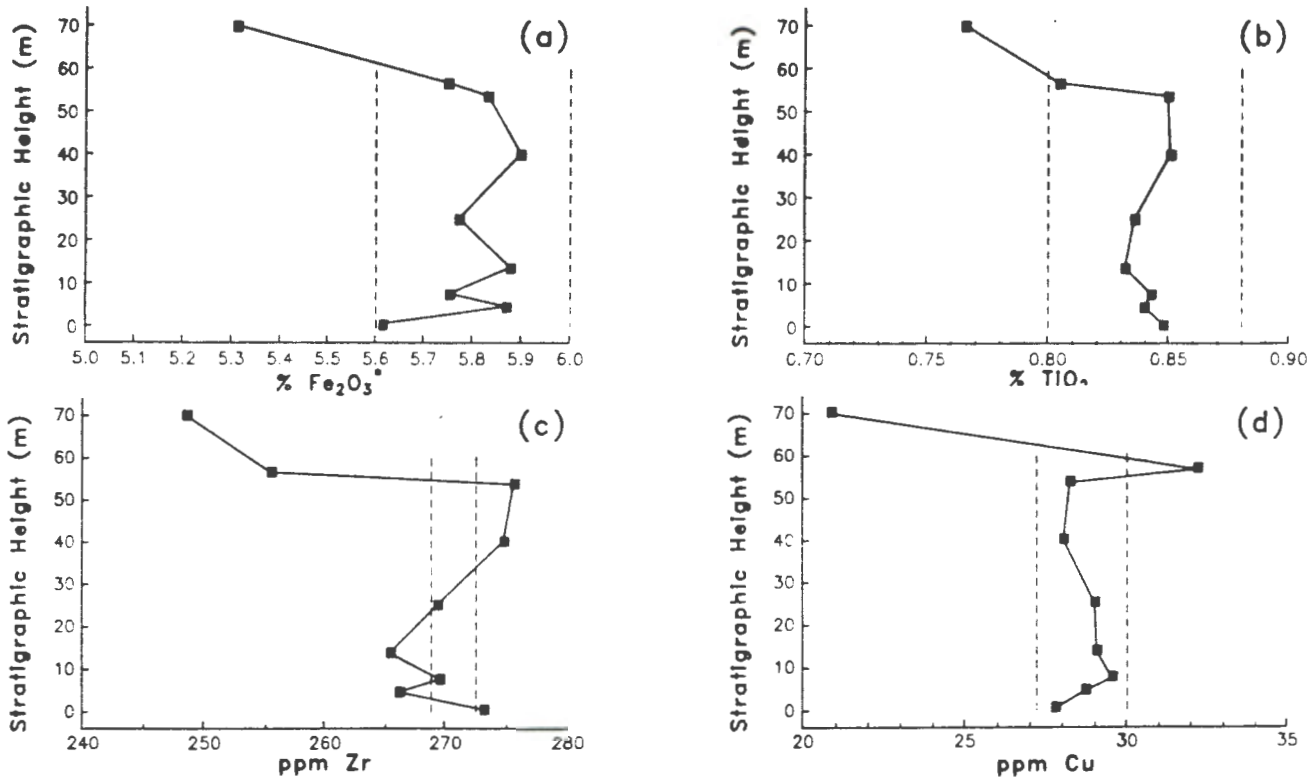

Fig. 5: Variation in the concentration of $Fe_2O_3^*$ (total Fe expressed as Fe_2O_3), TiO_2, Zr and Cu as a function of stratigraphic height within the lower Tafelberg quartz latite unit in a single section on the farm Wêreldsend. The dashed vertical lines represent 2 sigma analytical errors added and subtracted to the mean of the lowermost 7 samples in the section. For $Fe_2O_3^*$ and TiO_2 the errors are estimated from 6 replicate analyses, for Zr and Cu they are estimated from XRF counting statistics only.

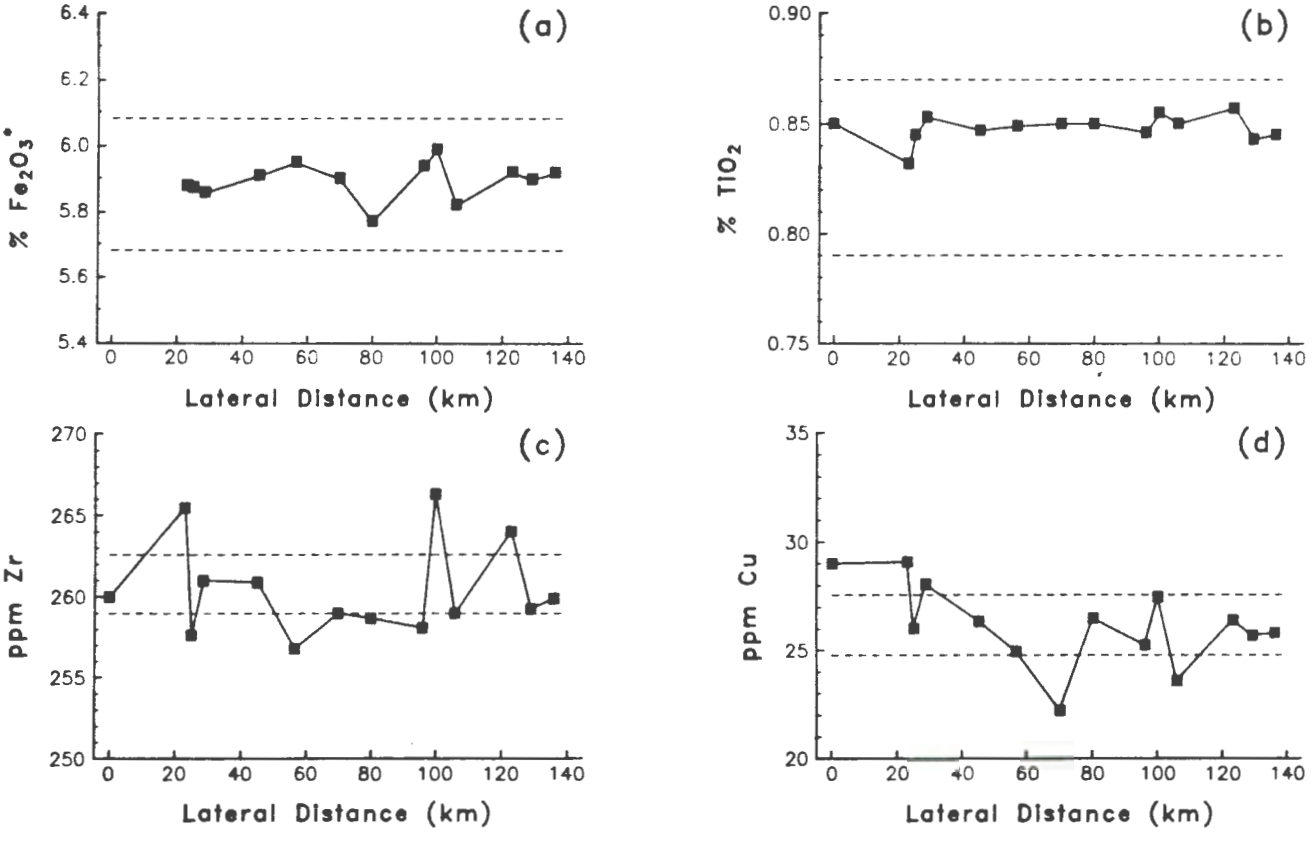

Fig. 6: Variation in the concentration of $Fe_2O_3^*$, TiO_2, Zr and Cu as a function of lateral distance within the lower Tafelberg quartz latite. The section runs from Tafelberg (0 km) eastwards in the vicinity of the Bergsig - Torra Bay road to the Ambrosius Berg Fault Zone (80 km) and then southwards along strike to Ambrosius Berg (140 km). The dashed horizontal lines represent 2 sigma analytical errors added and subtracted to the mean of all samples in the traverse.

1986, for a geological map showing these localities). Fig. 6 shows the variation of Fe_2O_3*, TiO_2, Zr and Cu with lateral distance. For the most part, the compositional range of these elements lies within the limits of analytical error and highlights the extremely uniform chemical composition of individual quartz latite units.

5. GEOCHEMICAL CORRELATION OF QUARTZ LATITE UNITS

5.1 Compositional Differences

Despite the overall compositional uniformity displayed by the Etendeka quartz latites, small but significant compositional differences do occur between some of the units. The principle discriminating elements are TiO_2, Fe_2O_3* and Cu. On the plot of TiO_2 vs. Fe_2O_3* the Springbok quartz latites can be distinguished from the Tafelberg and Interbedded Coastal groups by relatively higher Fe_2O_3* content (Fig. 7). The lower and upper Springbok units are not clearly separated on this diagram, although the lower Springbok samples fall at the high TiO_2 and high Fe_2O_3* end of the lower trend where they are associated with samples from Albin beacon (Erlank *et al.*, 1984) and the Gobobosebberge lava field surrounding the Messum Complex. The lower Tafelberg and lower Interbedded Coastal quartz latites form a single grouping that can be distinguished from samples of the middle Interbedded Coastal and upper Tafelberg groups. Data for the Upper Interbedded Coastal quartz latites and the Tafelberg Beacon unit plot at the high TiO_2 and Fe_2O_3* end of the upper trend, forming a cluster of points distinct from the other Tafelberg and Interbedded Coastal quartz latites. It is interesting to note that successive units in the Tafelberg and Interbedded Coastal quartz latites show a trend of increasing Fe_2O_3* and TiO_2 with increasing stratigraphic height. Quartz latite units within the Springbok group, however, show a decrease in Fe_2O_3* and TiO_2 with increasing stratigraphic height.

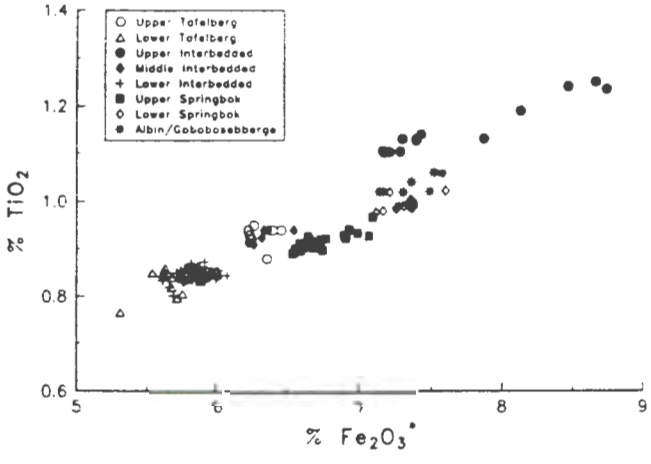

Fig. 7: Plot of TiO_2 against Fe_2O_3*; note that in the legend "Interbedded Coastal" subgroups of quartz latites have been abbreviated to "Interbedded".

A diagram of Cu vs. Fe_2O_3* demonstrates the Cu is a more effective discriminant than TiO_2 for the groups discussed so far (Fig. 8). The Springbok quartz latites define a discrete population with a completely different trend to the Tafelberg and Interbedded Coastal groups. Although the lower Interbedded Coastal quartz latites have slightly higher Cu values than those of the lower Tafelberg unit, this plot does not permit a further separation of the Tafelberg and Interbedded Coastal Samples from the three groups recognised in Fig. 7.

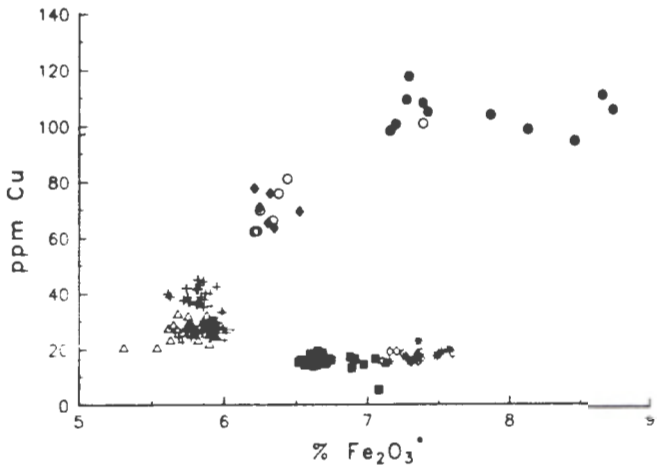

Fig. 8: Plot of Cu against Fe_2O_3* for the quartz latite units of the Etendeka Formation. See Fig. 7 for legend.

5.2. Discriminant Function Analysis

The objective of discriminant function analysis (DFA) is to examine how far it is possible to distinguish between members of various groups on the basis of observations made upon them. DFA is a comparative analysis of data which have already been pre-classified into groups using criteria different from those entered in the discriminant function; it is also possible to classify "unknown" samples in terms of the groups defined.

Geochemical data which can be related to different formations or lithological groups, like the quartz latites of the Etendeka, are ideally suited to this type of statistical treatment (Le Maitre, 1982). A full description of the methods employed here can be found in Duncan *et al.* (1984).

A discriminant function is a combination of variables which best describes the inter-group variance of a data set and reduces its dimensionality. In the program used (BMDP7M; Dixon *et al.*, 1981) the variables are chosen in a step-wise selection procedure and entered into the function on the basis of their ability to discriminate between groups. Variables which are strongly correlated with those already

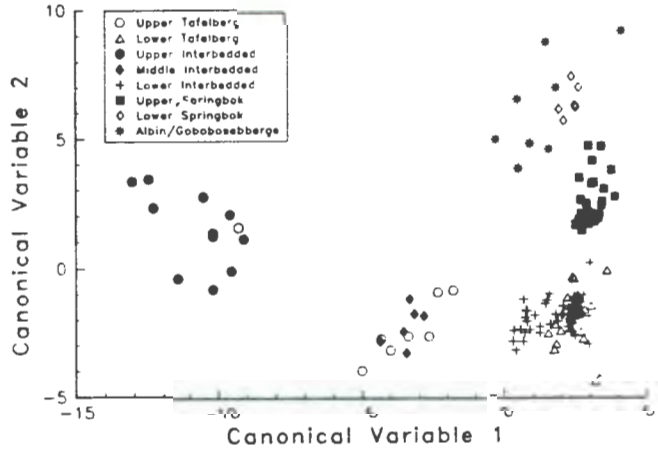

Fig. 9: Discriminant function analysis (DFA) diagram illustrating the maximum possible compositional discrimination between the Tafelberg, Interbedded and Springbok quartz latite units. The formulae for calculating the two canonical variables are given in the Appendix. Note that in the legend "Interbedded Coastal" subgroups of quartz latites have been abbreviated to "Interbedded".

in the function are excluded, as they contribute little to increasing the resolving power of the function. The discriminant function is expressed in terms of canonical variables which are a linear combination of weighted variables. The first canonical variable score describes the maximum variance between groups and successive canonical variables the maximum residual variance orthogonal to the previous score. It is important to note that the selection of discriminant elements and the canonical variable scores are dependent upon the sample groups used in the DFA, and that they change according to the groups used to define the function.

Fig. 9 presents a DFA diagram where all the main quartz latite groups and units were used to define the discriminant function; also plotted are samples from Albin beacon and the Gobosebberge. This diagram is similar in many respects to Fig. 8, however, a distinct separation is observed between the upper and lower Springbok units. The Albin beacon and Gobobosebberge samples plot apart from the Lower Springbok samples, a feature not observed on previous diagrams. The separation of the Tafelberg and Interbedded Coastal units into the three groupings recognised in the previous section is not improved.

To increase the discrimination between the Tafelberg and Interbedded Coastal quartz latites, these groups were processed through DFA without the Springbok group (Fig. 10). The lower Tafelberg unit and lower Interbedded Coastal subgroup remain closely associated, although some of the lower Interbedded Coastal samples plot towards the middle Interbedded Coastal subgroup and upper Tafelberg unit. The middle Interbedded Coastal subgroup and upper Tafelberg unit also show a slight separation. In the third cluster of points the single sample from Tafelberg beacon still plots within the upper Interbedded Coastal quartz latite subgroup.

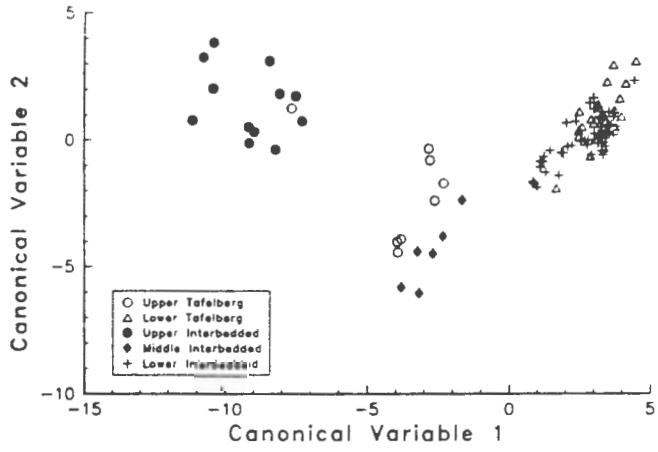

Fig. 10: DFA diagram illustrating the maximum possible compositional discrimination between the Tafelberg and Interbedded Coastal quartz latite units. The formulae for calculating the two canonical variables are given in the Appendix.

Discriminant functions were also calculated for several combinations of quartz latite group pairs in order to maximise the discrimination between them. The following conclusions were reached from the DFA investigation:

(1) The upper and lower Springbok units can be discriminated from each other and from the other quartz latite groups.
(2) Quartz latites from Albin beacon (Erlank *et al.*, 1984) and the Gobobosebberge lava field surrounding the Messum Complex are similar to the lower Springbok quartz latites. However, they can be separated into a diffuse field of their own when DFA is used to compare them with only the upper and lower Sprinbok units.
(3) The "Lower Tafelberg" quartz latites from either side of the Ambrosius Berg Fault Zone are compositionally indistinguishable and represent the same unit.
(4) The lower Tafelberg middle Tafelberg and Lower Interbedded Coastal quartz latites cannot be discriminated.
(5) The middle Interbedded Coastal subgroup and upper Tafelberg unit are not significantly different from one another and cannot be discriminated with any degree of confidence.
(6) The upper Interbedded Coastal quartz latites form a separate group which includes a sample from the Tafelberg beacon unit.

6. STRATIGRAPHIC INTERPRETATION

Based on the correlations discussed above a stratigraphic reconstruction and correlation of the Tafelberg and Interbedded Coastal successions across the southern Etendeka lava field is proposed (Table 2). Because of the different number of quartz latite units encountered in the Tafelberg and Interbedded Coastal sections, the comparison of quartz latite groups in Table 2 is not intended as an absolute correlation of individual units. We suggest that correlated units represent one or more eruptive units from the same 'batch' of quartz latite magma which were deposited over wide areas of the Etendeka during a particular eruptive cycle.

TABLE 2: Stratigraphic correlation of quartz latite units.

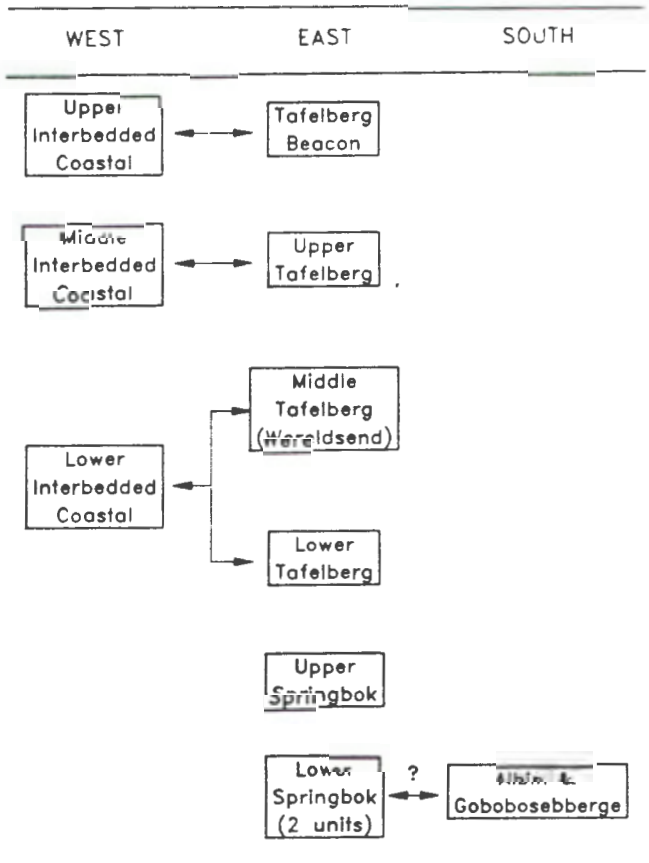

A schematic section of the Etendeka Formation illustrates the differences in stratigraphy and structure encountered in the eastern and western areas of the Etendeka lava field (Fig. 11a). The main structural break is the Ambrosius Berg Fault Zone (ABFZ). The increasing eastward dip in successive fault blocks to the west of the ABFZ suggests that the faults bounding these blocks are listric in character. Most of the faulting is probably post-volcanic, although some syn-volcanic movements may also have occurred in the period between the eruption of the upper Springbok and lower Tafelberg quartz latite units.

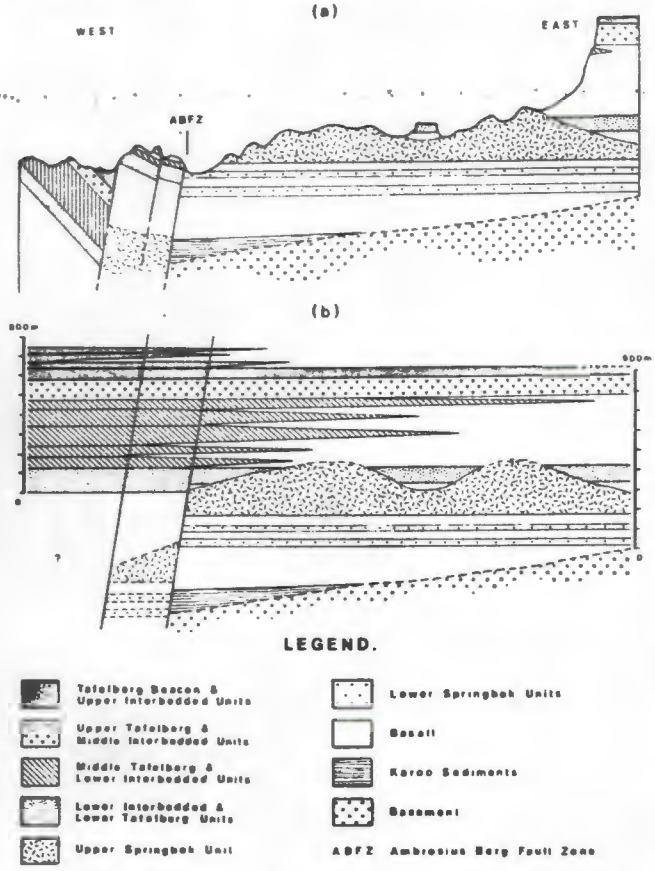

Fig. 11: (a) Schematic cross-section of the Etendeka Formation from Tafelberg (east) to the coast (west). Note that the lower Tafelberg quartz latite is correlated with the basal portion of the lower Interbedded Coastal quartz latite sequence on the basis of petrography. (b) Schematic stratigrahic reconstruction based on (a) but with the effects of post-volcanic faulting removed and without regard to present topography. Note that in the legend "Interbedded Coastal" subgroups of quartz latites have been abbreviated to "Interbedded".

A reconstruction of the Etendeka lava succession, based on the correlations in Table 2, is illustrated in Fig. 11b. The vertical scales on this diagram indicate the approximate thickness of the Tafelberg and Interbeded Coastal sequences, and of the individual units involved (Milner, 1986). Many of the quartz latite units appear to thin and terminate towards the east suggesting that the source area for these quartz latites was in the west.

It is tentatively suggested that the quartz latites from the Albin beacon and the Gobobosebberge lava field form part of the Springbok succession, although a more detailed knowledge of the Gobobosebberge lava succession and its geochemistry is required to substantiate this.

7. CONCLUSIONS

(1) Pitchstones and devitrified quartz latites have been affected by secondary alteration. The combination of low concentrations of K_2O and high LOI in the former implies a low temperature hydration event, and an apparent loss of CaO and Na_2O in the latter are related to the alteration of plagioclase.

(2) The extremely uniform composition displayed by the Etendeka quartz latite units indicates that their magma reservoirs were not compositionally zoned.

(3) Small, but significant, variations of certain element abundances allow the correlation of quartz latite units across most of the Etendeka area. Discriminant function analysis further enhances our ability to make geochemical correlations.

(4) A stratigraphic model for the Etendeka Formation is proposed on the basis of these correlations. The thick succession of quartz latites in the west thins and is intercalated with basaltic units in the east. Bellieni *et al.* (1984) have described 200-300 m thick interbedded dacite to rhyolite units in the upper portions of the Serra Geral Formation in the Parana Basin of Brazil. These units are the apparent equivalents of the Etendeka quartz latites in a pre-drift Gondwanaland reconstruction, although no direct geochemical correlation with the units described by Bellieni *et al.* (1984) can be attempted until possible inter-laboratory analytical variations have been assessed.

8. ACKNOWLEDGEMENTS

We owe particular thanks to Roy Miller for his earlier mapping of the Etendeka Formation and for many hours of fruitful discussion in the field. We have also benefitted greatly from discussions with Tony Erlank, Goonie Marsh and the late Peter Betton. Our work in the Etendeka area has been supported by a grant from the SWA/Namibia Committee for Research Priorities (CRP). We acknowledge thorough and constructive reviews of the manuscript by Roger Scoon and Brian Hoal.

9. REFERENCES

Bellieni, G., Brotzu, P., Comin-Chiaramonti, P., Ernesto, M., Melfi, A., Pacca, I.G., and Piccirillo, E.M. 1984. Flood basalt to rhyolite suites in the southern Parana Plateau (Brazil): Palaeomagnetism, petrogenesis and geochemical implications. *J. Petrol.*, **25**, 579-618.

Cerling, T.E., Brown, F.H., Bowman, J.R. 1985. Low-temperature alteration of volcanic glass: Hydration, Na, $K^{18}O$ and Ar mobility. *Chem. Geol.*, **52**, 281-293.

Dixon, W.J., Brown, M.B., Engelman, L., Frane, J.W. Hill, M.A., Jennrich, R.I. and Toporek, J.D. 1981. *BMDP statistical software.* Univ. of California Press, Berkeley, 785 pp.

Duncan, A.R., Erlank, A.J. and Marsh, J.S. 1984. Regional geochemistry of the Karoo Igneous Province. *Spec. Publ. geol. Soc. S. Afr.*, **13**, 355-388.

Erlank, A.J., Marsh, J.S., Duncan, A.R., Miller, R.McG., Hawkesworth, C.J., Betton, P.J. and Rex, D.C. 1984. Geochemistry and petrogenesis of the Etendeka volcanic rocks from S.W.A./Namibia. *Spec. Publ. geol. Soc. S. Afr.*, **13**, 195-245.

Hildreth, W. 1979. The Bishop Tuff: evidence for the origin of compositional zonation in magma chambers. *Spec. publ. geol. Soc. Am.*, **180**, 43-75.

Hildreth, W. 1981. Gradients in silicic magma chambers: implications for lithospheric magmatism. *J. geophys. Res.* **86**, 10153-10192.

Jezek, P.A. and Noble, D.C. 1978. Natural hydration and ion exchange of obsidian: an electron microprobe study. *Am. Miner.*, **63**, 266-273.

Le Maitre, R.W. 1982. *Numerical Petrology.* Elsevier, 281 pp.

Mackenzie, D.E. and Chappell, B.W. 1972. Shoshonitic and calc-alkaline lavas from the highlands of Papua New Guinea. *Contrib. Mineral. Petrol.*, **35**, 50-62.

Milner, S.C. 1986. The geological and volcanological features of the quartz latites of the Etendeka Formation. *Communs geol. Surv. S.W. Africa/Namibia*, **2**, 109-116.

Peccerillo, A. and Taylor, S.R. 1976. Geochemistry of Eocene calc-alkaline volcanic rocks from the Kastamonu area northern Turkey. *Contrib. Mineral. Petrol.*, **58**, 63-81.

Ritchey, J.L. 1980. Divergent magmas at Crater Lake, Oregon: products of fractional crystallisation and vertical zoning in a shallow, water-undersaturated chamber. *J. Volcan. Geotherm. Res.*, **7**, 373-386.

Smith, R.L. and Bailey, R.A. 1966. The Bandelier Tuff: a study of ash flow eruption cycles from zoned magma chambers. *Bull. volcan.*, **29**, 83-104.

Smith, R.L. 1979. Ash flow magmatism. *Spec. Publ. geol. Soc. Am.*, **180**, 5-27.

Williams, H. 1942. The geology of Crater Lake National Park. *Carnegie Instn. Wash. Publ.*, **540**, 1-162.

Zielinski, R.A. 1982. The mobility of uranium and other elements during alteration of rhyolite ash to montmorillonite: a case study in the Troublesome Formation, Colorado, U.S.A. *Chem. geol.*, **35**, 185-204.

APPENDIX

The canonical variable scores are calculated according to the equations given below. Major oxide concentrations were expressed in weight % and trace element concentrations in ppm, the data were not normalised to 100% on a volatile-free basis prior to calculating canonical variable (CV) scores.

Fig. 9:

$$CV1 = -(TiO_2 * 27.952) + (Al_2O_3 * 0.41343) + (Fe_2O_3 * 1.0670) - (P_2O_5 * 14.870) + (Ba * 0.00458) + (Zr * 0.05536) - (Cu * 0.08252) + 3.3561$$

$$CV2 = -(TiO_2 * 2.3059) - (Al_2O_3 * 0.35222) + (Fe_2O_3 * 3.1557) - (P_2O_5 * 46.007) + (Ba * 0.00435) + (Zr * 0.12755) - (Cu * 0.02577) - 36.302$$

Fig. 10:

$$CV1 = -(TiO_2 * 21.337) + (Al_2O_3 * 1.1980) + (Ba * 0.00036) + (Nb * 0.18515) - (V * 0.04694) - (Cu * 0.07132) + (Y * 0.10051) + 1.8007$$

$$CV2 = +(TiO_2 * 14.657) - (Al_2O_3 * 2.6432) + (Ba * 0.00754) + (Nb * 0.85879) - (V * 0.12429) - (Cu * 0.03202) + (Y * 0.01077) + 4.1757$$